MICROCOPY RESOLUTION TEST CHART

NATIONAL BUREAU OF STANDARDS 1963 A

Report No. CG-D-29-80

DETONATION-FLAME ARRESTER DEVICES

FOR GASOLINE CARGO VAPOR RECOVERY SYSTEM

R. A. BJORKLUND AND P. R. RYASON

FINAL REPORT

MARCH 1980

Document is available to the public through the
National Technical Information Service,
Springfield, Virginia 22151

Prepared for

U.S. DEPARTMENT OF TRANSPORTATION
United States Coast Guard
Office of Research and Development
Washington, D.C. 20590

80 6 26 042

NOTICE

Technical Report Documentation Page

1. Report No. CG-D-29-80	2. Government Accession No. AD-A086 062	3. Recipient's Catalog No. (11) Mar 80

4. Title and Subtitle	5. Report Date
DETONATION-FLAME ARRESTER DEVICES FOR GASOLINE CARGO VAPOR RECOVERY SYSTEMS	March 1980
	6. Performing Organization Code

7. Author(s) R.A. Bjorklund and P.R. Ryason	8. Performing Organization Report No. JPL Publication 80-18

9. Performing Organization Name and Address Jet Propulsion Laboratory California Institute of Technology 4800 Oak Grove Drive Pasadena, California 91103	10. Work Unit No. (TRAIS)
	11. Contract or Grant No. Z-70099-7-74328-H

12. Sponsoring Agency Name and Address United States Coast Guard Marine Technology Division, Office of Research and Development 2100 Second Street, S.W. Washington, D.C. 20593	13. Type of Report and Period Covered Final Report
(14) JPL-PUB-80-18	14. Sponsoring Agency Code

15. Supplementary Notes

Technical effort accomplished through an agreement with the National Aeronautics and Space Administration. (15) MIPR-Z-70099-7-74328-H

16. Abstract   An experimental program was carried out to (1) develop empirical data on the deflagration-to-detonation run-up distance for flowing mixtures of gasoline and air in 15.2-cm- (6.0-in.-) diameter piping simulating a vapor recovery system, and (2) evaluate the quenching capability of eight selected flame control devices subjected to repeated stable detonations. The deflagration-to-detonation run-up distance was found to be 11.2 m (36.7 ft), or a length-to-diameter ratio of 74. The relative roughness of the run-up length of piping was 0.010 to 0.015. The stable detonation downstream of the transition point had a velocity of 1800 m/s (5906 ft/s) with a stable peak pressure of 1900 kN/m^2 (275 psia). There appeared to be no discernable correlation between the initial flow velocity used in testing and the resulting run-up distance. Detonations were obtained only at equivalence ratios greater than 0.8; however, there was no correlation between equivalence ratio and run-up distance for equivalence ratios ranging from 0.9 to 1.4. The successful detonation-flame arresters were: (1) spiral-wound, crimped aluminum ribbon, (2) foamed nickel-chrome metal, (3) vertically packed bed of aluminum Ballast rings, and (4) water-trap or hydraulic back-pressure valve. Installation configurations for two of the more applicable arresters, the spiral-wound, crimped stainless-steel ribbon and the vertically packed bed of aluminum Ballast rings, were further optimized by a series of parametric tests. The final configuration of these two arresters were demonstrated with repeated detonation tests at conditions that simulated vapor recovery system operation. On these tests, the combustible mixture of gasoline and air continued to flow through the piping for periods up to 120 seconds after the initial detonation had been arrested. There was no indication of continuous burning or reignition occurring on either side of the test arresters.

17. Key Words	18. Distribution Statement
Inorganic Chemistry Safety Engineering Environment Pollution Combustion and Ignition	Document is available to the U.S. public through the National Technical Information Service, Springfield, Virginia 22161.

19. Security Classif. (of this report)	20. Security Classif. (of this page)	21. No. of Pages	22. Price
Unclassified	Unclassified	240	

Form DOT F 1700.7 (8-72)   Reproduction of completed page authorized

PREFACE

ABSTRACT

An experimental program was carried out to (1) develop empirical data on the deflagration-to-detonation run-up distance for flowing mixtures of gasoline and air in 15.2-cm- (6.0-in.-) diameter piping simulating a vapor recovery system, and (2) evaluate the quenching capability of eight selected flame control devices subjected to repeated stable detonations.

The deflagration-to-detonation run-up distance was found to be 11.2 m (36.7 ft), or a length-to-diameter ratio of 74. The relative roughness of the run-up length of piping was 0.010 to 0.015. The stable detonation downstream of the transition point had a velocity of 1800 m/s (5906 ft/s) with a stable peak pressure of 1900 kN/m^2 (275 psia). There appeared to be no discernable correlation between the initial flow velocity used in testing and the resulting run-up distance. Detonations were obtained only at equivalence ratios greater than 0.8; however, there was no correlation between equivalence ratio and run-up distance for equivalence ratios ranging from 0.9 to 1.4.

The successful detonation-flame arresters were: (1) spiral-wound, crimped aluminum ribbon, (2) foamed nickel-chrome metal, (3) vertically packed bed of aluminum Ballast rings, and (4) water-trap or hydraulic back-pressure valve. Installation configurations for two of the more applicable arresters, the spiral-wound, crimped stainless-steel ribbon and the vertically packed bed of aluminum Ballast rings, were further optimized by a series of parametric tests. The final configuration of these two arresters were demonstrated with repeated detonation tests at conditions that simulated vapor recovery system operation. On these tests, the combustible mixture of gasoline and air continued to flow through the piping for periods up to 120 seconds after the initial detonation had been arrested. There was no indication of continuous burning or reignition occuring on either side of the test arresters.

CONTENTS

viii

ix

Tables

SECTION I

SUMMARY

An experimental program was conducted to gather empirical data on
the detonation of combustible mixtures of gasoline and air flowing in a
15.2-cm- (6.0-in.-) diameter simulated vapor recovery piping system, and
to evaluate flame control devices capable of arresting the detonation.
A special test facility had to be assembled in a suitable location to
conduct these potentially hazardous experiments. Facility check-out tests
were performed to develop reliable methods of generating stable detonations
and to verify the operation of dynamic instrumentation used to measure flame
velocities and peak-pressure pulses. A series of calibration tests, using
both propane/air mixtures and gasoline/air mixtures, were made to determine
the run-up distance to detonation, the flame velocity and peak-pressure
pulse in both the transition and stable stages of detonation, and the pres-
sure buildup resulting from reflected detonation shock waves. These tests
were then followed by the experimental evaluation of eight selected flame
arrester test assemblies to demonstrate their operating characteristics;
these characteristics included pressure drop, flame quenching capability,
and structural durability before and after repeated exposures to stable
detonations. Two of the more successful flame arrester configurations
were further evaluated with a series of parametric tests designed to reduce
the level of the peak-pressure pulse passing through the device after
the detonation had been arrested, and to optimize the overall size of the
arrester configuration. A final series of tests were made to demonstrate
the ability of these optimized configurations to arrest a detonation in
simulated vapor recovery system piping under the condition where the
combustible mixture of gasoline and air continued to flow through the
system for periods up to 120 seconds after the initial deflagration-
to-detonation transition had occurred.

The facility check-out tests using propane and air mixtures revealed
that flame acceleration up to detonation transition could not be achieved
in the smooth-bored shock-tube piping at the maximum available run-up dis-
tance of 31.5 m (103.5 ft). However, stable detonations were obtained
after expanded metal tube liners were inserted into several lengths of run-
up piping to create turbulence in the combustion process. Flame propagating
velocities were determined using photomultiplier tube optical flame sen-
sors. Peak-pressure pulse levels in the detonation wave were measured
using quartz piezoelectric transducers. All dynamic data were recorded
on FM tapes and analyzed using playbacks on oscillograph recorders at an
expanded time base.

Calibration tests with both propane/air and gasoline/air mixtures
determined that 13.7 m (45 ft) of turbulence-inducing liners were required
to produce repeatable stable detonations in the combustion process. Ad-
ditional calibration tests, using gasoline and air mixtures in a modified
test configuration that included flame sensing instrumentation in the lined
sections, showed that the run-up distance to detonation was 11.2 m (36.7 ft),
or an L/D of 74 for the 15.2-cm- (6.0-in.-) diameter pipe system. These
results generally held true for equivalence ratios ranging from 0.9 to
1.4 and initial flow velocities from 0 to 6.1 m/s (0 to 20 ft/s). The
flame velocity in a stable detonation was measured at 1830 m/s (6000 ft/s),

and the peak-pressure level at 1630 kN/m^2 (235 psia). During the de-flagration-to-detonation transition, flame velocities were measured up to 2700 m/s (8858 ft/s), and peak pressures exceeded 4000 kN/m^2 (580 psia). The peak pressure measured in a reflected detonation wave 30 cm (12 in.) from the reflecting surface was 3300 kN/m^2 (479 psia), or about twice the level in the approaching wave.

A series of air-flow-only calibration tests were made to measure pressure drop through the lined and unlined piping. This pressure loss was used to determine the internal wall Darcy friction factor (f) and the relative roughness (ϵ/D). For the lined piping, the friction factor ranged from 0.040 to 0.047 and the relative roughness from 0.010 to 0.015. This relative roughness is approximately equivalent to that of commercial riveted steel pipe. The unlined shock-tube piping had a friction factor around 0.020 and a relative roughness less than 10^{-6}, which is lower than any commercial smooth piping.

The flame control devices experimentally evaluated for arresting detonations in simulated vapor recovery system piping consisted of two arrangements of standard high-pressure pipe fittings with rupture-disc assemblies, four commercially manufactured flame arresters or prototype models, and two JPL-manufactured arrester assemblies. All of these de-vices were subjected to a series of stable detonations resulting from the ignition of a flowing combustible mixture of gasoline and air. A standard condition for each repeated test firing was established at an equivalence ratio of 1.1 (air-to-gasoline weight ratio of 13.3), and an initial flow velocity of 4.6 m/s (15 ft/s). Depending on ambient conditions, the mixture temperature just before ignition ranged from 30 to 60°C (86 to 150°F). Pressure level in the piping system was just slightly above ambient, as determined by the arrester pressure drop. The results of these test firings using an upstream ignition location are tabulated in Table 1-1 and briefly summarized as follows:

(1) The pipe-tee and rupture-disc in-line test assembly sustained four detonations. Both rupture discs were blown out, but there was no physical damage. The detonation passed through the device in every test with very little reduction in flame velocity and peak pressure. Pre- and posttest pressure loss average was 0.20 kN/m^2 (0.029 psid).

(2) The pipe tee, rupture-disc not-in-line, and pipe-elbow test assembly sustained four detonations. The rupture disc was blown out in each test, but there was no physical damage. The detonation passed through the device in every test with an intermittent moderate loss of flame velocity and peak pressure. Pre- and posttest pressure loss average was 0.214 kN/m^2 (0.031 psid).

(3) The Shand and Jurs spiral-wound, crimped aluminum ribbon arrester test assembly sustained nine detonations without serious damage. The detonation did not pass through the arrester. Pre- and posttest pressure loss averaged 0.152 kN/m^2 (0.022 psid).

Table 1-1. Summary of Test Results for Detonation-Flame Arrester Assemblies

Ignition Location, and Type and Size of Arrester	Number of Detonations Sustained	Detonations Arrested		Air Velocity, (Averaged)		Pressure Loss, (Averaged)	
		Yes	No	m/s	(ft/s)	kN/m²	(psid)
A. Upstream Ignition							
Two 15.2-cm- (6.0-in.-) diam pipe tees, rupture discs, and a 8.192-cm- (3.225-in.-) diam orifice plate	4		4	4.68	(15.35)	0.200	(0.029)
A 15.2-cm- (6.0-in.-) diam pipe tee and pipe elbow, rupture disc, and a 8.192-cm- (3.225-in.-) diam orifice plate	4		4	4.71	(15.46)	0.214	(0.031)
Shand and Jurs spiral wound, crimped aluminum ribbon, 30.5-cm (12.0-in.) diam by 15.2-cm (6.0-in.) depth, 0.137-cm (0.054-in.) crimp height, and 0.114-cm (0.045-in.) hydraulic diam	9	9		4.68	(15.35)	0.152	(0.022)
Amal spiral wound, crimped stainless-steel ribbon, 25.4-cm (10.0-in.) diam by 3.81-cm (1.5-in.) depth, 0.046-cm (0.018-in.) crimp height, and 0.038-cm (0.015-in.) hydraulic diam	4	1	3	4.69	(15.39)	0.428	(0.062)

Table 1-1. Summary of Test Results for Detonation-Flame Arrester Assemblies (Continuation 1)

Ignition Location, and Type and Size of Arrester	Number of Detonations Sustained	Detonations Arrested		Air Velocity, (Averaged)		Pressure Loss, (Averaged)	
		Yes	No	m/s	(ft/s)	kN/m2	(psid)
A. Upstream Ignition (contd)							
Whessoe 80-grade Retimet foamed nickel-chrome alloy, 25.4-cm (10.0-in.) diam by 1.3-cm (0.5-in.) depth	3	3		4.74	(15.54)	0.241	(0.035)
Whessoe 45-grade Retimet foamed nickel-chrome alloy 25.4-cm (10.0-in.) diam by 1.3-cm (0.5-in) depth	1		1	4.78	(15.68)	0.130	(0.019)
Water trap with water, 15.2-cm- (6.0-in.-) diam pipe inlet and outlet, 43.2-cm- (17.0-in.-) diam pipe vessel with 15.2-cm (6.0-in.) water depth	5	5		4.66	(15.29)	1.655	(0.240)
Water trap without water (same dimensions as that with water)	1		1	4.84	(15.88)	0.028	(0.004)
Vertical bed of aluminum Ballast rings, 43.2-cm (17.0-in.) diam by 63.5-cm (25.0-in.) depth with 2.54-cm- (1.0-in.-) diam by 2.54-cm- (1.0-in.-) long rings	5	5		4.64	(15.23)	0.048	(0.007)

Table 1-1. Summary of Test Results for Detonation-Flame Arrester Assemblies (Continuation 2)

Ignition Location, and Type and Size of Arrester	Number of Detonations Sustained	Detonations Arrested		Air Velocity, (Averaged)		Pressure Loss, (Averaged)	
		Yes	No	m/s	(ft/s)	kN/m^2	(psid)
A. Upstream Ignition (contd)							
Linde hydraulic back-pressure valve with water, 10.2-cm- (4.0-in.-) diam pipe inlet and outlet, 20.3-cm- (8.0-in.-) diam pipe vessel with 15.2-cm (6.0-in.) water depth	6	6		4.65	(15.27)	2.027	(0.294)
Linde hydraulic back-pressure valve without water (same dimensions as that with water)	3		3	4.63	(15.20)	0.407	(0.059)
B. Downstream Ignition							
Linde hydraulic back-pressure valve with water (same dimensions as that for upstream ignition)	6	6		1.61	(5.28)	1.917	(0.278)
Water trap with water (same dimensions as that for upstream ignition)	5	5		1.52	(5.0)	1.393	(0.202)

(4)   The Amal spiral-wound, crimped stainless-steel ribbon arrester
        test assembly sustained four detonations without any visible
        damage. The detonation was arrested in the first firing,
        but passed through in the other three. Pre- and posttest
        pressure loss averaged 0.428 kN/m^2 (0.062 psid).

(5)   The Whessoe foamed metal arrester test assembly using the 80-
        grade Retimet nickel-chrome alloy core element sustained three
        detonations. The detonation was stopped for all three tests,
        but the core element fractured during the last test. Pre-
        and posttest pressure loss before failure averaged 0.241
        kN/m^2 (0.035 psid). One additional test firing with a
        45-grade Retimet nickel-chrome alloy core element failed
        to stop the detonation.

(6)   The water-trap arrester test assembly sustained six detona-
        tions without damage, but did display a measurable loss in
        water volume due primarily to evaporation. The detonation
        did not pass through the arrester as long as it contained
        water at or near the prescribed level. Pre- and posttest
        pressure loss averaged 1.655 kN/m^2 (0.240 psid).

(7)   The vertical bed of the Ballast rings arrester test assembly
        sustained five detonations with only minor distortion of the
        rings caused by bed compacting. The detonation did not pass
        through the arrester. Pre- and posttest pressure loss aver-
        aged 0.048 kN/m^2 (0.007 psid).

(8)   The Linde hydraulic back-pressure valve arrester test assembly
        sustained ten detonations without damage, but like the water
        trap, it did display a measurable loss in water volume due
        primarily to evaporation. The detonation was stopped for six
        test firings where the water level was at or near the prescribed
        level and was stopped for one test firing where there was only
        a small amount of water remaining in the arrester. The
        detonation was not stopped for three test firings with
        a dry arrester. Pre- and posttest pressure loss averaged
        2.027 kN/m^2 (0.294 psid).

Two of the arrester test assemblies were evaluated using a downstream
ignition configuration. The maximum initial flow velocity was limited to
1.5 m/s (5.0 ft/s) because of the difficulty in getting the flame to pro-
pagate back upstream against the flowing gasoline and air mixture. The
results of these test firings are tabulated in Table 1-1 and briefly summarized
as follows:

(1)   The Linde hydraulic back-pressure valve arrester test assembly
        sustained six more detonations without damage. Some water was
        lost due to evaporation, but an additional quantity was dis-
        placed upstream by the force of the detonation wave. The
        detonation was stopped for all six test firings. Pre- and
        posttest pressure loss averaged 1.92 kN/m^2 (0.278 psid).

(2)   The water-trap arrester test assembly sustained five more
        detonations without damage. The detonation was stopped for
        every test firing. Some water was lost from the arrester
        due to evaporation. However, no liquid appeared to be dis-
        placed by the incoming detonation wave. Pre- and posttest
        pressure loss average was 1.393 kN/m^2 (0.202 psid).

The two arrester assemblies selected for parametric testing were (1)
the Shand and Jurs spiral-wound, crimped stainless-steel ribbon arrester
and (2) the vertical bed of aluminum Ballast rings arrester. The Shand
and Jurs arresters all had the same ribbon crimp height and same core
diameter, but three different core lengths. Both an indirect and a direct
inlet pipe configuration with rupture-disc assembly were used. With the
direct inlet installed, the rupture-disc pressure rating was increased in
four steps to a blanked-off condition. The vertical bed of rings arrester
was tested with four decreasing bed diameters, three decreasing bed lengths,
and three increasing sizes of aluminum Ballast rings. The inlet pipe
configuration was not varied, but the inlet rupture-disc pressure rating
was increased in four steps up to a blanked-off condition. All of the
parametric arrester configurations were subjected to a series of stable
detonations developed in a flowing mixture of gasoline and air at the
same standard test condition established for the preceding screening
tests. The results of the parametric testing are tabulated in Tables
1-2 and 1-3, and briefly summarized as follows:

(1)   The 15.2-cm- (6-in.-) long stainless-steel Shand and Jurs
        arrester configuration, with the indirect inlet piping and a
        690-kN/m^2 (100-psid) rupture disc, arrested four detonations.
        On the fifth test, the detonation passed through the arrester.
        Posttest inspection revealed a small separation in the crimped
        ribbon winding. Pre- and posttest pressure loss averaged
        0.151 kN/m^2 (0.022 psid). Downstream pressure pulse measure-
        ments averaged 344 kN/m^2 (49.9 psia).

(2)   The 20.3-cm-(8-in.-) long stainless-steel Shand and Jurs arrester
        configuration, with the indirect inlet piping and a 690-kN/m^2
        (100-psid) rupture disc, arrested six detonations. Pre- and
        posttest pressure loss averaged 0.152 kN/m^2 (0.022 psid). Down-
        stream pressure pulse measurements averaged 320 kN/m^2 (46.4 psia),
        or 7% lower than the 15.2-cm- (6-in.-) long core element.

(3)   The 30.5-cm- (12-in.-) long stainless-steel Shand and Jurs arrester
        configuration, with the indirect piping and a 690-kN/m^2 (100-
        psid) rupture disc, arrested six detonations. Pre-and posttest
        pressure loss averaged 0.230 kN/m^2 (0.033 psid). Downstream
        pressure pulse measurements averaged 260 kN/m^2 (37.7 psia),
        or 25% lower than the 15.2-cm-(6-in.-) long core element.

(4)   The 20.3-cm-(8-in.-) long stainless-steel Shand and Jurs arrester
        configuration, with the direct inlet piping and rupture
        disc assembly, arrested six more detonations. During the
        first three tests, the inlet rupture-disc pressure rating
        was increased in steps through 690, 2068, and 4137 kN/m^2
        (100, 300, and 600 psid). On the last three tests, the

Table 1-2. Summary of Parametric Test Results for the Shand and Jurs Spiral-Wound, Crimped Stainless-Steel Ribbon Arrester Assemblies

Arrester Core Size		Inlet Pipe Connection Configuration	Rupture Disc Pressure Rating, kN/m² (psid)	Number of Detonations Arrested		Run-Up Pipe Air Velocity, (Averaged) m/s (ft/s)	Arrester Pressure Loss, (Averaged) kN/m² (psid)	Downstream Pressure Pulse, (Averaged) kN/m² (psid)
Diameter, cm (in)	Length, cm (in)			Yes	No			
30.5 (12)	15.2 (6)	Indirect	690 (100)	4	1	4.78 (15.68)	0.151 (0.022)	344 (49.9)
30.5 (12)	20.3 (8)	Indirect	690 (100)	6	0	4.58 (15.89)	0.152 (0.022)	320 (46.4)
30.5 (12)	30.5 (12)	Indirect	690 (100)	6	0	4.48 (14.70)	0.230 (0.033)	260 (37.7)
30.5 (12)	20.3 (8)	Direct	690 (100)	1	0	4.35 (14.27)	0.134 (0.019)	318 (46.1)
30.5 (12)	20.3 (8)	Direct	2068 (300)	1	0	4.38 (14.37)	0.138 (0.020)	334 (48.4)
30.5 (12)	20.3 (8)	Direct	4137 (600)	1	0	4.55 (14.93)	0.138 (0.020)	325 (47.1)
30.5 (12)	20.3 (8)	Direct	Blanked-off	3	0	4.46 (14.63)	0.138 (0.020)	323 (46.8)

1-8

Table 1-3. Summary of Parametric Test Results for the Vertical Bed of
Aluminum Ballast Rings Arrester Assemblies

Arrester Bed Size		Ballast Ring Size (Diam. & length)		Rupture Disc Pressure Rating		Number of Detonations Arrested		Run-Up Pipe Air Velocity (Averaged)		Arrester Pressure Loss (Averaged)		Downstream Pressure Pulse (Averaged)	
Diameter, cm (in)	Depth, cm (in)	cm	(in)	kN/m²	(psid)	Yes	No	m/s	(ft/s)	kN/m²	(psid)	kN/m²	(psid)
43.2 (17)	63.5 (25)	2.45	(1.0)	690	(100)	6	0	4.52	(14.82)	0.075	(0.011)	181	(26.3)
43.2 (17)	45.7 (18)	2.45	(1.0)	690	(100)	6	0	4.62	(15.14)	0.053	(0.008)	197	(28.6)
43.2 (17)	22.9 (9)	2.45	(1.0)	690	(100)	4	2	4.59	(15.04)	0.052	(0.007)	236	(34.2)
43.2 (17)	63.5 (25)	3.81	(1.5)	690	(100)	2	2	4.73	(15.52)	0.067	(0.010)	290	(42.1)
43.2 (17)	63.5 (25)	5.08	(2.0)	690	(100)	1	2	4.68	(15.35)	0.056	(0.008)	304	(44.1)
33.7 (13.3)	63.5 (25)	2.45	(1.0)	690	(100)	6	0	4.55	(14.93)	0.131	(0.019)	149	(21.6)
30.5 (12)	63.5 (25)	2.45	(1.0)	690	(100)	6	0	4.51	(14.78)	0.147	(0.021)	142	(20.6)
25.4 (10)	63.5 (25)	2.45	(1.0)	690	(100)	-	0	4.62	(15.14)	0.278	(0.040)	132	(19.1)
25.4 (10)	45.7 (18)	2.45	(1.0)	690	(100)	1	0	4.55	(14.93)	0.162	(0.023)	142	(20.6)
25.4 (10)	45.7 (18)	2.45	(1.0)	2068	(300)	1	0	4.53	(14.86)	0.197	(0.028)	141	(20.4)
25.4 (10)	45.7 (18)	2.45	(1.0)	4137	(600)	1	0	4.60	(15.09)	0.197	(0.028)	141	(20.4)
25.4 (10)	45.7 (18)	2.45	(1.0)	Blanked-off		3	0	4.57	(14.99)	0.220	(0.032)	164	(23.8)

rupture-disc assembly was blanked-off. This variation in rupture-disc pressure rating made little difference in the downstream pressure pulse measurements, which averaged 324 kN/m^2 (47.0 psia), or about the same level as that obtained with the indirect inlet piping. Pre- and posttest pressure loss on these tests averaged 0.138 kN/m^2 (0.020 psid).

(5)   Three vertical bed arrester configurations, with a full-size bed diameter of 43.2 cm (17 in.), and decreasing bed depths of 63.5 cm (25 in.), 45.7 cm (18 in.), and 22.9 cm (9 in.) packed with 2.54-cm- (1.0-in.-) size aluminum Ballast rings, were each subjected to six stable detonations. The two longer bed configurations arrested all six detonations. The shortest bed configuration arrested four detonations, but then allowed two to pass through. Posttest inspections of this arrester showed some evidence of channeling through the compacted bed of rings. Pre- and posttest averaged pressure loss dropped slightly from 0.075 to 0.052 kN/m^2 (0.011 to 0.007 psid) with the decrease in bed depth. The averaged downstream pressure pulse for an arrested detonation increased from 181 to 236 kN/m^2 (26.3 to 34.2 psia) with the decrease in bed depth.

(6)   Two full-size vertical bed arresters having a 43.2-cm- (17-in.-) diameter by 63.5-cm- (25-in.-) depth bed, one packed with 3.81-cm- (1.5-in.-) size aluminum Ballast rings and the other with 5.08-cm- (2.0 in.-) size aluminum Ballast rings, were tested. The configuration with the 3.81-cm- (1.5-in.-) size rings arrested two detonations and then allowed two to pass through. The configuration with the 5.08-cm- (2.0-in.-) size rings arrested only one detonation before allowing two to pass through. Posttest inspection revealed considerable distortion of these enlarged-size Ballast rings from the detonation impacts. Pre- and posttest averaged pressure loss decreased slightly with the enlarged ring sizes of 0.067 and 0.056 kN/m^2 (0.010 and 0.008 psid). Averaged downstream pressure pulse for an arrested detonation increased to 290 and 304 kN/m^2 (42.1 and 44.1 psia).

(7)   Three vertical bed arrester configurations, with a full-size bed depth of 63.5 cm (25 in.) and decreasing bed diameters of 33.7 cm (13.3 in.), 30.5 cm (12 in.), and 25.4 cm (10 in.) packed with 2.54-cm- (1.0-in.-) size aluminum Ballast rings, were each subjected to six or more stable detonations. All three configurations arrested the detonations. Posttest inspections showed about 30% compaction of the beds due to distortion of the rings. Pre- and posttest averaged pressure loss increased with each succeeding smaller bed diameter. The 25.4-cm- (10-in.-) diameter bed pressure loss was 0.278 kN/m^2 (0.040 psid), which is about four times higher than the 0.075-kN/m^2- (0.011-psid-) loss for the full size 43.2-cm- (17-in.-) diameter bed. The averaged downstream pressure pulse decreased from 181 kN/m^2 (26.3 psia) for the full-diameter bed to 132 kN/m^2 (19.1 psia) for the smallest 25.4-cm- (10-in.-) diameter bed.

(8)   The 25.4-cm- (10-in.-) diameter vertical bed arrester packed
        with 2.54-cm- (1.0-in.-) size aluminum Ballast rings to a reduced
        bed depth of 45.7 cm (18 in.) arrested six more detonations.
        During the first three tests, the inlet piping rupture-disc
        pressure rating was increased in steps through 690, 2068, and
        4137 kN/m^2 (100, 300, and 600 psid). On the last three tests,
        the rupture-disc assembly was blanked-off. The averaged
        downstream pressure pulse for the three test firings with
        rupture discs installed was around 141 kN/m^2 (20.4 psia).
        When the rupture-disc assembly was blanked-off, the averaged
        downstream pressure pulse increased slightly to 164 kN/m^2
        (23.8 psia). Pre- and posttest averaged pressure loss
        measurements increased from 0.162 kN/m^2 (0.023 psid) after the
        first detonation to 0.220 kN/m^2 (0.032) after the sixth
        detonation, due to a 28% compaction of the bed.

        The two optimized detonation arrester configurations, developed from
the parametric tests, were further evaluated after test facility modifica-
tions were made to provide continuous combustible mixture flow capability
and an extended exit section with 16.5 m (54 ft) of 15.2-cm- (6.0-in.-)
diameter pipe added to witness lingering flames or reignitions occuring
downstream of the test arrester. The vertical bed of Ballast rings arrester
configuration had a bed size 25.4 cm (10 in.) in diameter by 45.7 cm (18
in.) long packed with 2.54-cm- (1.0-in.-) size aluminum rings. An indirect
inlet configuration for this arrester consisted of a not-in-line pipe tee,
a blanked-off rupture-disc assembly, and a pipe elbow. The Shand and Jurs
spiral-wound, crimped stainless-steel ribbon arrester configuration had
a core size 30.5 cm (12 in.) in diameter by 20.3 cm (8 in.) long. A direct
inlet configuration for this arrester was an in-line pipe tee with a blanked-
off rupture-disc assembly. Both of these arresters were tested with a flow-
ing combustible mixture of gasoline and air at the standard test conditions.
The mixture continued to flow through the test piping for periods up to
120 seconds after the ignition and detonation had occurred. The results
of these tests are tabulated in Table 1-4 and briefly summarized as follows:

        (1)   The vertical bed of aluminum Ballast rings arrester test
                assembly arrested eight detonations. The first two detonation
                tests were followed by continuous mixture flow for a period
                of 30 seconds. On each succeeding two-test series, the
                flow periods were extended in steps through 60, 90, and
                120 seconds. There was no indication of reignition or
                lingering flames either upstream or downstream of the test
                arrester on any of these firings. Pre- and posttest averaged
                pressure loss was 0.031 kN/m^2 (0.044 psid) and appeared
                to increase slightly during testing due to compaction of
                the bed of rings. The downstream pressure pulse averaged
                14.6 kN/m^2 (21.1 psia) and had an average velocity of 398
                m/s (1304 ft/s) through the pipe extension section. There
                was no evidence of increasing wave velocity or pressure
                in the extension section.

        (2)   The Shand and Jurs spiral-wound, crimped stainless-steel
                arrester test assembly arrested eight detonations. The first
                two detonation tests were followed by continuous mixture flow

Table 1-4. Summary of Continuous-Flow Test Results for Two Detonation-Flame Arrester Assemblies

Arrester Type, Size, and Inlet Configuration	Continuous-Flow Time, s	Number of Detonations Arrested		Run-Up Pipe Air Velocity, (Averaged) m/s (ft/s)		Arrester Pressure Loss, (Averaged) kN/m² (psia)		Downstream Pressure Pulse, (Averaged) kN/m² (psia)		Downstream Wave Velocity, (Averaged) m/s (ft/s)	
		Yes	No								
Vertical bed of aluminum Ballast rings, bed size: 25.4-cm (10-in.) diam. by 45.7-cm (18.0-in.) depth, ring size: 2.54-cm (1.0-in.) diam. by 2.54-cm (1.0-in.) long, indirect inlet with blanked-off rupture disc.	30	2	0	4.62	(15.14)	0.279	(0.041)	145	(21.0)	400	(1313)
	60	2	0	4.74	(15.55)	0.321	(0.046)	145	(21.0)	398	(1306)
	90	2	0	4.48	(14.68)	0.274	(0.040)	149	(21.6)	397	(1304)
	120	2	0	4.52	(14.82)	0.331	(0.048)	144	(20.8)	395	(1296)
Shand and Jurs spiral-wound, crimped stainless-steel ribbon, core size: 30.5-cm (12-in.) diam. by 20.3-cm (8-in.) long, direct inlet with blank-off rupture disc.	30	2	0	4.58	(15.02)	0.140	(0.020)	300	(43.6)	550	(1805)
	60	2	0	4.55	(14.92)	0.138	(0.020)	296	(42.9)	549	(1800)
	90	2	0	4.62	(15.15)	0.135	(0.019)	296	(42.9)	552	(1812)
	120	2	0	4.69	(15.38)	0.129	(0.019)	296	(42.9)	563	(1848)

for a period of 30 seconds. On each succeeding two-test series, the flow periods were extended in steps through 60, 90, and 120 seconds. There was no indication of reignition or lingering flames either upstream or downstream of the test arrester on any of these firings. Pre- and posttest averaged pressure loss was 0.136 kN/m^2 (0.020 psid). The downstream pressure pulse averaged 297 kN/m^2 (43.1 psia) and had an average velocity of 555 m/s (1816 ft/s) through the pipe extension section. There was an indication of decreasing wave velocity and pressure in the extension section. Posttest inspection revealed no damage or distortion to the arrester core assembly and only minor distortion of the arrester retainer grid ring.

The following is a listing of source information for commercial flame arresters and components used in this program.

(1)   Shand and Jurs, spiral-wound, crimped metal ribbon arresters; G.P.E. Controls, 6511 Oakton Street, Morton Grove, Illinois, 60053.

(2)   Amal, spiral-wound, crimped metal ribbon arrester; Amal Ltd., Birmingham, England.

(3)   Retimet foamed metal arresters; Whessoe Systems and Controls, Ltd., Brinkburn Road, Darlington, Co., Durham DL3 6DS, England.

(4)   Linde hydraulic back-pressure valve arrester; Union Carbide, Linde Division, Gas Products Division, P. O. Box 42, 239 Old New Brunswick Road, Piscataway, New Jersey, 08854.

(5)   Ballast Rings; Glitsch, Inc., P. O. Box 6227, Dallas, Texas, 75222.

SECTION II

INTRODUCTION

The Clean Air Act of 1970 requires the Environmental Protection Agency (EPA) to establish air quality standards for principal air pollutants, and directed individual states to develop and implement plans to meet these standards. Regulations requiring the recovery of vapors emitted during the loading and unloading of gasoline and other volatile compounds from ships and barges have been considered, but their implementation has been repeatedly postponed because of the lack of information and experience in safe handling of combustible fuel and air mixtures in closed ducting.

The U.S. Coast Guard, under the Ports and Waterways Safety Act (PL 92340), is responsible for keeping U.S. ports and vessels within these ports safe from the inherent hazards of handling petroleum products. When U.S. cargo vessels and loading terminals are required to install vapor recovery systems (VRS) to reduce the amount of hydrocarbons released to the atmosphere, it will be imperative that the U.S. Coast Guard have data and experience factors concerning the adequacy of flame control devices used in the VRS installations.

Within certain limits of composition, combustible mixtures may burn in either of two modes: deflagration (flame) or detonation (explosion). Deflagration velocities are subsonic and the pressure change across the combustion front is small. Detonation velocities are supersonic, and a large step increase in pressure occurs across the combustion front. Under certain circumstances, a deflagration may accelerate and become a detonation. Flame propagation in a long tube filled with a quiescent combustible gas mixture and closed at the end at which ignition occurs provides the classic example of flame acceleration and the deflagration-to-detonation transition (DDT) (Reference 2-1). Since the tube is closed, the burned gas is not in motion; the hydrodynamic equations for flame propagation require the unburned gas to be in motion. (Reference 2-2). A shock wave that precedes the flame front is the means by which the unburned gas is set in motion. Not only does the shock set the unburned gas in motion, it also heats it. Flame speeds increase with increasing unburnt gas temperatures; hence the flame front accelerates as it proceeds into the shock-heated gas. In turn this strengthens the shock, and the rate of acceleration increases. However, this process accounts for only part of the observed flame acceleration. For the particular situation of flame propagation in a tube, a boundary layer develops on the tube wall behind the shock. Marked increases in flame propagation velocity occur when the boundary layer becomes turbulent, and a transition from laminar to turbulent burning occurs (Reference 2-3). As the preflame shock is further strengthened, the shock becomes sufficiently strong at some point to allow a transition to detonation. Several intermediate specific events, either singly or in combination, may immediately precede the actual development of detonation (Reference 2-4). Autoignitions (point explosions) in the shock-heated gas may provide the final impetus. Successive sudden increases in flame propagation produced by turbulence in the boundary layer of the shocked, unburned gases may result in several successive shock waves;

as these waves coalesce, the transition to detonation may occur. Transition may also occur immediately behind the shock front, if it is of sufficient strength.

Clearly, the deflagration-to-detonation transition is a complex phenomenon and depends not only on the properties of the burned and unburned gases, but also upon the conditions at the boundary of the combustible mixture. The distance required for development of detonation (the "run-up distance") is known to be shorter, e.g., in rough-walled tubes (Reference 2-5), since wall roughness will at first enhance nonuniformity of the boundary layer, and eventually enhance the transition to turbulence. Tube dimension effects are also to be expected, in that propagation times for transverse shocks or combustion fronts will be longer for larger tubes. Abundant evidence exists showing that the deflagration-to-detonation transition is not a one-dimensional phenomenon, but involves transverse compression waves and combustion fronts in tubes (References 2-6 and 2-7).

One other characteristic of this transition is the rapid pressure increase, which is of importance in considering safety precautions under conditions where detonations may develop. At the time of transition, pressure pulses in excess of the steady detonation pressure are often observed (References 2-4 and 2-8). Although these pulses are of very short duration, the pressure may be three to four times the steady detonation pressure. Neither the occurrence nor the magnitude of these pressure pulses is predictable; hence prudence demands that personnel be adequately shielded in the event the detonation tube shatters. These intense pressure pulses are related to another well-known detonation phenomenon, that of spinning detonation (References 2-9 and 2-10). Spinning detonation is a near-limit mode of detonation propagation. It is characterized by a rotating triple-shock intersection that propagates axially. Combustion occurs behind the triple-shock interaction, creating a localized region of high temperatures and pressures. Multiple fronts are also observed. Helical damage patterns in the DDT region are due to spinning fronts. Such fronts, in mixtures well inside the detonation limits, are unstable and do transform to stable planar detonation fronts as the transition process is completed (Reference 2-11).

In evaluating hazards, a number of factors need to be considered. Among these are the pressure developed behind a detonation wave in the combustible mixture in question, the run-up distance for the transition, and the quenching requirements. Other factors of importance that will not be dealt with here are actual mixture compositions and sources of ignition. The particular application of interest in this work is the lengthy, large-diameter piping required for vapor recovery systems at marine terminals. Hydrocarbon/air mixtures will be present in this piping. Maximum detonation velocities and maximum detonation pressures in such mixtures occur at equivalence ratios of about 1.1. Maximum pressure ratios across the wave for hydrocarbon/air mixtures are about 20, corresponding to an impulse pressure of about 2070 kN/m^2 (300 psia). If it is impractical to construct the vapor recovery system of pipe sufficiently strong to contain a detonation of maximum strength, the run-up distance becomes very important in that it establishes the minimum spacing of flame arresters required to prevent the development of detonation. If, on the other hand, the system can be constructed of piping that will contain the detonation, then the question

of the need for detonation arresters becomes important. Detonation arresters in the piping serve to prevent detonation from propagating into the large volumes (shipboard and dockside storage tanks) associated with the vapor recovery apparatus.

A review of literature on the deflagration-to-detonation transition was concerned with rationalizing (if possible) the available information on run-up distances, with a view toward developing correlations of run-up distances with pipe geometry and combustion characteristics, and with predicting detonation and reflected detonation pressures. The information developed was utilized in the design of the test apparatus and in the analysis of the results.

Many workers have studied the acceleration of flames and the trans-formation of a flame to a detonation wave (Reference 2-12). Emphasis has been on the details of the transition, rather than on measurements of run-up distance as such. In recent years, elegant laser methods of elucidating the sequence of events in the DDT have revealed, for H_2/O_2 mixtures, a rich and complex set of physiochemical interactions that contribute to this striking phenomenon (Reference 2-4). It must be observed, however, that systematic studies of run-up distances per se are few. Bollinger and coworkers have provided a consistent set of data for several combustible mixtures in small diameter tubes (References 2-8 and 2-13). These workers have reported data on H_2/O_2, C_2H_2/O_2, C_2H_2/air, CH_4/O_2, CO/O_2, $H_2/O_2/N_2$, $H_2/O_2/air$, and $H_2/O_2/CO_2$ mixtures at initial pressures of 1, 5, 10, and 25 atm. Correlations were developed for some of the mixtures, relating run-up distance to properties of the combustible gas and tube geometry. A function, K, was defined,

$$K = Re_b \left(\frac{S_u}{a_b} \right) \left(\frac{T_c}{T_b} \right) \tag{2-1}$$

where: Re_b is the Reynolds number based on unburned gas conditions, the normal burning velocity, and the pipe diameter;

S_u is the burning velocity of the gas mixture;

a_b is the speed of sound in the unburned gas;

T_c is the combustion (detonation) temperature; and

T_b is the unburned gas temperature.

Detonation induction distances were correlated with K for CO/O_2 and H_2/O_2 mixtures, but not for CH_4/O_2 mixtures. Whereas all the data for H_2/O_2 and CO/O_2 mixtures lay on a single correlating curve, that for CH_4/O_2 mixtures divided into two groups, depending on mixture ratio. Neither group of CH_4/O_2 data fell on the correlating curve for the H_2/O_2 and CO/O_2 mixtures. The authors attempted to account for this as a manifestation of the increased ion concentrations observed in hydrocarbon flames as compared with those in H_2/O_2 or CO/O_2 flames. Unfortunately, their argument is not internally self-consistent. They state: "It is suspected that certain ionized

particles are created at the elevated temperature and pressure conditions across the shock discontinuities. The ionization probes are triggered by these ionized particles before the flame arrives..." They then discuss the well-established large concentrations of ions in hydrocarbon/air (or hydrocarbon/O_2) flames in terms of ionization of carbon particles formed in rich hydrocarbon flames. Not all the ionization in hydrocarbon flames is properly attributable to ionization of carbon particles; but it is inappropriate to discuss this subject, which is deserving of separate treatment, in this report. The important point is that the authors argue on the one hand that ionizing particles are formed behind the shock wave and this flame front arrival, and on the other hand that the particles are the products of flames. Now, it is well documented that precursor ionization occurs in shock waves (Reference 2-14). However, this is probably due to photoionization, the short-wavelength radiation originating from the highly-ionized heated gas in the case of strong shocks (Reference 2-14), and from chemiluminescence in the case of flames in which CO is oxidized (Reference 2-15). These precursors precede the shock wave.

While the arguments of Bollinger and coworkers (References 2-8 and 2-14) cannot be accepted, the possibility of precursor ionization must be admitted. However, this ionization should be present in their CO/O_2 cases, as well as the CH_4/O_2 cases, and thus is not unique. It must be noted that Bollinger, et al. (References 2-8 and 2-14), use Strauss and Edse's (Reference 2-16) methane-burning velocity data, which show that the burning velocity increases with increasing pressure. More recent work shows that methane burning velocities decrease with increasing pressure (Reference 2-17). Unfortunately, the direction of correction produced by this trend is to increase the difference between the CH_4/O_2 data and the H_2/O_2 and CO/O_2 data in the Bollinger, et al., correlation (References 2-8 and 2-14). A more likely explanation of the unique behavior of CH_4 as a fuel in these DDT studies lies in its ignition kinetics, which differ from those of CO/O_2 and of H_2/O_2.

Yet another approach to predicting run-up distances has been taken by Shchelkin and Troshin (Reference 2-18), who derive the expression:

$$x_1 \sim \frac{c_1^2 \, d}{C^3 \, K^3 \, (\sigma_3 - 1)^2 \, U_k} \tag{2-2}$$

where: x_1 is the run-up distance;

c_1 is the speed of sound in the quiescent unburned gas;

d is the tube diameter;

C is a coefficient accounting for the enlargement of flame surface by nonuniform flow in the tube behind the shock front;

K is the Karman number, the ratio of the mean velocity of turbulent fluctuations, V', and the velocity of the disturbed unburned gas, w ($K = V'/w$);

σ_3 is the ratio of the density of unburned and burned gas across the detonation front ($\sigma_3 = \rho_1/\rho_3$), and

U_k is the burning velocity of the mixture.

Shchelkin and Troshin note that $0.6 \leq KC \, (\sigma_3 - 1) \leq 2$; which is to say $KC \, (\sigma_3 - 1)$ is of the order of 1, and further C is of the order of 2 or 3. The model used in deriving this expression, however, is that of successive shock waves forming during flame acceleration, and detonation occurring at the point of coalescence. They admit the possibility that detonation may occur after the point of coalescence. Experimentally, shock coalescence is but one mechanism for the transition to detonation. They concede (Reference 2-18) that the expression (2-2) is qualitative in nature and they offer no experimental evidence supporting it. Since the model fits but one of several modes of DDT, it is not surprising that it is of limited usefulness. In particular, no confidence may be placed in run-up distances computed from expression (2-2) in attempts to estimate hazards in the design of piping runs containing detonatable mixtures.

Holzapfel and Schoen (Reference 2-19) obtained an experimental DDT run-up distance of approximately 12 m (39.9 ft) for propane/air mixtures at an equivalence ratio of 1.15 in a 15.0-cm- (5.9-in.-) diam stainless-steel pipe closed off at the ignition end. The internal wall finish of the pipe was stated to be of "technical grade roughness," but was not otherwise characterized. It was also noted that shorter DDT run-up distances were observed in a test configuration in which the flame was ignited in a vessel connected to the inlet end of the pipe. Safety considerations based on the knowledge of DDT run-up distances must take this effect into account.

Run-up distances, for propane/air and gasoline/air mixtures, were estimated from expression (2-2) to be about 30.5 m (100 ft). In fact, for the Coast Guard work described herein, no detonations developed in the shock tube filled with stoichiometric propane/air mixtures in 31.5 m (104 ft) before the tube was modified. Originally, this shock tube had been designed to provide a test gas volume of known properties. It has, therefore, been carefully honed and polished to eliminate surface irregularities. To obtain DDT within the available tube length of 31.5 m (104 ft), it was necessary to insert tube liners of expanded metal, thereby increasing internal wall roughness.

Neither expression (2-1) nor (2-2) explicitly allows for wall roughness. To be sure, expression (2-1) includes a Reynolds number; however, it is based on tube diameter. This is clearly inappropriate for large tubes such as the one employed in this work, or those for proposed vapor recovery systems. A more appropriate characteristic length would be related to boundary layer thickness behind the accelerating shock wave, or related to average surface profiles of the pipe interior wall. The importance of turbulence in flame acceleration has long been recognized. However, the time-dependent flow of DDT has resisted analysis, and is likely to do so for some time, in view of the complexity of the problem. Until better theoretical models are available, empirical correlations will be needed.

To provide the Coast Guard with needed information on the adequacy of flame control devices that could be used in vapor recovery systems and to develop empirical data on run-up distance to detonation for gasoline/air

mixtures, a test facility for experimental evaluation had to be constructed of full-scale hardware. The safety of operating personnel and adjacent activities was of prime concern in selection of the test site location and of pressure rating the test components. To this end, preliminary calculations of detonation pressures and of reflected detonation pressures were carried out for three selected hydrocarbon/air mixtures. The Lewis C.E.C. 71 computer program (Reference 2-20) was used in these computations. While steady detonation pressures are directly computed by this program, which uses stored thermodynamic data and composition data specified in the input data, reflected detonation pressures are not automatically computed. The velocity of the reflected shock wave was computed from the particle velocity ahead of the reflected wave (equal to the particle velocity behind the detonation wave) and the knowledge that behind the reflected shock the particle velocity is zero (the gas is brought to rest by the rigid wall) (Reference 2-21). Using the reflected shock velocity and postdetonation gas properties as input data, the reflected shock wave properties were computed using the "SHOCK" subroutine of the Lewis program.

The results of these calculations are shown in Figures 2-1, 2-2, and 2-3, which detail detonation wave velocities, pressures, and temperatures for toluene, N-heptane, and propane mixed with air at several stoichiometries. Reflected shock wave properties were computed for the same fuel/air mixtures at one stoichiometry, $\emptyset$ = 1.1. The detonation wave and reflected shock wave properties are summarized in Table 2-1. The value of 1.1 was chosen for the equivalence ratio because gasoline and air mixtures have maximum flame speed at about $\emptyset$ = 1.1 (Reference 2-22), hence this was considered the most hazardous condition. Qualitatively, the higher the flame speed, the shorter the run-up distance, and although $\emptyset$ = 1.1 does not correspond to the maximum detonation wave pressure, the differences between the detonation pressures at $\emptyset$ = 1.1 and the maximum value is not great and would not compromise normal safety factors. A nominal working pressure of 4137 kN/m^2 (600 psia) was chosen as a design working pressure for the piping and component in the test assembly. A safety factor of somewhat less than four would result if the full reflected shock pressure were realized. One notes, however, that these pressures are for plane reflection from a rigid wall. In the actual experiment, reflection from a flame arrester would never result in the full pressure development due to flow through the arrester. Similarly, reflection at a pipe bend would result in an expansion wave (soon developing into a detonation) in the downstream leg of the bend, and again the full reflected shock pressure on the bend wall would not be realized.

Since it is not possible to calculate peak pressures during the transition, it was judged that the hazard could not be computed with sufficient certainty to assure that the run-up pipe would remain intact at the time of transition. The experimental hardware was therefore required to be located at a well-protected test site where the fuel-and-air mixing and firing could be conducted remotely.

The experimental program was performed at the Jet Propulsion Laboratory's Edwards Test Station (ETS) where suitable safety protection and support activities were available. A new facility that utilized the piping, structural supports, components, and instrumentation from the JPL-Pasadena shock-tube facility was installed on an existing test site. A photograph of this test facility is shown in Figure 2-4.
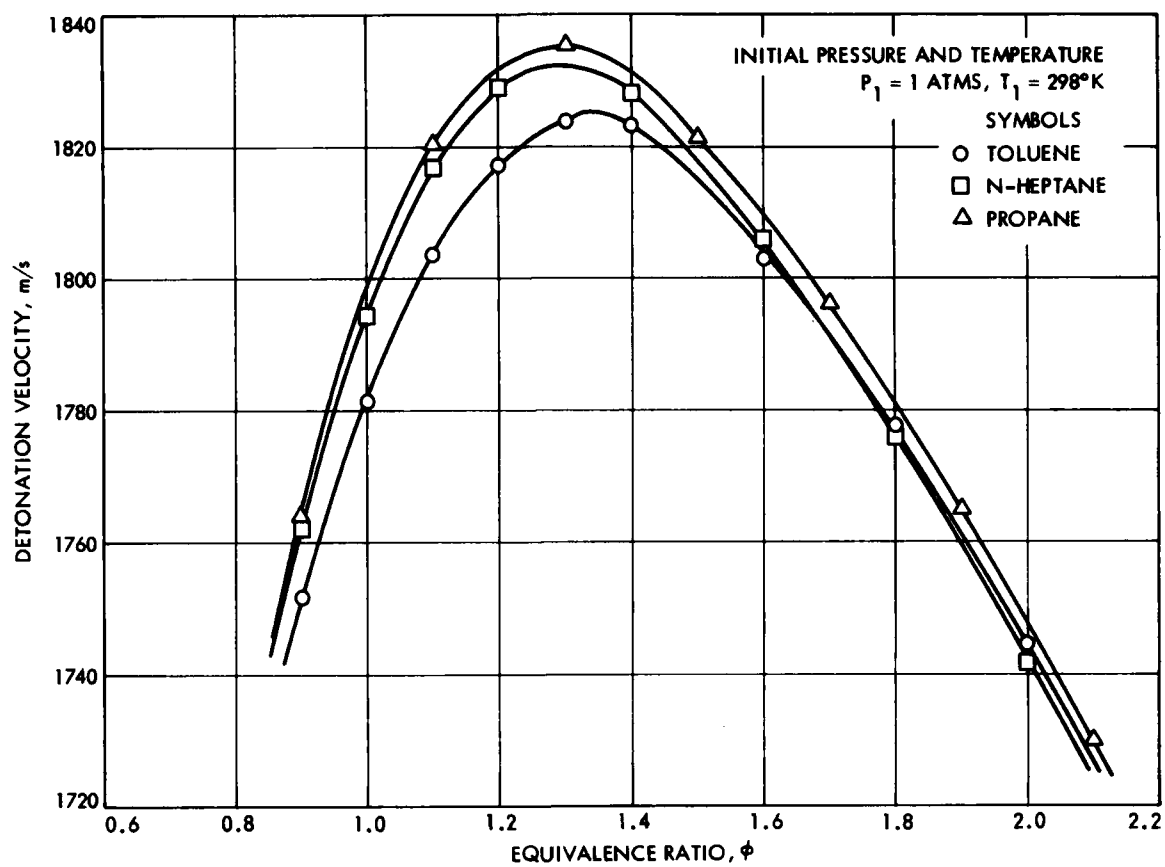
Figure 2-1.   Hydrocarbon and Air Mixture Theoretical
Detonation Velocity vs Equivalence Ratio
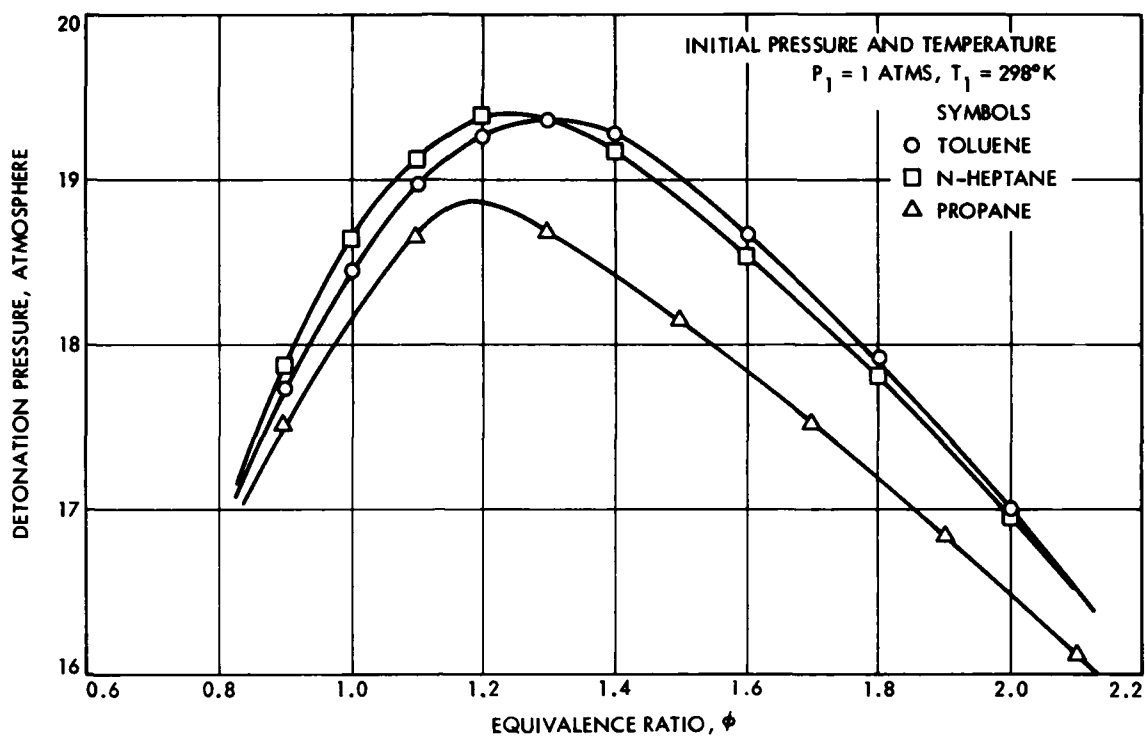
Figure 2-2.   Hydrocarbon and Air Mixture Theoretical
             Detonation Pressure vs Equivalence Ratio
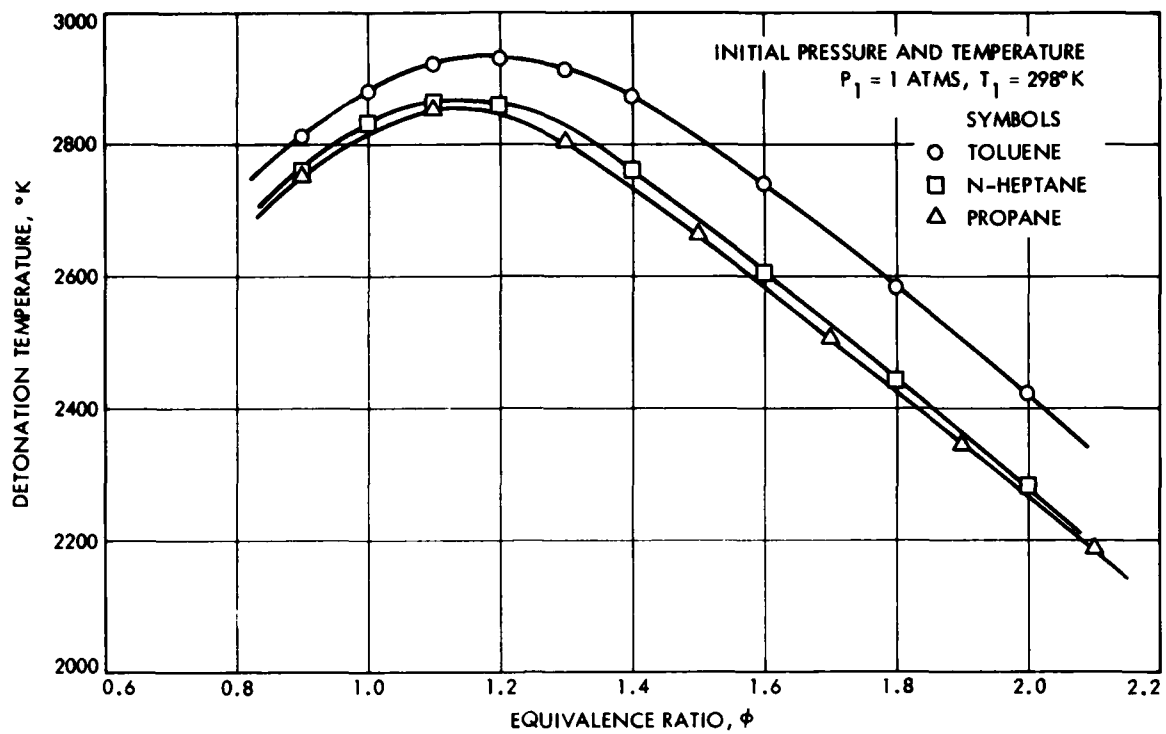
Figure 2-3. Hydrocarbon and Air Mixture Theoretical
Detonation Temperature vs Equivalence Ratio

Figure 2-4. B-Stand Facility, Edwards Test Station

Table 2-1. Detonation Wave and Reflected Shock Properties for Hydrocarbon and Air Mixtures[a]

	Detonation Wave			Reflected Shock		
Fuel	Pres- sure, atm	Tempera- ture, K	Wave Velo- city, m/s	Pressure, atm	Tempera- ture, K	Wave Velo- city, m/s
Toluene	19.0	2920	1805	51.2	3300	715
N-Heptane	19.2	2870	1817	51.3	3280	723
Propane	18.7	2860	1820	49.2	3260	726

[a]Initial Pressure: 1 atm
 Initial Temperature: 298 K
 Equivalence Ratio: 1.1

SECTION III

TEST FACILITY DESCRIPTION

A.   GENERAL

All testing was performed at the B-Stand facility of the Jet Propulsion Laboratory's (JPL) Edwards Test Station (ETS). This is a remote site in the Mojave desert leased from Edwards Air Force Base for hazardous testing. B-Stand is one of five test installations in the liquid propulsion area of the test station. Other adjacent areas include solid propulsion, environmental simulation, solar thermal electrical power, and electrical vehicle testing. Most areas are remotely controlled and monitored from a barricaded building called the "blockhouse," which contains the control consoles and a central data recording system. The blockhouse is connected with the test stands by a series of underground walk-through tunnels containing electrical power conduits, high-pressure gas lines, instrumentation, and control cables. The B-Stand test area contains an air compressor system, fuel system, fuel vaporizer and condenser loop, fuel and air induction system, and the detonation test piping. The test facility flow system schematic diagram is shown in Figure 3-1. Table 3-1 gives a description of the symbols used in the diagram. A Firex system provides emergency water deluge to the fuel system, vaporizer and condenser loop, and the test section piping in the case of fire. A bank of lead-acid batteries at the stand provides emergency back-up power for the 28-Vdc electrical power in the control systems.

B.   AIR COMPRESSOR SYSTEM

Air flow for testing was provided by a Spencer Model 80 x 10 SOH multi-stage centrifugal turbine compressor, rated at 7.79 m^3/min (275 icfm) at 38.6 kN/m^2 (5.6 psid), that is driven by a 7.46-kW (10-hp) electrical motor. The compressor was provided with an inlet filter to assure clean air and a 41.4-kN/m^2 (6-psid) pressure relief valve in the event of complete system blockage. Air flow in the 10.2-cm- (4-in.-) diameter induction piping system was controlled by the remote positioning of an air metering valve and air by-pass valve. Valve position was controlled and monitored in the blockhouse. Air flow was determined by measuring upstream total pressure and differential pressure loss across a Meriam Laminar Flow Element (LFE). The air was heated by compression up to 32°C (90°F) above the ambient inlet temperature. The measured air temperature and flowmeter pressures were used by the on-line data system to calculate air mass flow for continuous display and digital data recording.

C.   FUEL SYSTEM

Liquid fuel was supplied from a 0.049-m^3 (13-gal) spherical aluminum pressure vessel with a 6895-kN/m^2 (1000-psia) working pressure. It was pressurized for fuel expulsion by means of a remotely-regulated gaseous nitrogen supply, with remotely-operated valves to deliver and vent the pressurant.

3-1
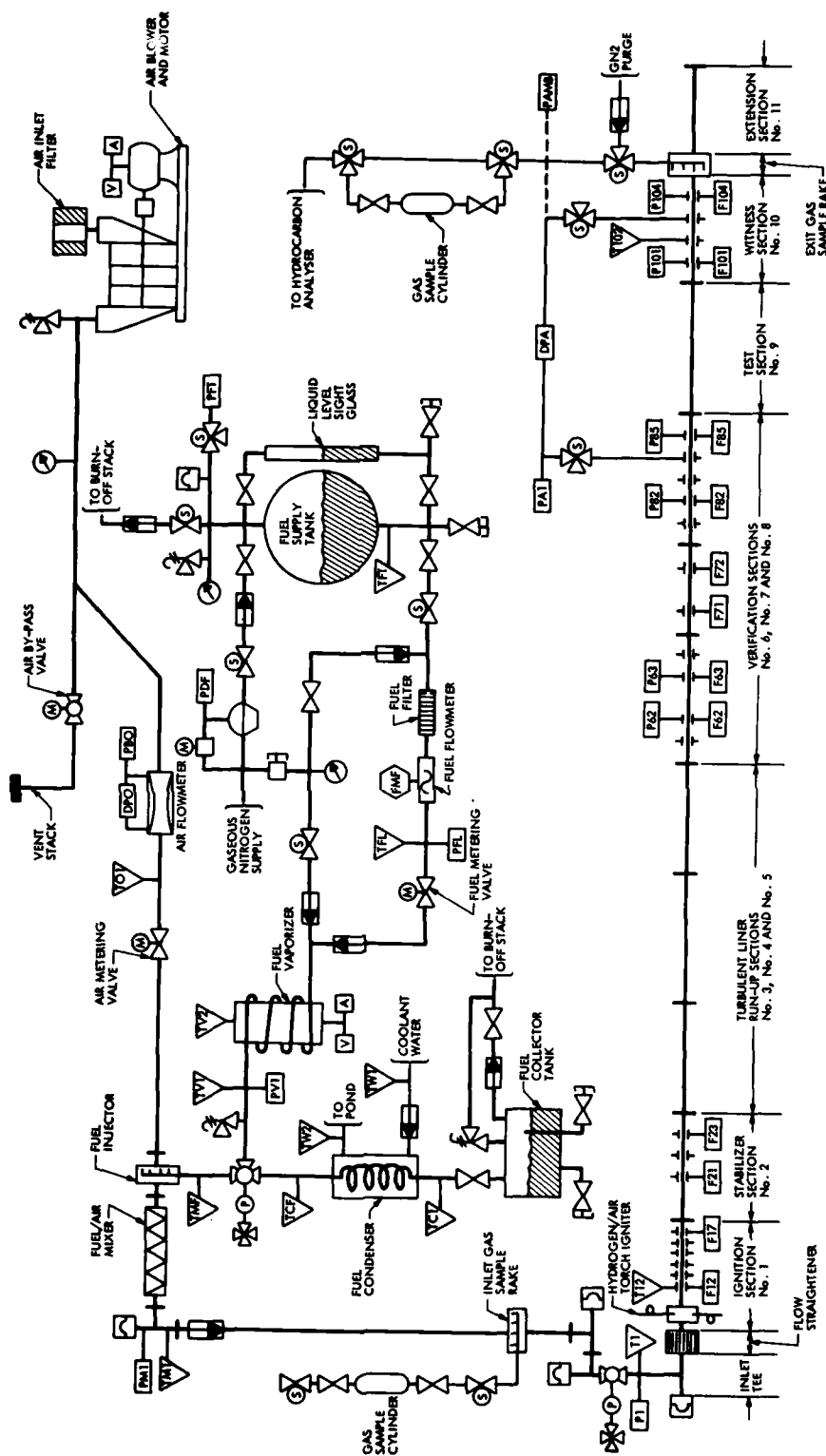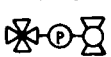
Figure 3-1. Test Facility Flow System Schematic Diagram with Instrumentation Locations for Detonation Testing

3-2

Table 3-1. Symbols and Description for Flow System Schematic
           Diagram

Symbol	Description
▷◁	Manual Globe Valve
▷◁(S)	Electric solenoid operated valve
▷◁(M)	Electric motor operated valve
▷◁(M)	Electric motor operated ball valve
✳–(P)–⊐⊏	Air piston operated ball valve
◄▭	One-way flow check valve
⌀	Pressure relief safety valve
⊖	Dome pressure regulator valve
⊡	Manual set pressure regulator valve
(M)⊡	Electric motor operated pressure Regulator valve (dome loader)
⌂	Pressure rupture-disc assembly
⊘	Pressure gage
Ⓥ	Voltmeter transducer
Ⓐ	Ammeter transducer
▽TXX	Temperature transducer
PXX	Pressure transducer
FXX	Flame sensor transducer
⟨FXX⟩	Flowmeter transducer

The fuel tank valve, pressure relief valve, and rupture disc were all manifolded to a burn stack fired by natural gas. A gaseous nitrogen purge kept the venting lines clear of fuel vapors. Liquid level in the fuel tank was determined from a high-pressure sight glass. Liquid fuel was delivered through a 0.95 cm-(0.375-in.-) diameter line containing a manual isolation valve, remote isolation valve, 10-micron filter, turbine flowmeter, and remote metering valve for flow control. Valve positioning was controlled and monitored in the blockhouse. Fuel temperature and pressure, and turbinemeter hertz were used by the data system to calculate fuel mass flow for continous display and digital data recording. The data system also calculated and displayed air-to-fuel mass flow ratio and equivalence ratio.

D.   FUEL VAPORIZER AND CONDENSER LOOP

An electrical heater was used to vaporize the fuel before injection into the flowing air stream. The vaporizer consisted of a 10.2-cm- (4.0-in.-) diameter by 36.6-cm- (14.4-in.-) long aluminum cylinder heated by four 2.5-kW electrical resistance elements. Thirteen turns of fuel line were coiled around the aluminum core and insulated with a Fiberfrax ceramic fiber blanket. A sheet-metal housing provided weather protection. The vaporizer heater power was controlled by motor-driven Powerstat Model No. 60 MB-1256-DT-2S with the input voltage and current monitored in the blockhouse. A controller limit switch in the heater circuit, triggered by a thermocouple measuring core temperature, was used to prevent overheating of the vaporizer.

A fuel condenser loop was used to prevent the exhausting of vaporized fuel into the atmosphere during pretest warm-up and system stabilization. In the "condenser" position, a remotely-operated three-way fuel mixer valve directed the vaporized fuel into a water-cooled heat exchanger, where most of the fuel was reliquified and collected in a storage tank for later disposal. The noncondensables were vented through the collector tank and passed along to the burn stack. With the three-way fuel mixer valve energized in the "run" position, the vaporized fuel was directed to the fuel and air induction system.

E.   FUEL AND AIR INDUCTION SYSTEM

A 4.9-m- (16-ft-) long induction system consisting of 10.2-cm- (4-in.-) diameter standard weight pipe and fittings was used to assure thorough mixing of the vaporized fuel and air in the detonation run-up piping. Fuel was injected at the start of this pipe run through the seven-tube manifold shown in Figure 3-2. Each tube discharged into an equal portion of the cross-sectional flow area of the pipe. Initially it was positioned to inject the fuel vapor in the downstream direction, but was later reversed to inject upstream against the flow of air to improve the fuel-to-air distribution. A four-element Komax triple-action motionless mixer was installed downstream of the injector for additional turbulent mixing. This was followed by a 90-deg turn in flow through a pipe tee containing a low-pressure rupture-disc assembly in one branch and a one-way flow check valve in the other branch. A gas-sample collection rake was located further downstream, just ahead of two additional pipe
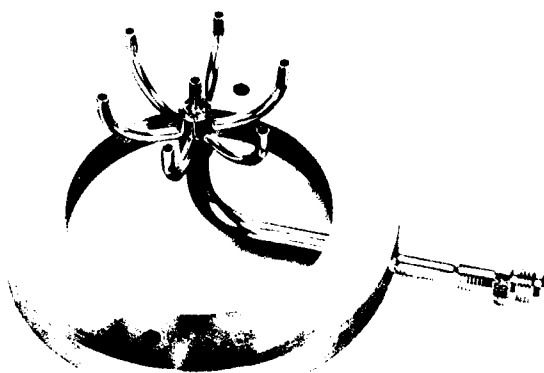
Figure 3-2. Vaporized Fuel Injector Manifold

tees containing low-pressure rupture-disc assemblies. The induction
system was terminated by a remotely-operated high-pressure isolation
valve at the inlet to the detonation test piping. A photograph of the
combined air, fuel, vaporizer, condenser, and induction systems is shown
in Figure 3-3.

F.   DETONATION TEST PIPING

Most of the piping, *structural supports, and components* used in the
detonation test system were obtained from the JPL-Pasadena shock-tube
facility. The piping was made from heavy-walled stainless-steel tubes
that were bored, honed, and polished to a 15.32-cm (6.03-in.) internal
diameter with a very smooth finish. Special extra-strong stainless-steel
flanges, with O-ring seals, were used to join the pipe section. These
flanges were drilled with an eight-bolt hole pattern that required an
adapter plate for mating with the twelve-bolt hole pattern in the standard
extra-strong 15.2-cm- (6-in.-) diameter pipe flanges used on the newly-
fabricated test components.

The upstream end of the detonation test piping began with a 15.2-cm-
(6-in.-) diameter extra-strong pipe tee mounted in a thrust support stand
bolted to a concrete foundation slab to absorb the axial force of the
detonation. The induction system piping was attached to the side branch
of the inlet tee and a high-pressure rupture-disc assembly was mounted
on the upstream branch. A flow straightener made from a spiral-wound,
crimped stainless-steel ribbon assembly 15.2 cm (6 in.) in diameter by 5.08
cm (2 in.) long, shown in Figure 3-4, was mounted on the downstream branch
of the tee at the inlet to the ignition section (No. 1 of Figure 3-1).
This flow straightener was later changed to a Shand and Jurs spiral-wound,
crimped aluminum ribbon flame arrester for the final phase of testing
performed under conditions of continuous mixture flow. All of the
detonation test piping mounted downstream of the thrust stand were
supported by a pair of overhead I-beams with trolley hangers and saddles
for easy servicing and flexibility in making various piping arrangements.

3-5

The number of pipe sections used and their order of installation depended on the specific test requirements. The total number of shock-tube piping sections available was eleven, which provided a total assembly length of 31.5 m (103.5 ft). A brief description of the various shock-tube pipe sections shown schematically in Figure 3-1, their normal function, and instrumentation capabilities follow:

(1) Ignition section (No. 1): one piece 1.68 m (5.5 ft) long containing the hydrogen-air-spark igniter, two flame sensors, and one temperature sensor.

(2) Flame stabilization section (No. 2): one piece 3.05 m (10 ft.) long containing two flame sensors.

(3) Run-up sections (No. 3, No. 4, and No. 5): three pieces each 4.57 m (15 ft) long containing an expanded metal tube liner to generate turbulence in the propagating flame. No instrumentation ports were available in these sections.

(4) Verification sections (No. 6, No. 7, and No. 8): three pieces: one 3.05 m (10 ft) long with two flame sensors and two pressure sensors, one 1.52 m (5 ft) long with two flame sensors and two pressure sensors added later in the program, and one 1.83 m (6 ft) long with two flame sensors, two pressure sensors, one temperature sensor, and one pressure port for test section upstream differential pressure measurement.

(5) Test section (No. 9): one piece 3.05 m (10 ft) long with no instrumentation. This section was replaced with the experimental detonation arrester during evaluation tests.

(6) Witness section (No. 10): one piece 1.52 m (5 ft) long with two flame sensors, two pressure sensors, one temperature sensor, and one pressure port for the test section downstream differential pressure measurement.

(7) Extension section (No. 11): one piece 2.13 m (7 ft) long with no instrument ports, used to minimize the amount of ambient light entering the witness section.

Two additional extension sections (No. 12 and No. 13), each 6.8 m (22.4 ft.) long and made from standard weight 15.2-cm- (6-in.-) diameter pipe, were added later for the final test phase.

The exit gas sample rake was normally installed between the flanges of the witness section and the extension section. Individual fuel/air mixture samples were collected for laboratory analysis at this location or a continuous sample was fed directly into the on-site hydrocarbon gas analyzer described in the next section of this report. In either case, the sample line was closed-off by a remotely operated valve 10 seconds before the detonation test to protect the collection system from possible high-pressure shock waves. For this same reason, the
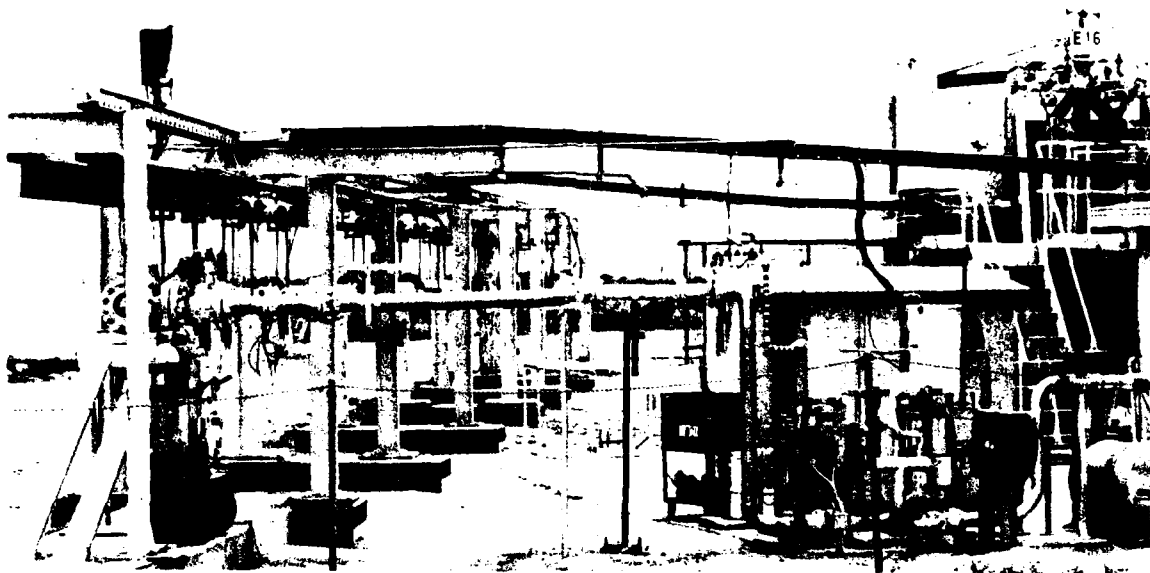
Figure 3-3. Combined Air, Fuel, Vaporizer, Condenser, and Induction Systems on B-Stand
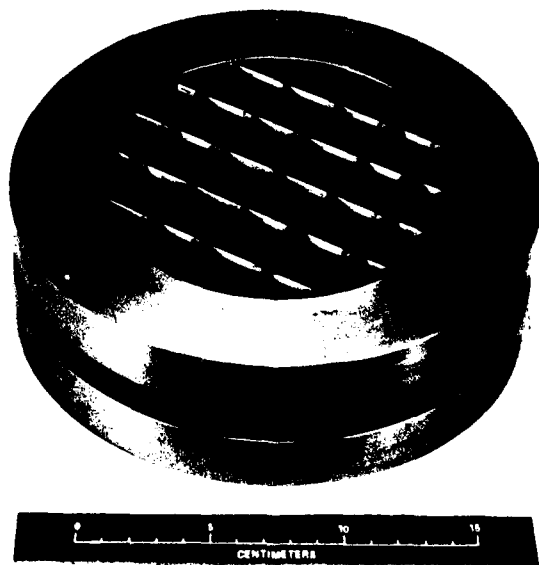
Figure 3-4. Spiral-Wound, Crimped Stainless-Steel, Ribbon Air Flow Straightener

highly sensitive pressure transducers used to measure the air-flow
pressure loss across the test section arrester before and after each
detonation test were also isolated by remotely operated valves.

G.   HYDROGEN-AIR-SPARK IGNITER

The hydrogen-air-spark igniter installation shown in Figure 3-5
consisted of two insulated high-voltage electrodes, Auburn Model I-28,
extending into the center of the flowing stream from opposite sides of
the ignition section pipe. A spark gap of 0.24 cm (0.094 in.) was main-
tained between the two electrodes. Power for the spark igniter was obtained
from a Webster Model 312 high-voltage transformer having a 120-vac, 2.2-
A, 60-Hz primary and a 10,000-vac, 0.023-A secondary. Directly upstream
of the electrodes, a small injector head discharged a stoichiometric
mixture of hydrogen and air through the spark gap. The flow of hydrogen
and air could be be adjusted to suit the ignition energy required by the
fuel/air mixture flow conditions. The initiation of spark current and
the operation of the hydrogen and air solenoid-operated valves were all
controlled simultaneously by a preset sequence timer to assure accurate
and repeatable ignition timing. The igniter "on-time" was normally set at
500 ms, but was later reduced to 180 ms during the final phase of testing.
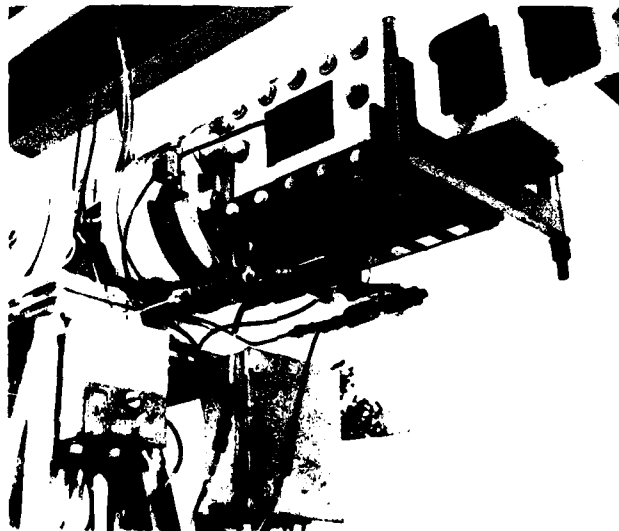
Figure 3-5. Hydrogen-Air-Spark Igniter
Installation

SECTION IV

INSTRUMENTATION AND CONTROLS

A.   GENERAL DESCRIPTION

The potentially hazardous nature of detonation testing required that
all instrumentation and controls be remotely operated and monitored. Test
system parameters were measured at the test site using electrical transducers
with their signals conducted to the blockhouse for conditioning, recording,
and display. Location and identification of all the principle instrumenta-
tion parameters and controls are shown in Figure 3-1. Table 4-1 is a
listing of the nomenclature for instrumentation and calculated parameters.

Test system parameters were divided into two groups: (1) steady-
state (low-speed) data and (2) transient-state (high-speed) data. Steady-
state data includes all the measured and calculated parameters for the
air system, fuel system, fuel vaporizer and condenser loop, fuel and air
induction system, hydrocarbon gas analyzer, and the pre- and posttest
pressure loss measured across the test arrester. Transient-state data
includes the measured and calculated flame velocities and peak pressures
developed in the facility piping during the transition from deflagation
to detonation and the success or failure of the detonation flame arrester.
Steady-state data was recorded and calculated on the JPL-developed Integra-
ted Digital Acquisition and Controls System (IDAC). Transient-state data
was recorded on two high-frequency FM tape recorders and played back on
an *oscillograph* at an expanded time scale. Flame velocities and peak
pressures were manually scaled and calculated from the oscillograph traces.

All critical control functions were either manually positioned on
the control console or automatically operated by the preset sequence timer.
These operations were selectively recorded using contact closures on IDAC,
FM tape, or a second high-speed oscillograph. This latter oscillograph
also recorded several important facility parameters to provide a time
history of the test facility operations during detonation firings that
could be used to diagnose any malfunctions or unusual incidents.

Two strategically-placed television cameras, with displays in
the blockhouse, monitored the fuel systems area and the test section
piping during test operations. A motion picture camera also recorded
any events at the test section during actual test firings. Visual
coverage and controlled access to the test area were maintained by a
safety monitor in an observation tower located over the blockhouse.

B.   STEADY-STATE DATA

Air-mass flow was calculated from measurements made on a Meriam
LFE Model 50 MC2-4 flowmeter. A Statham Model PL 280 TC pressure trans-
ducer was used to measure the upstream total pressure, and a Statham
model PM 5 TC pressure transducer was used to measure the differential
pressure across the flow element. Air temperature was measured with
a Thermo-Electrical Model K18G-1600 chromel-alumel thermocouple.

Table 4-1. Instrumentation and Calculated Test Parameters Nomenclature

Steady State Parameters	Units S.I. (Engr.)	Description
PBO	kN/m^2 (psig)	Air flowmeter inlet pressure
DPO	kN/m^2 (psid)	Air flowmeter differential pressure
TOI	$^{\circ}$C ($^{\circ}$F)	Air flowmeter temperature
PFT	kN/m^2 (psig)	Fuel tank pressure
TFT	$^{\circ}$C ($^{\circ}$F)	Fuel tank temperature
PDF	kN/m^2 (psig)	Fuel tank dome loader pressure
PFL	kN/m^2 (psig)	Fuel line pressure
TFL	$^{\circ}$C ($^{\circ}$F)	Fuel line temperature
FMF	Hz (cps)	Fuel flowmeter frequency
PVI	kN/m^2 (psig)	Fuel vaporizer outlet pressure
TVI	$^{\circ}$C ($^{\circ}$F)	Fuel vaporizer outlet temperature
TV2	$^{\circ}$C ($^{\circ}$F)	Fuel vaporizer core temperature
TMF	$^{\circ}$C ($^{\circ}$F)	Fuel injector inlet temperature
PMI	kN/m^2 (psig)	Fuel/air mixer outlet pressure
TMI	$^{\circ}$C ($^{\circ}$F)	Fuel/air mixer outlet temperature
TCF	$^{\circ}$C ($^{\circ}$F)	Fuel condenser inlet temperature
TCI	$^{\circ}$C ($^{\circ}$F)	Fuel condenser outlet temperature
TWI	$^{\circ}$C ($^{\circ}$F)	Coolant water inlet temperature
TW2	$^{\circ}$C ($^{\circ}$F)	Coolant water outlet temperature
P1	kN/m^2 (psig)	Inlet tee pressure
TI	$^{\circ}$C ($^{\circ}$F)	Inlet tee temperature
T12	$^{\circ}$C ($^{\circ}$F)	Ignition section temperature
PA1	kN/m^2 (psig)	Test section inlet pressure
DPAI	kN/m^2 (psid)	Test section differential pressure-pretest
DPA2	kN/m^2 (psid)	Test section differential pressure-posttest
PAMB	kN/m^2 (psia)	Test area ambient pressure
T102	$^{\circ}$C ($^{\circ}$F)	Test section exit temperature
HCA	%	Test section total hydrocarbon analysis
F12	s (sec)	Ignition section inlet flame sensor
F17	s (sec)	Ignition section exit flame sensor
F21	s (sec)	Stabilizer section inlet flame sensor
F23	s (sec)	Stabilizer section exit flame sensor
F62	s (sec)	Verification sec. No. 6 inlet flame sensor
F63	s (sec)	Verification sec. No. 6 exit flame sensor
F71	s (sec)	Verification sec. No. 7 inlet flame sensor
F72	s (sec)	Verification sec. No. 7 exit flame sensor
F82	s (sec)	Verification sec. No. 8 inlet flame sensor
F85	s (sec)	Verification sec. No. 8 exit flame sensor
F101	s (sec)	Witness section inlet flame sensor
F104	s (sec)	Witness section exit flame sensor
P62	kN/m^2 (psig)	Verification sec. No. 6 inlet pressure
P63	kN/m^2 (psig)	Verification sec. No. 6 exit pressure
P71	kN/m^2 (psig)	Verification sec. No. 7 inlet pressure
P72	kN/m^2 (psig)	Verification sec. No. 7 exit pressure
P82	kN/m^2 (psig)	Verification sec. No. 8 inlet pressure
P85	kN/m^2 (psig)	Verification sec. No. 8 exit pressure
P101	kN/m^2 (psig)	Witness section inlet pressure
P104	kN/m^2 (psig)	Witness section exit pressure

Table 4-1. Instrumentation and Calculated Test Parameters Nomenclature
(Continuation 1)

Calculated Parameters	Units S.I. (Engr.)	Description
MA	kg/h (lb/h)	Air mass flow
MF	kg/h (lb/h)	Fuel mass flow
A/F	ratio	Air mass flow to fuel mass flow ratio
Ø	ratio	Equivalence ratio
VA	m/s (ft/sec)	Air flow velocity through 15.2-cm- (6.0-in.-) diam. pipe

Fuel-mass flow was calculated using measurements made with a Cox Model LF-G-1 turbine flow meter to determine volumetric flow, a Taber Model 206 pressure transducer measured fuel pressure, and a Thermo-Electrical Model K18G-1600 chromel-alumel thermocouple measured fuel temperature. Fuel pressure and temperature were used to determine fuel density from standard tables stored in the computer memory.

The air-to-fuel mass ratio and equivalence ratio in the induction system were determined from the calculated air-mass flow and fuel-mass flow noted above. The equivalence ratio of the air and fuel mixture passing through the test arrester and into the witness section was determined by a gas sample fed directly into an on-line total hydrocarbon gas analyzer. A detailed description of this system and the method of calculation is presented later in this section.

Operating pressures in the fuel vaporizer and condenser loop and the fuel/air mixer were measured with Taber Model 217 pressure transducers. Temperature measurements in the vaporizer fuel outlet line, fuel injector line, fuel/air mixer, and fuel condenser loop were all made with chromel-alumel thermocouples.

Pre- and posttest pressure loss measured across the test arrester were made with air only flowing through the facility piping. The upstream total pressure was measured with a Statham Model PL 280 TC pressure transducer and the differential pressure across the arrester was measured with a Statham Model PM 80 TC pressure transducer.

All of the preceding pressure measurements were made using either gage-type pressure transducers or differential pressure transducers with the low side vented to ambient pressure. To convert these measurements to an absolute pressure level, the barometric pressure had to be added. Local barometric pressure was obtained from the weather station at Edwards Air Force Base. A Taber Model 254 absolute pressure transducer installed at the test stand was adjusted to read this value of barometric pressure at the beginning of each test series. The IDAC computer program used this locally varying barometric pressure input for all calculations.

C. TRANSIENT-STATE DATA

The detonation facility piping flame sensors were DuMont Type 6291, 10-stage multiplier phototubes with flat end-window photo cathodes. These instruments have an average luminous sensitivity of 60 A/lm and a spectral response from 3500 A to 5850 A with maximum response at 4400 ±500 A. The blue-colored stoichiometric hydrocarbon/air flame falls well within this response range. These optical sensors have been successfully used in the JPL shock-tube facility for many years to detect very-high-velocity shock waves generated by a high-capacitance arc discharge driver. The phototube viewing port was constructed with front and rear collimating slots 1.27 cm (0.50 in.) high by 0.013 cm (0.005 in.) wide, separated at a distance of 7.62 cm (3.0 in.). These slots limit the amount of light that reaches the phototubes and eliminate reflected beams. The result is a very sharp signal with a rise time response on the order of microseconds, which was required for shock-wave velocity determination. The flame sensor slots required only minor modifications for the deflagration-to-detonation flame velocity measurements.

There were three distinct flame intensity sections in the detonation piping. In the ignition section (No. 1) and stabilization section (No. 2), flame intensity was weak; however, the flame velocity was beginning to accelerate. It was necessary to remove the rear collimator slot from the viewing port and to increase the amplification gain to record a good signal. In the verification sections (No. 6, No. 7, and No. 8) the detonation flame was very intense, with a velocity of around 1800 m/s (5900 ft/s). Both front and rear slots were used in the viewing ports and the amplifier gain was normally low. The third region was the witness section (No. 10). Here it was important to detect any flame that may have penetrated the detonation arrester; therefore, the rear slot was removed from the viewing ports and the amplifier gain was high.

High-response pressure sensors were installed directly opposite the flame sensors in two verification sections (No. 6 and No. 8) and in the witness section. These were PBC Piezotronic Model 113 AP quartz-crystal, high-frequency pressure transducers flush-mounted to the inside wall of the pipe. They were capable of measuring peak pressure levels up to 20,700 kN/m^2 (3000 psi) with a frequency response of 100,000 Hz for the advancing and reflected detonation shock waves. PBC Model 402 in-line amplifiers were installed with the pressure transducers to drive the signals over the long transmission lines to the blockhouse.

During the last two phases of the test program, the two quartz-crystal pressure transducers in the witness section were relocated upstream to unused ports in the verification section (No. 7). In their place, two Statham Model PG 856 G bonded strain-gage-type pressure transducers were installed in the witness section. These lower-range instruments provided higher accuracy in measuring the peak-pressure pulses passing through the arrester from an arrested detonation flame.

A 100-Hz coded time pulse and the spark igniter current were recorded on both high-frequency FM tape recorders and the on-line oscillograph. These signals were used as reference points for test initiation and time correlation between recorders. Typical examples of transient-state data

from the FM tape recorders played back on an oscillograph with an expanded time base of 32 to 1 are shown in Figure 4-1.

D.   GAS-SAMPLE ANALYSIS SYSTEM

A gas-sample analyzer was installed at the test site to provide an on-line indication of the gasoline and air mixture flowing through the test section piping. The laboratory analysis method using individual gas-sample cylinders, that was used for propane and air mixtures during the facility check out, was too slow and costly for routine testing. The laboratory analysis method, however, did provide an accurate verification of the instrumentation measurements for on-line calculations of air flow and fuel flow. It also demonstrated the effectiveness of the vaporized fuel injection and mixing techniques by showing that very little of the vaporized propane condensed on the cold walls of the test system piping. This was not the case with vaporized gasoline and air mixtures because of the lower condensation temperature of gasoline. The amount of gasoline vapor that would be condensed was a function of many variables including: ambient air temperature, vaporized fuel temperature, fuel-and-air-flow rates, equivalence ratio, and pretest run-in time. To assure that a combustible mixture would be flowing through the test arrester at the time of ignition, an on-line total hydrocarbon gas analyzer was required.

The gas-analyzer system was designed to use an existing Beckman Model 400 hydrocarbon analyzer instrument. This analyzer automatically and continuously measures the concentration of hydrocarbons in a flowing gas sample, utilizing the flame ionization method of detection. A premixed fuel gas consisting of 40% hydrogen (H_2) and 60% nitrogen (N_2) was used to obtain the analyzer's highest rated hydrocarbon sensitivity of 10% methane (CH_4) equivalence. For propane (C_3H_8), this sensitivity is r juced to 1/3 or 3.3% CH_4 equivalence because of the greater number of carbon atoms per molecule.

The precentage of propane in the fuel/air mixture at an equivalence ratio ($\emptyset$) of 1.0 is about 4.0%. At the established standard test condition, where the equivalence ratio is 1.1, the percentage of propane is about 4.4%. In either case, the percentage of hydrocarbons in the test sample to be analyzed is beyond the upper range of the Beckman analyzer. The test sample had to be diluted with a known amount of air to be within the measurement range.

A 2% C_3H_8 + N_2 gas mixture was selected as the calibration span gas to adjust the gas analyzer to read 50% of full scale. A second calibration gas containing 4% C_3H_8 + N_2 was diluted by an air mixing system with one part air to one part gas mixture so that it would also read 50% of full scale. Using the same dilution ratio, a 4.4% C_3H_8 plus air test sample gas mixture would record about 56% of full scale on the gas analyzer.

The Indolene HO III clear gasoline used in this test program was analyzed to have a total carbon-to-hydrogen ratio of 1.93 ($CH_{1.93}$). In :alculating a stoichiometric air-to-fuel ratio it was assumed that the gasoline has a simplified molecular structure containing 8 carbon molecules or a chemical formula of $C_8H_{15.44}$. The balanced chemical equation for ideal combustion of Indolene gasoline and air would then be as follows:
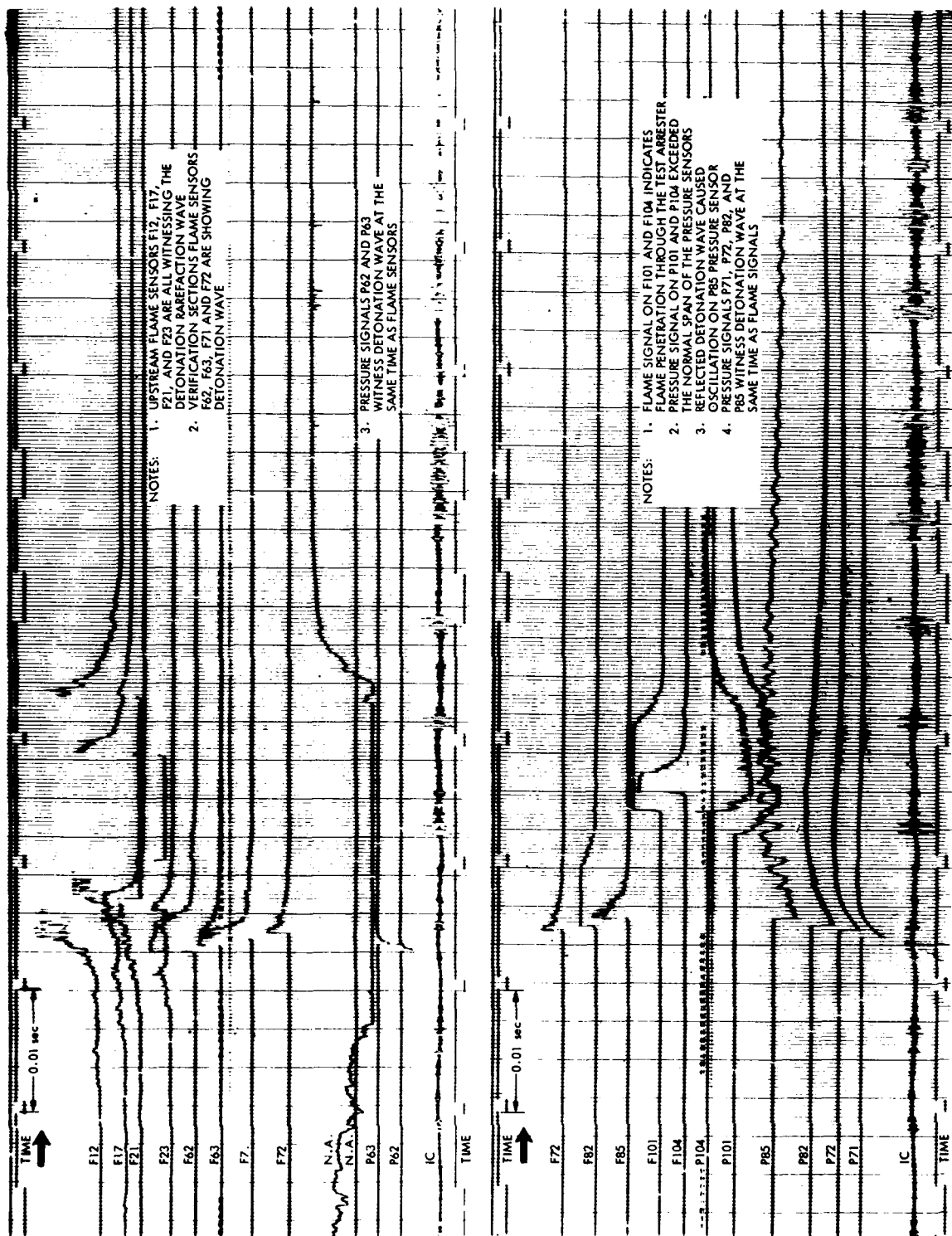
Figure 4-1. Typical Example of Transient-State Data Played
Back on an Oscillograph at an Expanded Time Base
of 32 to 1

$$C_8H_{15.44} + 11.86\ O_2 + 44.62\ N_2 = 8\ CO_2 + 7.72\ H_2O + 44.62\ N_2$$
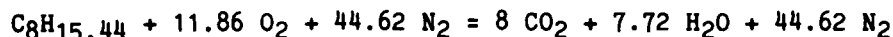
The stoichiometric air to fuel ratio (A/F) on a weight basis was calculated to be 14.62 ($\emptyset$ = 1.0). For the standard test condition ($\emptyset$ = 1.1), A/F = 13.29 and the percentage of gasoline in air is 1.92%. Using the 2% C_3H_8 + N_2 calibration gas to span the analyzer to 50% of full scale and the same one-to-one air dilution rate for the gasoline-and-air mixture sample, the carbon ratio between propane and gasoline is 3 to 8, which should give an analyzer reading of 64% of full scale.

A significant amount of vaporized gasoline will condense out of the flowing mixture onto the cold walls of the test facility piping. An extremely rich fuel mixture would be required at the upstream injection section to provide the ideal mixture ($\emptyset$ = 1.1) at the downstream test section. It was doubtful that a fuel-rich mixture at the upstream ignition location would result in the rapidly accelerating flame needed to produce a detonation. On the other hand, any gasoline condensed on the piping walls should be reevaporated by the propagating flame front and enter into the combustion process. It was determined to maintain the ideal mixture ratio at the point of injection, and monitor the test section exit for evidence of a combustible mixture. The lower flamability limit of gasoline at the nominal test condition would be an A/F = 20.89 ($\emptyset$ = 0.7), and the gas analyzer should read 41% of full scale.

The hydrocarbon gas analyzer was located as close to the test section exit as practical, to minimize response time. It was placed in a steel-walled protective enclosure, which unfortunately had no provision for thermal control. Although the Beckman Model 400 analyzer has an internal controller for maintaining the desired 40°C (120°F) operating temperature under normal laboratory conditions, it was doubtful that it could accommodate the broad range of temperatures to be experienced on the test site. The absolute accuracy of this instrument was not determined; however, a 1-to-2% zero shift was noticed during the morning, midday, and late-afternoon calibrations. Used primarily as an indicator for the existence of a combustible mixture in the test section, a gasoline and air test firing was made whenever the analyzer reading exceeded 41% of full scale.

A flow-system schematic diagram of the hydrocarbon analyzer and air dilution system is shown in Figure 4-2. Starting with the gas-sample rake in the test section piping, the sample mixture is directed into a close-coupled three-way solenoid valve. When deenergized, this valve isolates the sample rake and allows a continuous flow of 100% N_2 at low pressure to purge the sample delivery line. When the valve is energized, the purge is closed off and the sample gas is directed into either a sample collection cylinder or through a by-pass line into a visual flowmeter. The gas-sample pressure level at this point is witnessed on a pressure gage and relayed to a combination air- and spring-loaded pressure regulator. This regulator delivers the dilution air from a compressor and receiver tank, at the same pressure as the gas sample, to a second visual flowmeter. Flow-control needle valves at the inlet of each flowmeter are used to proportion the air and gas-sample flow rates to the desired dilution level. A gas-transfer pump then delivers the diluted sample through a third visual flowmeter to the total hydrocarbon analyzer. To minimize system response time, an internal sample-bypass feature provides high-velocity sample flow through
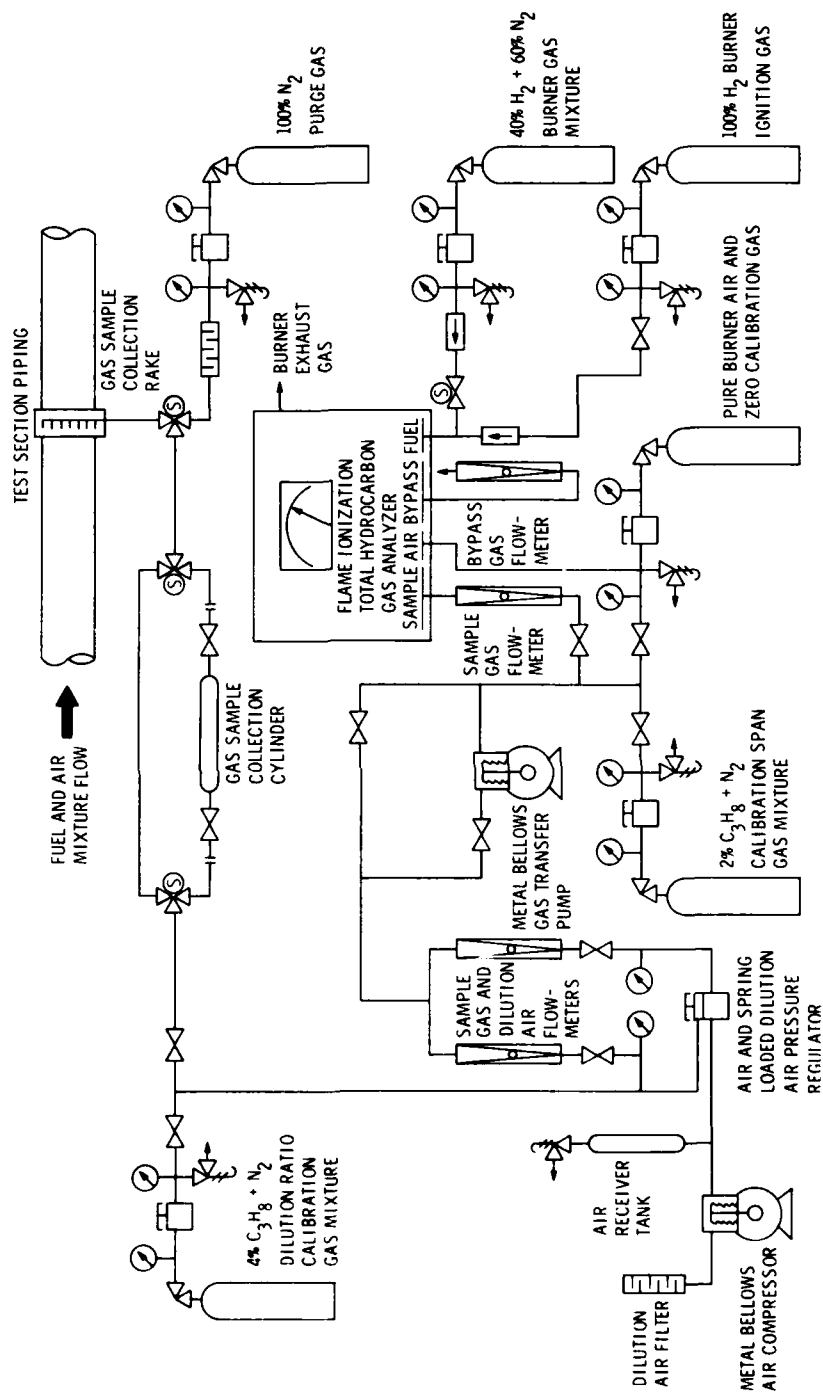
Figure 4-2. Hydrocarbon Gas Sample Analyzer and Air Dilution Flow System Schematic Diagram

the analyzer, with only a small portion of the sample fed into the ionization flame burner. The bypass flow is witnessed on a fourth visual flowmeter.

A regulated supply of 100% H_2 was used to enrich the ionization flame burner only during the ignition and start-up procedure. The ionization flame is maintained by the pressure-regulated flows of 40% H_2 + 60% N_2 gas mixture and 100% pure (oil-free) air. The pure air can also be directed into the analyzer inlet for zero calibrations. A pressure-regulated supply of 2% C_3H_8 + N_2 gas mixture, which can be directed into the analyzer inlet, is used for calibration span of the visual output indicator. A second pressure-regulated supply of 4% C_3H_8 + N_2 gas mixture can be directed into the sample line ahead of the dilution system to verify the desired dilution ratio setting.

The only difficulty with this gas-analyzer installation, other than the lack of adequate temperature control, was that the detonation shock wave, blowing out through either the rupture disc port or the exit of the extension piping, would extinguish the ionization flame burner. Consequently, after each test, the burner had to be relit and stabilized. The 100% H_2 enrichment greatly simplified this reignition operation. Analyzer response time after actuation of the three-way sample solenoid valve was 30 seconds, plus another 30 seconds to fully stabilize the reading. Line length between the sample rake and the analyzer inlet was approximately 6.1 m (20 ft.)

E.   PARAMETER MEASUREMENT AND CALCULATION UNCERTAINTIES

To get maximum accuracy from the instrumentation systems used at ETS, an end-to-end system calibration method is employed. All calibration signals are initiated at the transducer or between the transducer and the first piece of signal conditioning equipment, and recorded on the digital recorder, FM recorders, and oscillograph recorder. All calibration signals recorded are at known values and are independent of amplifier gain changes and power supply setting inaccuracies.

Three calibration points are recorded for each instrumentation parameter: (1) "Cal Low", (2) "Cal Ambient," and (3) "Cal High." Cal low is a power-off or shorted input signal. Cal ambient is an ambient pressure, temperature, voltage, etc. For gage pressures and voltages, this is normally a zero condition; if a zero condition is not possible, the cal ambient is a known pressure or voltage. Cal high is a voltage substitution or a known unbalance condition on top of the ambient calibration. For thermocouple readings, voltages, and most special parameters, known substitute voltages are recorded. For bridge measurements, an external shunt resistor is used to unbalance the bridge.

The Integrated Digital Data and Control System (IDAC) is the primary recorder for steady-state data. The system also has computer capability that converts input data to engineering units, and outputs it on a printer or the television (TV) monitors. A special IDAC software program was written for the air and fuel systems data to calculate air-mass flow, fuel-mass flow, air-to-fuel mixture ratio, and equivalence ratio.

Each IDAC input channel, calculation parameter, or calculation result can be displayed singly on the TV monitor to five significant figures, with engineering units and channel identification number. Alternate preselected displays with up to four parameter values, but without engineering units or channel identifications, can also be monitored on TV.

The IDAC printer is capable of outputting 50 lines per second, with one channel per line, of real-time data in engineering units from assigned channels. The printer output was used as prime steady-state data reporting the test results. All IDAC data was also recorded on magnetic tape for off-line computer reduction if required. The following is a summary of the detailed analysis of the uncertainties associated with pressure and temperature measurements and the IDAC program-calculated parameters presented in Appendix A. These values can be assured with only a 95% (2σ) probability.

(1)   Uncertainty for pressure measurement is ± 0.39% of transducer full-scale range.

(2)   Uncertainty for temperature measurement in percent of reading is:

    (a)   10.0 to 31.8°C (50 to 100°F) = ± 2.7%
    (b)   37.8 to 93.3°C (100 to 200°F) = ± 1.4%
    (c)   93.7 to 148.9°C (200 to 300°F) = ± 0.85%
    (d)   148.9 to 204.4°C (300 to 400°F) = ± 0.65%
    (e)   204.4 to 276.7°C (400 to 530°F) = ± 0.49%
    (f)   276.7 to 1260°C (530 to 2300°F) = ± 0.43%

(3)   Uncertainty for air-velocity or air-mass-flow calculations is ± 1.82% of value.

(4)   Uncertainty for fuel-mass-flow calculation is ± 1.93% of value.

(5)   Uncertainty for calculated air-to-fuel mixture ratio and equivalence ratio is ± 2.65% of value.

Using the uncertainties listed above, the maximum uncertainty that can be expected for the measured and calculated test parameters associated with the standard test condition are listed in Table 4-2.

The transient-state data were recorded on an Ampex Model FR 2200 and an Ampex Model FR 3020 high-frequency FM tape recorders. Photodetector flame sensors were the primary instruments used to determine flame velocities. Quartz-crystal pressure transducers were primarily used to measure peak-pressure pulses in the detonation wave, but they also served as back-up instruments to determine wave velocities. There was usually good agreement in calculated velocities between the flame sensors and the pressure sensors witnessing a stable detonation wave. This was not the case, however, when the sensors were located in the deflagration-to-detonation transition zone. The spinning detonation phenomenon, reported in References 2-9 and 2-10, would most likely explain this discrepancy.

Flame sensor and pressure sensor test data, along with the pre-and posttest calibrations recorded on the FM tapes, were played back on an oscillograph at an expanded time base of 32 to 1. The peak-pressure

pulse deflections and the calibration parameter equivalents were scaled from these recordings and used to calculate the detonation wave pressures. The elapsed time between sequential flame sensor signals (or pressure sensor signals) were also scaled from the oscillograph recordings. Using this time data and the known distances between adjacent instrumentation transducer ports, the average flame velocities through each succeeding section of the detonation test piping were calculated.

The following is a summary of the Appendix A detailed analysis of uncertainties associated with transient-state measured detonation peak-pressure pulses and rise-time response limits of data recorded on FM tapes with a 32-to-1 time-expanded playback onto an oscillograph. These values can be assured with only a 95% (2σ) probability.

(1)   The uncertainty for the peak-pressure pulse measurement is ±3.1% of transducer span.

(2)   The response time limit for photodetectors and quartz-crystal pressure transducers is:

(a)   3.5   s on Ampex Model FR 3020 recorder.

(b)   7.0   s on Ampex Model FR 2200 recorder.

Using the uncertainties listed above, combined with an oscillograph readability uncertainty of ±5.0% and a measured transducer spacing uncertainty of ±0.25%, the maximum uncertainty that can be expected for measured and calculated parameters associated with a stable detonation wave at standard test conditions are listed in Table 4-2.

Table 4-2. Maximum Uncertainty for Measured and Calculated
Parameters at the Standard Test Condition

Parameter	Symbol	Uncertainty
Steady-State Data		
Air flowmeter inlet pressure	PBO	$\pm$ 0.27 kN/m^2 ($\pm$ 0.039 psia)
Air flowmeter differential pressure	DPO	$\pm$0.0083 kN/m^2 $\pm$ 0.0012 psid)
Air flowmeter exit temperature	TOI	$\pm$ 1.3°C ($\pm$ 2.8°F)
Fuel line pressure	PFL	$\pm$ 14.0 kN/m^2 ($\pm$ 2.0 psia)
Fuel line temperature	TFL	$\pm$ 1.0°C ($\pm$ 2.7°F)
Fuel flowmeter frequency	FMF	$\pm$ 0.8 Hz
Test section inlet pressure	PAI	$\pm$ 0.27 kN/m^2 ($\pm$ 0.039 psia)
Test section differential pressure	DPA	$\pm$ 0.028 kN/m^2 ($\pm$ 0.004 psid)
Test area ambient pressure	PAMB	$\pm$ 0.538 kN/m^2 ($\pm$ 0.078 psia)
Air mass flow	MA	$\pm$ 5.67 kg/h ($\pm$ 12.5 lb/hr)
Air velocity	VA	$\pm$ 0.08 m/s ($\pm$ 0.27 ft/s)
Fuel mass flow	MF	$\pm$ 0.05 kg/h ($\pm$ 1.00 lb/hr)
Air to fuel mass ratio	A/F	$\pm$ 0.35
Equivalence ratio	ϕ	$\pm$ 0.12
Transient-State Data		
Detonation peak-pressure pulse	PXX	$\pm$ 241 kN/m^2 ($\pm$35 psia)
Detonation flame velocity	FXX-FYY	$\pm$ 98 m/s ($\pm$322 ft/s)
Detonation pressure wave velocity	PXX-PYY	$\pm$ 98 m/s ($\pm$322 ft/s)

SECTION V

TEST OPERATING PROCEDURES

A. GENERAL SAFETY REQUIREMENTS

All test operating procedures involving fuel transfer, or performed with the fuel system pressurized, required the safety tower operator to be in position, monitor all communication on a headset, and control access to the test area with the safety status lights. The test stand is normally in a GREEN condition, which permits open access to all personnel. Fuel transfers and test preparations were performed in an AMBER condition, which restricts nonoperating personnel to the workshop area, unless permission is granted to enter other areas. A RED condition was used during actual tests, which isolates the test stand and the surrounding designated area from all personnel.

A minimum of two men was required at the site during fuel transfers and test preparations. Personnel safety equipment included hard hats, face shields, gloves, and fire-retardant coveralls. Additional safety equipment was available including MSA breathing devices, safety showers, eye washes, and the Firex water deluge system. All operations, except the servicing and reconfiguration of the test arrester section, were performed using formal procedures in the form of check lists, with individual pages dated and timed, and with each step initialed by two persons witnessing the event.

An ignition-completion key switch, which prevented the actuation of the hydrogen-air-spark igniter except during checkouts and test operations, was located at the test stand. Igniter checkouts required that the air compressor be in operation to minimize the build-up of combustible mixtures in the test piping.

B. OPERATING PROCEDURE CHECK LISTS

The following is a description of the operating procedures and check lists used in the detonation tests.

1. Pretest System Checkouts

    a. <u>Preliminary Check</u>. This check confirms proper installation of the test item, instrumentation and control cable connections, readiness of the nitrogen pressurant and purge systems, requested photographic coverage, and that the safety system is operational.

    b. <u>Electromechanical Checkouts</u>. These checks examine, at the test stand, the overall control system readiness by individual confirmation of proper operation of each control in the blockhouse.

    c. <u>Sequence Timer/Emergency Circuit Checkout</u>. This checkout operates the preset automatic sequence timer, without actual fuel flow, while recording control-element actuations on the facility oscillograph.

Sequence times of the various elements were measured and adjusted where necessary. The sequence was then repeated, adding a shutdown with the emergency switch to confirm proper emergency switch actuations.

    d.   <u>Leak Checks</u>. These checks provide a gaseous nitrogen system leak check at maximum operating pressure for the fuel system, fuel vaporizer and condenser loop, fuel induction system, and the air-compressor system.

NOTE: The four check-list procedures described above were not performed before each test, but were done when special circumstances, such as component changes, malfunctions, or severe weather, were encountered.

2.   Fuel Transfer Procedures

    a.   <u>Propellant (fuel) Fill Check Lists</u>. These procedures are provided for transferring either propane or gasoline from their storage containers into the test stand fuel supply tank. Propane was transferred via its own vapor pressure. Gasoline was transfered from drums by means of an air-motor-driven pump. It was common to expect up to six separate tests in a day, each of which required approximately 4.6×10^{-3} m^3 (1 gal) of fuel. Therefore, the fuel supply tank was topped off for each test day.

    b.   <u>Propellant (fuel) Offload</u>. These transfers from the fuel supply tank were normally returned to the appropriate storage container. Small quantities of propane could also be disposed of through the burn stack. Gasoline from the vaporizer/condensor loop remaining in the collector tank was not suitable for recycling and was disposed of as waste. It was necessary to empty the collector tank after every two days of testing.

3.   Test Preparations

    The Test Preparations Check List for instrumentation and test systems was completed concurrently on the day of testing. In the blockhouse, all patchboard connections were completed and instrumentation was setup. An end-to-end instrumentation system calibration was performed. At the test stand, various safety check and facility setups were made: condenser cooling water was turned on, the hydrocarbon analyzer was put in operation, and the hydrogen and air gas pressures were adjusted for the igniter. At the control console, the air compressor was started and the air flow adjusted by means of the air metering valve and the air bypass valve. After the air system temperature and flow were stabilized at the desired values, the test item's pretest pressure loss was measured and recorded.

    The fuel vaporizer heater was activated, and nitrogen purge gas flowed through the heater coils and into the condenser for the preheat cycle. The test stand safety condition was changed from GREEN to AMBER. The fuel supply tank was pressurized with nitrogen up to the desired operating pressure. When the heater core reached approximately 260°C

(500°F), the nitrogen purge gas was turned off and fuel flow was metered at a low level. The fuel flow was increased up to the desired test condition as the vaporizer heater reached the operating temperature.

Final visual checks were made of the test stand area, and the ignition completion key switch was turned on. All operating personnel evacuated the test stand area and its safety condition was changed to RED.

4. Blockhouse Preparation

Blockhouse preparation begins with a weather station confirmation of wind velocity and direction and the local barometric pressure. Control console circuits for ignition and emergency shutdown functions were armed and each significant panel switch had its position confirmed. With all test personnel at their operating position, the test conditions where reviewed and confirmed. A pretest instrumentation calibration was recorded and the countdown procedure was begun.

5. Countdown

A typical "countdown" procedure follows:

(1) An announcement was made over the public address system to alert personnel in the general area that a detonation would occur. Generally, the detonation noise was very intense and sharp, capable of creating an indirect hazard. A horn signal was also sounded.

(2) The IDAC tape, printer, and the oscillograph were turned on to a slow speed.

(3) The hydrocarbon analyzer purge was turned off, allowing the analyzer to sample the mixture flowing through the witness section.

(4) The fuel mixer valve was changed to the RUN position, allowing fuel to flow to the test piping for the first time in the test sequence. The burn stack purge valve was opened to sweep out combustible gases from the collector tank vent line. The oscillograph was turned off.

(5) As the fuel and air mixture traveled through the test piping, the hydrocarbon analyzer responded with a steadily increasing signal. The countdown timer was then stopped for a HOLD period, while fuel and air-flow rates were confirmed or adjusted, if necessary.

(6) When the countdown was resumed, the IDAC tape and printer were switched to continuous mode and the oscillograph and movie camera were turned on.

(7)   The hydrocarbon analyzer purge was turned on, again
       isolating it from the test piping to protect it from
       the detonation pressure wave.

(8)   Valves were actuated to isolate the low-pressure
       transducers from the detonation pressure wave.

(9)   The igniter was armed by a console switch, the high-
       frequency tape recorders were turned on, and the
       oscillograph was switched to high speed.

(10)   The sequence timer was turned on. For the noncontinuous
       flow tests, this first automatically changed the
       fuel mixer valve to the CONDENSER position, preventing
       further fuel flow from entering the induction section
       of the test piping. Residual fuel downstream of
       the injector was sufficient for ignition on this
       type of test. The sequence timer then fired the
       igniter, turned on the vaporizer warm-up purge valve,
       closed the fuel-tank outlet valve, and turned off
       the vaporizer heater. For the continuous flow tests,
       the sequence timer was used only to fire the igniter,
       and the other items were performed manually by means
       of the emergency cutoff switch after the desired
       flow time had elapsed. Temperatures in the test
       piping on each side of the test arrester were monitored
       on the video display during the continuous flow of
       fuel after ignition and detonation to check for flame
       penetration and flame holding.

(11)   The igniter was unarmed, the oscillograph changed to
       low speed, and the high-frequency tape turned off.

(12)   The fuel metering valve was closed and the movie
       camera was turned off.

(13)   Fuel supply tank pressure transducers were vented
       and a posttest calibrate was performed on the
       instrumentation.

(14)   Fuel supply tank pressure transducers and the test
       arrester pressure transducers were reopened to the test
       system, the oscillograph turned off, and the IDAC tape
       and printer were switched to a slow speed.

(15)   Compressor air flow was maintained to purge residual
       fuel and combustion by-products from the test piping.

6.   Posttest

    The Posttest procedure included a visual inspection of the test
stand. The test stand safety condition was changed to AMBER. Reentering
personnel inspected all rupture disc assemblies. If they were intact,

a posttest pressure loss across the test item was measured and recorded. If any rupture disc was blown out, the air compressor was turned off while the discs were replaced. The air compressor was then turned back on, the air flow stabilized, and the posttest measurement recorded.

If a repeat test was to be made, the hydrocarbon analyzer was checked out; normally, it had to be reignited because the detonation shock wave usually blew out the ionization flame. The Test Preparation procedure would then be restarted from the point of fuel vaporizer heater activation.

Following the last test of the day, a posttest end-to-end calibration of the instrumentation system was made. Fuel in the induction system was pushed back into the supply tank and the system thoroughly purged with nitrogen gas.

Immediately after each test, the data recorded on the FM tape recorder was played back onto a quick-look oscillograph at an expanded time scale of 8 to 1. This data told the test conductor that he did or did not get ignition and detonation, or that the flame arrester worked or did not work.

After a day of testing, a playback record was made of the FM tape data at an expanded time scale of 32 to 1. This record contains both calibration and test data for all parameters, and was used for reductions of flame velocities and peak pressure pulse data.

SECTION VI

FACILITY CHECK-OUT TESTS

A number of tests were required to check out facility systems that were designed and installed specifically for the Detonation Flame Arrester Evaluation Program. During the facility check-out tests, it was determined that propane and air mixtures would not ignite and burn predictably with spark ignition only. The test procedure allowed 0.50 second from fuel shut-off to spark initiation to clear the fuel/air induction system and prevent flash-back flame damage. A hydrogen-air-spark ignition system was developed that produced the desired results. The only disadvantage in this method was that the addition of hydrogen to the fuel/air mixture imparted an initially higher velocity to flame propagation in the pipe than would normally be associated with an hydrocarbon/air mixture alone. It required about 10 to 12 pipe diameters to diminish this effect.

Chemically pure (CP) propane was used during the check-out tests to allow a reliable determination of the effectiveness of the fuel injection and air mixing procedure, as well as to verify the accuracy of flow measuring instrumentation. Gas samples were collected at both the inlet and outlet of the test piping (see Figure 3-1 for location of sampling rakes and collection cylinders). The samples were analyzed in the laboratory using a gas chromatograph mass spectrometer (GCMS). Adjustments were made to the fuel/air systems until an acceptable agreement was obtained between the measured flow and the GCMS analyzer results. One effective change involved the redirection of the fuel injector from a parallel-flow orientation with the air stream to a counter-flow orientation. This modification provided better mixing, which was confirmed by the inlet sample results. An eventual close agreement between the inlet and outlet samples showed that there was little condensation of propane on the walls of the test piping. The GCMS analysis indicated from 4.0- to 4.2-mole-percent propane in the samples at a flow-measured equivalence ratio of 1.1 (air-to-propane mass mixture ratio of 14.3).

The initial length of 15.2-cm- (6.0-in.-) diameter piping in the check-out test configuration (see Appendix B) was 8.4 m (25.5 ft). In some tests, the individual pipe sections were modified and used for alternate functions as noted in Appendix B. Test firings were made at an initial flow velocity of 4.6 m/s (15.0 ft/s) and a propane/air equivalence ratio of 1.1. A detonation was not obtained at this run-up distance, so an additional section of pipe was installed. Test firings were repeated that did not result in detonations, so additional sections of piping were added to test configuration Nos. 100 to 117. This procedure continued until all available piping was installed, resulting in a total run-up distance of 31.5 m (103.5 ft). Both equivalence ratio and initial flow velocities were varied, but none of these test conditions produced a detonation. The maximum flame velocities recorded were around 244 m/s (800 ft/s).

The chemically pure propane was removed from the fuel supply tank and replaced with commercial grade (CG) propane. Test firings

were made at an equivalence ratio of 1.1 and varying initial flow rates, but no detonations were obtained. The recorded flame velocities were about the same as those obtained with CP propane. It was theorized that the smooth-bored, honed, and polished shock-tube piping did not develop sufficient turbulence in the boundary layer flow, even during combustion, to accelerate the propagating flame up to the stable detonation velocity. To increase turbulence, a coil of 0.32-cm- (0.13-in.-) diameter wire was stretched through one of the 4.6-m- (15-ft-) long run-up pipe sections with a coil spacing of about one every 0.3 m (1.0 ft). This configuration produced one detonation, but failed to produce any more in subsequent firings. Posttest inspection revealed that the coils had been displaced by the rarefaction wave following detonation and was compressed together at the inlet end of the pipe in which it was installed. The coil of wire was replaced by a cylindrical liner of rolled and welded expanded metal mesh (shown in Figure 6-1) that fitted closely against the pipe inner wall. This test configuration (No. 117) produced detonations at initial flow velocities of 3.0, 4.6, and 6.1 m/s (10, 15, and 20 ft/s), but not at 1.5 m/s (5 ft/s). Enough data on detonations was obtained during these tests to complete the instrumentation check-out of optical flame sensors, dynamic pressure transducers, and the high-speed FM data recording system.
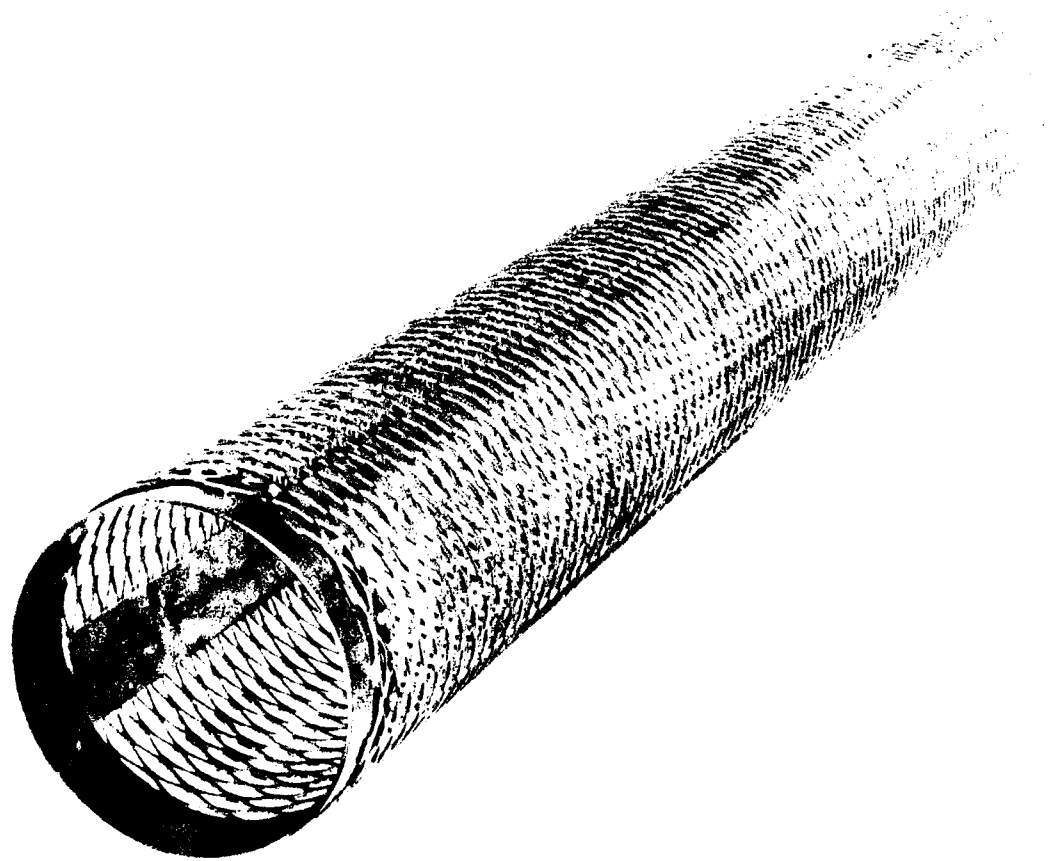
Figure 6-1. Expanded Metal Tube Liner

SECTION VII

CALIBRATION TESTS

The calibration tests for detonation run-up distance with CG propane were started with a test assembly configuration (No. 118) similar to the one shown in Figure 3-1, the difference being that there were only two lengths of 4.6-m- (15-ft-) long run-up pipe lined with the turbulence-producing, expanded metal-mesh tubes. This test assembly produced detonations at all initial flow velocities from 0 to 6.1 m/s (0 to 20 ft/s) (see Appendix C).[1] The flame velocity after transition to detonation stabilized around 1830 m/s (6000 ft/s). The peak pressure pulses recorded during transition ranged broadly between 1000 to 5000 kN/m^2 (145 to 725 psia), but stabilized around 2000 kN/m^2 (290 psia) after transition (see Appendix D).[1] Based on these measured flame velocities and peak pressures, the location of detonation transition appeared to be very close to the downstream end of the 9-m (30-ft) length of lined run-up piping or at a total distance of 20 m (66 ft) from the point of ignition. A plot of flame velocity and peak pressure as a function of pipe length for these tests is shown in Figure 7-1.

To evaluate the influence a flame arrester may have on the run-up distance, a sharp-edged orifice plate with an 8.192-cm- (3.225-in.-) diameter bore, designed to simulate the back pressure an arrester may produce, was installed on the exit of the extension section (No. 11). With this test configuration (No. 119), the flame accelerated down the pipe, reaching a maximum velocity of only 1000 m/s (3281 ft/s) at a distance of 23 m (75.5 ft), and then decelerated through the remaining length of run-up pipe. The peak pressures reflected the same phenomena, obtaining a maximum level of 1200 kN/m^2 (366 psia) and then decreased, as shown in Figure 7-1. Since these velocities and pressures were below the required stable detonation levels, the test configuration was judged to be unstable.

The orifice plate was removed and another 4.6-m (15-ft) length of expanded metal tube liner was installed into the remaining run-up pipe section (No. 5), making the total pipe length with turbulent liners 13.7 m (45 ft). This test configuration (No. 120), shown in Figure 3-1, produced a very stable detonation in the verification sections (No. 6, No. 7, and No. 8). The flame velocity averaged around 1800 m/s (5960 ft/s) at a peak pressure of 1650 kN/m^2 (240 psia) for a stable detonation wave. After one firing, the orifice plate was installed at the inlet of the test section (No. 9) (Test configuration No. 121). On the subsequent firings, a fully-developed and stable detonation was recorded in the verification sections. A reflected shock wave was evident 0.3 m (1.0 ft) upstream of the orifice plate, where peak pressures of about 3000 kN/m^2 (435 psia) were recorded. Both the flame

---

[1]Parameter nomenclature is presented in Table 4-1.

velocity and the peak pressure in the detonation wave normally decreased after passing through the orifice plate into the witness section (No. 10). However, in one test firing (No. 1431 E) they were only slightly reduced. A plot of the results of these tests is shown in Figure 7-2.

After development of a successful configuration for stable detonation with CG propane and air mixtures, the next step was to determine if it were equally suited for gasoline and air mixtures. The CG propane was replaced in the fuel supply tank with Indolene HO III clear (unleaded) gasoline. Indolene, a product of the Standard Oil Division of Amoco Oil Company, complies with the EPA specifications in the Federal Register for standard test motor fuel (Reference 7-1). Test conditions for gasoline and air were the same as for propane and air. Initial flow velocities were reduced from 6.1 to 1.5 m/s (20 to 5 ft/s) The test configuration (No. 122) without the orifice plate produced /e.·y stable detonations where the flame velocity through the test section was about 1830 m/s (6000 ft/s) and peak pressure was about 1630 kN/m^2 (235 psia). The deflagration-to-detonation transition location appeared to be well within the turbulent liner run-up pipe sections. This provided some distance for the detonation wave to stabilize in the verification sections before entering the test section. With the orifice plate installed at the inlet to the test section, the reflected peak-pressure wave measured 30 cm (12 in.) upstream showed a sharp increase, reaching a level of 3300 kN/m^2 (479 psia). This pressure level reduced quickly as it moved upstream. Both the flame velocities and peak pressures decreased significantly after passing through the orifice plate into the witness section. A plot of the results of these tests is shown in Figure 7-3.

The successful attainment of stable detonations with gasoline and air mixtures completed the calibration test series. The test program was started to evaluate selected flame arrester devices subjected to a fully-developed detonation. To reduce the required number of comparative tests, a standard test condition was established that would use an equivalence ratio of 1.1 and an initial flow velocity of 4.6 m/s (15 ft/s) for all subsequent arrester evaluation tests.

TEST NO.	SYMBOL	φ	VA, m/s	ORIFICE PLATE
1429-A		1.1	1.5	NONE
B			3.0	
C			4.6	
D			6.1	
E			0	
F			0	NONE
1430-A			4.6	INSTALLED ON EXIT
B			4.6	INSTALLED ON EXIT
C			4.6	NONE
D		1.1	4.6	NONE

○ OPEN SYMBOLS – FLAME SENSORS
● CLOSED SYMBOLS – PRESSURE SENSORS
⌀ EQUIVALENCE RATIO, PROPANE/AIR
VA   INITIAL FLOW VELOCITY

PIPE LENGTH WITH TURBULENT LINER
9.14 m (30 ft)

FLAME VELOCITY, m/s

PIPE LENGTH, m

Figu[

F12 F17 F31 F32 F41 F43

FLAME VELOCITY AND PEAK PRESSURE VERSUS PIPE LENGTH
TEST CONFIGURATION NO. 118 AND NO. 119
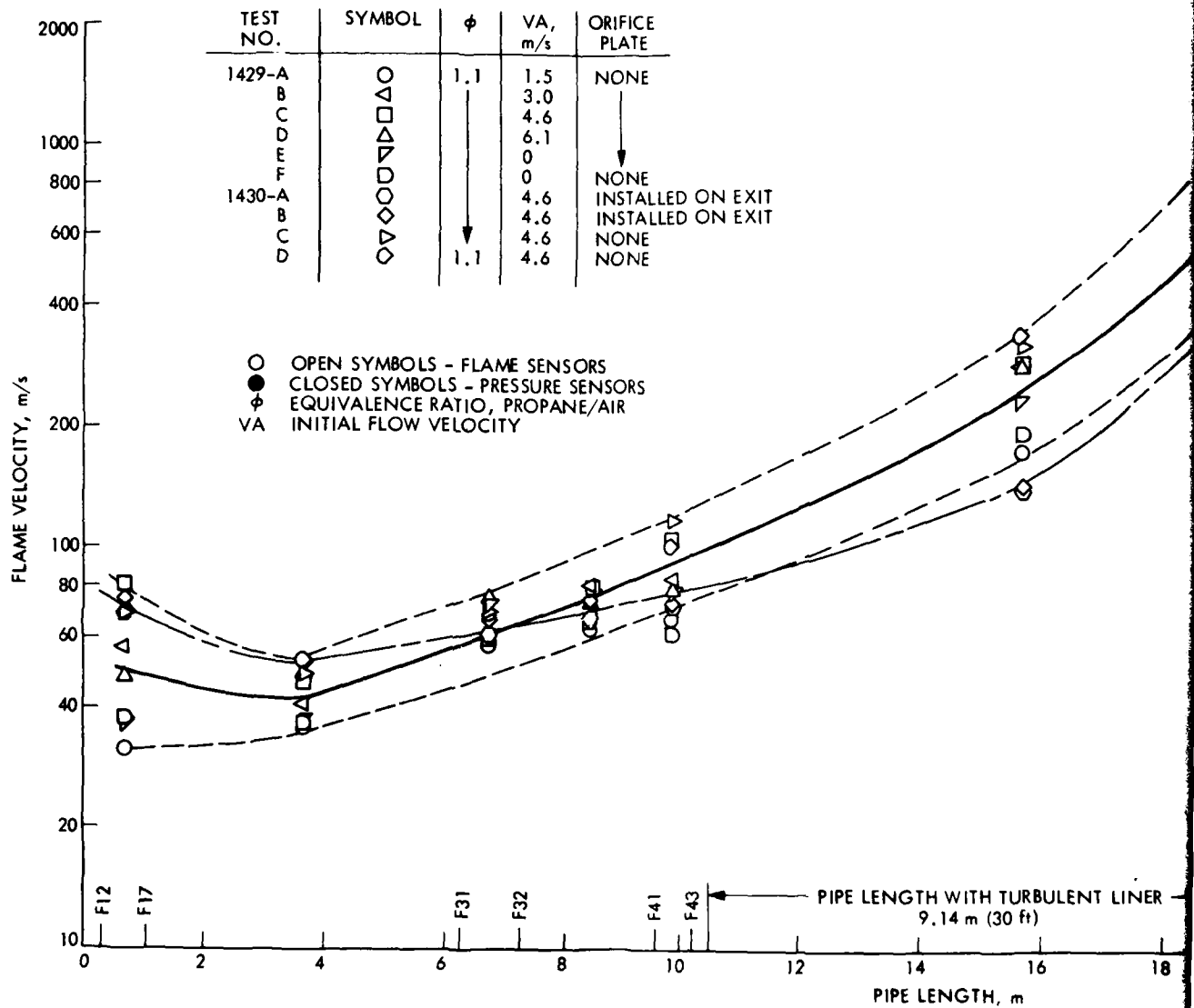
Figure 7-1. Calibration Test Results for Detonation Run-Up
Distance with Commercial Grade Propane and Air
Mixture -- Unstable

TEST NO.	SYMBOL	ϕ	VA, m/s	ORIFICE PLATE
1431-A	O	1.1	4.6	NONE
B	▷	↓	↓	INSTALLED
C	□			INSTALLED
D	△			INSTALLED
E	◇	1.1	4.6	INSTALLED

O OPEN SYMBOLS – FLAME SENSORS
● CLOSED SYMBOLS – PRESSURE SENSORS
ϕ EQUIVALENCE RATIO, PROPANE/AIR
VA INITIAL FLOW VELOCITY

PIPE LENGTH WITH TURBULENT LINER
13.72 m (45 ft)

FLAME VELOCITY, m/s
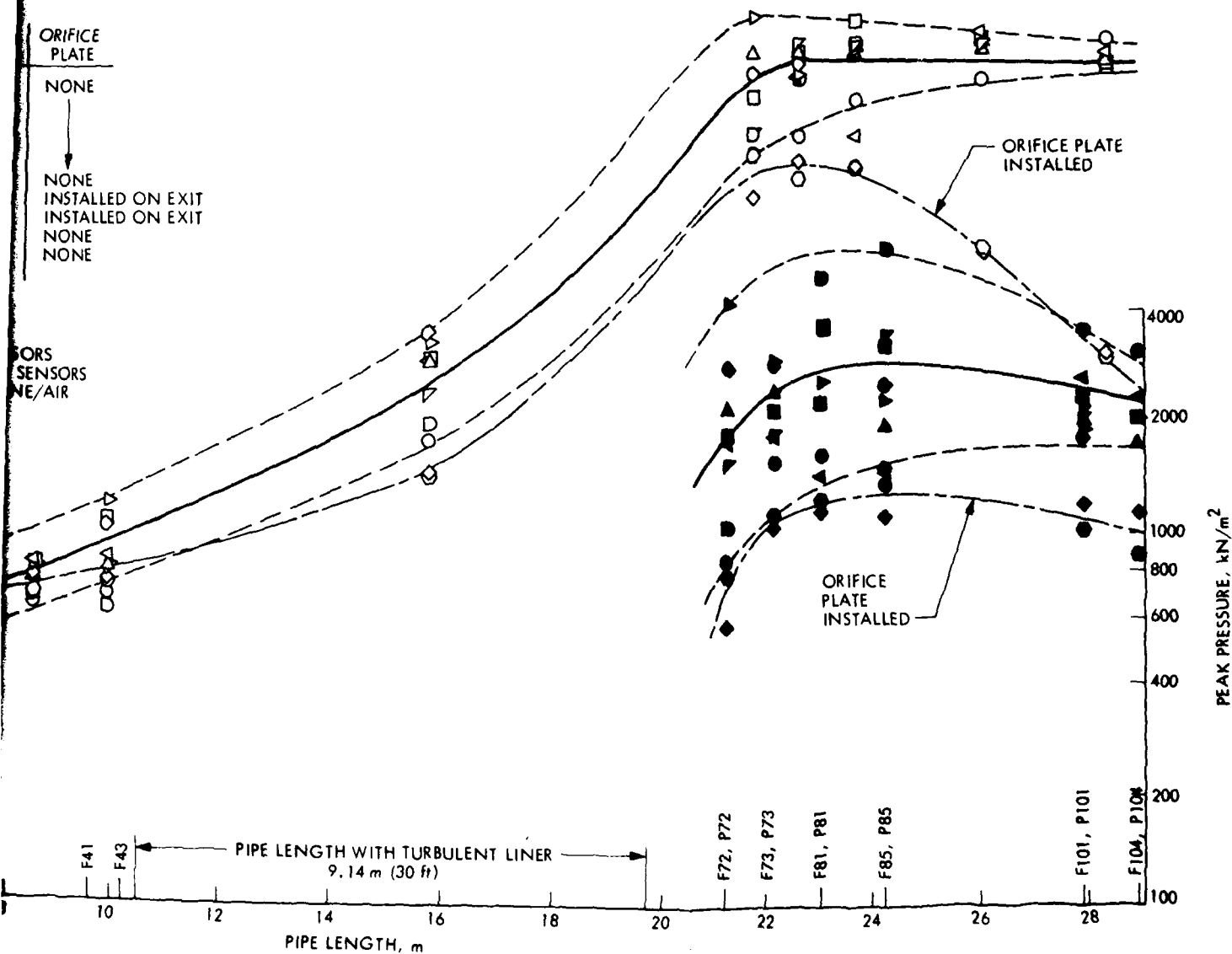
PIPE LENGTH, m

Figure 7-

FLAME VELOCITY AND PEAK PRESSURE VERSUS PIPE LENGTH
TEST CONFIGURATION NO. 120 AND NO. 121

ORIFICE
PLATE

NONE
INSTALLED
INSTALLED
INSTALLED

SORS
SENSORS
NE/AIR

ORIFICE PLATE
INSTALLED

ORIFICE PLATE
INSTALLED

PEAK PRESSURE kN/m²

4000

2000

1000
800

600

400

200

0

PIPE LENGTH WITH TURBULENT LINER
13.72 m (45 ft)

F62, P62
F63, P63
F71
F72
F81, P81
F85, P85
ORIFICE PLATE
F101, P101
F104, P104

8   10   12   14   16   18   20   22   24   26   28

PIPE LENGTH, m

Figure 7-2. Calibration Test Results for Detonation Run-Up
Distance with Commercial Grade Propane and Air
Mixture -- Stable

7-5

TEST NO.	SYMBOL	φ	VA, m/s	ORIFICE PLATE
1432-A		1.1	6.1	NONE
B			4.6	
C			3.0	
D			1.5	
1433-A			4.6	NONE
B				INSTALLED
C				INSTALLED
D				INSTALLED
E		1.1	4.6	INSTALLED

O OPEN SYMBOLS – FLAME SENSORS
● CLOSED SYMBOLS – PRESSURE SENSORS
φ EQUIVALENCE RATIO, GASOLINE/AIR
VA INITIAL FLOW VELOCITY

FLAME VELOCITY, m/s

PIPE LENGTH WITH TURBULENT LINER
13.72 m (45 ft)

F12 F17 F21 F23

F62, P62   F63, P63

PIPE LENGTH, m

Figure 7-3.

FLAME VELOCITY AND PEAK PRESSURE VERSUS PIPE LENGTH
TEST CONFIGURATION NO. 122 AND NO. 123
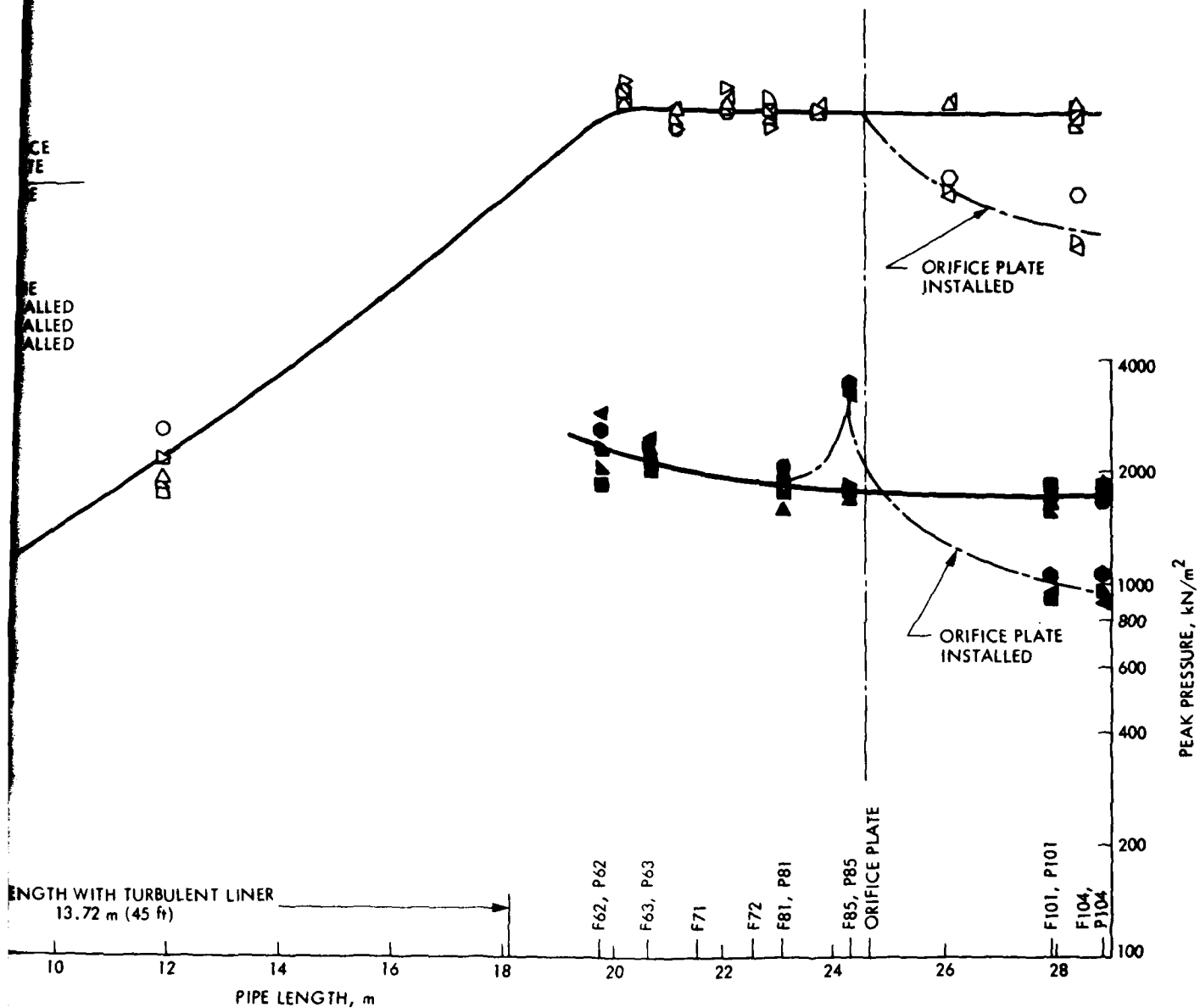
Figure 7-3. Calibration Test Results for Detonation Run-Up
Distance with Gasoline and Air Mixture

SECTION VIII

ARRESTER EVALUATION TESTS

A. PIPE TEES AND RUPTURE-DISC IN-LINE TEST ASSEMBLY

The first device to be evaluated was not an arrester in the true sense, but a combination of two extra-strong 15.2-cm- (6.0-in.-) diameter pipe tees and rupture discs. They were assembled in an arrangement that caused the detonation wave to make two 90-deg turns before proceeding along the length of pipe. The test section was removed from the test assembly and replaced with the pipe tees as shown schematically in Figure 8-1. The first rupture disc was placed in the leg of the pipe tee in-line with the approaching detonation wave. A second rupture disc was placed in the leg of the tee in line with the receding detonation wave. The restricter orifice plate was installed in the downstream side of the second tee, just ahead of the witness section.

Four test firings were made with variations of this test configuration (No. 124 to No. 127), where the pressure ratings of both rupture discs were reduced in the following steps: 4137, 2068, 690, and 345 kN/m^2 (600, 300, 100, and 50 psid). Both rupture discs were blown out in all test firings and the detonation passed through the test assembly. There was only a slight reduction in flame velocity and peak pressure in the witness section downstream of the orifice plate. There appears to be no correlation between the magnitude of this loss and the rupture-disc pressure rating. A plot of the results of these tests is shown in Figure 8-2. The measured pressure drop across the test assembly, including the orifice plate, averaged 0.20 kN/m^2 (0.029 psid) at an average air-flow velocity of 4.68 m/s (15.35 ft/s).

B. PIPE TEE, RUPTURE-DISC NOT-IN-LINE, AND PIPE ELBOW TEST ASSEMBLY

The safest orientation for a rupture disc in a pipeline is normally vertically-up so that the release of flame and high-pressure gas will not impact adjacent installations. The pipe tee, rupture-disc not-in-line, and pipe elbow test assembly was developed to provide this orientation and to lower the piping inlet interface with an arrester. This lower interface was also used with two of the selected arrester test assemblies, which were evaluated later. This test assembly is shown schematically in Figure 8-3.

Four test firings were made with this test configuration (No. 128 to No. 131) where the pressure rating of the rupture disc was reduced in the same steps as above. The rupture disc was blown out in all test firings and the detonation passed through the test assembly. Figure 8-4 is a plot of the results for these tests. For two tests, the flame velocity and peak pressure in the witness section showed only a slight drop in levels. For the two other tests, the drop was more significant. However, there is still no apparent correlation between this loss and the rupture-disc pressure rating. It appears to be a random phenomenon. The measured pressure drop across the test
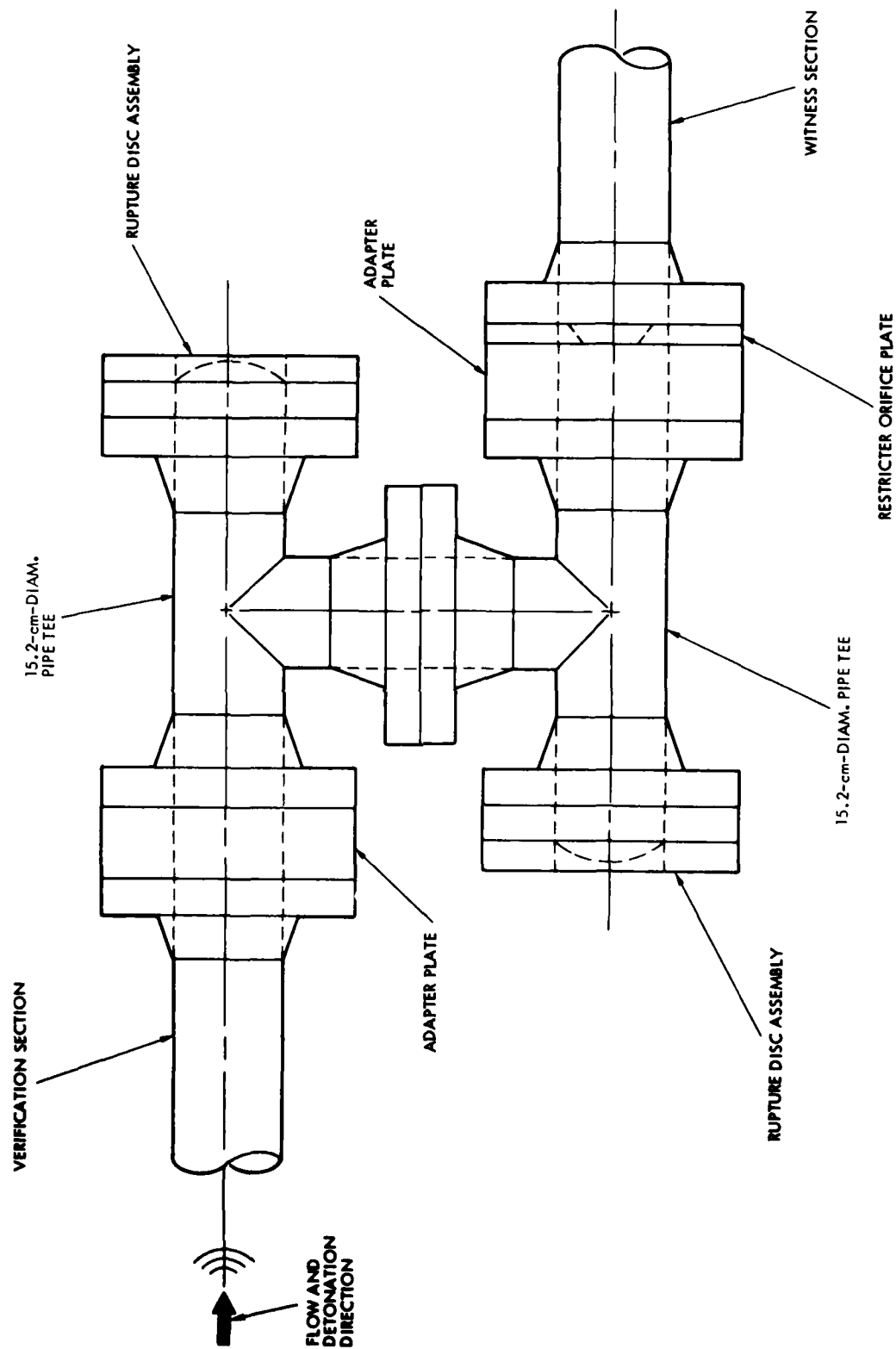
Figure 8-1. Pipe Tees and Rupture Disc In-Line Test Assembly
Schematic Drawing

FLAME VELOCITY AND PEAK PRESSURE VERSUS PIPE LENGTH
TEST CONFIGURATION NO. 124 TO NO. 127

TEST NO.	SYMBOL	ϕ	VA, m/s	PD, kN/m^2
1434-A	O	1.1	4.6	4137
B	△	1.1	4.6	2068
C	□	1.1	4.6	690
D	◁	1.1	4.6	345

O   OPEN SYMBOLS – FLAME SENSORS
●   CLOSED SYMBOLS – PRESSURE SENSORS
ϕ EQUIVALENCE RATIO, GASOLINE/AIR
VA   INITIAL FLOW VELOCITY
PD   RUPTURE DISC PRESSURE RATING

Figure 8-2.

FLAME VELOCITY AND PEAK PRESSURE VERSUS PIPE LENGTH
TEST CONFIGURATION NO. 124 TO NO. 127

A, /s	PD, kN/m²
.6	4137
.6	2068
.6	690
.6	345

ME SENSORS
RESSURE SENSORS
GASOLINE/AIR
TY
RE RATING

DETONATION
PASSED THROUGH TEST
ASSEMBLY ON ALL TESTS

PRESSURE PULSE
PASSED THROUGH TEST
ASSEMBLY ON ALL TESTS

PEAK PRESSURE, kN/m²

4000
2000
1000
800
600
400
200
100

F62, P62
F63, P63
F71
F72
F81, P81
F85, P85
TWO TEES
ORIFICE PLATE
F101, P101
F104, P104

PIPE LENGTH, m

8   10   12   14   16   18   20   22   24   26   28

Figure 8-2. Pipe Tees and Rupture Disc In-Line Assembly
Test Results

8-3
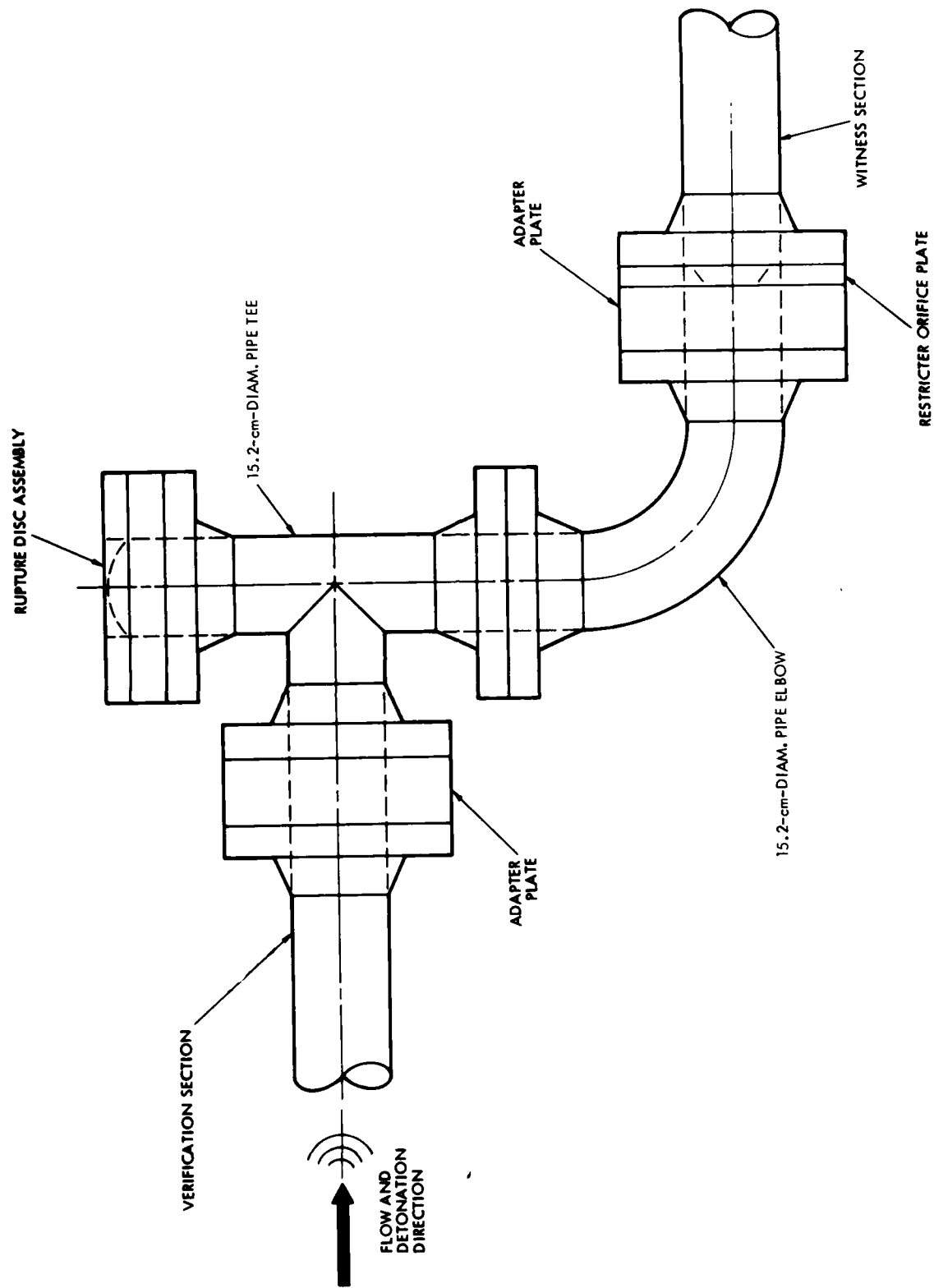
Figure 8-3. Pipe Tee, Rupture Disc Not-In-line, and Pipe Elbow Assembly Schematic Drawing

8-5

assembly, including the orifice plate, averaged 0.214 kN/m^2 (0.031 psid) at an average air flow velocity of 4.71 m/s (15.46 ft/s).

C.   SHAND AND JURS SPIRAL-WOUND, CRIMPED ALUMINUM RIBBON ARRESTER
      TEST ASSEMBLY

The spiral-wound, crimped aluminum ribbon core element was removed from a Shand and Jurs commercial flame arrester housing model No. 94/305/16/11. The 15.2-cm (6.0-in.) wide (L) aluminum ribbon had a crimp height (H) of 0.137 cm (0.054 in.), which gives a flow passage hydraulic diameter (D_h) of 0.114 cm (0.045 in.) and a length-to-diameter ratio (L/D_h) of 133. This core element was installed into a high-pressure housing made from an extra strong 30.5-cm- (12-in.-) diameter pipe 15.2 cm (6.0 in.) long. A mounting ring with a retainer grid was placed on each end of the housing as shown in Figure 8-5. The arrester test assembly consisted of a pipe tee, rupture disc not in line, and pipe elbow on the upstream side of a pair of 30.5- to 15.2-cm- (12-to 6-in.-) diameter concentric and eccentric extra-strong flanged pipe reducers. The arrester housing assembly was mounted between the two 30.5-cm- (12-in.-) diameter flanges as shown in Figure 8-6.

The Shand and Jurs arrester test configurations (No. 132 to No. 136) were subjected to nine stable detonations. There was no evidence in the witness section that detonation passed through the arrester. A low-level peak pressure pulse of around 290 kN/m^2 (42 psia) was measured at the downstream side in the witness section. In four tests, the rupture-disc pressure rating of the inlet pipe tee was increased in four steps from 690 to 4137 kN/m^2 (100 to 600 psid). This had no effect on the capability of the arrester in stopping the detonation, even when the highest rated disc failed to blow out. In the final test firing, the arrester housing was removed from the test assembly and the two 30.5-cm- (12-in.-) diameter flanges were bolted together. The rupture disc was blown out and the detonation passed through the test assembly, verifying the functional capability of the flame sensors in the witness section. The results of these tests are plotted in Figure 8-7.

The pre- and posttest-measured pressure drop across the arrester test assembly averaged 0.152 kN/m^2 (0.022 psid) at an average air flow velocity of 4.68 m/s (15.35 ft/s). Posttest inspection of the arrester showed a slight indentation of the retainer grid on the downstream side of the core element. The retainer grid was bowed downstream about 0.16 cm (0.063 in.) at the axial center line. There was a separation of the crimped ribbon layers near the outer perimeter of the core at the upstream interface with the mounting ring as shown in Figure 8-8. This separation continued through the full depth of the core in some places. It was probably caused by the radial component of the detonation wave reflected off the inner pipe wall or the inlet of the mounting ring.

TEST NO.	SYMBOL	ϕ	VA, m/s	PD, kN/m^2
1435-A	O	1.1	4.6	4137
B	△	1.1	4.6	2068
C	□	1.1	4.6	690
D	◁	1.1	4.6	345

O   OPEN SYMBOLS – FLAME SENSORS
●   CLOSED SYMBOLS – PRESSURE SENSORS
ϕ EQUIVALENCE RATIO, GASOLINE/AIR
VA   INITIAL FLOW VELOCITY
PD   RUPTURE DISC PRESSURE RATING

Figure 8-4. Pip
E1

FLAME VELOCITY AND PEAK PRESSURE VERSUS PIPE LENGTH
TEST CONFIGURATION NO. 128 TO NO. 131

DETONATION
PASSED THROUGH
TEST ASSEMBLY
ON ALL TESTS —

PRESSURE PULSE
PASSED THROUGH
TEST ASSEMBLY
ON ALL TESTS —

PEAK PRESSURE, kN/m^2

4000

2000

1000

800

600

400

200

100

F62, P62
F63, P63
F71
F72
F81, P81
F85, P85
TEE AND ELBOW
ORIFICE PLATE
F101, P101
F104, P104

8   10   12   14   16   18   20   22   24   26   28
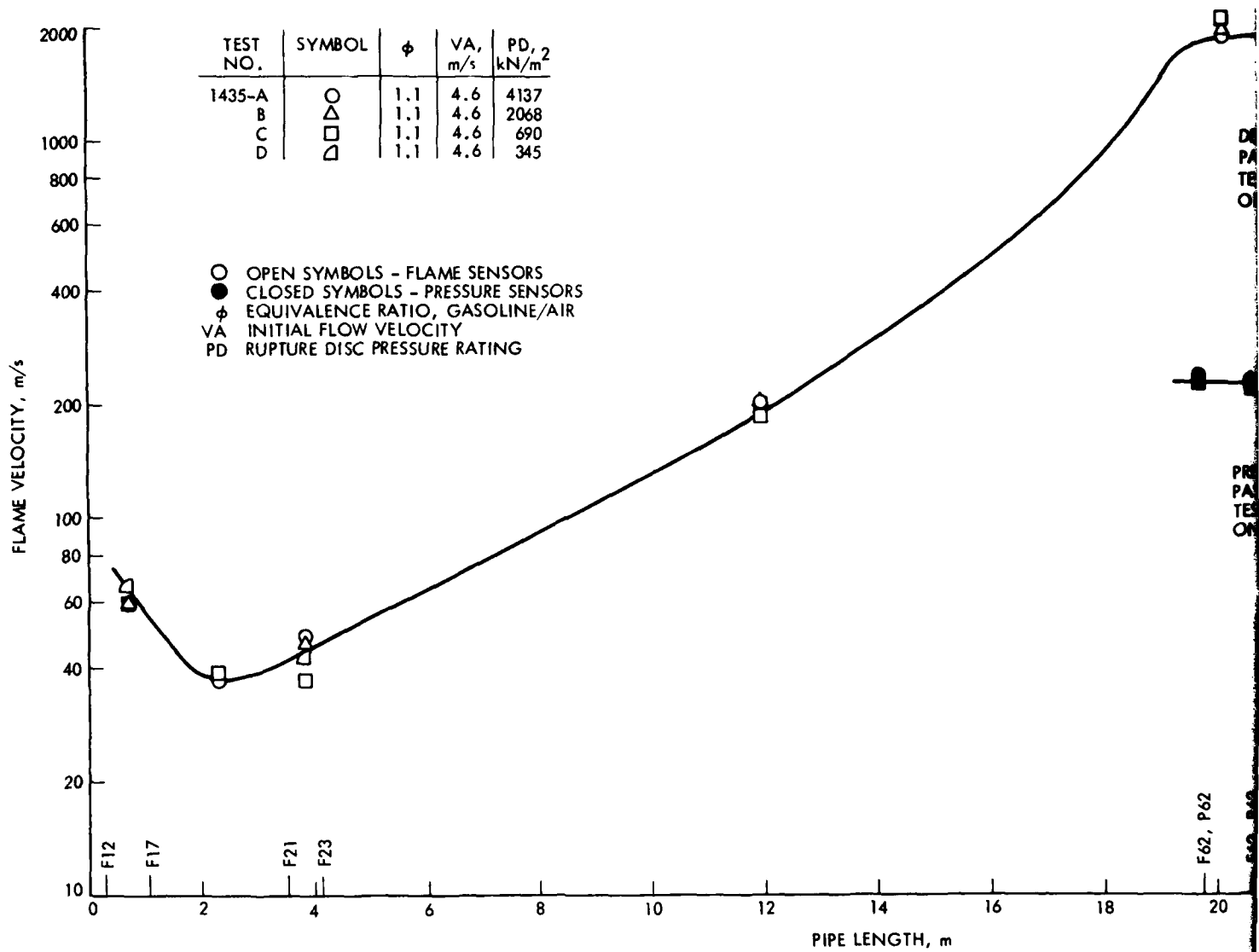
PIPE LENGTH, m

Figure 8-4. Pipe Tee Rupture Disc Not-In-line, and Pipe
Elbow Assembly Test Results

8-7

2
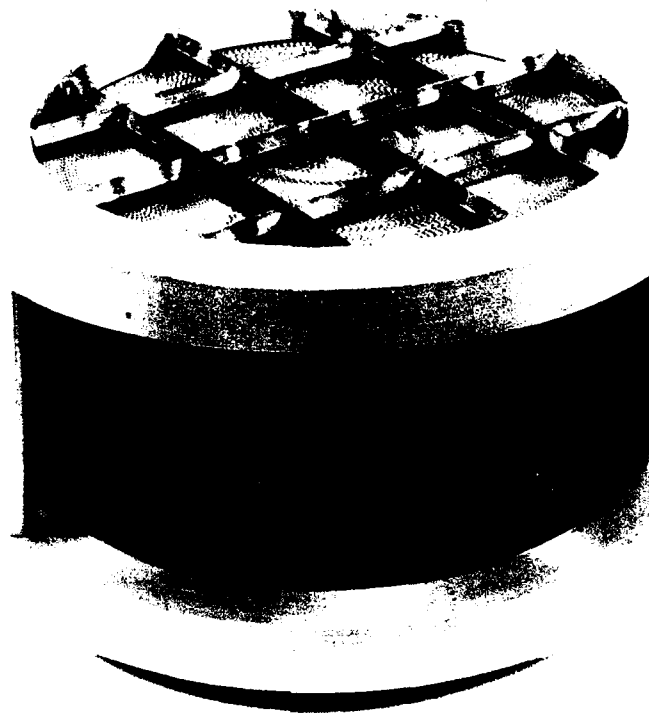
Figure 8-5. Shand and Jurs Spiral-Wound, Crimped Aluminum
Ribbon Arrester Assembly

D.   AMAL SPIRAL-WOUND, CRIMPED STAINLESS-STEEL RIBBON ARRESTER
      TEST ASSEMBLY

The Amal spiral-wound, crimped stainless-steel ribbon arrester core
element was a model No. 188/905/15/18/CN. The stainless-steel ribbon was
3.81 cm (1.5 in.) wide with a crimp height of 0.046 cm (0.018 in.), which
gives a flow passage hydraulic diameter of 0.038 cm (0.015 in.) and a
length-to-hydraulic-diameter ratio of 100. This core element was
installed in a high-pressure housing of 25.4-cm (10-in.) diameter by
3.8-cm (1.5-in.) length. Mounting rings with support grid, similar to
the Shand and Jurs arrester, were placed on each end. Figure 8-9 is
a photograph of this arrester assembly. The test assembly was also
similar, except that the extra-strong pipe reducers were 25.4 to 15.2 cm
(10 to 6 in.) in diameter to accommodate the smaller core size. A rupture-
disc pressure rating of 690 kN/m^2 (100 psid) was used. Figure 8-10
is a photograph of this test installation.
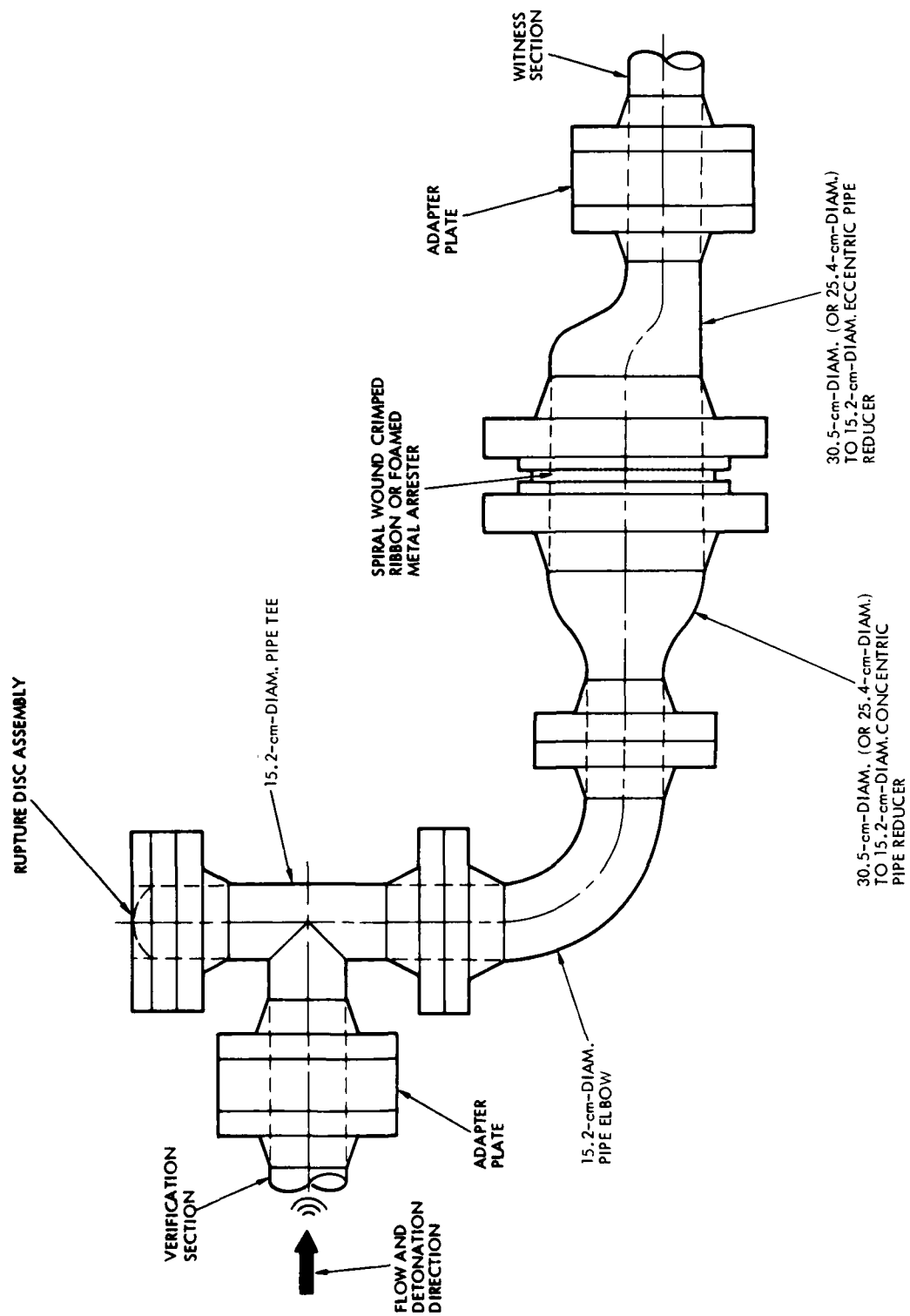
Figure 8-6. Spiral-Wound, Crimped Ribbon and Foamed Metal
Arresters Assembly Schematic Drawing

TEST NO.	SYMBOL	PD, kN/m^2
1436-A	○	690
B	□	
C	◇	
D	△	
E	◁	↓
1437-A	◁	690
B	◇	1379
C	◁	2068
D	○	4137
E	◁	4137 (CORE ELEMENT REMOVED)

$\phi = 1.1$
VA $= 4.6$ m/s

○ OPEN SYMBOL – FLAME SENSOR
● CLOSED SYMBOL – PRESSURE SENSOR
ϕ EQUIVALENCE RATIO, GASOLINE/AIR
VA INITIAL FLOW VELOCITY
PD RUPTURE DISC PRESSURE RATING

FLAME VELOCITY AND PEAK PRESSURE VERSUS PIPE LENGTH
TEST CONFIGURATION NO. 132 TO NO. 136

PD, 2
kN/m²
───
690

↓

690
1379
2068
4137
4137 (CORE ELEMENT REMOVED)

$\phi = 1.1$
VA = 4.6 m/s

FLAME SENSOR
PRESSURE SENSOR
IO, GASOLINE/AIR
LOCITY
SSURE RATING

DETONATION PASSED
THROUGH ARRESTER ONLY
WHEN CORE ELEMENT WAS
REMOVED ON THE LAST TEST

HIGH-LEVEL PRESSURE PULSE
PASSED THROUGH ARRESTER
ON LAST TEST

LOW-LEVEL PRESSURE
PULSE PASSED THROUGH
ARRESTER ON ALL TESTS

PEAK PRESSURE, kN/m²

4000

2000

1000
800
600

400

200

100

F62, P62
F63, P63
F71
F72
F81, P81
F85, P85
SHAND AND JURS
F101, P101
F104, P104

14   16   18   20   22   24   26   28

PIPE LENGTH, m

Figure 8-7. Shand and Jurs Spiral-Wound, Crimped Aluminum
Ribbon Arrester Assembly Test Results

8-11
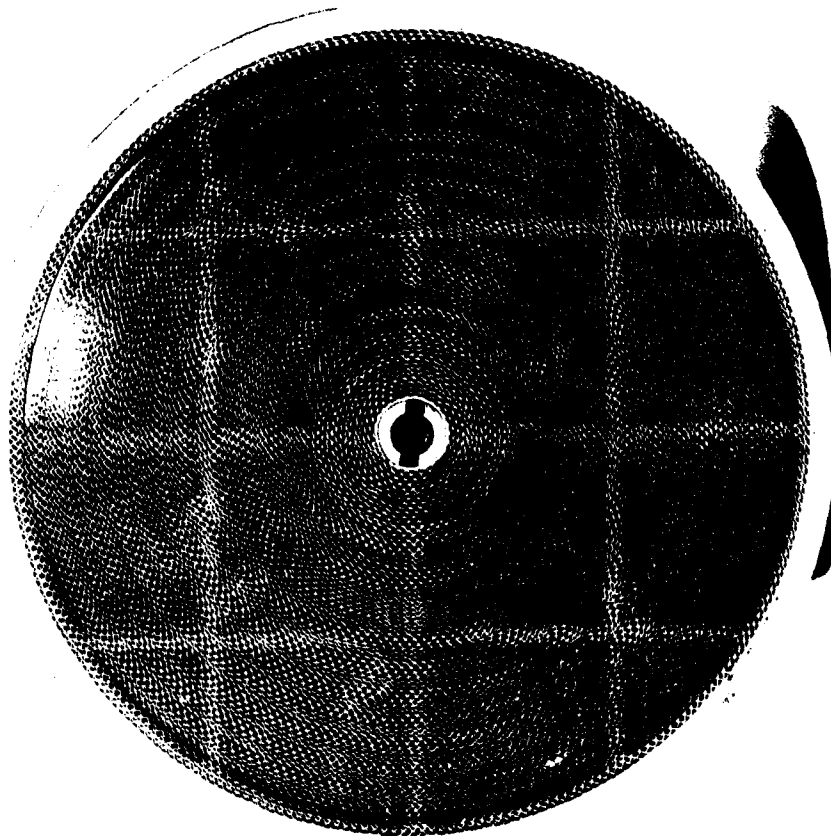
Figure 8-8. Shand and Jurs Spiral Wound, Crimped Aluminum
Ribbon Arrester Core Posttest Showing Ribbon
Separation

The Amal arrester test configuration (No. 137) was successful
in stopping the detonation in only the first of four test firings.
The rupture disc was blown out on all tests. Flame velocity recorded
in the witness section was only 600 m/s (1968 ft/s) in the last three
tests. When the detonation was stopped, the peak pressure pulse down-
stream of the arrester measured about 360 kN/m^2 (52 psia), but increased
to 600 kN/m^2 (87 psia) when the flame penetrated. A plot of the results
of these tests is shown in Figure 8-11.

The pre- and posttest pressure drop across the Amal arrester test
assembly did not vary appreciably. It averaged 0.428 kN/m^2 (0.062 psid)
for an average air flow velocity of 4.78 m/s (15.68 ft/s). Posttest
inspection of the core element showed no evidence of damage that could
have caused the failure. The retainer grid was bowed downstream 0.64 cm
(0.25 in.) at the axial centerline, indicating that some distortion had
occurred to the core element under the detonation wave loading, but
apparently the core element had returned to its original shape.

8-13
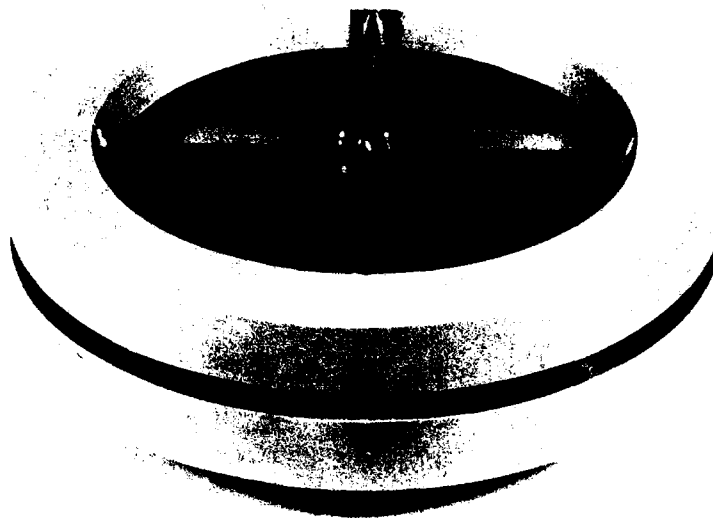
Figure 8-9. Amal Spiral-Wound, Crimped Stainless-Steel
Ribbon Arrester Assembly

E.   WHESSOE FOAMED METAL ARRESTER TEST ASSEMBLY

The Retimet 80-grade foamed nickel-chrome alloy core element was
removed from a prototype Whessoe arrester and installed into a high-
pressure housing 25.4-cm (10-in.) diameter by 1.3-cm (0.5-in.) length.
Mounting rings with support grids were placed on each side. Figure 8-12
is a photograph of the arrester components before assembly. This arrester
assembly was mounted between the same pipe reducers used for the Amal
arrester tests. A rupture-disc pressure rating of 690 kN/m^2 (100 psid)
was used.

The Whessoe arrester test configuration (No. 138) was successful in
stopping the detonation in three tests. The rupture disc was blown out
on all tests. Pre- and posttest pressure drop measured across the arrester
test assembly averaged 0.241 kN/m^2 (0.035 psid) at an average air flow
velocity of 4.74 m/s (15.54 ft/s). After the third test, the measured
pressure loss dropped to 0.110 kN/m^2 (0.016 psid). Posttest inspection
revealed that a section of the Retimet foamed metal core element had been
extruded through the downstream retainer grid, leaving a large hole as
shown in Figure 8-13.
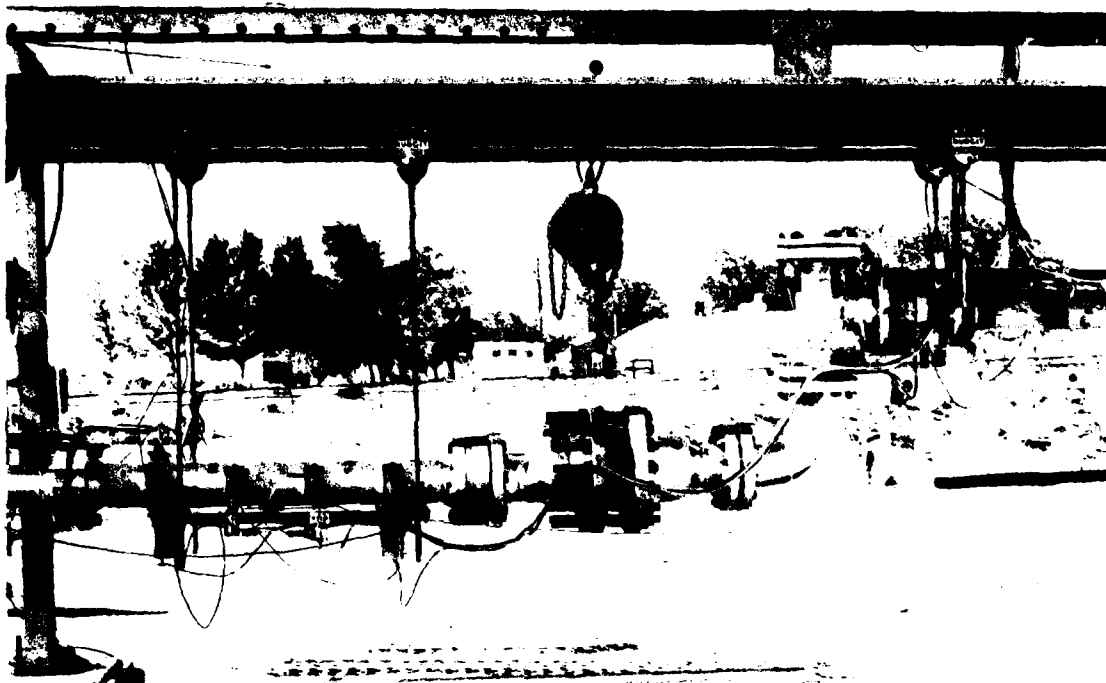
Figure 8-10. Amal Spiral-Wound, Crimped Stainless-Steel
Ribbon Arrester Test Installation

The 80-grade foamed metal was replaced in the housing with the
alternate 45-grade foamed metal and reinstalled into the arrester test
configuration (No. 139). One additional test firing was made, but this
arrester failed to stop the detonation. The test results presented
in Figure 8-14 show a large drop in flame speed to 45 m/s (148 ft/s) at
the downstream side of the arrester after penetration. A low-level peak
pressure pulse ranging from 250 to 470 kN/m^2 (36 to 68 psia) was measured
in the witness section on all test firings. Pre- and posttest pressure
loss measured across the 45-grade foamed-metal arrester test assembly was
0.130 kN/m^2 (0.019 psid) at an air-flow velocity of 4.78 m/s (15.68 ft/s).
The posttest inspection showed no damage to this arrester core element.

F.   WATER-TRAP ARRESTER TEST ASSEMBLY

The water-trap arrester test assembly was installed into the
test section. This arrester vessel was made using 45.7-cm- (18.0-in.-)
diameter extra-strong piping 91.4 cm (36 in.) long with a pipe cap
on the lower end and a flanged cover containing a blowout port on the
top. There were two 15.2-cm- (6.0-in.-) diameter flanged side ports.
One of these ports contained a pipe elbow inside the vessel with a
30.5- to 15.2-cm- (12- to 6-in.-) diameter concentric pipe reducer

8-15

directed towards the bottom. The lower end of the reducer had three rows of 2.54-cm- (1.0-in.-) diameter holes drilled through the wall so that the assembly functioned as a bell-mouth diffuser. A schematic drawing of this arrester assembly is shown in Figure 8-15. The inlet piping consisted of a pipe tee, not-in-line rupture disc, and a pipe elbow. A similar reversed assembly was used at the arrester exit. A third rupture-disc assembly was installed on the blow-out port of the water-trap vessel cover. All rupture discs had a burst pressure rating of 690 kN/m^2 (100 psid). Water was added to the arrester vessel until the inlet piping and top row of holes in the diffuser bell were immersed 15.2 cm (6.0 in.) below the surface. A photograph of the test installation is shown in Figure 8-16.

Five test firings were made with the water-trap test configuration (No. 140), and the detonation was stopped for all tests. The upstream rupture disc on the inlet pipe tee was blown out in each firing. The downstream rupture discs on the arrester cover and exit pipe tee remained intact. There was no measurable peak-pressure pulse passing through the witness section in any of these firings. Water level in the arrester was reduced by 0.64 to 1.91 cm (1/4 to 3/4 in.) during testing and was replaced before the next firing. This amounts to 1/2 to 2 liters of water loss that can be related to the length of air-flow run time before each test firing. There was no evidence of water in the downstream piping or at the shock tube exit, so the loss had to be due to evaporation and convection caused by air flow. Pre- and posttest pressure loss measured across the water-trap arrester test assembly averaged 1.655 kN/m^2 (0.240 psid) at an average air-flow velocity of 4.66 m/s (15.29 ft/s).

In the sixth test, all the water was drained from the arrester vessel before firing. The detonation passed through the arrester test configuration (No. 141), as shown in the plot of these test results in Figure 8-17. Flame velocity in the witness section was measured at 950 m/s (3117 ft/s) and a peak-pressure pulse at around 900 kN/m^2 (130 psia) was experienced. All the rupture discs were blown out in this last test firing. Posttest inspection showed no damage to the arrester test assembly.

G.   VERTICAL BED OF ALUMINUM BALLAST RINGS ARRESTER
     TEST ASSEMBLY

The vertical bed arrester test assembly utilized the water-trap vessel for the lower housing. The vessel was disconnected from the inlet pipe elbow and reversed 180 deg, exchanging the inlet and outlet ports. A blind flange was used to close off the unused outlet port. The vessel cover was removed and a 45.7-cm- (18-in.-) diameter flange pipe spool section, 91.4 cm (36 in.) long, was installed on top of the lower housing. The outlet pipe elbow and pipe tee were inverted and relocated to an outlet port on the downstream side of the spool section. A support grid ring covered with heavy wire mesh was installed into the housing assembly just above the inlet port. The internal volume between the inlet port and the outlet port, a distance of 63.5 cm (25 in.), was filled with 2.54-cm- (1.0-in.-) diameter by 2.54-cm- (1.0-in.-) long aluminum Ballast rings (identical in conformation to Pall rings) obtained

FLAME VELOCITY AND PEAK PRESSURE VERSUS PIPE LENGTH
TEST CONFIGURATION NO. 137
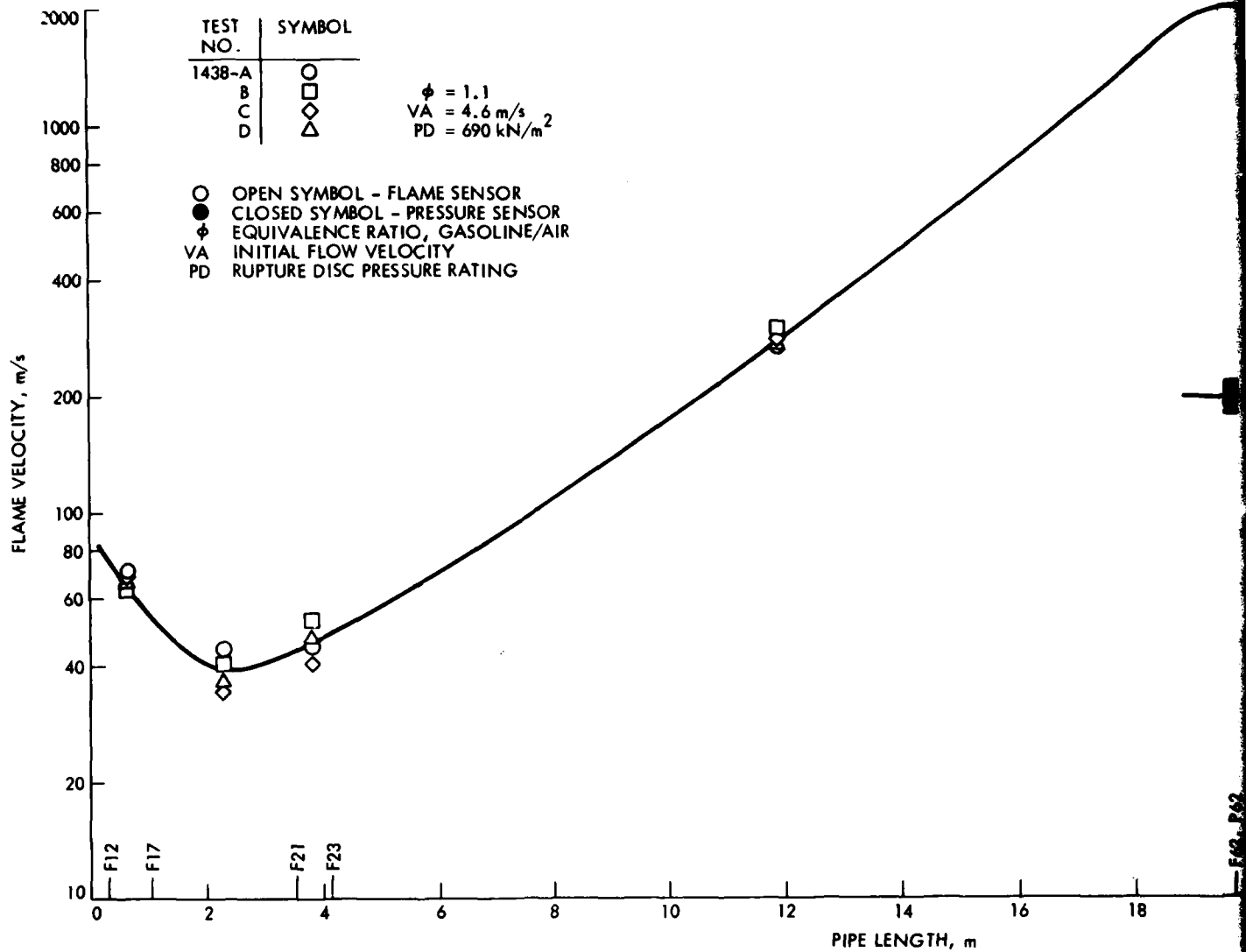
Figure 8-11.

FLAME VELOCITY AND PEAK PRESSURE VERSUS PIPE LENGTH
TEST CONFIGURATION NO. 137
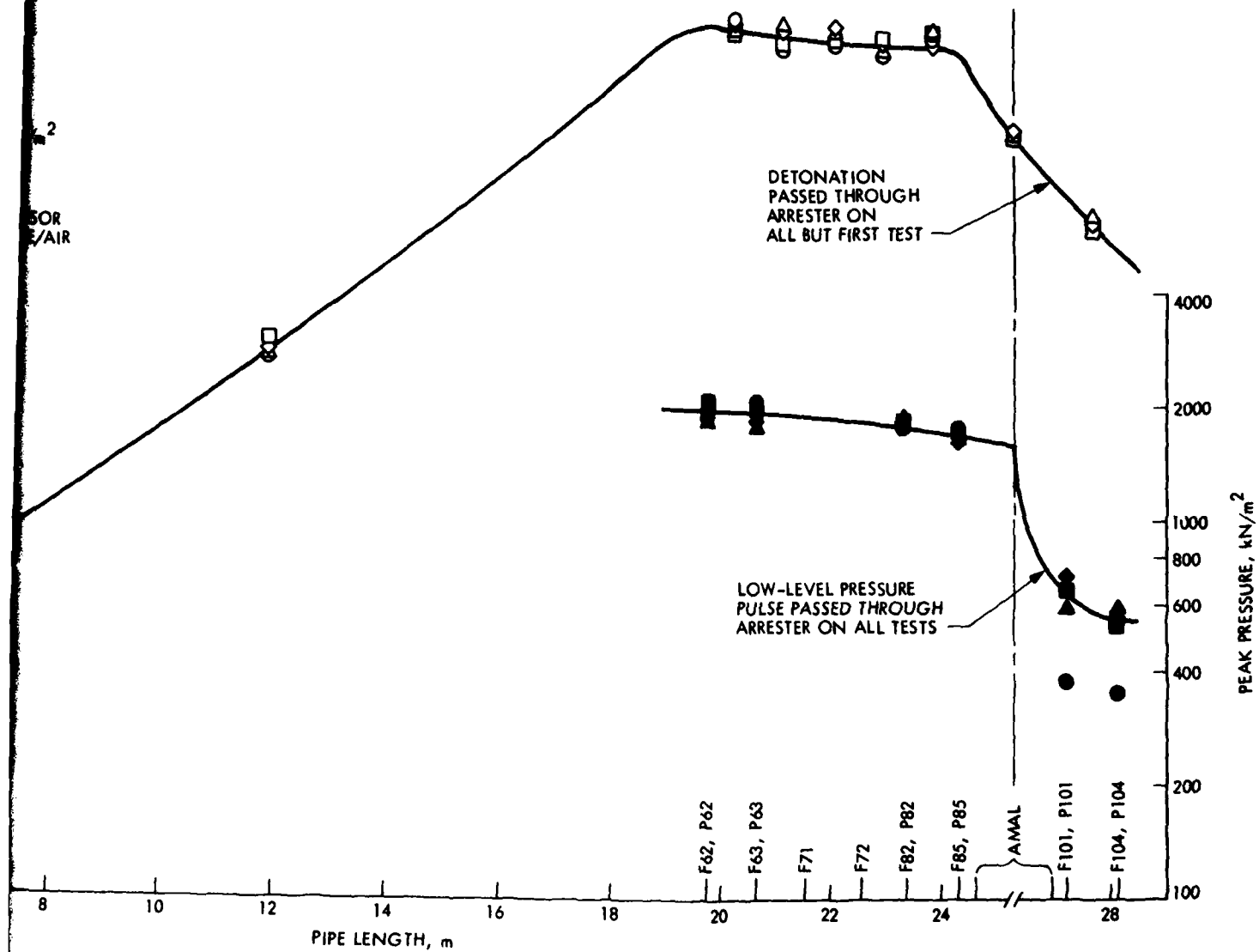
Figure 8-11.   Amal Spiral-Wound, Grimped Stainless-Steel
Ribbon Arrester Assembly Test Results

8-17

2
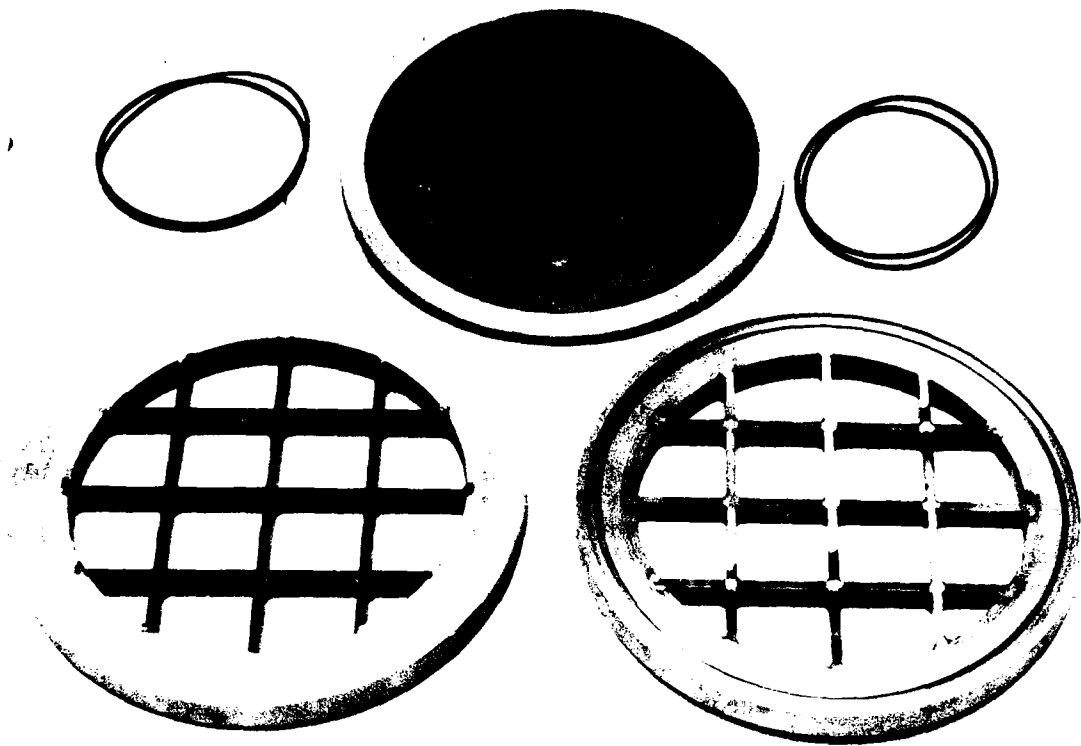
Figure 8-12. Whessoe Foamed Metal Arrester Test Assembly Exploded View
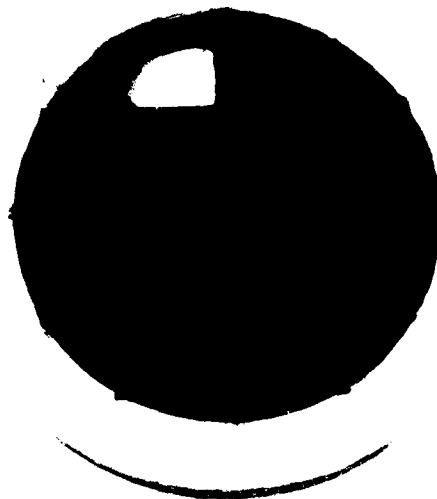
Figure 8-13. Whessoe Foamed Metal Arrester
Test Assembly Posttest Showing
Damaged Core

from Glitsch, Inc. A second wire-mesh-covered grid ring was installed on top of the bed of rings and held securely in place. The vessel cover, with a rupture disc, was installed on the top of the spool section. A water spray injector for the top of the bed was installed, but was not plumbed in. Figure 8-18 is a schematic drawing of the vertical bed arrester test assembly and a photograph of the test installation is shown in Figure 8-19.

Five test firings were made with the vertical bed arrester test configuration (No. 142); 690 kN/m^2 (100 psid) rupture discs were installed on all blow-out ports. The detonation was arrested in all tests and only the rupture disc on the inlet tee was blown out. There were no measurable peak-pressure pulses passing through the witness section. A plot of these test results is shown in Figure 8-20.

Pre- and posttest pressure loss measured across the arrester test assembly averaged 0.050 kN/m^2 (0.007 psid) at an average air-flow velocity of 4.64 m/s (15.23 ft/s). Posttest inspection of the arrester assembly revealed compaction of the bed due to distortion of the Ballast rings. This was probably caused by the fact that the lower support grid ring was not restrained in the vertical direction. The incoming detonation pressure wave forced the bottom grid ring up, crushing the bed of rings against the top restrained grid ring. Both support grid rings were to be restrained against any vertical forces in later tests.

The repeated success with the dry bed of Ballast rings in arresting the detonation eliminated the need for water irrigation that would have been used to increase the available heat sink. Therefore, the irrigated bed configuration was deleted from the test series.

H. LINDE HYDRAULIC BACK-PRESSURE VALVE ARRESTER TEST ASSEMBLY

The Linde Model No. H-20 hydraulic back-pressure valve was a standard commercial unit, that had to be modified slightly by removing a 7.6-cm- (3.0-in.-) diameter one-way check valve on the inlet piping and the enlargement of the inlet port to a 10.2-cm- (4.0-in.-) diameter nominal pipe size. Two 15.2- to 10.2-cm- (6.0- to 4.0-in.-) diameter pipe reducer elbows were used to adapt this arrester to the 15.2-cm- (6.0-in.-) diameter pipe tees on the inlet and outlet piping as shown on the schematic drawing in Figure 8-21. The rupture discs had to be installed on the vertically-down legs of both the inlet and outlet pipe tees. The Linde arrester was filled with water up to the gaging port. This placed the lower end of the 10.2-cm- (4.0-in.-) diameter inlet port approximately 15.2 cm (6.0 in.) under the water in the two parallel 20.2-cm- (8.0-in.-) diameter vertical pipe chambers. A photograph of this test installation is shown in Figure 8-22.

Five test firings were made on the Linde arrester test configuration (No. 143) with 690 kN/m^2 (100 psid) rupture discs installed on the two blow-out ports. The detonation was arrested for all tests. Only the rupture disc on the inlet pipe tee was blown out. There was no measurable peak pressure pulse passing through the witness section. These test results are plotted in Figure 8-23. The water level loss

FLAME VELOCITY AND PEAK PRESSURE VERSUS PIPE LENGTH
TEST CONFIGURATION NO. 138 AND NO. 139

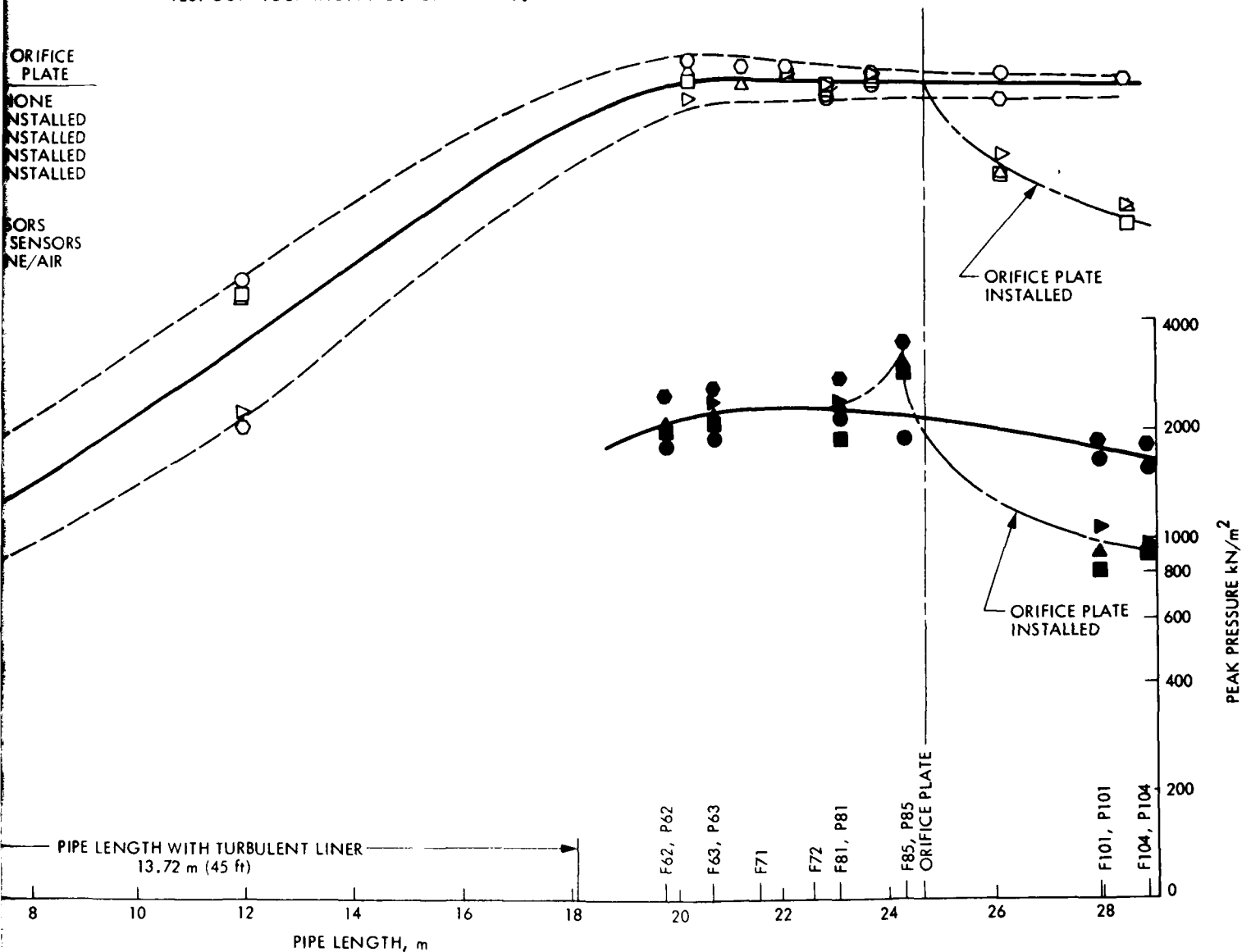| TEST NO.	SYMBOL	GRADE
1439-A	○	80
B	□	80
C	◇	80
D	△	45

ϕ = 1.1
VA = 4.6 m/s
PD = 690 kN/m^2

○ OPEN SYMBOL – FLAME SENSOR
● CLOSED SYMBOL – PRESSURE SENSOR
ϕ EQUIVALENCE RATIO, GASOLINE/AIR
VA INITIAL FLOW VELOCITY
PD RUPTURE DISC PRESSURE RATING

DETON
THRO
ONLY

LOW-LEV
PULSE PA
ARRESTE

F12 F17 F21 F23 F62, P62 F63, P63

FLAME VELOCITY, m/s

PIPE LENGTH, m

Figure 8-14. Whessoe Foam

Figure 8-14. Whessoe Foamed Metal Arrester Assembly Test Results

WITNESS SECTION

ADAPTER PLATE

15.2-cm-DIAM. PIPE ELBOW

15.2-cm-DIAM. PIPE TEE

LIQUID LEVEL SIGHT GAGE

DRAIN VALVE

RUPTURE DISC ASSEMBLIES

15.2-cm-DIAM. PIPE TEE

WATER LEVEL GAGING VALVE

45.7-cm-DIAM. PIPE TRAP

ADAPTER PLATE

15.2-cm-DIAM. PIPE ELBOW

VERIFICATION SECTION

FLOW DIRECTION
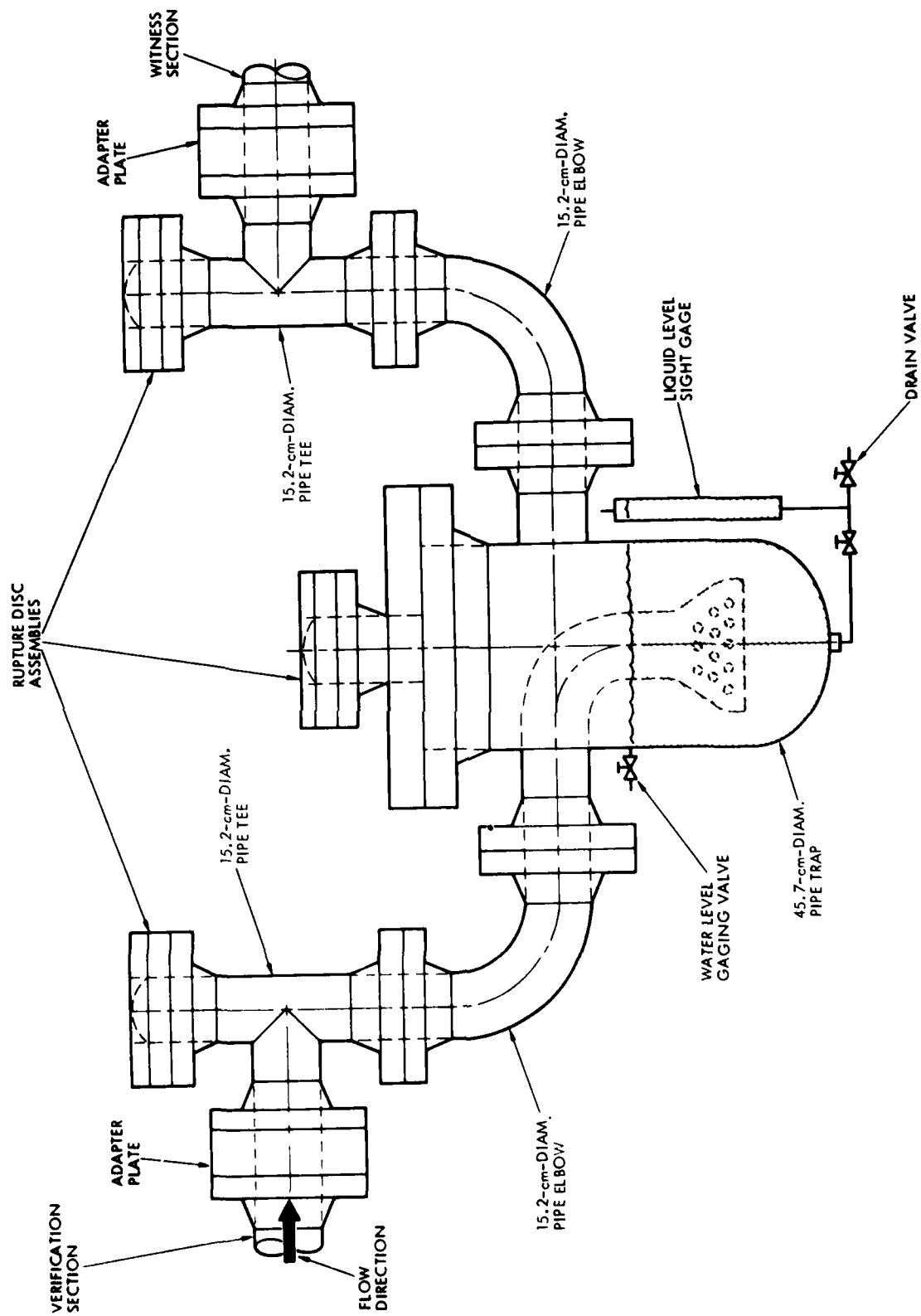
Figure 8-15. Water-Trap Arrester Test Assembly Schematic Drawing
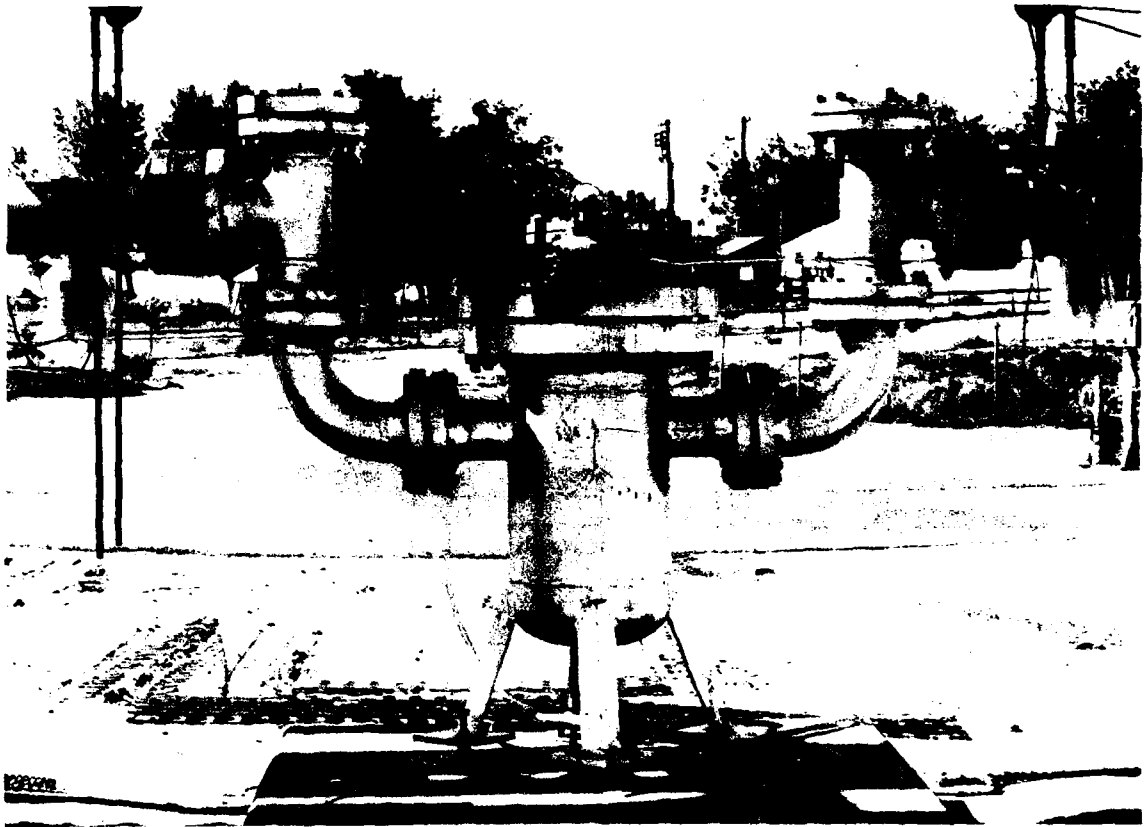
Figure 8-16. Water-Trap Arrester Test Installation

ranged from 0.63 to 4.45 cm (1/4 to 1 3/4 in.), depending on the length of run-in time. The volume of water loss was equivalent to 1/2 to 3 liters and was replaced after each test. No visible quantity of water was detected in the downstream piping or at the exit of the shock tube. Pre- and posttest pressure loss across the arrester averaged 2.027 kN/m^2 (0.294 psid) at an average air-flow velocity of 4.65 m/s (15.27 ft/s).

The water was removed from the Linde arrester through a drain valve, and a sixth test firing made. The detonation was arrested and only the inlet rupture disc was blown out. This was an unexpected turn of events that required further investigation. The drain valve, along with the mounting pipe reducer bushing, was removed for closer inspection. A small amount of water remaining in the bottom of the arrester was drained out. The drain valve was reinstalled and two more test firings were made with the dry Linde arrester configuration (No. 144) with 690 kN/m^2 (100 psid) rupture discs installed. The detonation was not arrested and both the inlet and outlet rupture discs were blown out.

In trying to duplicate the previous anomaly, the arrester was again filled with water up to the gaging port. Another test firing was made

8-24
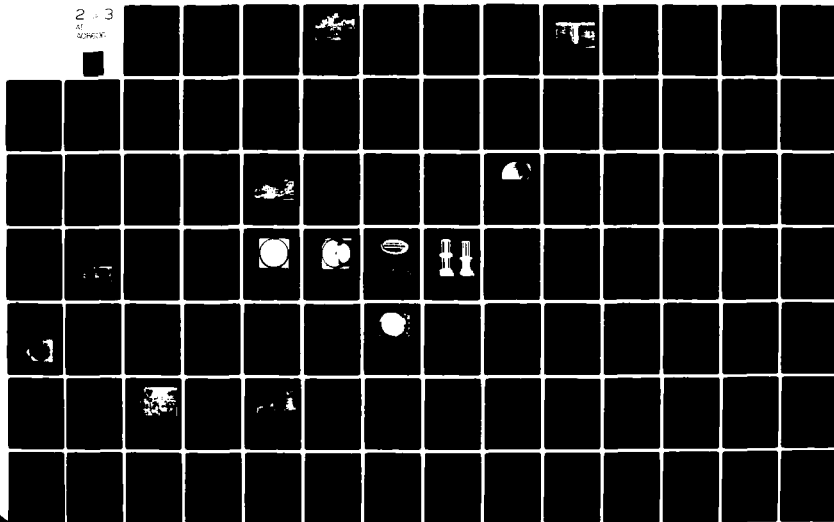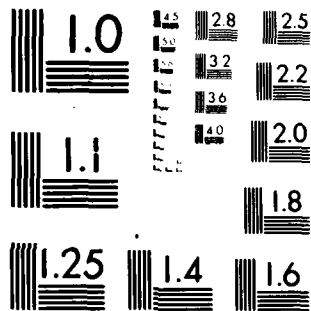
MICROCOPY RESOLUTION TEST CHART

NATIONAL BUREAU OF STANDARDS 1963 A
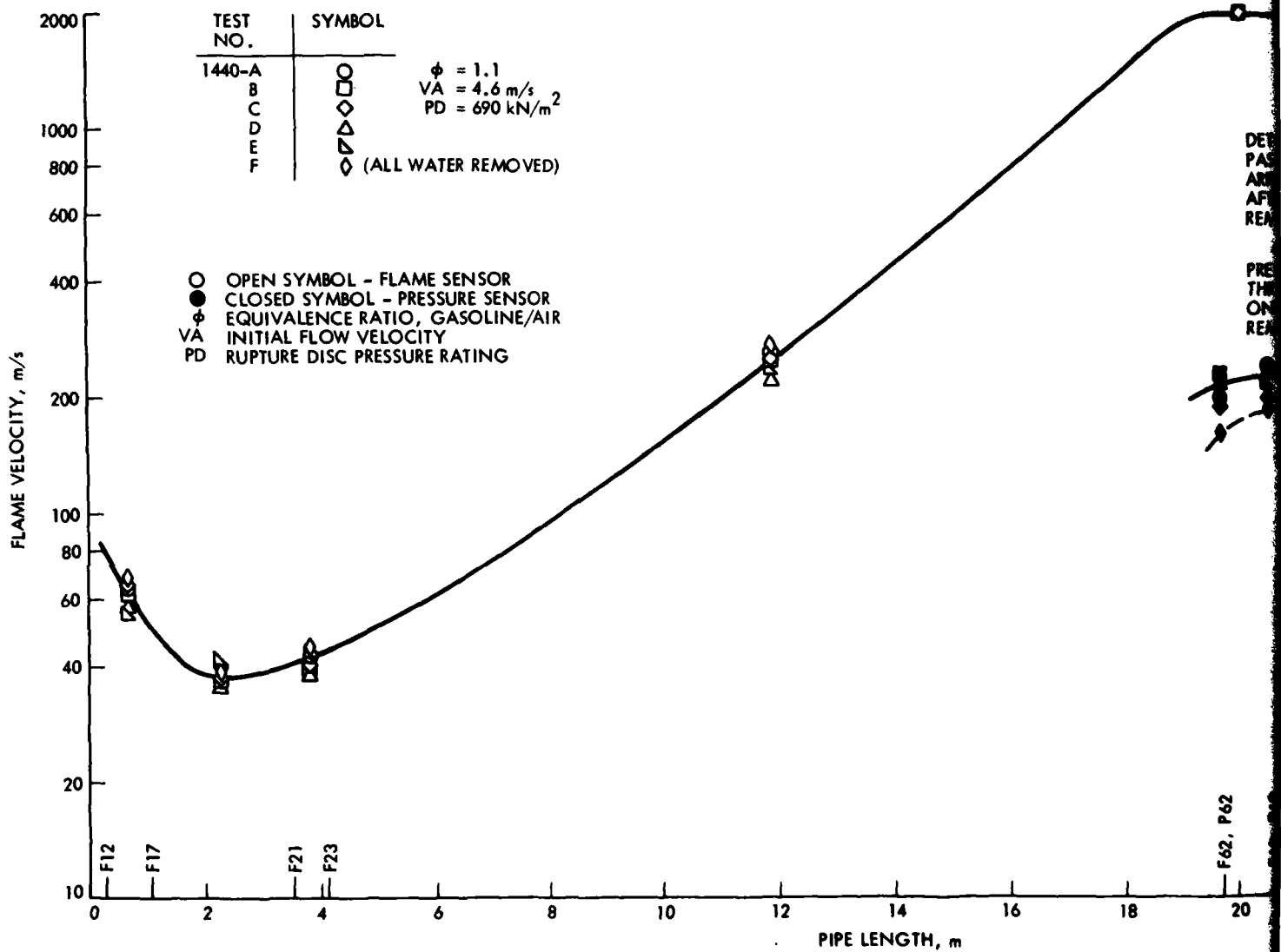
FLAME VELOCITY AND PEAK PRESSURE VERSUS PIPE LENGTH
TEST CONFIGURATION NO. 140 AND NO. 141

Figure 8-17.

FLAME VELOCITY AND PEAK PRESSURE VERSUS PIPE LENGTH
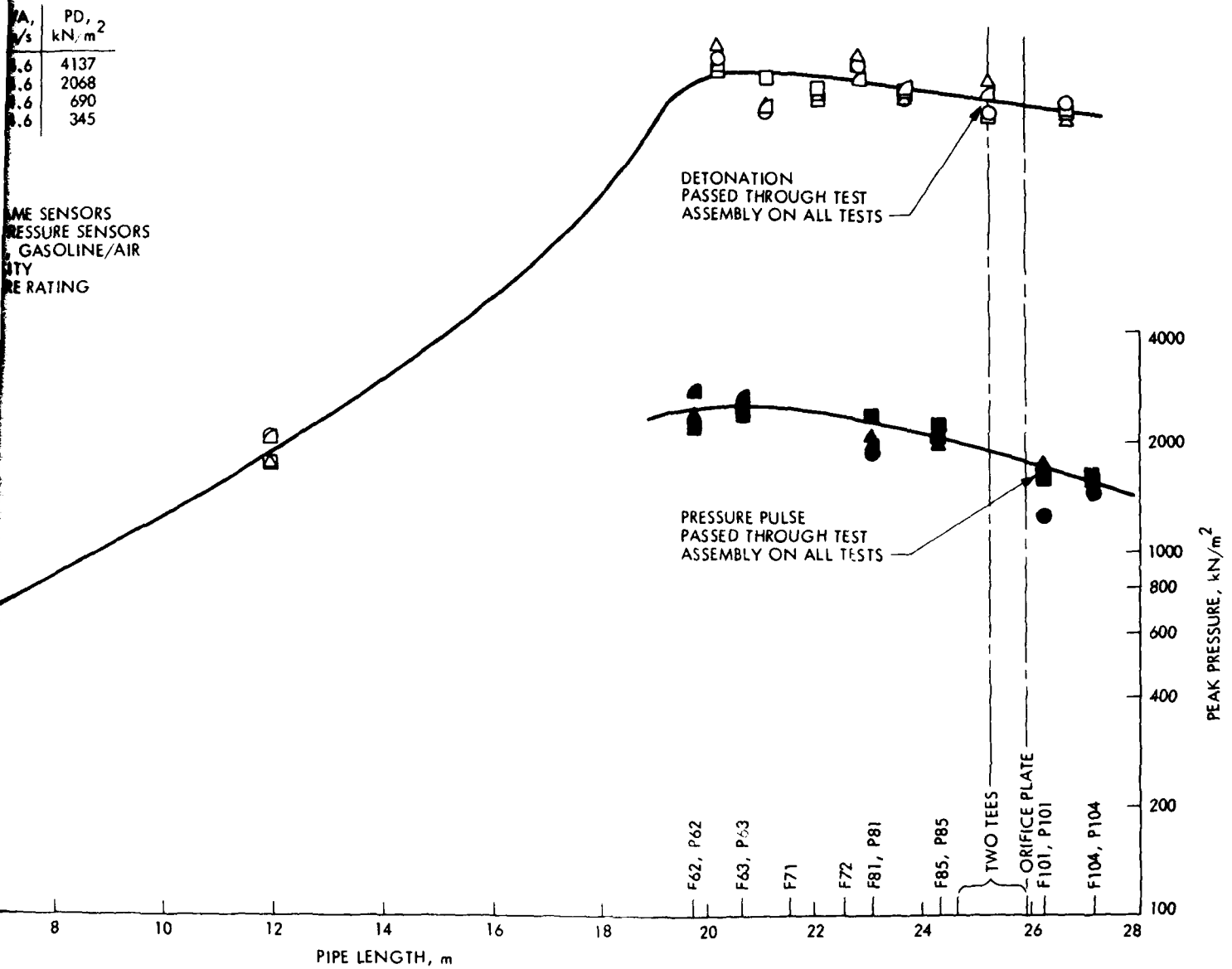TEST CONFIGURATION NO. 140 AND NO. 141

1.1
4.6 m/s
690 kN/m^2

(REMOVED)

SOR
SENSOR
OLINE/AIR

NG

DETONATION
PASSED THROUGH
ARRESTER ONLY
AFTER WATER WAS
REMOVED ON LAST TEST

PRESSURE PULSE PASSED
THROUGH ARRESTER
ONLY AFTER WATER WAS
REMOVED ON LAST TEST

PEAK PRESSURE, kN/m^2

4000

2000

1000
800

600

400

200

100

F62, P62
F63, P63
F71
F72
F82, P82
F85, P85
WATER TRAP
F101, P101
F104, P104

8   10   12   14   16   18   20   22   24   28   30

PIPE LENGTH, m
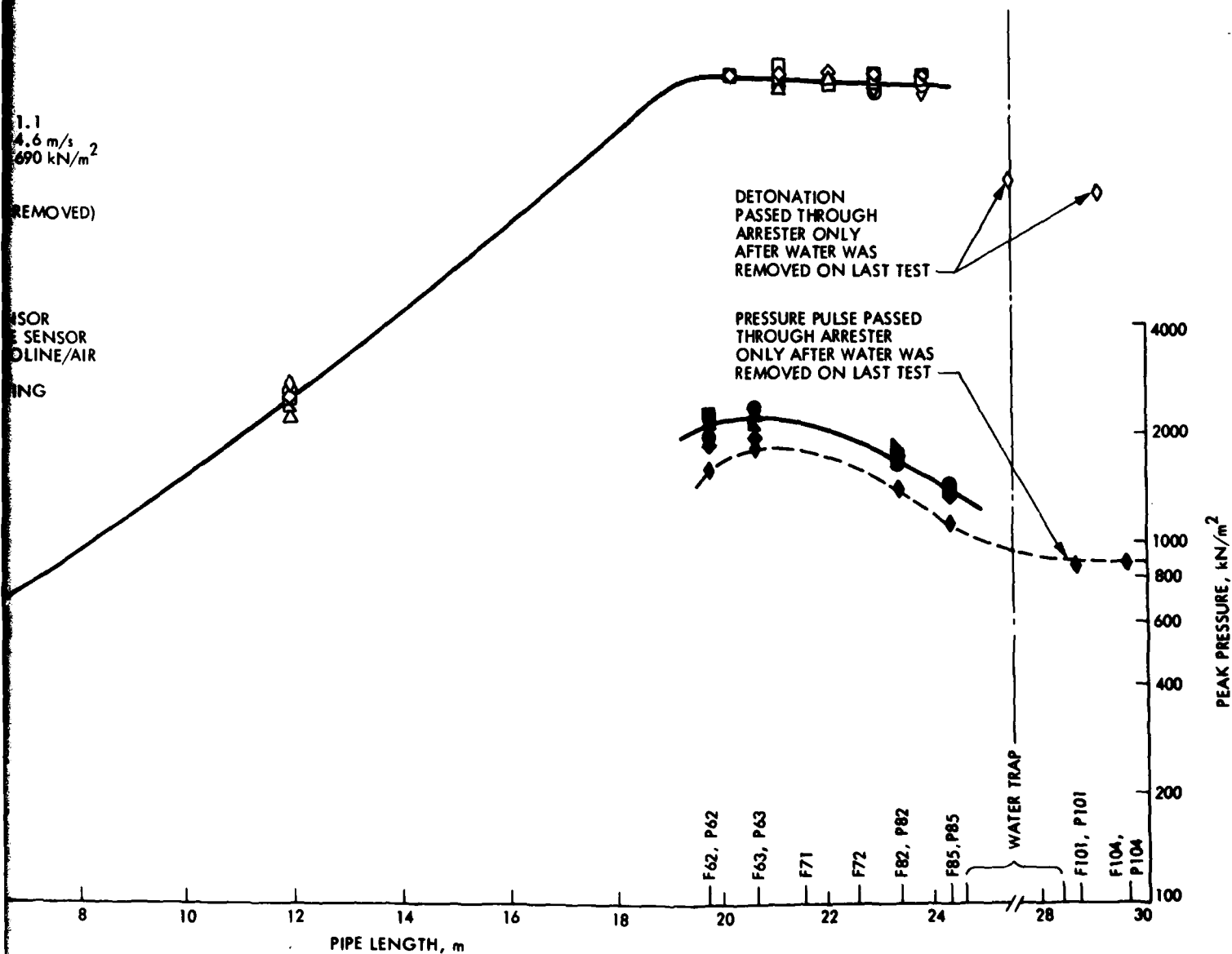
Figure 8-17.   Water-Trap Arrester Assembly Test Results

8-25
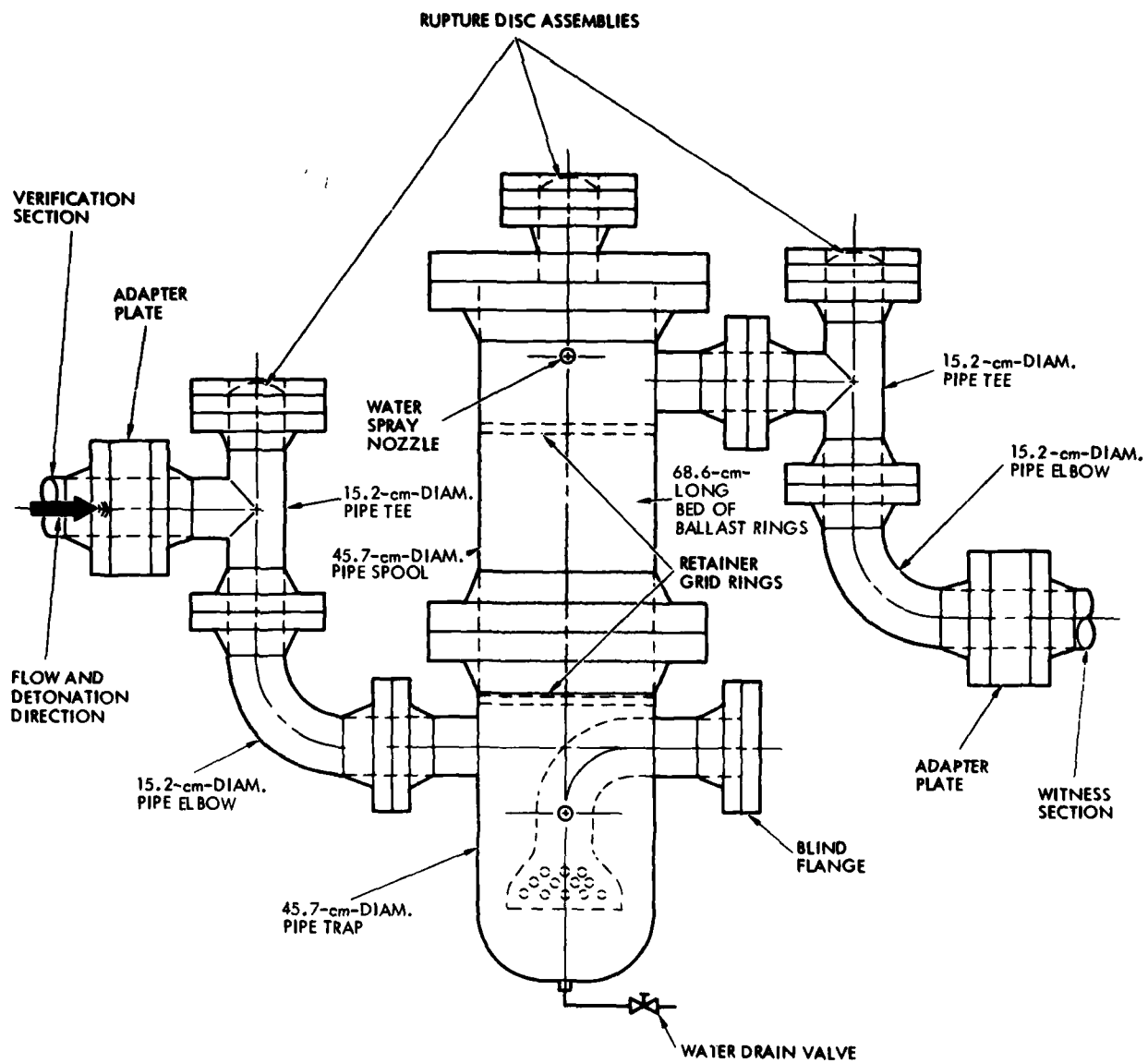
Figure 8-18.   Vertical Bed of Ballast Rings Arrester
Test Assembly Schematic Diagram
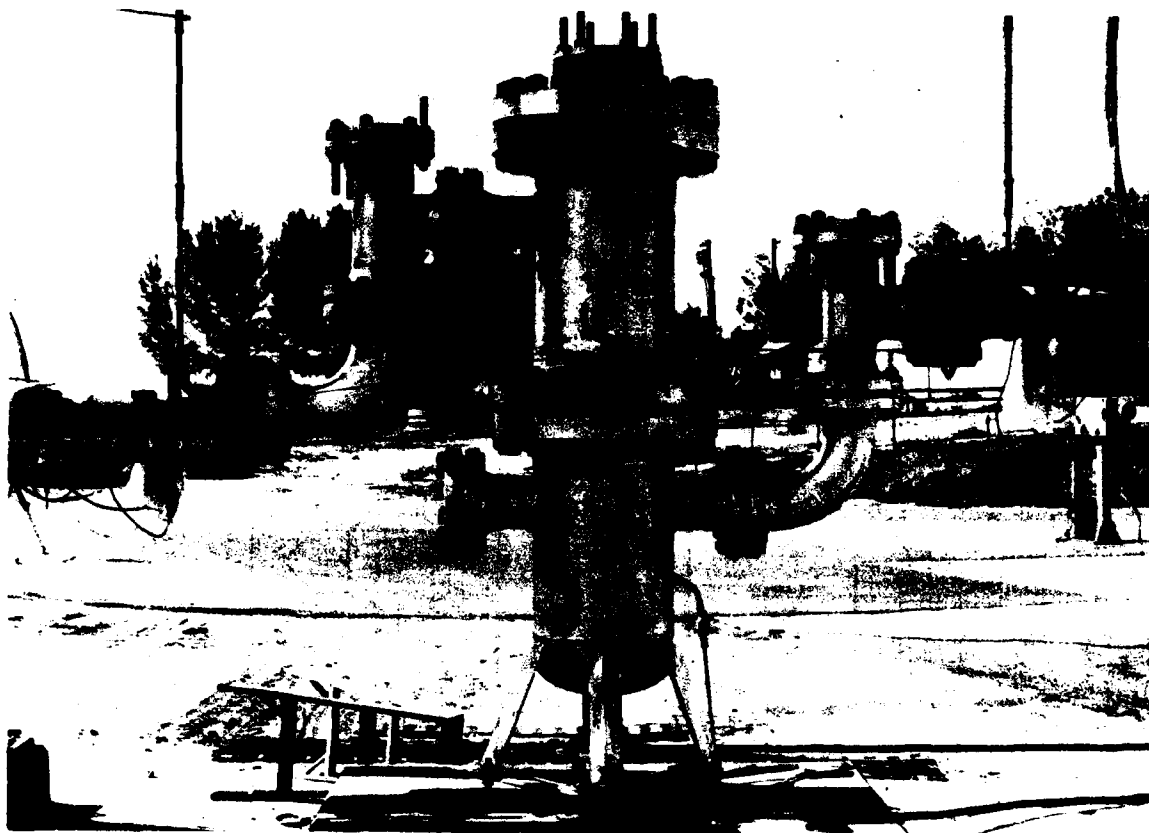
Figure 8-19. Vertical Bed of Ballast Rings Arrester Test Installation

where the detonation was arrested and only the inlet rupture disc was blown out. At this point, the water was removed from the arrester through the drain valve, just as in the previous test series. A final test firing was made with the dry arrester. The detonation was not arrested and both rupture discs were blown out. It is believed that the drain valve became plugged with some foreign object in the first attempt to remove the water, and this small amount of water caused the unexpected quenching of the detonation in the supposedly dry test firing. Pressure loss across the dry arrester averaged 0.407 kN/m^2 (0.059 psid) at an average air-flow velocity of 4.63 m/s (15.2 ft/s). Posttest inspection showed no damage to the Linde arrester.

FLAME VELOCITY AND PEAK PRESSURE VERSUS PIPE LENGTH
TEST CONFIGURATION NO. 142
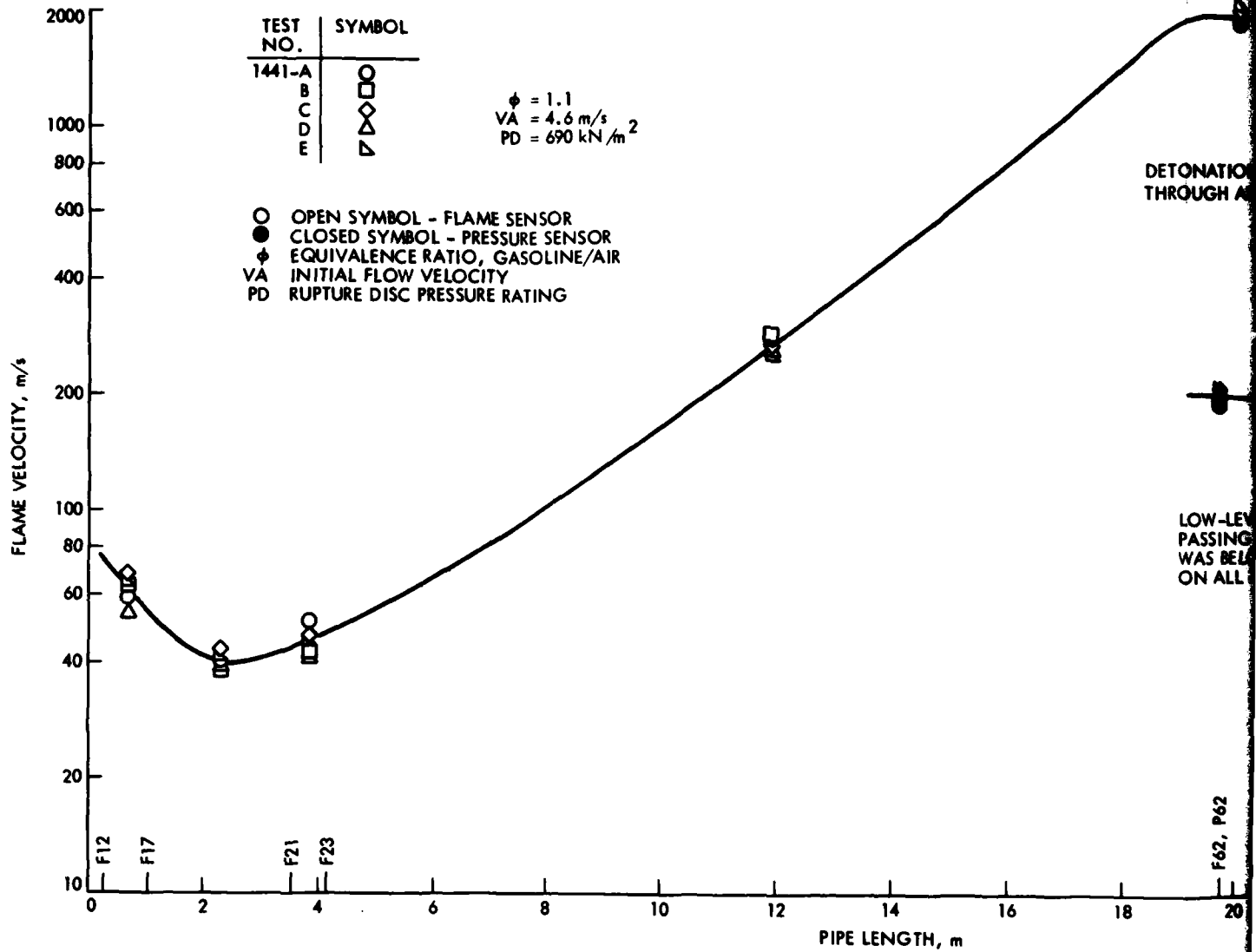
TEST NO.	SYMBOL
1441-A	○
B	□
C	◇
D	△
E	▷

ϕ = 1.1
VA = 4.6 m/s
PD = 690 kN/m^2

○ OPEN SYMBOL – FLAME SENSOR
● CLOSED SYMBOL – PRESSURE SENSOR
φ EQUIVALENCE RATIO, GASOLINE/AIR
VA INITIAL FLOW VELOCITY
PD RUPTURE DISC PRESSURE RATING

DETONATIO
THROUGH A

LOW-LEV
PASSING
WAS BEL
ON ALL

FLAME VELOCITY, m/s

F12   F17   F21   F23   F62, P62

PIPE LENGTH, m

Figure 8-2

FLAME VELOCITY AND PEAK PRESSURE VERSUS PIPE LENGTH
TEST CONFIGURATION NO. 142

ϕ = 1.1
VA = 4.6 m/s
PD = 690 kN/m^2

DETONATION DID NOT PASS
THROUGH ARRESTER ON ANY TEST

– FLAME SENSOR
L – PRESSURE SENSOR
ATIO, GASOLINE/AIR
VELOCITY
RESSURE RATING

LOW-LEVEL PRESSURE PULSE
PASSING THROUGH ARRESTER
WAS BELOW SENSOR RANGE
ON ALL TESTS

PEAK PRESSURE, kN/m^2

F62, P62
F63, P63
F71
F72
F82, P82
F85, P85
VERTICAL BED
F101, P101
F104, P104

PIPE LENGTH, m
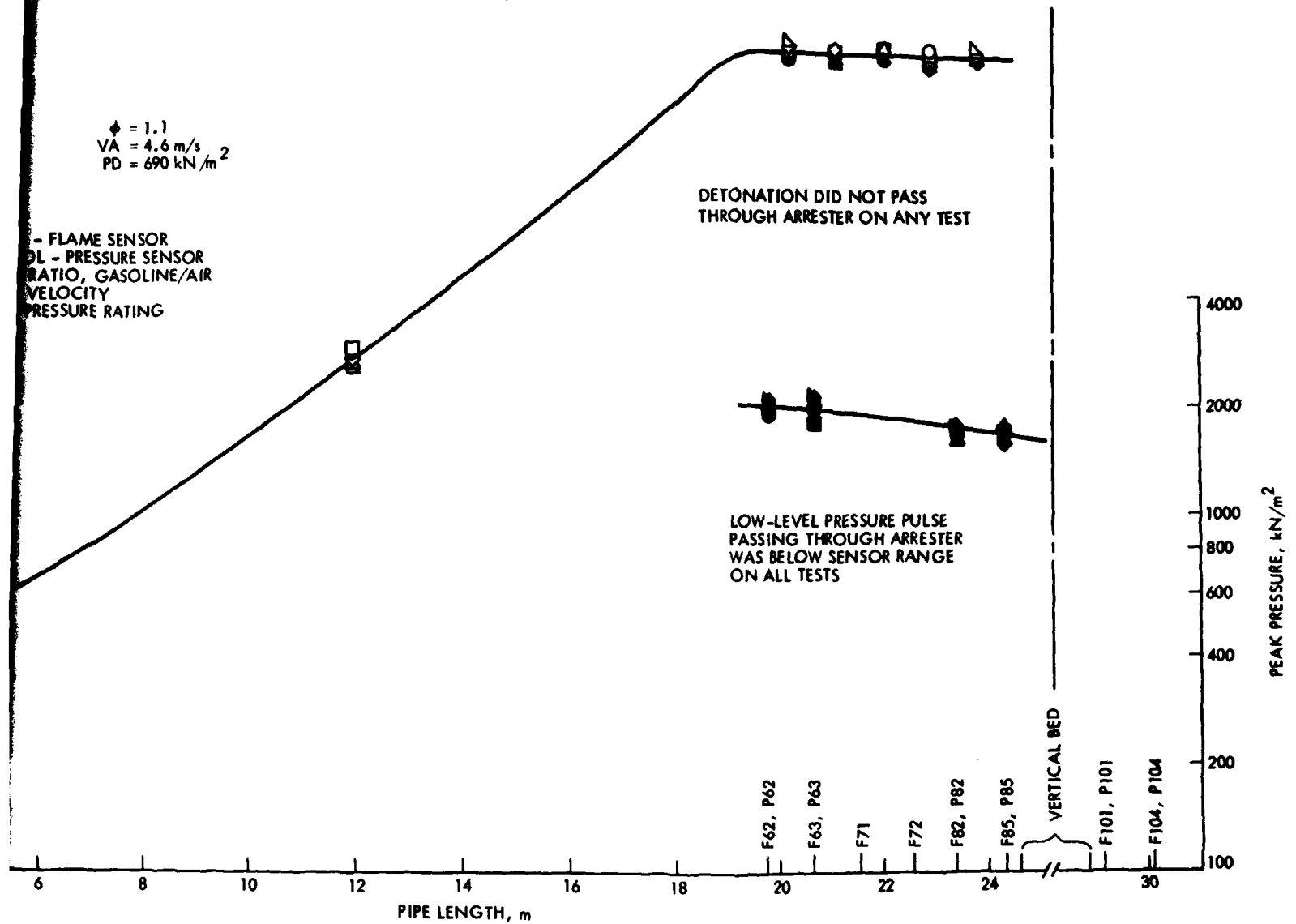
Figure 8-20.   Vertical Bed of Ballast Rings Arrester
Assembly Test Results

8-29
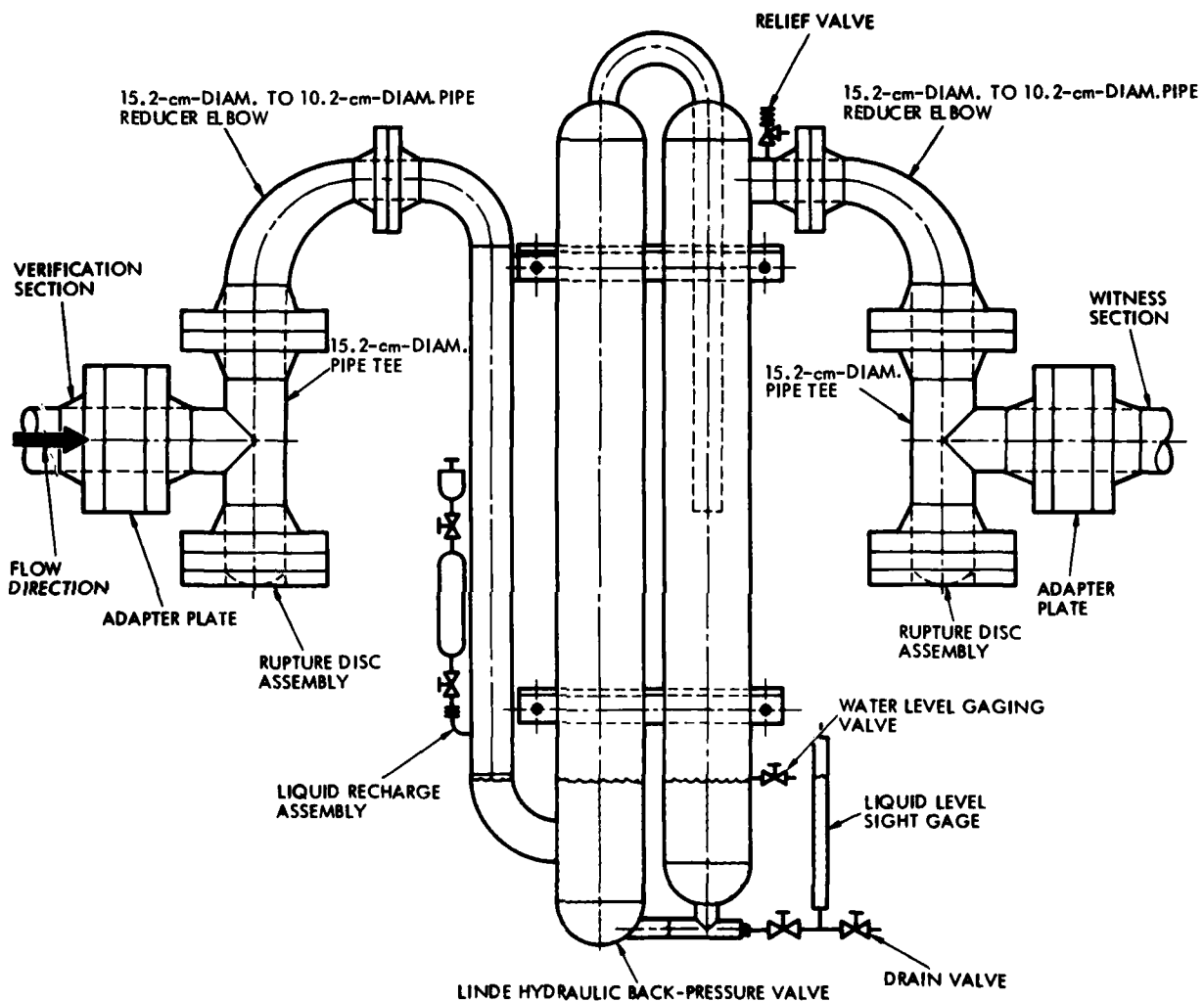
Figure 8-21. Linde Hydraulic Back-Pressure Valve Arrester
Test Assembly Schematic Drawing
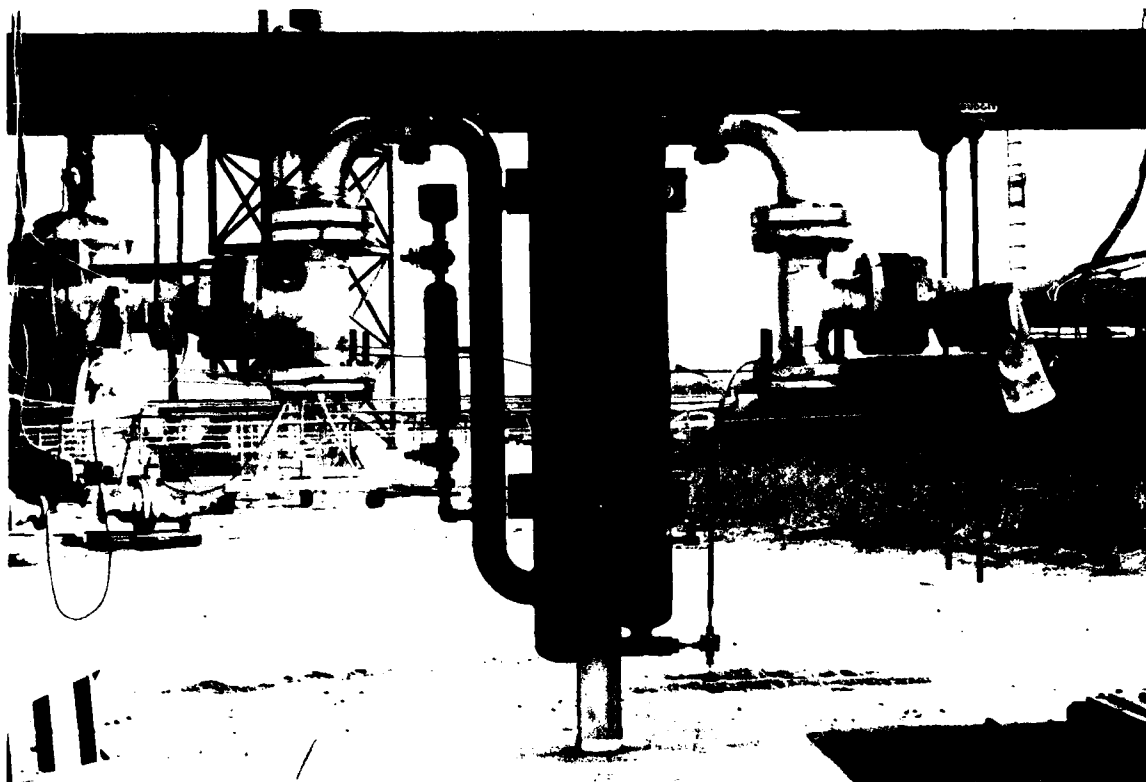
Figure 8-22. Linde Hydraulic Back-Pressure Valve Arrester
Test Installation

FLAME VELOCITY AND PEAK PRESSURE VERSUS PIPE LENGTH
TEST CONFIGURATION NO. 143 AND NO. 144
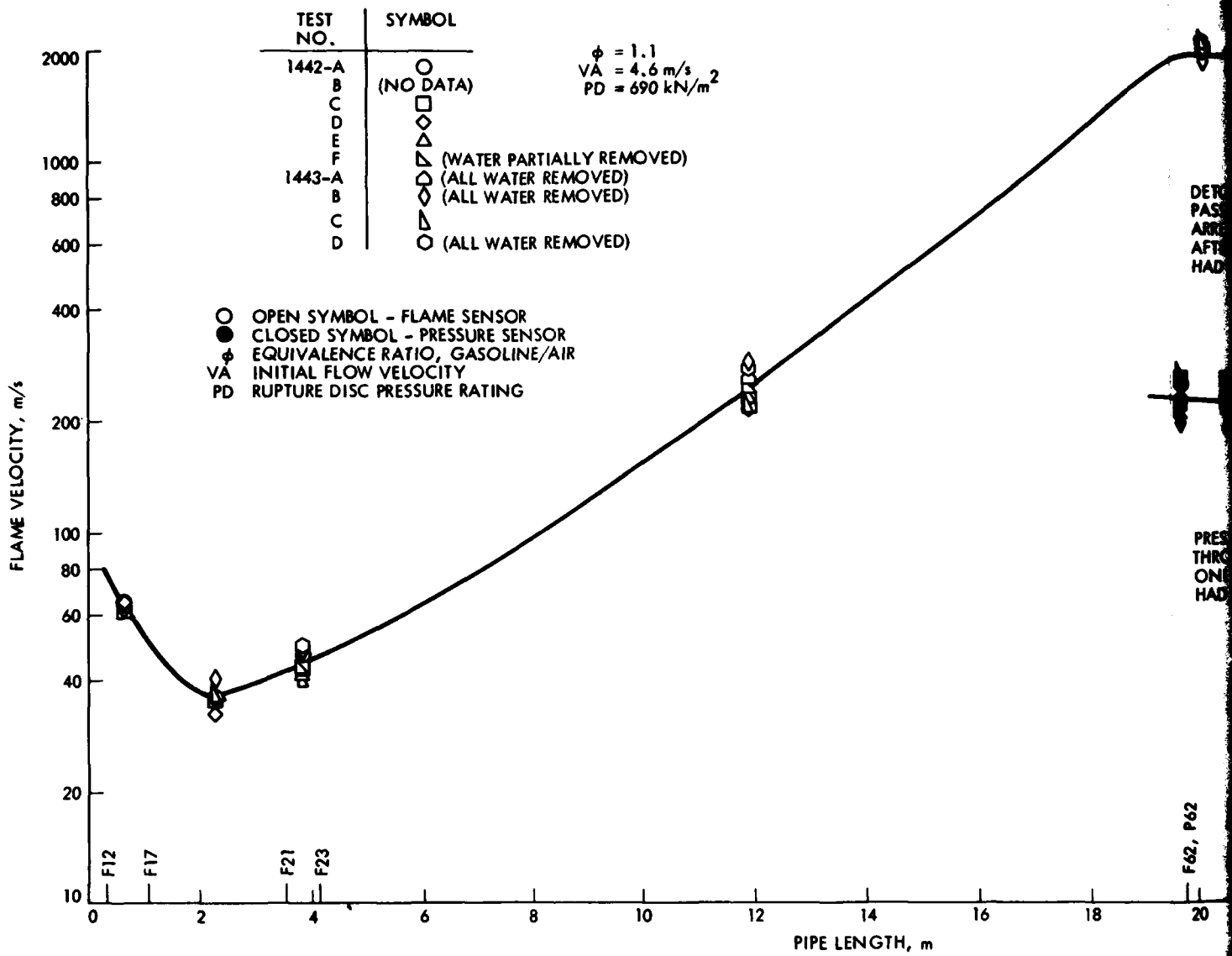
Figure 8-23. Line
Asso

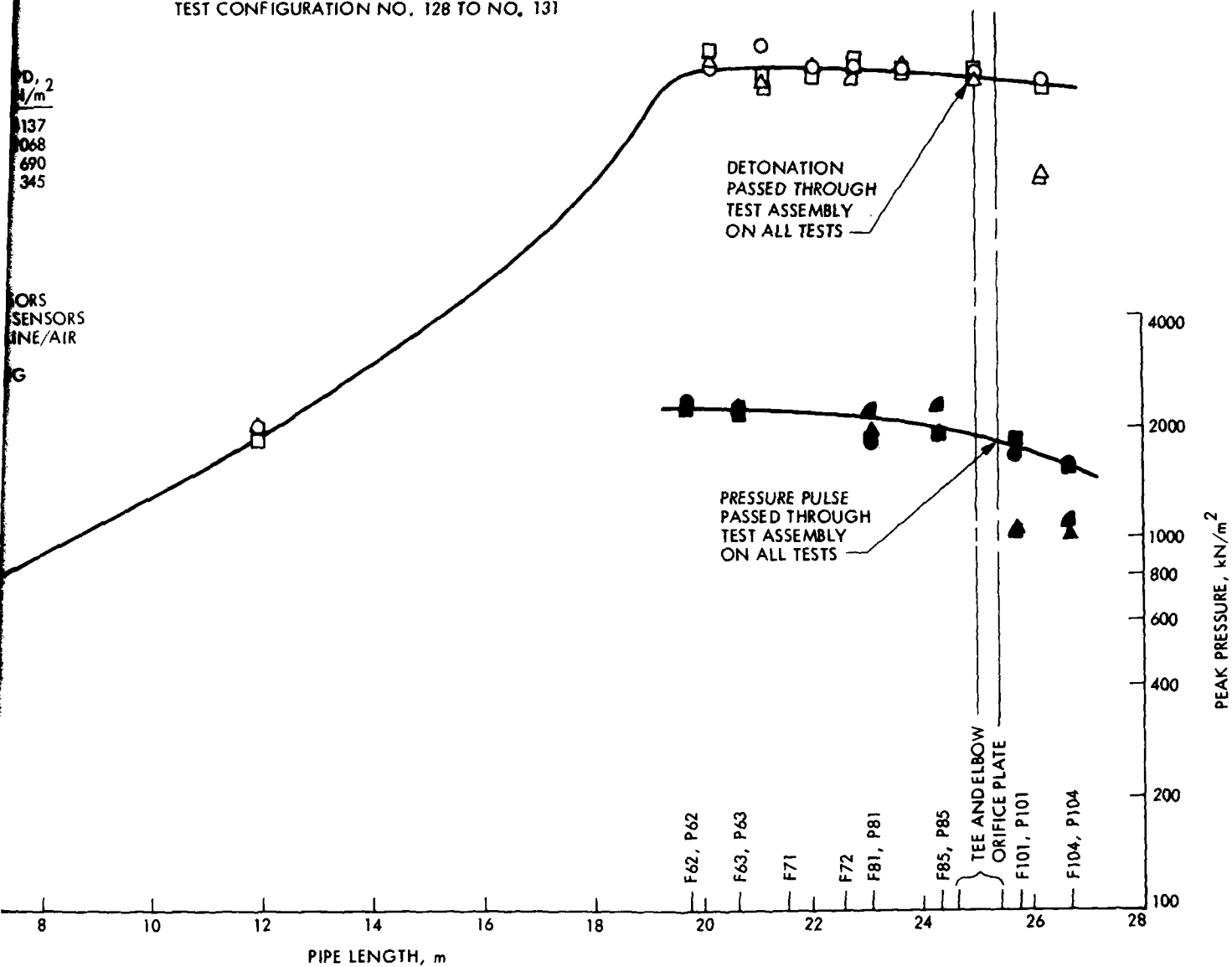FLAME VELOCITY AND PEAK PRESSURE VERSUS PIPE LENGTH
TEST CONFIGURATION NO. 143 AND NO. 144

$\phi = 1.1$
VA $= 4.6$ m/s
PD $= 690$ kN/m^2
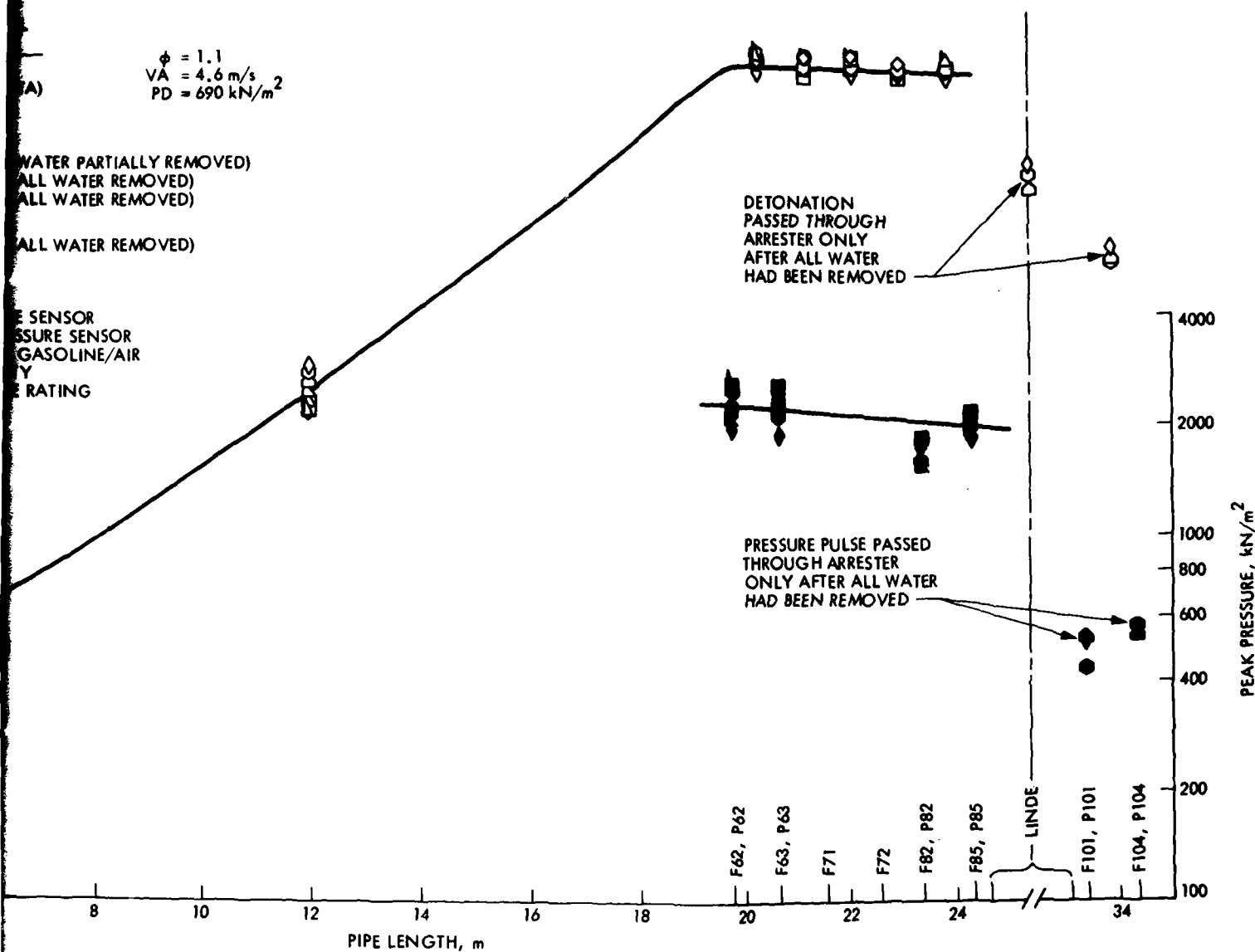
Figure 8-23. Linde Hydraulic Back-Pressure Valve Arrester
Assembly Test Results

8-33

SECTION IX

ARRESTER EVALUATION TESTS USING DOWNSTREAM IGNITION

A. REVERSAL OF TEST FACILITY PIPING

The test facility 15.2-cm- (6.0-in.-) diameter piping was completely removed and reassembled for the downstream ignition tests. All of the pipe sections between the inlet tee section and the exit extension section (No. 11) were reversed 180 deg. This was done to retain continuity in the test configuration and instrumentation locations from the ignition section (No. 1) to the witness section (No. 10). The hydrogen-air-spark igniter was oriented to fire downstream with the gasoline-and-air-mixture flow directed into the extension section. The orifice restricter plate was installed at the exit of the extension section to assist flame propagation back upstream against the flow. The exit gas sampling rake remained in its original position at the entrance to the extension section. All of the flame sensors and pressure transducers remained in their same locations and retained the same identification in relation to flame propagation direction from the ignition section to the witness section.

The water-trap and the Linde arresters were the only two arresters selected for evaluation with downstream ignition. Both of these devices have significant differences in the geometric arrangements between the inlet and outlet configurations. Also, they accept flow-through in only one direction.

B. LINDE HYDRAULIC BACK-PRESSURE VALVE ARRESTER TEST ASSEMBLY

The Linde arrester was installed in the upstream test section (No. 9). Oriented in the normal flow-through direction, the same inlet and outlet adapter piping shown in Figure 8-21 was used with 690 kN/m^2 (100 psid) rupture discs installed in the blow-out ports. Water was added to the arrester up to the gaging port.

For the first test using downstream ignition configuration (No. 145), the initial flow velocity was 1.5 m/s (5.0 ft/s). Ignition was obtained, but there was no detonation. Flame did not propagate upstream beyond the ignition section. The second test was made with the inlet valve closed after the piping was filled with the gasoline and air mixture, so there was no mixture flowing at the time of ignition. Ignition was obtained, but again there was no detonation. The flame had propagated up through the stabilizer section (No. 2), but did not continue through the turbulent liner run-up sections (Nos. 3, 4, and 5). A third test at no-flow condition was made after the injection direction of the hydrogen-air-spark igniter was reversed 180 deg from downstream to upstream orientation. Again, ignition was obtained, but no detonation. The flame had not propagated through the turbulent liner run-up sections. To eliminate any influence water vapor may have had on flame propagation, the water was drained from the Linde arrester. A final test firing was made with the no-flow condition, but the results were no different.

At this point a configuration change was made in the piping test assembly. The ignition section (No. 1) and the stabilizer section (No. 2) were interchanged, placing the ignition section upstream adjacent to the turbulent liner sections, and the stabilizer section downstream next to the extension section. Also, the orifice plate was relocated upstream at the flanged joint between the ignition section and the stabilizer section, so that it was positioned just downstream of the hydrogen-air-spark igniter. A facility piping schematic diagram of this test assembly is shown in Figure 9-1.

The Linde arrester in this test configuration (No. 148) was refilled with water up to the gaging port. Three test firings were made with no initial flow velocity; all resulted in ignitions and detonations. The detonation was arrested for all tests. Only the downstream rupture discs were blown out.

Three additional test firings were made with this same Linde test configuration at an initial flow velocity of 1.5 m/s (5.0 ft/s). Ignition and detonation were again obtained for each test. The detonation was arrested for all tests and only the downstream rupture disc was blown out. The test results, plotted in Figure 9-2, show no significant change in the detonation wave terminal velocity or peak pressure pulse from the levels obtained in the no-flow tests. There was no measurable peak pressure pulse passing into the witness section.

Pre- and posttest pressure loss measured across the arrester assembly averaged 1.92 kN/m^2 (0.278 psid) at an average air-flow velocity of 1.61 m/s (5.28 ft/s). Water level in the arrester had dropped 2.54 to 3.18 cm (1 to 1-1/4 in.) during each test. This represents a loss of 1-1/2 to 3 liters of water, which was replaced after each test. Some of the water displaced from the arrester was driven upstream by the detonation and collected in the vertically-down leg of the inlet pipe tee. This water was drained off after each test by loosening the flange bolts retaining the rupture-disc assembly.

C.   WATER-TRAP ARRESTER TEST ASSEMBLY

The water-trap arrester was installed into the upstream test section (No. 9). Oriented in the normal flow-through direction, the same inlet and outlet adapter piping shown in Figure 8-15 was used with 690 kN/m^2 (100 psid) rupture discs installed on the pipe tee blow-out ports. A blind flange was installed on the blow-out port in the water-trap vessel cover. Water was added to the arrester vessel up to the gaging port.

Five downstream ignition test firings were made with the water-trap arrester test configuration (No. 149) at an initial flow velocity of 1.5 m/s (5.0 ft/s). Ignition and detonation were obtained for each test. The detonation was arrested and only the downstream rupture disc was blown out. There was no measurable peak-pressure pulse passed into the witness section. A plot of the test results is shown in Figure 9-3.
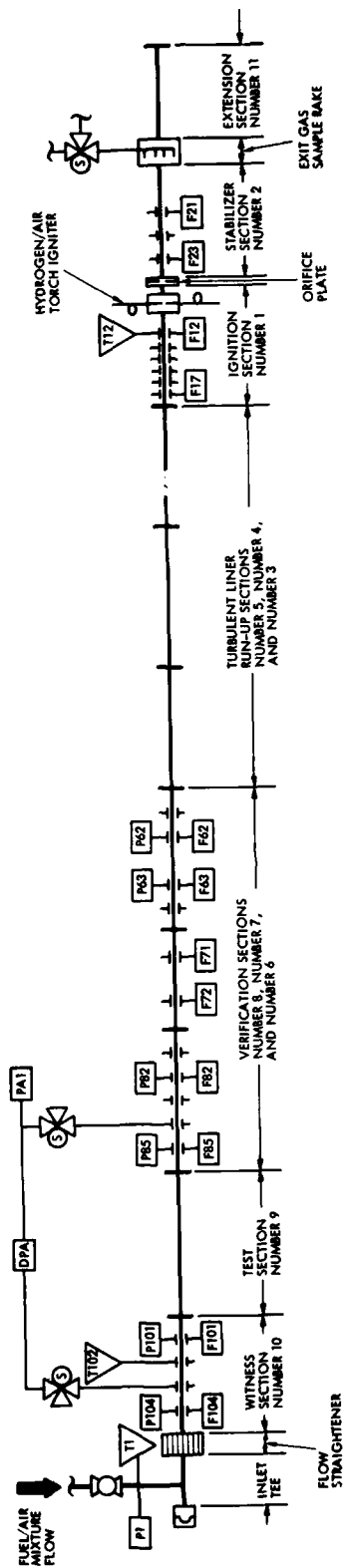
Figure 9-1. Facility Piping Schematic Diagram for Detonation
Testing with Downstream Ignition

The water level in the arrester vessel dropped around 0.48 to 2.22 cm (3/16 to 7/8 in.) during each test. This represents a loss of 1/2 to 2 liters of water, which was replaced after each test. There was no visible sign of water in the upstream piping, possibly because there were no traps in the line, as was the case with the Linde arrester. Posttest air flowing through the piping would normally blow any water collected upstream back into the arrester vessel. Pre- and posttest pressure loss measured across the arrester assembly averaged 1.39 kN/m^2 (0.202 psid) at an average air flow velocity of 1.52 m/s (5.0 ft/s).

A summary of the test results for all the detonation-flame arresters is presented in Table 1-1.

FLAME VELOCITY AND PEAK PRESSURE VERSUS PIPE LENGTH
TEST CONFIGURATION NO. 148
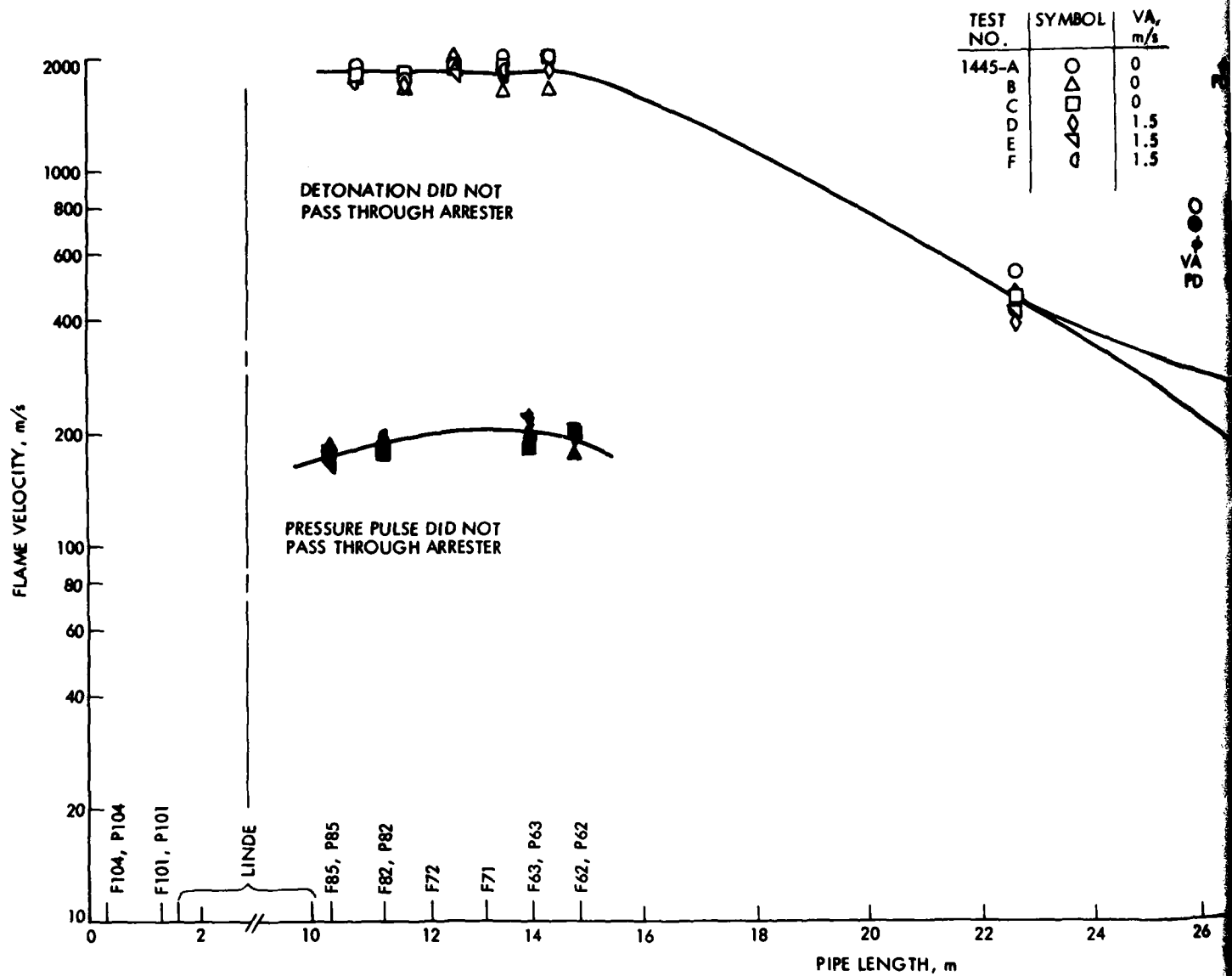
TEST NO.	SYMBOL	VA, m/s
1445-A	○	0
B	△	0
C	□	0
D	◇	1.5
E	◁	1.5
F	◖	1.5

DETONATION DID NOT
PASS THROUGH ARRESTER

PRESSURE PULSE DID NOT
PASS THROUGH ARRESTER

Figure 9-2. Linde
Asse

FLAME VELOCITY AND PEAK PRESSURE VERSUS PIPE LENGTH
TEST CONFIGURATION NO. 148

TEST NO.	SYMBOL	VA, m/s
1445-A	O	0
B	△	0
C	□	0
D	◇	1.5
E	◁	1.5
F	◁	1.5

$\phi = 1.1$
$PD = 690 \text{ kN/m}^2$

O OPEN SYMBOL – FLAME SENSOR
● CLOSED SYMBOL – PRESSURE SENSOR
ϕ EQUIVALENCE RATIO, GASOLINE/AIR
VA INITIAL FLOW VELOCITY
PD RUPTURE DISC PRESSURE RATING
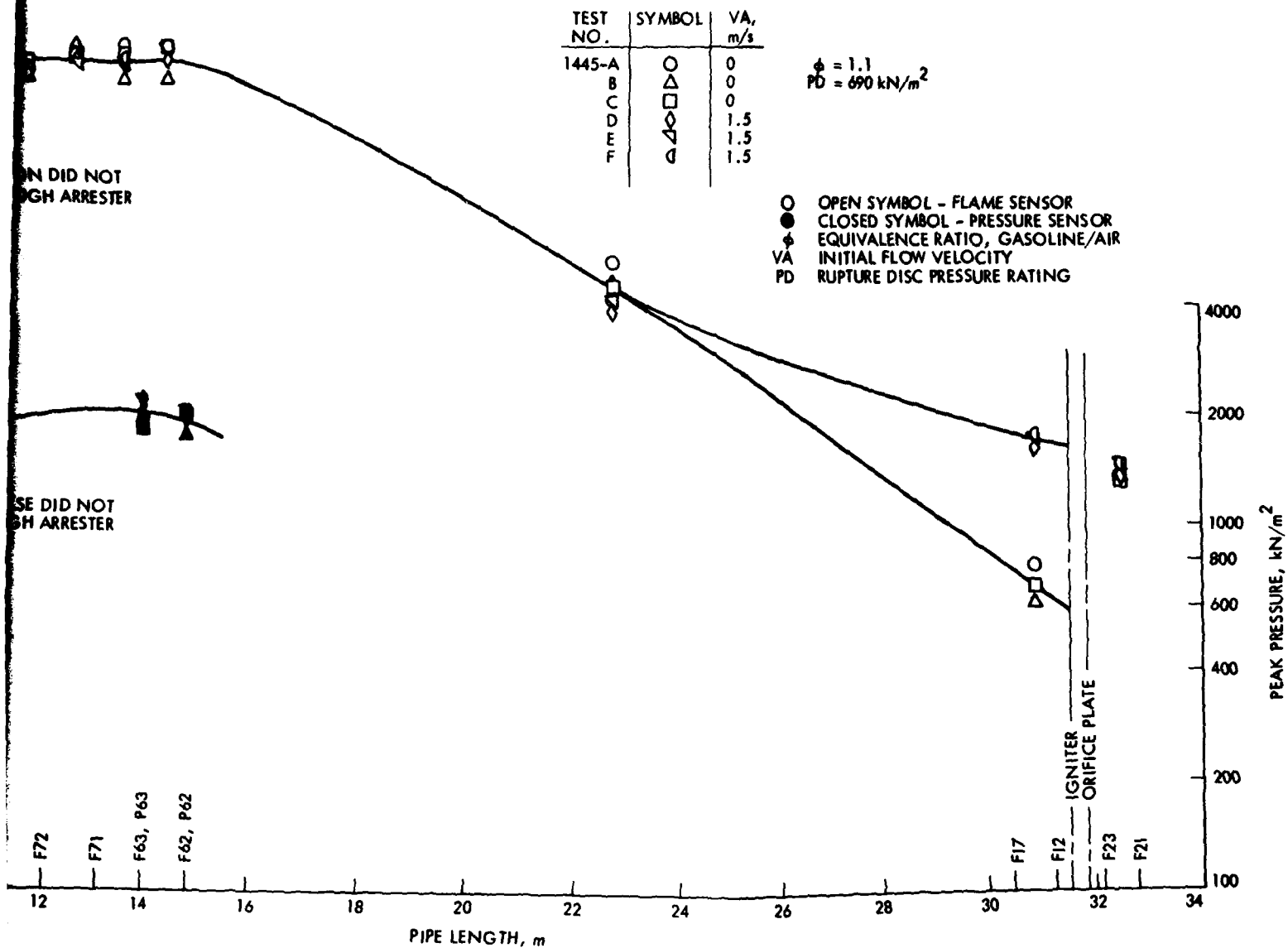
Figure 9-2. Linde Hydraulic Back-Pressure Valve Arrester
Assembly Test Results with Downstream Ignition

9-5

FLAME VELOCITY AND PEAK PRESSURE VERSUS PIPE LENGTH
TEST CONFIGURATION NO. 149
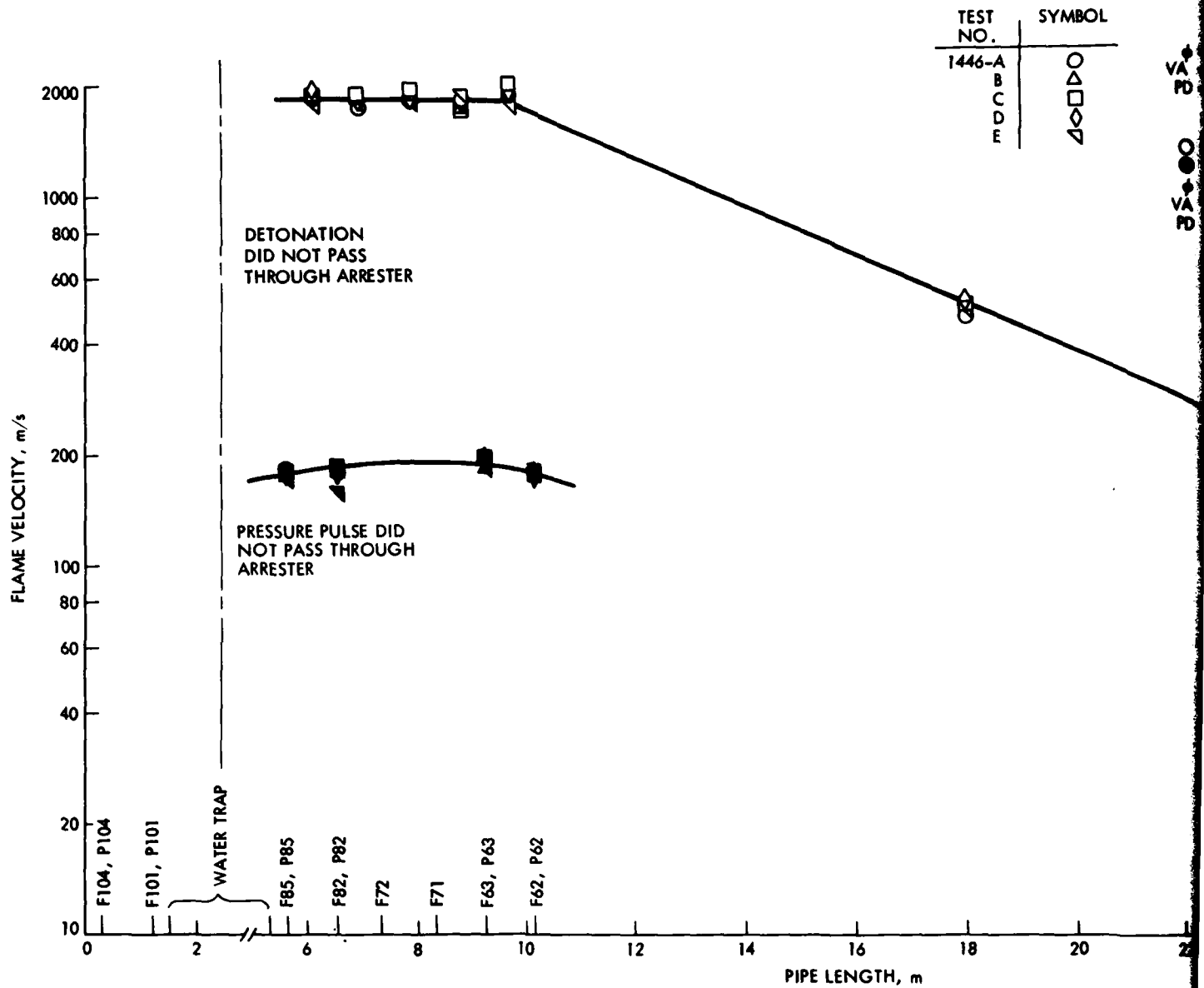
Figure 9-3. Wat
Dow

FLAME VELOCITY AND PEAK PRESSURE VERSUS PIPE LENGTH
TEST CONFIGURATION NO. 149

TEST NO.	SYMBOL
1446-A	○
B	△
C	□
D	◇
E	◁

$\phi = 1.1$
VA $= 1.5$ m/s
PD $= 690$ kN/m^2

○ OPEN SYMBOL - FLAME SENSOR
● CLOSED SYMBOL - PRESSURE SENSOR
ϕ EQUIVALENCE RATIO, GASOLINE/AIR
VA INITIAL FLOW VELOCITY
PD RUPTURE DISC PRESSURE RATING

PEAK PRESSURE, kN/m^2

4000

2000

1000
800
600

400

200

100

F63, P63
F62, P62

F17
F12
IGNITER
ORIFICE PLATE
F23
F21

10   12   14   16   18   20   22   24   26   28   30

PIPE LENGTH, m

Figure 9-3. Water-Trap Arrester Assembly Test Results with Downstream Ignition

9-7

SECTION X

CHEMICALLY PURE PROPYLENE DETONATION TESTS

A detonation was never obtained in the facility check-out tests using chemically pure (CP) propane, whereas calibration tests with commercial grade (CG) propane resulted in stable detonations. California Liquid Gas Corporation, the suppliers of the CG propane used, could not provide specific information on the composition of their propane, but they did indicate that it was in compliance with the Gas Producers Association Liquified Petroleum Gas Specification. According to this specification, the composition is required to be predominantly propane and/or propylene. Matheson Gas Products provided a more definitive specification for CG propane as having a minimum purity of 65.0 mole percent propane, with the main impurity being propylene.

Initial in-house efforts to determine the CG propane composition using gas chromatography analysis were unsuccessful. While this problem was being worked out, a series of tests was conducted to determine the detonation capability of CP propylene.

The test facility piping was reassembled into the upstream ignition configuration that was successful in producing detonation with CG propane during the calibration tests. This is the configuration (No. 150) shown in Figure 3-1. Gasoline in the fuel supply system was replaced with CP propylene. Test firings were made at an initial flow velocity of 4.6 m/s (15.0 ft/s) and a propylene/air equivalence ratio of 1.1. Ignition was obtained, but the transition to detonation did not occur. The restricter orifice plate was removed from the test assembly and a second test firing was made at the same condition. Ignition and detonation were achieved with this test configuration (No. 151). A third test firing was made at the same test condition. Ignition and detonation were achieved, but there was an unexplained slow flame velocity transition through the turbulent liner sections. All attempts to obtain a stable, repeatable detonation with CP propylene were unsuccessful so the tests were terminated.

The previous problem with the gas chromatography analysis was solved by the acquisition of a new "Porasil-B" column and by the revision of the analytical method. The CG propane being used was found to have a composition of 97% propane, 1.2% ethane, 0.2% butane, less than 0.1% propylene, with the balance being heavier hydrocarbons. The values used in the propane quantitation determination were checked against certified samples and found to be accurate within approximately ±3%.

The calibration test results and gas chromatography analysis support the possibility that a small percentage of ethane and butane mixed with propane will produce stable detonation in pipe run-up testing. CP propylene and CP propane appear to have poorly defined detonation properties.

SECTION XI

DEFLAGRATION-TO-DETONATION TRANSITION LOCATION TESTS

In the initial calibration tests, a pipe run-up configuration was developed that would produce stable and repeatable detonations with gasoline and air mixtures. The deflagration-to-detonation transition location was well within the run-up piping containing the turbulent liners. Limited variations in test conditions, including initial flow velocity, mixture ratio, and back pressure, did not suppress the detonation. The actual location of the point of transition remained to be identified. A relocation of flame sensors and dynamic pressure sensors into the lined run-up piping was required to make this determination.

The last run-up section (No. 5) was removed from the test assembly, and its turbulent liner was removed, modified, and reinstalled into three instrumented sections (Nos. 7, 8, and 10). Special holes had to be cut into the liner and aligned with the instrumentation ports to give a clear field of view for the flame sensors and pressure sensors. The instrumented lined sections were moved upstream to join the first two uninstrumented lined sections (Nos. 3 and 4). The unlined run-up section (No. 5) was reinstalled downstream between the remaining verification section (No. 6) and the orifice plate at the inlet to test section (No. 9). Overall make-up length of the test piping remained the same.

A series of three test firings was made with the new test configuration (No. 165) at an initial flow velocity of 4.6 m/s (15.0 ft/s) and a gasoline/air equivalence ratio of 1.1. A detonation was produced in each test. The transition from deflagration to detonation appeared to be located either in the first instrumented lined section (No. 7) or just upstream from it, but the actual location was not well defined.

A second uninstrumented run-up section (No. 4) was removed from the test assembly. The turbulent liner was withdrawn, modified, and reinserted into the remaining instrumented verification section (No. 6). These two sections were then interchanged to produce the facility piping assembly shown in the schematic diagram in Figure 11-1. Thirteen test firings were made with this test configuration (No. 166 and No. 167). Initial flow velocity was varied through 0, 1.5, 3.0, 4.6, and 6.1 m/s (0, 5, 10, 15, and 20 ft/s) with the gasoline/air equivalence ratio of 1.1. The results of these tests are plotted in Figure 11-2. Although there is some scatter in both flame velocity and peak pressure data, attesting to the complexity of the transitional process, the preponderance of data indicates that the location of the transition point is about 15.4 m (50.5 ft) from the point of ignition. The run-up length through turbulent liner pipe was 11.2 m (36.7 ft) giving an L/D of 74. There appears to be no discernible correlation between the initial flow velocity used in testing and the resulting run-up length. The stable detonation wave velocity downstream of the transition is 1800 m/s (5906 ft/s) with a peak pressure of 1900 kN/m^2 (276 psia). Some

11-1
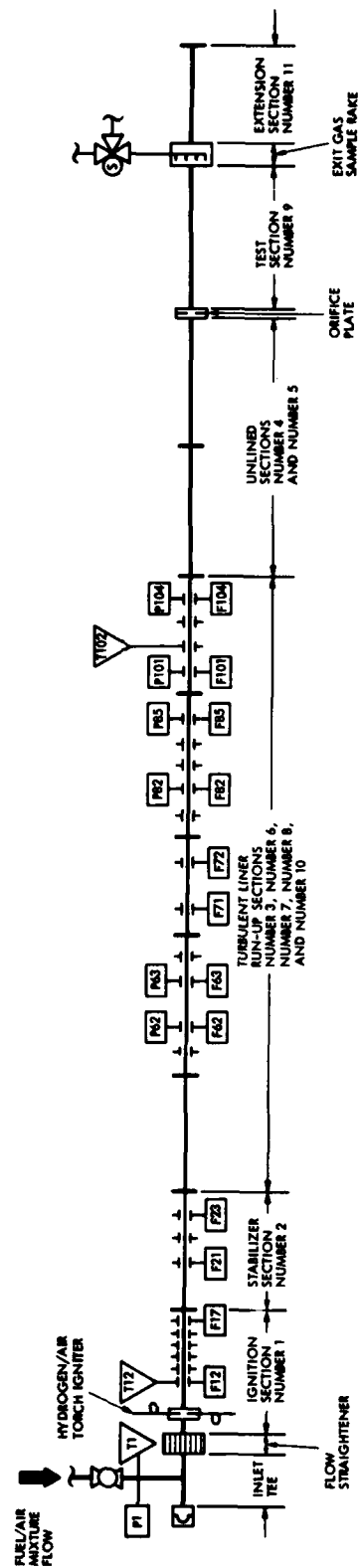
Figure 11-1. Facility Piping Schematic Diagram for Calibration Testing to Determine Location of Deflagration-to-Detonation Transition

FLAME VELOCITY AND PEAK PRESSURE VERSUS PIPE LENGTH
TEST CONFIGURATION NO. 165, NO. 166, AND NO. 167

TEST NO.	SYMBOL	ϕ	VA, m/s
1458-A		1.1	4.6
B			4.6
C			4.6
1459-A			4.6
D			6.1
E			4.6
F			3.0
1460-A			0
B			0
C			1.5
D			1.5
E			3.0
F		1.1	6.1

O OPEN SYMBOLS – FLAME SENSORS
● CLOSED SYMBOLS – PRESSURE SENSORS
ϕ EQUIVALENCE RATIO, GASOLINE/AIR
VA INITIAL FLOW VELOCITY

TRANSITION POINT

DEFLAGRATION ←   → DETONATION

DETONATION VELOCITY =

DETONATION PRESSURE = 19

FLAME VELOCITY, m/s

PIPE LENGTH, m

F12 F17   F21 F23   F62 F63 F71, P71 F72, P72 F82, P82 F85, P85 F101, P101 F104, P104

F71 F72 F82, P82 F85, P85 F101, P101 F104, P104 F82, P82
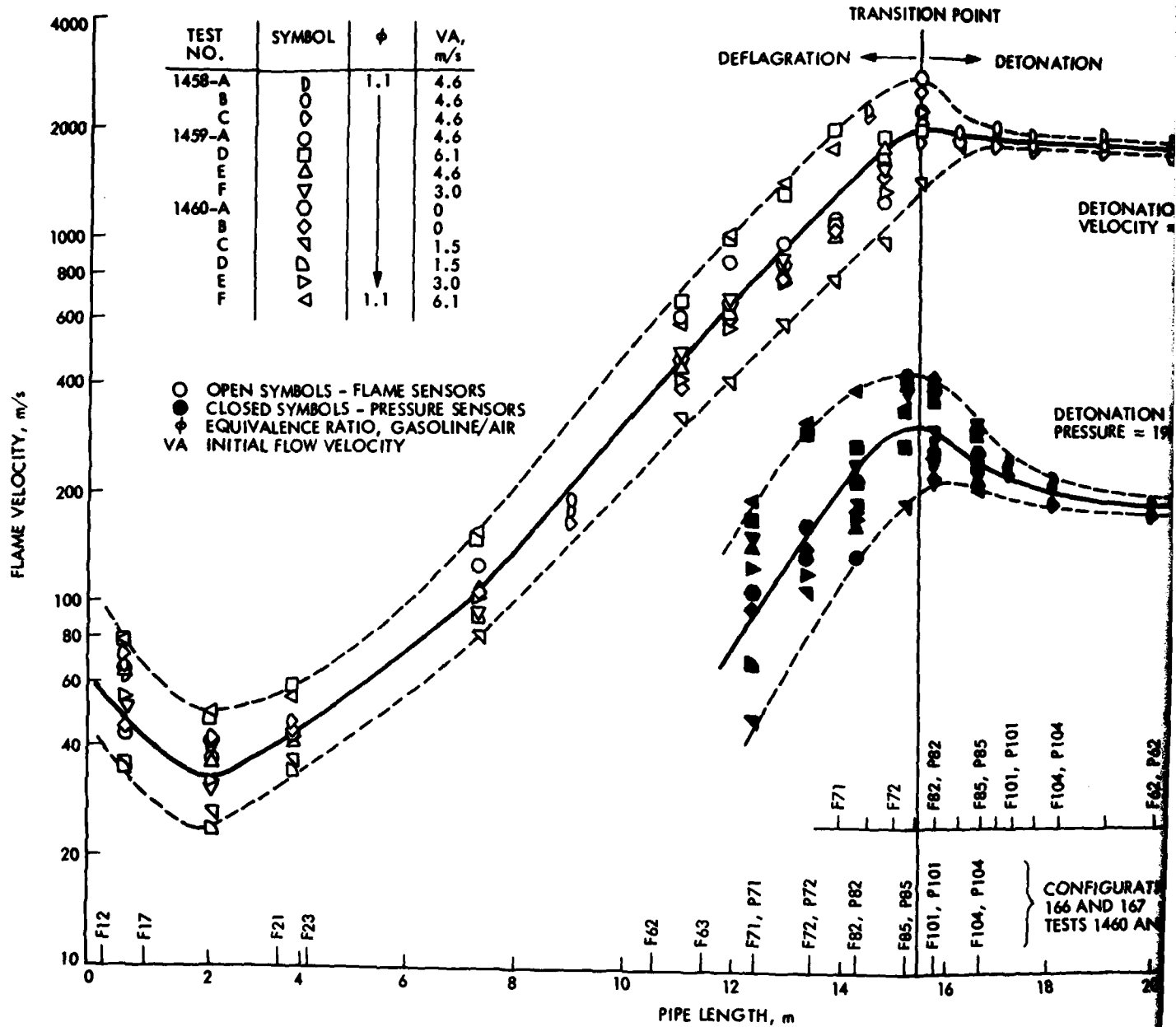
CONFIGURATI
166 AND 167
TESTS 1460 AN

Figure 11-2. Deflagration-to-Detonatio
for Gasoline and Air Mixt
Flow Velocities
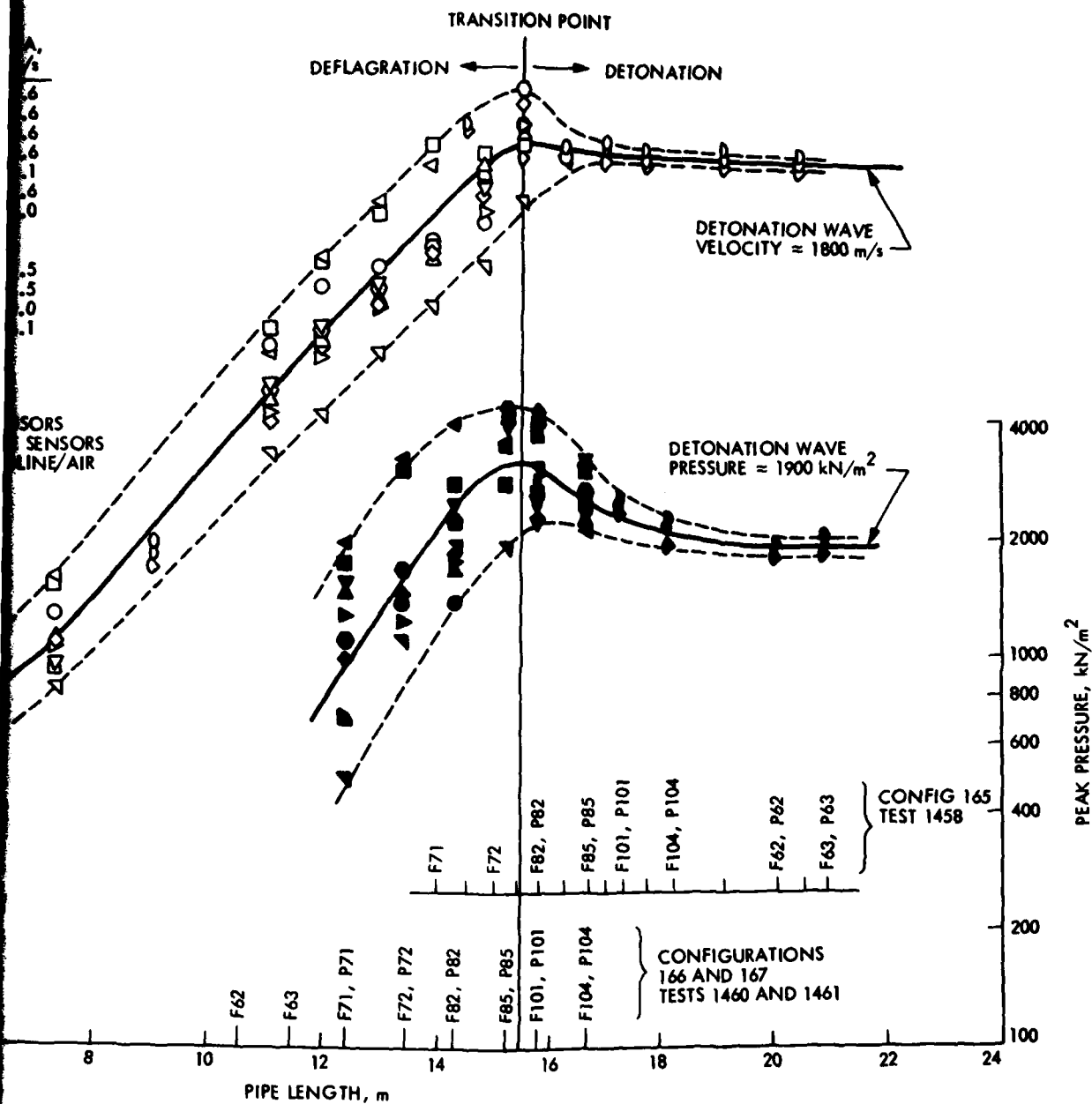
Figure 11-2. Deflagration-to-Detonation Transition Test Results
for Gasoline and Air Mixtures at Selected Initial
Flow Velocities

peak pressures measured near the point of transition exceeded 4000 kN/m^2 (580 psia).

To determine the influence the equivalence ratio has on the detonation run-up length, nine additional test firings were made at a constant initial velocity of 4.6 m/s (15.0 ft/s). The equivalence ratio was varied from 0.7 to 1.4 in steps of 0.1 for these tests. The results of these tests are plotted in Figure 11-3. At an equivalence ratio of 0.7, the flowing gasoline and air mixture would not ignite. Increasing the gasoline flow to an equivalence ratio of 0.8, the flowing mixture was ignited, but the flame acceleration was too slow to reach detonation velocity within the test length of run-up piping. The maximum flame velocity in this test was measured at 600 m/s (1969 ft/s) and the peak pressure at 900 kN/m^2 (131 psia) in the last instrumented section (No. 10). Stable detonations were obtained for all test conditions where the equivalence ratio ranged from 0.9 to 1.4. The data are scattered to the extent that there is no obvious correlation between equivalence ratio and the run-up length. The location of the transition is at 15.4 m (50.5 ft) from the point of ignition, which is the same location determined in the previous test series. This is undoubtedly caused by the fact that the same data obtained at an initial velocity of 4.6 m/s (15.0 ft/s) and an equivalence ratio of 1.1 are used in both plots. It is these data that produce the maximum levels of flame velocity and peak pressure, which are the criterion used to identify the point of transition. Data at other test conditions, with the one exception, do not show any consistent results that influence a change in the apparent location of transition. A detonation run-up length of 11.2 m (36.7 ft) for the turbulent lined 15.2-cm- (6.0-in.-) diameter piping, or an L/D of 74, holds for all conditions tested except at an equivalence ratio of 0.8.

FLAME VELOCITY AND PEAK PRESSURE VERSUS PIPE LENGTH
TEST CONFIGURATION NO. 165, NO. 166, AND NO. 167
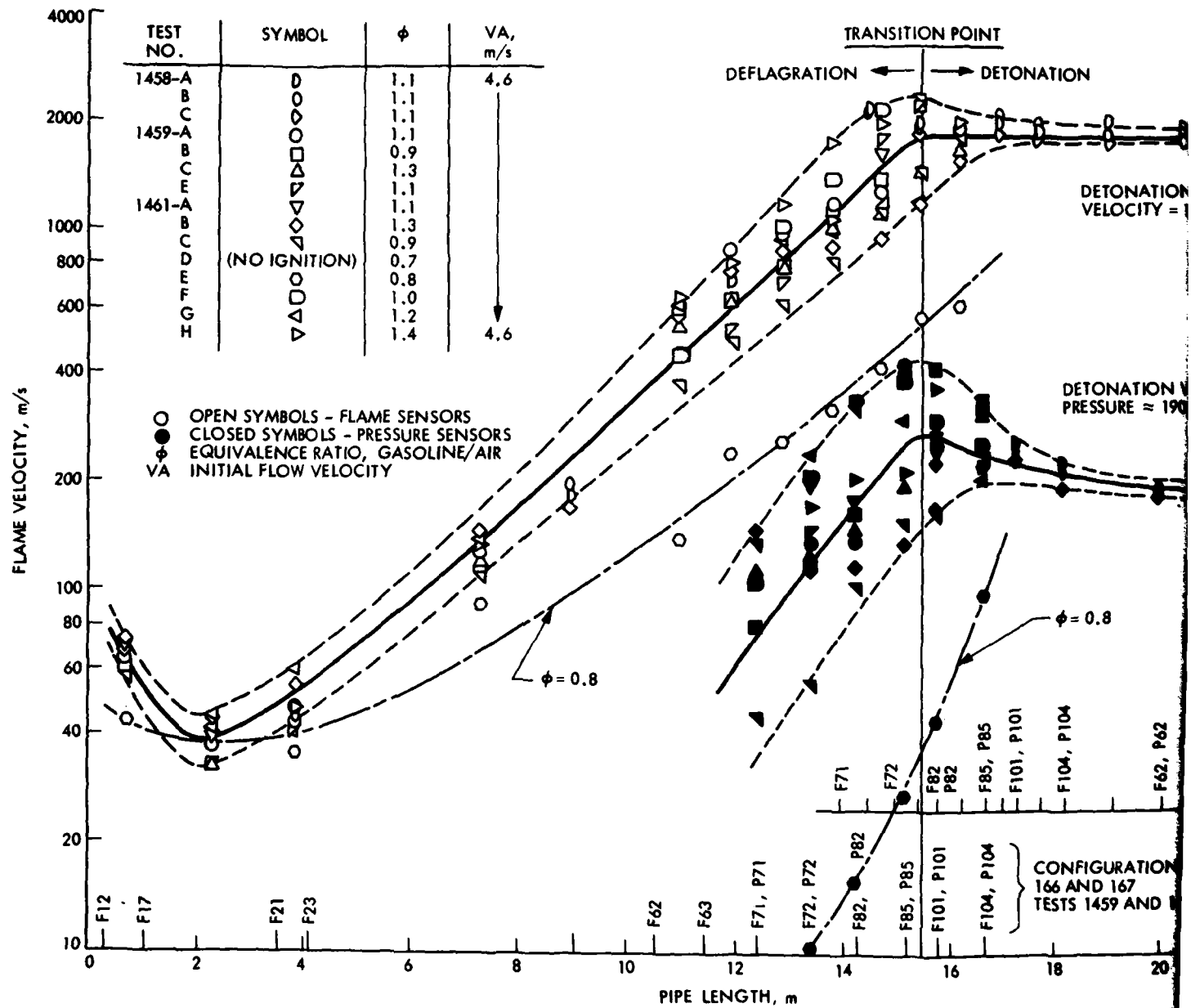
Figure 11-3. Deflagration-to-Detonation Trans
Gasoline and Air Mixtures at Sel

FLAME VELOCITY AND PEAK PRESSURE VERSUS PIPE LENGTH
TEST CONFIGURATION NO. 165, NO. 166, AND NO. 167
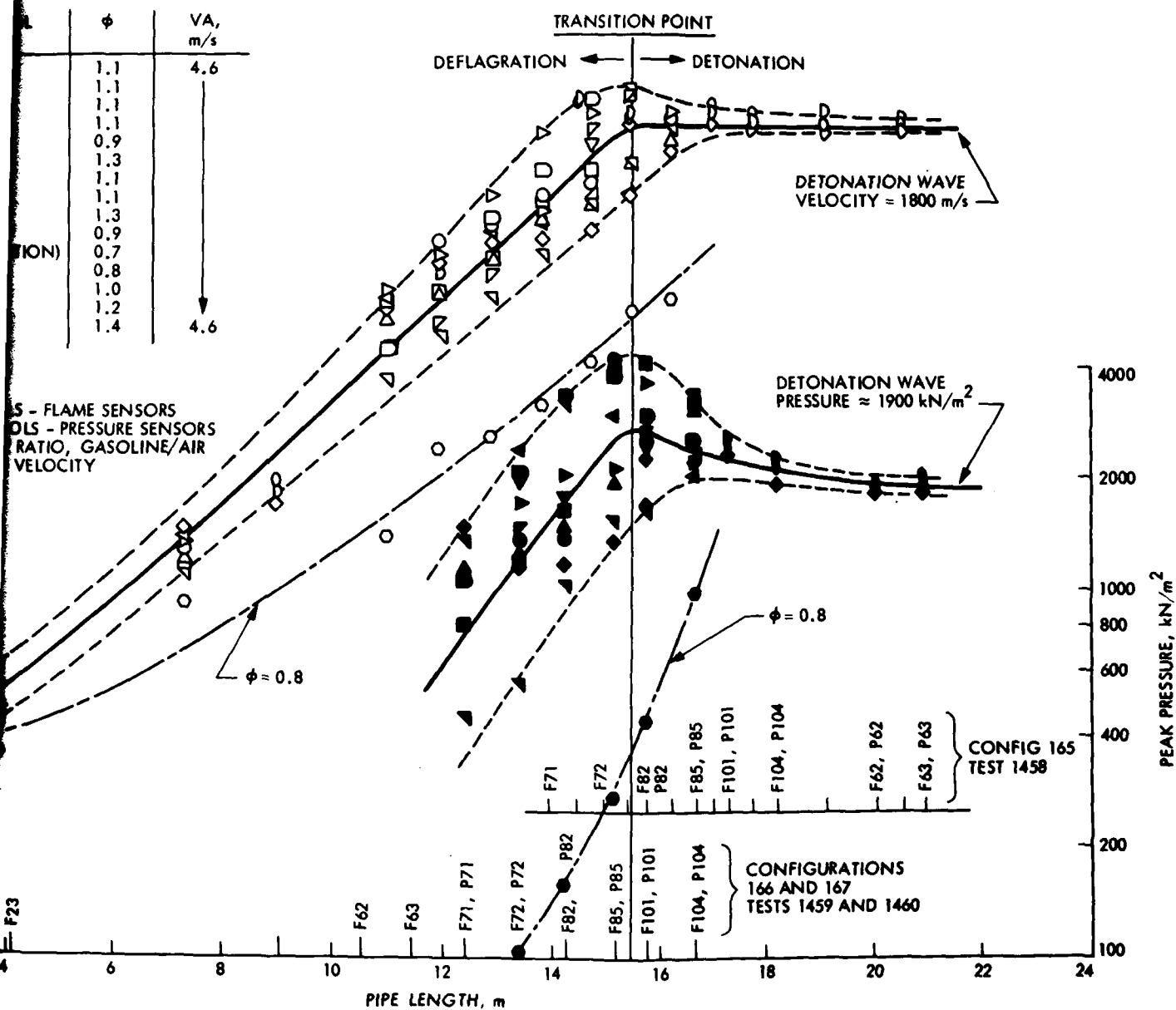
Figure 11-3.   Deflagration-to-Detonation Transition Test Results for
Gasoline and Air Mixtures at Selected Equivalence Ratios

SECTION XII

FACILITY PIPING RELATIVE ROUGHNESS DETERMINATION TESTS

The relative roughness of the turbulent liners in the facility piping was required to relate the experimental results of detonation run-up distance to standard commercial pipe. A series of air-flow tests was made to measure the pressure loss through the 15.2-cm- (6.0-in.-) diameter facility run-up piping with varying lengths of turbulent liners and without the liners. The measured data were used in the Darcy equation to determine the pipe wall friction factor (f) as follows:

    (1)   Darcy equation,

$$\Delta P = f\left(\frac{L}{A^2 D}\right)\left(\frac{\dot{m}^2}{2g_c \rho}\right)$$

    (2)   Solving for friction factor,

$$f = 2g_c\left(\frac{A^2 D}{L}\right)\left(\frac{\rho \Delta P}{\dot{m}^2}\right)$$

where g_c = gravitational conversion constant relating force and mass

    A   = internal cross-sectional area of pipe

    D   = inside diameter of pipe

    L   = length of pipe

    ρ = fluid density

    P   = pressure loss through pipe

    $\dot{m}$ = fluid mass flow

The friction factor is a dimensionless quantity, and at normally encountered pipe flows is a function of two other dimensionless quantities, the relative roughness (ϵ/D) and the Reynolds number (R_e), which are defined as follows:

    (1)   Relative roughness = ϵ/D

            where: ϵ = height of absolute roughness

    (2)   Reynolds number, $R_e = \dfrac{4\dot{m}}{\pi D \mu}$

        where μ = absolute viscosity of fluid

In Reference 12-1, L. F. Moody has presented two charts; one gives the functional relationship between f, R_e, and ϵ/D, and the second relates f, ϵ/D, and ϵ to those values typical of commercial pipe and tubing.

The first set of experimental pressure loss data, which was obtained with test configurations (No. 157 to No. 164) using the installed pressure transducers and steady-state recorders, proved to be unreliable. The total pressure and differential pressure measurements encountered were below the linear, repeatable range of the transducers employed. They were replaced by a visually read micromanometer to measure upstream pressure and an inclined manometer to measure pressure loss. The data obtained using these instruments were considered to be acceptable.

The air-flow tests were made at velocities of 1.5, 3.0, 4.6, and 6.1 m/s (5, 10, 15, and 20 ft/s) in both increasing and decreasing steps. The test configurations (No. 168 to No. 175) included lined pipe lengths of 12.6, 8.0, and 3.4 m (41.3, 26.2, and 11.2 ft), and an unlined pipe length of 10.6 m (34.9 ft). Pressure loss through each length was measured for the conditions of both an open outlet and for the orifice plate installed on the outlet. At the lowest air-flow velocity, 1.5 m/s, and the shortest pipe length, 3.4 m, the pressure measurements obtained were questionable because of their very low values. However, the measurements made at the other test conditions appeared good and produced the following results:

Pipe Condition	Length, m	R_e	f	ϵ/D
Lined	12.6, 8.0, and 3.4	2×10^{-4} to 5×10^{-4}	0.040 to 0.047	0.010 to 0.015
Unlined	10.6	2×10^{-4} to 5×10^{-4}	0.016 to 0.020	$< 10^{-6}$

The lined pipe had a friction factor and relative roughness comparable to riveted steel pipe 15.2 cm (6.0 in.) in diameter. The unlined, honed, and polished shock-tube pipe had a friction factor and relative roughness less than any commercial grade smooth pipe.

SECTION XIII

PARAMETRIC TESTS OF DETONATION-FLAME ARRESTERS

A.   DOWNSTREAM PRESSURE PULSE

A low-level pressure pulse that penetrated through the test arrester was measured in the witness section on two of the four generic types of flame control devices found to be effective in arresting a detonation. The pressure pulse level ranged from 250 to 470 kN/m^2 (36 to 68 psia) for the spiral-wound, crimped aluminum ribbon arrester and the foamed nickel-chrome metal arrester. The pressure pulse, if present, was below the lower sensitivity level of 207 kN/m^2 (30 psia) for the high-pressure, quartz-crystal-type pressure transducers installed in the witness section of the vertical bed of aluminum Ballast rings arrester, the water-trap arrester, and the Linde hydraulic back-pressure valve arrester. The existence of this low-level pressure pulse passing through the arrester caused some concern as to the possibility of a reignition occuring in the combustible fuel and air mixture in the piping at some distance beyond the arrester. Although reignition was not observed in the initial evaluation tests, it was not known whether this was due to the short length of piping in the witness section, which was only 1.5 m (5 ft), or due to the fact that operational procedures terminated the flow of gasoline into the induction section just prior to ignition. Both of these conditions were later evaluated by additional testing. A long length of extension piping was installed downstream of the arrester test section and a change in the operating procedure was made to allow gasoline and air mixture to flow continuously through the piping system for periods up to 120 seconds following ignition and detonation.

Before proceeding with continuous-flow detonation testing, two of the more applicable arrester configurations were further evaluated with a series of parametric tests designed to identify any existing relationships between the measured levels of downstream pressure pulse and the arrester size, inlet configuration, or rupture disc pressure rating. The two configurations selected were (1) The Shand and Jurs spiral-wound, crimped metal ribbon arrester and (2) the vertical bed of Ballast rings arrester. Both of these devices are considered to be readily adaptable to either shipboard or shore-based tank installations, and could be made compatible with a marine environment.

During the initial testing of Shand and Jurs spiral-wound, crimped aluminum ribbon arrester, a pressure pulse of about 290 kN/m^2 (42 psia) was measured on the downstream side (Figure 8-7). The detonation pressure wave on the upstream side was on the order of 1900 kN/m^2 (276 psia). Only 15% of the detonation wave pressure was transmitted through the 15.2-cm- (6-in.-) long arrester core element. An increase in core length would be expected to reduce the downstream pressure pulse even lower. The measured air-flow pressure loss across this core element averaged only 0.152 kN/m^2 (0.022 psid) at an average air velocity of 4.68 m/s (15.35 ft/s) (Table 1-1). It was apparent that the core length could be increased considerably and still operate at an acceptable pressure loss.

Testing of the vertical bed of aluminum Ballast rings arrester produced no measurable pressure pulse in the downstream piping. This original configuration was very large and heavy compared to the Shand and Jurs arrester assembly. The size of the bed of packed rings was designed to assure its flame arresting capability. This large size also resulted in the lowest measured air-flow pressure loss of all the arrester configurations tested. It was apparent that the packed bed of rings could be reduced in size without developing an unacceptable high-pressure loss, providing the detonation arresting capability was not lost. However, a significant reduction in bed size would undoubtedly be accompanied by an increase in the level of a pressure pulse that would pass through the arrester. A more sensitive lower-range pressure transducer had to be employed in the witness section to monitor any measurable variations in downstream pressure pulse.

A series of parametric tests were conducted to evaluate the following variations on the two selected types of detonation-flame arresters:

(1) The Shand and Jurs arrester was tested with the spiral-wound, crimped stainless-steel ribbon core elements having the same crimp height and diameter as the original aluminum core element, but with three different core lengths. The inlet configuration was eventually changed from the indirect pipe tee, rupture-disc and pipe-elbow assembly to a directly connected in-line pipe tee and rupture-disc assembly where the rupture-disc pressure rating was increased in four steps up to a blanked-off condition.

(2) The vertical bed of aluminum Ballast rings arrester was tested with four bed diameters, three bed depths, three Ballast ring sizes, and increasing rupture-disc pressure rating in four steps up to a blanked-off condition. The inlet and outlet configuration were the indirectly connected pipe tee, rupture-disc and pipe-elbow assemblies used with the existing pressure vessel housing.

B.   SHAND AND JURS SPIRAL-WOUND, CRIMPED STAINLESS-STEEL RIBBON ARRESTER TEST ASSEMBLIES

New spiral-wound, crimped stainless-steel ribbon core elements for the Shand and Jurs arrester test assemblies were obtained from G.P.E. Controls. They are manufactured in only two core lengths, 15.2 cm (6 in.) and 20.3 cm (8 in.), so the third experimental length was made by assembling two 15.2-cm- (6-in.-) long units in series in a single 30.5-cm- (12-in.-) long high-pressure housing. The new 20.3-cm (8-in.) and 30.5-cm (12-in.) arrester housings were identical, except in length, to the existing 15.2-cm (6-in.) housing, and could interchangeably use the two existing mounting rings with the grid retainers.

All three lengths of the stainless-steel Shand and Jurs arresters were initially tested using the same test assembly shown in the schematic drawing, Figure 8-6. This configuration used the indirect inlet connection consisting of a pipe tee, rupture disc not in line, and a pipe elbow on

the upstream side of a pair of 30.5- to 15.2-cm- (12- to 6-in.-) diameter
concentric and eccentric flanged pipe reducers. A photograph of the
20.3-cm- (8-in.-) long arrester test assembly is shown in Figure 13-1.
A rupture disc with a pressure rating of 690 kN/m^2 (100 psid) was installed
on all these tests. The two 20,685 kN/m^2 (3000 psia) quartz-crystal-type
pressure transducers were relocated from the witness section (No. 10) up-
stream to the verification section (No. 7) instrumentation pressure ports
(P71 and P72). Two 345 kN/m^2 (50 psia) strain-gage-type pressure transducers
were installed into the witness section instrumentation pressure ports
(P101 and P104). All test firings were made using gasoline and air mixtures
at the established standard conditions with the upstream ignition location.
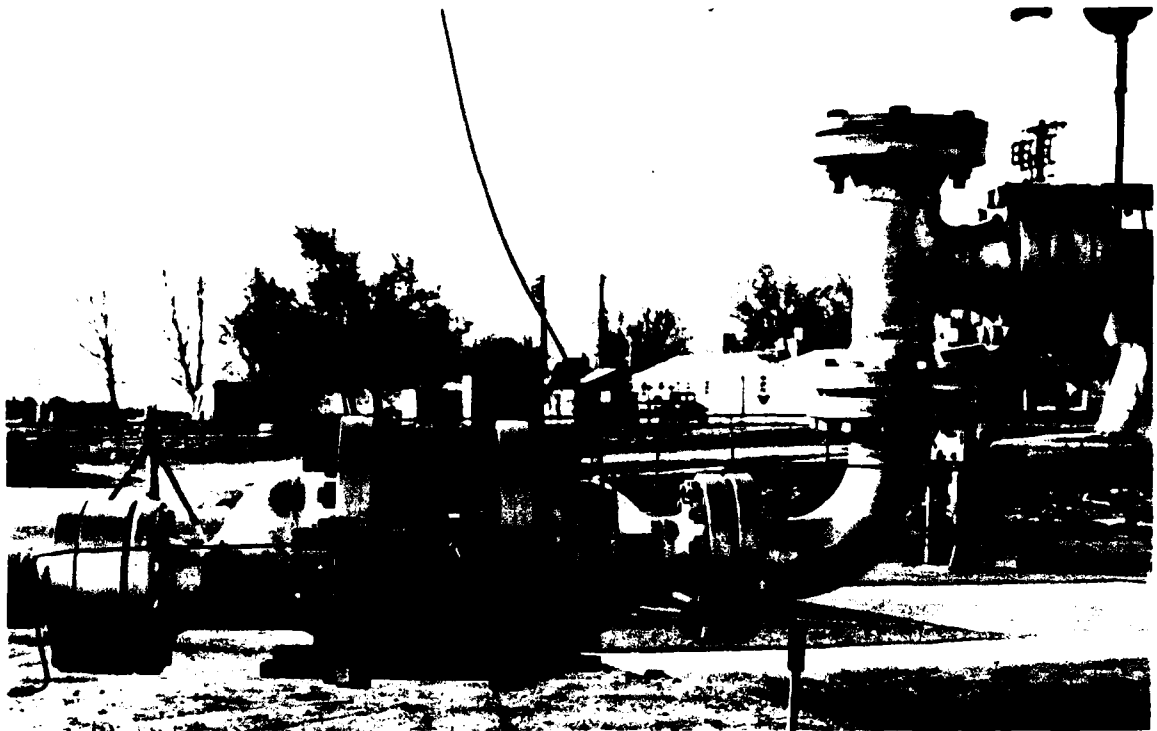
Figure 13-1. Shand and Jurs Spiral-Wound, Crimped Stainless-Steel
Ribbon Arrester Test Installation

The 15.2-cm- (6-in.-) long stainless-steel Shand and Jurs arrester
configuration (No. 176 and No. 177) was subjected to five stable deto-
nations. The rupture disc was blown out on all tests. Detonation was
arrested on the first four test firings, but on the fifth, the passage
of a flame traveling at 570 m/s (1870 ft/s) was recorded in the witness
section. When the detonation was arrested, the peak-pressure pulse
downstream of the arrester averaged 344 kN/m^2 (50 psia). This same
pressure increased to 460 kN/m^2 (67 psia) when the flame penetrated
the arrester. A plot of these test results are shown in Figure 13-2.

Pre- and posttest pressure loss across the arrester averaged 0.151 kN/m^2 (0.022 psid) at an average air-flow velocity of 4.78 m/s (15.68 ft/s). These are about the same values recorded for the 15.2-cm-(6-in.-) long aluminum core arrester (Table 1-1). Posttest inspection of the stainless-steel core element revealed that a circumferential displacement had occurred in an overlap joint at the middle of the spiral-wound, crimped ribbon windings. This produced a double-width gap in the windings, approximately 6.35-cm (2.5-in.) long, that extended through the full depth of the core. A photograph showing an enlarged view of this displacement is presented in Figure 13-3. It is believed that this was the path for flame passage through the arrester on the last test, since there was no other evidence of distortion or damage. Inspection of the other stainless-steel core elements disclosed that this particular unit was the only one that had been manufacturered with an overlap joint in the crimped ribbon windings.

The 20.3-cm- (8-in.-) long stainless-steel Shand and Jurs arrester configuration (No. 178) was subjected to six stable detonations. The rupture disc was blown out and the detonation was arrested on all test firings. A low-level peak-pressure pulse, which averaged 320 kN/m^2 (46 psia), was measured in the witness section. A plot of these test results are shown in Figure 13-4. Pre- and posttest pressure lost across the arrester averaged 0.152 kN/m^2 (0.022 psid) at an average air-flow velocity of 4.58 m/s (15.89 ft/s).

The 30.5-cm- (12-in.-) long stainless-steel Shand and Jurs arrester configuration (No. 179) was subjected to six stable detonations. The rupture disc was blown out and the detonation was arrested on all test firings. A low-level peak-pressure pulse, which averaged 260 kN/m^2 (38 psia), was measured in the witness section. A plot of these test results are shown in Figure 13-5. Pre- and posttest pressure loss across the arrester averaged 0.230 kN/m^2 (0.033 psid) at an average air-flow velocity of 4.48 m/s (14.70 ft/s).

The results of the parametric tests are summarized in Table 1-2. A plot of the arrester core length versus the downstream peak-pressure pulse is shown in Figure 13-6. If the apparent linear relationship between core length and peak-pressure pulse on this graph were to be extrapolated down to the atmosphere, (zero peak-pressure pulse) the corresponding arrester core length would be 58.5 cm (23 in.). It was impractical to verify this result by further testing since the required arrester core element was not commercially available. The 20.5-cm- (8-in.-) long Shand and Jurs arrester assembly was selected to be evaluated using a directly connected inlet pipe configuration.

The indirect inlet connection to all detonation-flame arresters was initially employed to reduce the severity of the impacting shock wave. The rupture-disc assembly was used to release the hot combustion gas from the pipeline detonation rather than allowing it to flow through the arrester. If this gas retained enough heat, it could cause a reignition of the flammable mixtures downstream of the arrester. The first assumption proved to be wrong, in that there was no evidence that the combustion-

FLAME VELOCITY AND PEAK PRESSURE VERSUS PIPE LENGTH
TEST CONFIGURATION NO. 176 AND NO. 177

TEST NO.	SYMBOL
1470-A	○
B	□
C	◇
1471-A	△
B	◁

$\phi = 1.1$
$VA = 4.6$ m/s
$PD = 690$ kN/m^2

○ OPEN SYMBOLS – FLAME SENSORS
● CLOSED SYMBOLS – PRESSURE SENSORS
ϕ EQUIVALENCE RATIO, GASOLINE/AIR
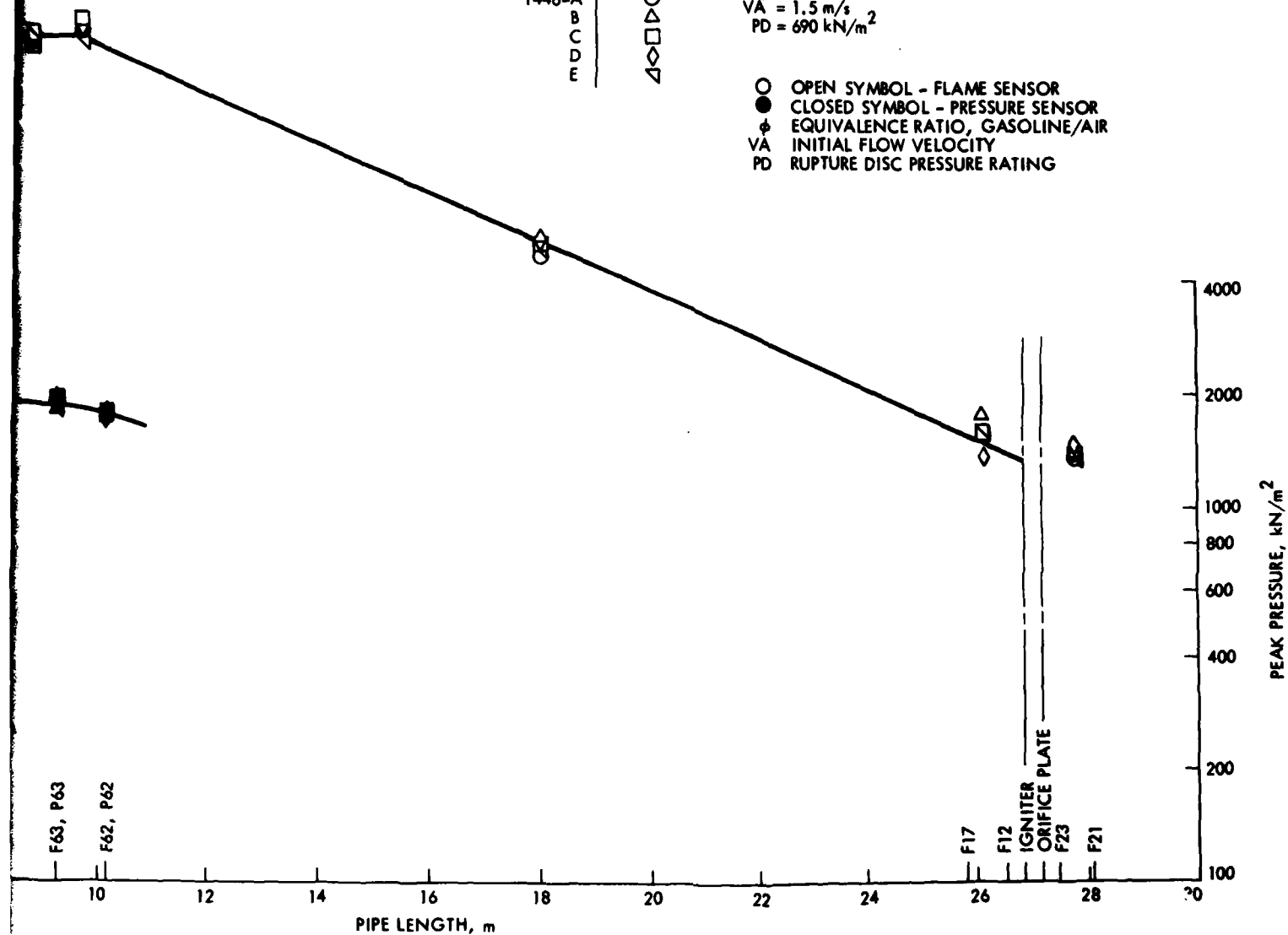VA INITIAL FLOW VELOCITY
PD RUPTURE DISC PRESSURE RATING

FLAME VELOCITY, m/s
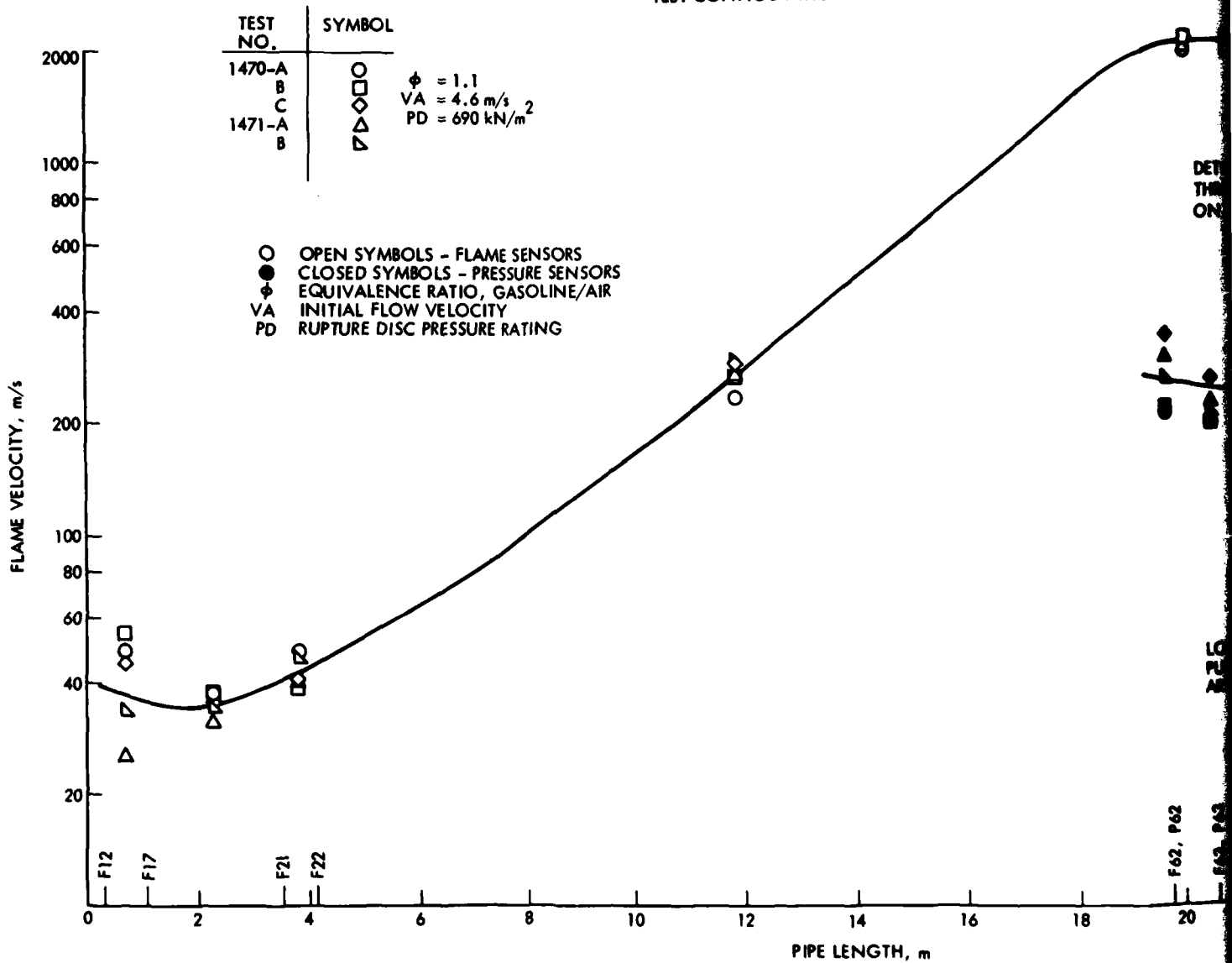
PIPE LENGTH, m

Figure 13-2.   Shand and Jur
Ribbon Arrest
Diameter by

FLAME VELOCITY AND PEAK PRESSURE VERSUS PIPE LENGTH
TEST CONFIGURATION NO. 176 AND NO. 177

1.1
4.6 m/s
690 kN/m^2

DETONATION PASSED
THROUGH ARRESTER
ON LAST TWO TESTS

FLAME SENSORS
– PRESSURE SENSORS
TIO, GASOLINE/AIR
OCITY
SSURE RATING

4000

LOW-LEVEL PRESSURE
PULSE PASSED THROUGH
ARRESTER ON ALL TESTS

2000

PEAK PRESSURE, kN/m^2

100
800
600

400

F62, P62
F63, P63
F71, P71
F72, P72
F82, P82
F85, P85
SHAND AND JURS
F101, P101
F104, P104

200

100

8   10   12   14   16   18   20   22   24   26   28

PIPE LENGTH, m
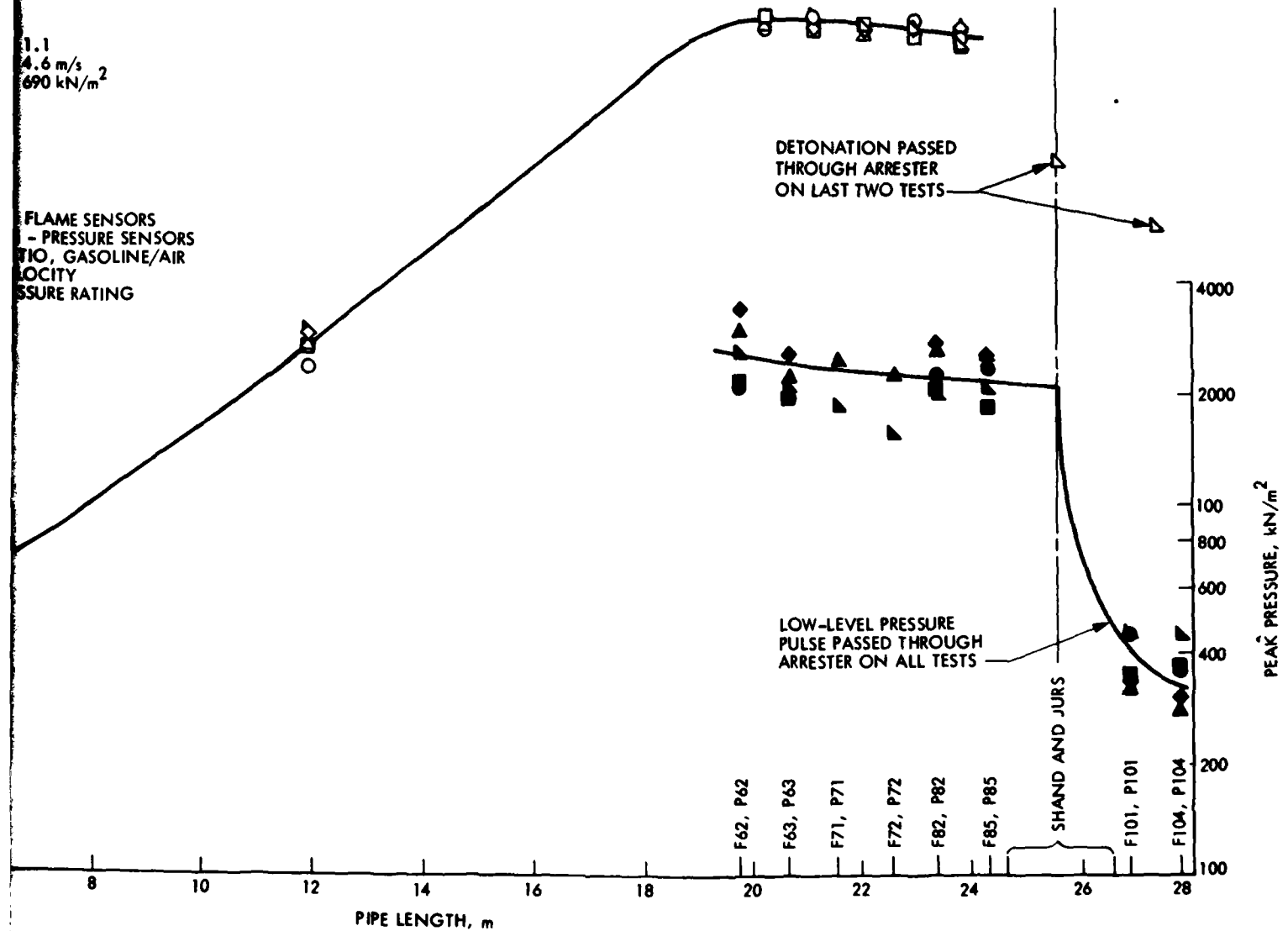
Figure 13-2.   Shand and Jurs Spiral-Wound, Crimped Stainless-Steel
Ribbon Arrester Assembly Test Results, Size: 30.5-cm
Diameter by 15.2-cm Length

13-5

2
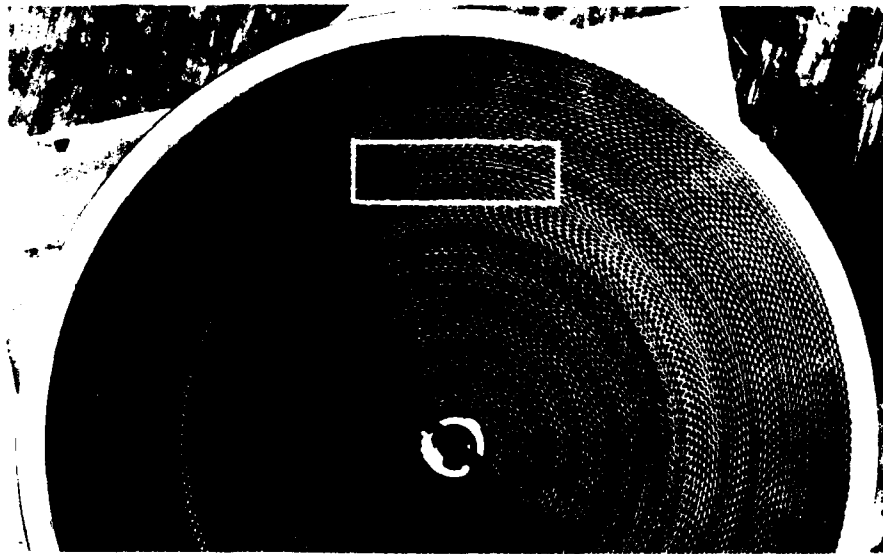
Figure 13-3. Spiral-Wound, Crimped Stainless-Steel Ribbon
Core Element, 30.5-cm Diameter by 15.2-cm
Length, Posttest

driven detonation wave was in any way diminished by combinations of
pipe tees and pipe elbows. The second assumption on combustion gasses
causing a reignition remained to be evaluated.

A direct connect inlet was made by rearranging the test assembly
inlet pipe tee to an in-line position with the arrester test assembly and
removing the inlet pipe elbow. The branch line of the pipe tee, contain-
ing the rupture-disc assembly, was directed vertically up as shown in
Figure 13-7. A photograph of this installation containing the 20.3-
cm- (8-in.-) long stainless-steel Shand and Jurs arrester test assembly
is presented in Figure 13-8. This configuration (No. 180 to No. 183)
was subjected to six stable detonations. In the first three tests,
the rupture-disc pressure rating was increased in steps through 690,
2068, and 4137 kN/m^2 (100, 300, and 600 psid). On the last three tests,
the rupture-disc assembly was blanked off with a blind flange. The
detonation was arrested on all test firings. A low-level peak-pressure
pulse that averaged 325 kN/m^2 (47 psia) was measured in the witness
section. The level of this pressure pulse was not noticeably influenced
by the rupture-disc pressure rating or when the blow-out port was blanked
off. Pre- and posttest pressure loss across the arrester averaged 0.138
kN/m^2 (0.020 psid) at an average air-flow velocity of 4.44 m/s (14.58
ft/s). A plot of the test results is shown in Figure 13-9 and summarized
in Table 1-2.

Posttest inspection of the arrester core element showed no distortion or damage to the spiral-wound, crimped stainless-steel ribbon windings. A photograph of the upstream side of the core element showing a flame imprint of the retainer grid, caused by carbon deposit, is presented in Figure 13-10. By contrast, the downstream side of the same element shown in Figure 13-11 appears very clean. The downstream retainer grid was bowed slightly at the axial center line as shown in Figure 13-12.

C.   VERTICAL BED OF ALUMINUM BALLAST RINGS ARRESTER TEST ASSEMBLIES

The vertical bed of Ballast rings arrester test assembly was installed into the test section in the same configuration used earlier as shown in Figure 8-18. New aluminum Ballast rings were obtained from Glitsch, Inc. in three sizes: (1) 2.54 cm (1.0 in.) in diameter by 2.54 cm (1.0 in.) long, (2) 3.81 cm (1.5 in.) in diameter by 3.81 cm (1.5 in.) long, and (3) 5.08 cm (2.0 in.) in diameter by 5.08 cm (2.0 in.) long. Figure 13-13 shows the three different sizes of Ballast rings used. The lower support grid ring covered with heavy wire mesh was installed into the arrester housing assembly just above the inlet port. This was followed by a welded spacer assembly made from two 2.54-cm (10-in.) diameter pipe rings and four 3.81-cm (1.5-in.) steel 90-deg angle bars. The spacer established the packed bed depth. A second support grid ring, also covered with heavy wire mesh, was placed on top of the first spacer and held down by a second spacer, which built the stack height up to the vessel cover. This stacked assembly is shown in Figure 13-14. The internal volume between the two grid support rings was packed with the selected size of aluminum Ballast rings. The spacers rigidly controlled the established bed depth by maintaining the position of the support grid rings against the displacing forces of the incoming detonation wave. Three sets of spacers, two in each set, provided the three variations in bed depth: (1) 63.5 cm (25 in.), (2) 45.7 cm (18 in.), and (3) 22.9 cm (9.0 in.), all at a constant bed diameter of 43.2 cm (17 in.).

The variations in bed diameters were accomplished with cylindrical pipe inserts that were flanged on the lower end to close-off the annular area between the inner wall of the housing vessel and the outer wall of the pipe insert. Internal diameter of the pipe insert controlled the packed bed flow path. The insert was lowered into the vessel housing on top of the lower support grid ring. The second support grid ring was then placed on top of the insert and held in place by a spacer, which built the stack height up to the vessel cover. This stacked assembly is shown in Figure 13-15. The volume between the two support grid rings were packed with the selected size of Ballast rings, both inside the cylindrical insert and in the surrounding annulus. The flow path is restricted to the internal diameter of the pipe insert. Including the unrestricted vessel housing and three sets of cylindrical inserts and spacers, the four variations in bed diameter are (1) 43.2 cm (17 in.), (2) 33.7 cm (13.25 in.), (3) 30.5 cm (12 in.), and (4) 25.4 cm (10 in.), all at a constant bed depth of 63.5 cm (25 in.).

FLAME VELOCITY AND PEAK PRESSURE VERSUS PIPE LENGTH
TEST CONFIGURATION NO. 178

TEST NO.	SYMBOL
1472-A	O
B	□
C	◇
D	△
E	◁
F	◊

ϕ = 1.1
VA = 4.6 m/s
PD = 690 kN/m^2

O   OPEN SYSBOL – FLAME SENSOR
●   CLOSED SYMBOL – PRESSURE SENSOR
ϕ EQUIVALENCE RATIO, GASOLINE/AIR
VA   INITIAL FLOW VELOCITY
PD   RUPTURE DISC PRESSURE RATING
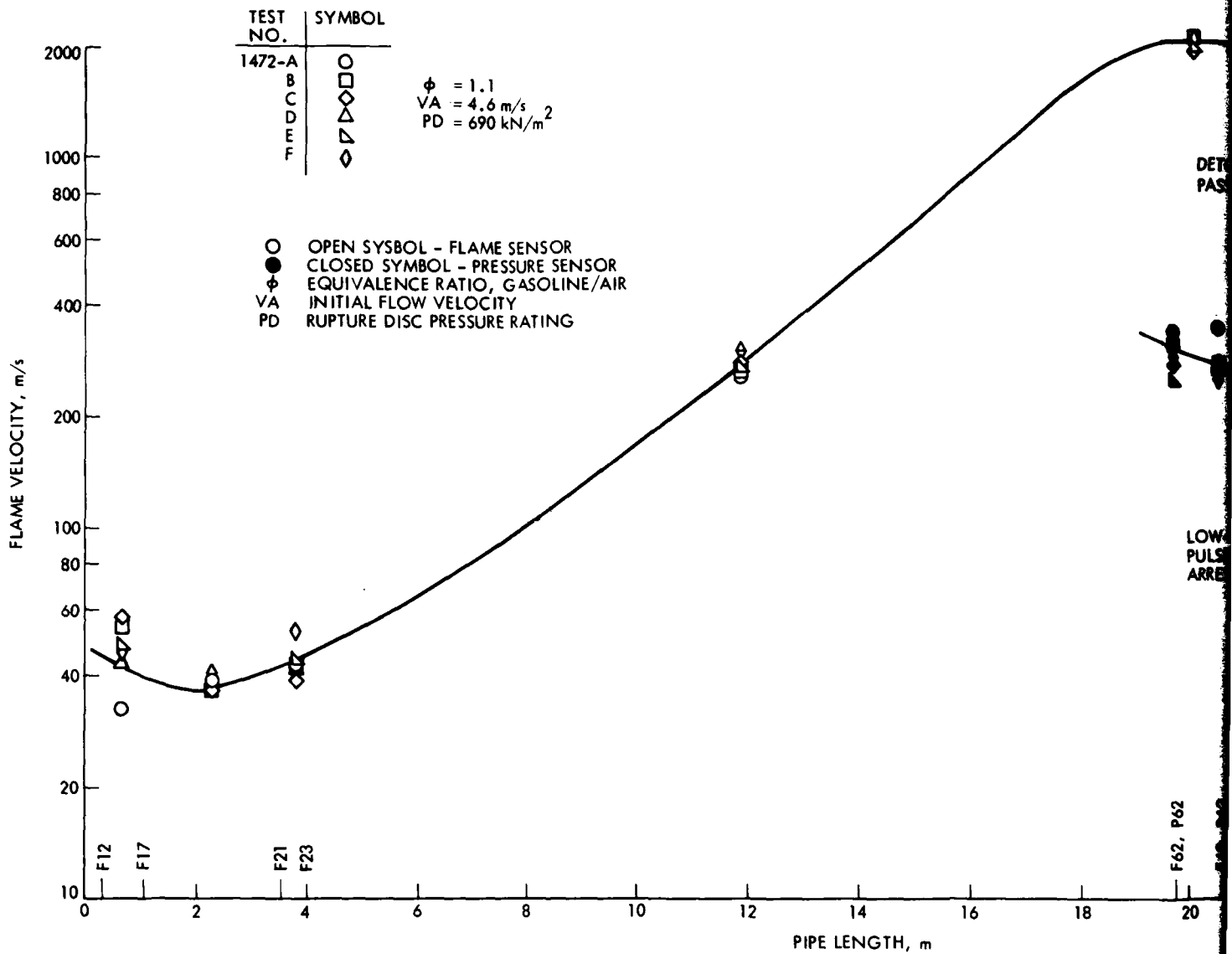
Figure 13-4.   Shand and Jurs
Ribbon Arrester
by 20.3-cm Leng

FLAME VELOCITY AND PEAK PRESSURE VERSUS PIPE LENGTH
TEST CONFIGURATION NO. 178

■ 1.1
■ 4.6 m/s
■ 690 kN/m²

DETONATION DID NOT
PASS THROUGH ARRESTER

LAME SENSOR
– PRESSURE SENSOR
TIO, GASOLINE/AIR
LOCITY
SSURE RATING

LOW-LEVEL PRESSURE
PULSE PASSED THROUGH
ARRESTER ON ALL TESTS

PEAK PRESSURE, kN/m²

4000

2000

1000
800

600

400

200

100

F62, P62
F63, P63
F71, P71
F72, P72
F82, P82
F85, P85
SHAND AND JURS
F101, P101
F104, P104

PIPE LENGTH, m

8   10   12   14   16   18   20   22   24   26   28
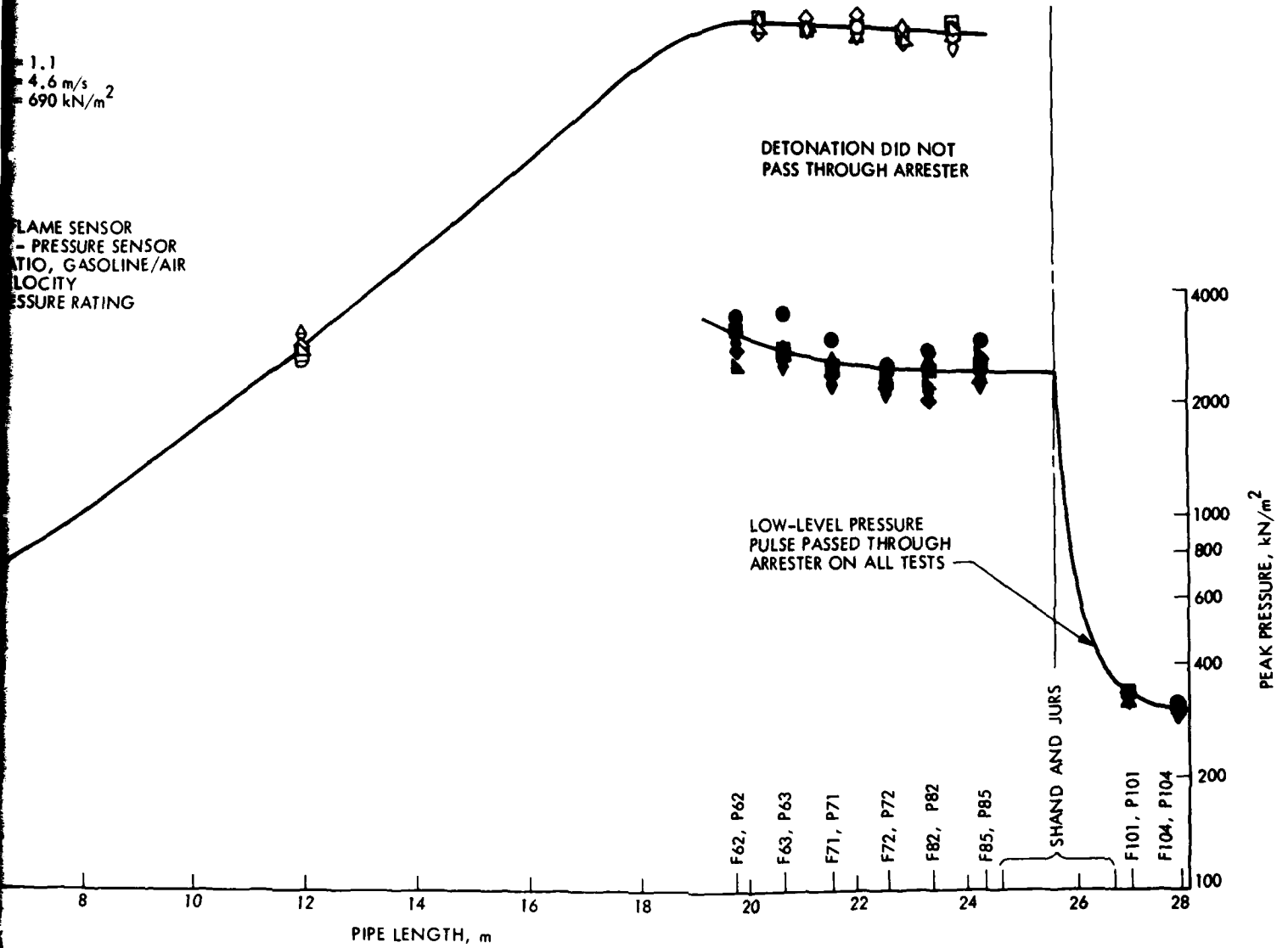
Figure 13-4.   Shand and Jurs Spiral-Wound, Crimped Stainless-Steel
Ribbon Arrester Assembly Test Results, 30.5-cm Diameter
by 20.3-cm Length

13-9

2

FLAME VELOCITY AND PEAK PRESSURE VERSUS PIPE LENGTH
TEST CONFIGURATION NO. 179
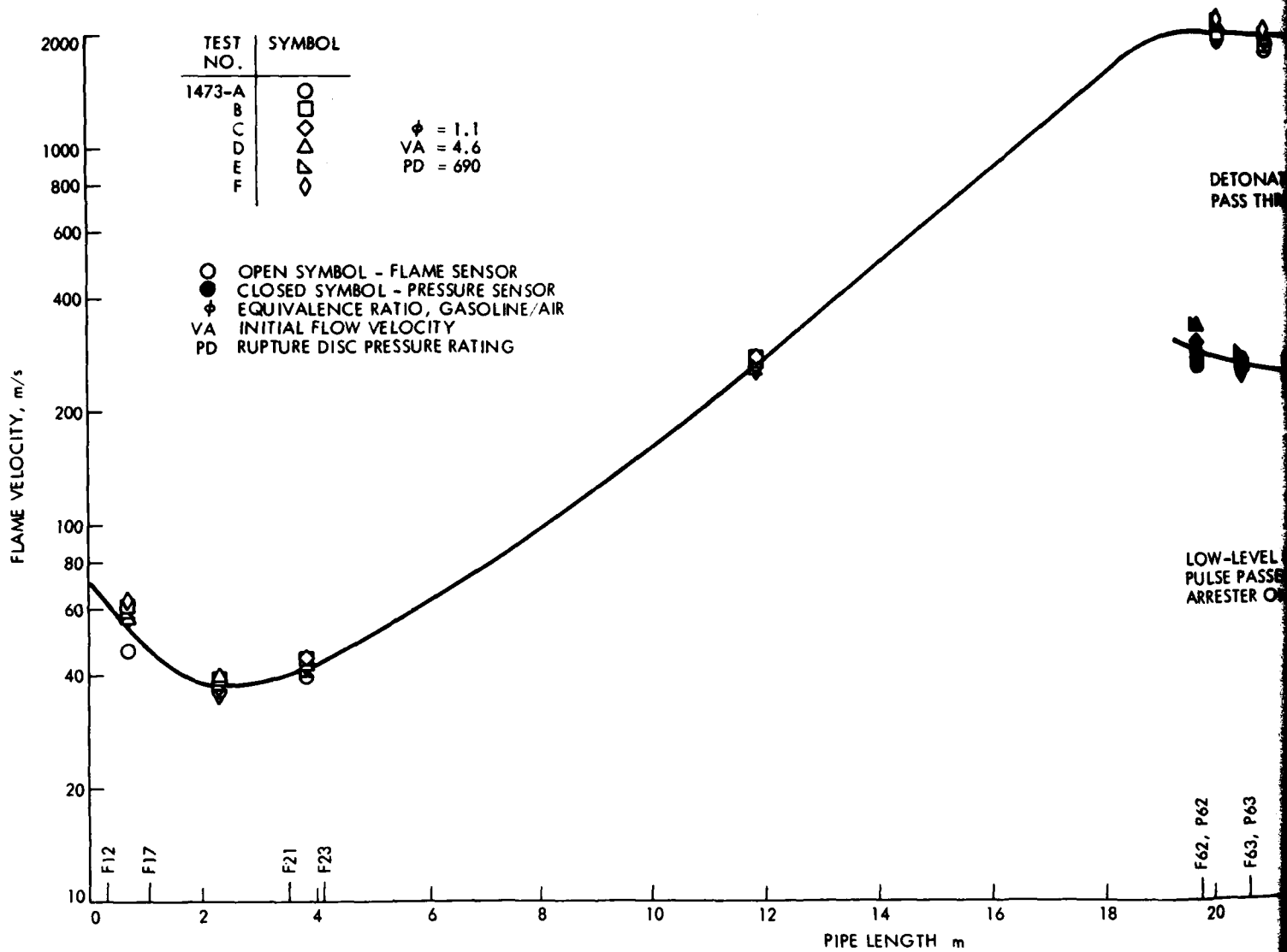
Figure 13-5. Shand and Jurs Sp
Ribbon Arrester A
by 30.5-cm Length

Figure 13-5. Shand and Jurs Spiral-Wound, Crimped Stainless-Steel
Ribbon Arrester Assembly Test Results, 30.5-cm Diameter
by 30.5-cm Length

13-11
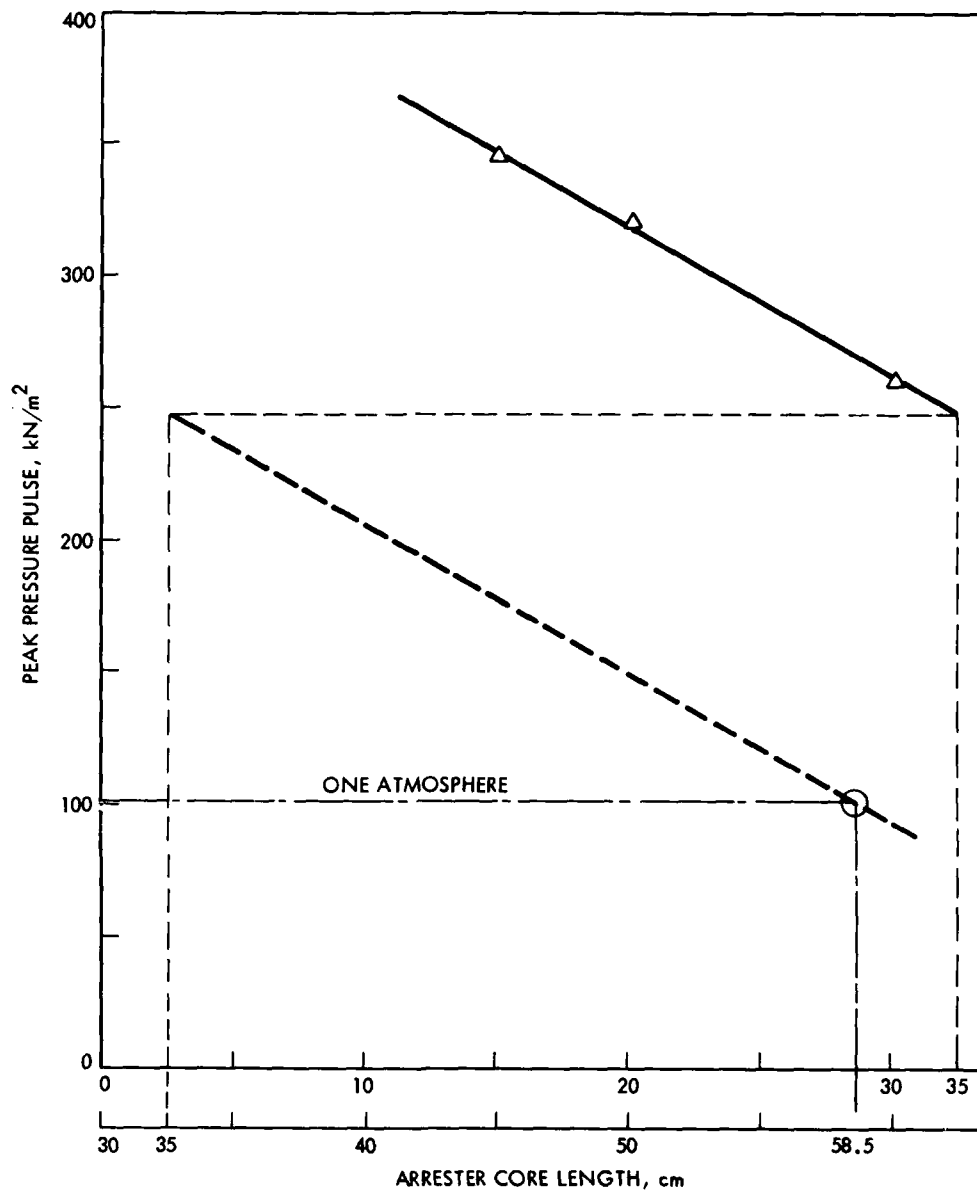
Figure 13-6. Shand and Jurs Spiral-Wound, Crimped Stainless-Steel
Ribbon Arrester Core Length Versus Downstream Peak-
Pressure Pulse
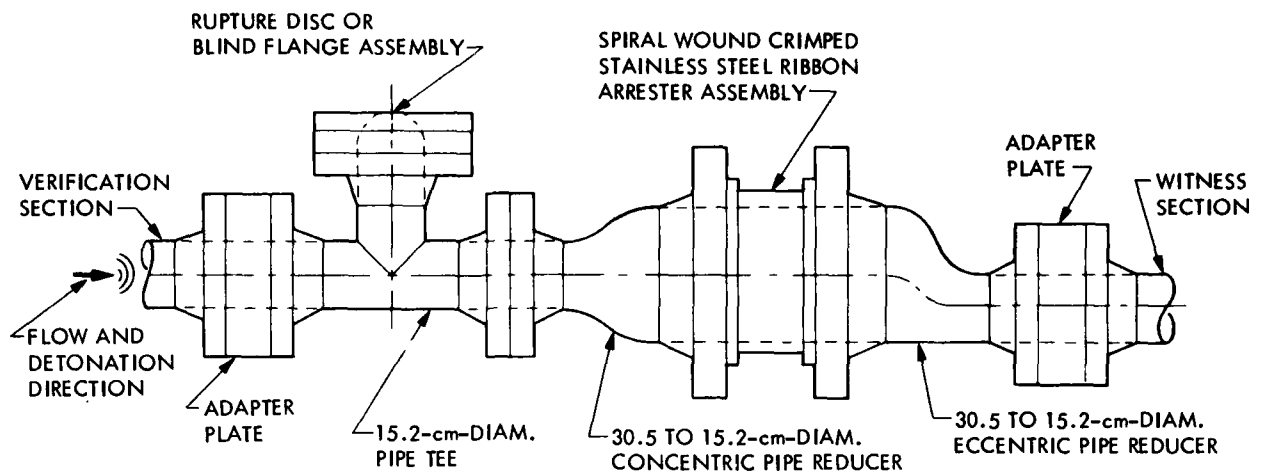
Figure 13-7. Shand and Jurs Spiral-Wound, Crimped Stainless-Steel Ribbon Arrester Test Assembly with Direct Connect Inlet Schematic Drawing

Figure 13-8. Shand and Jurs Spiral-Wound, Crimped Stainless-Steel Ribbon Arrester Test Installation with Direct Connect Inlet
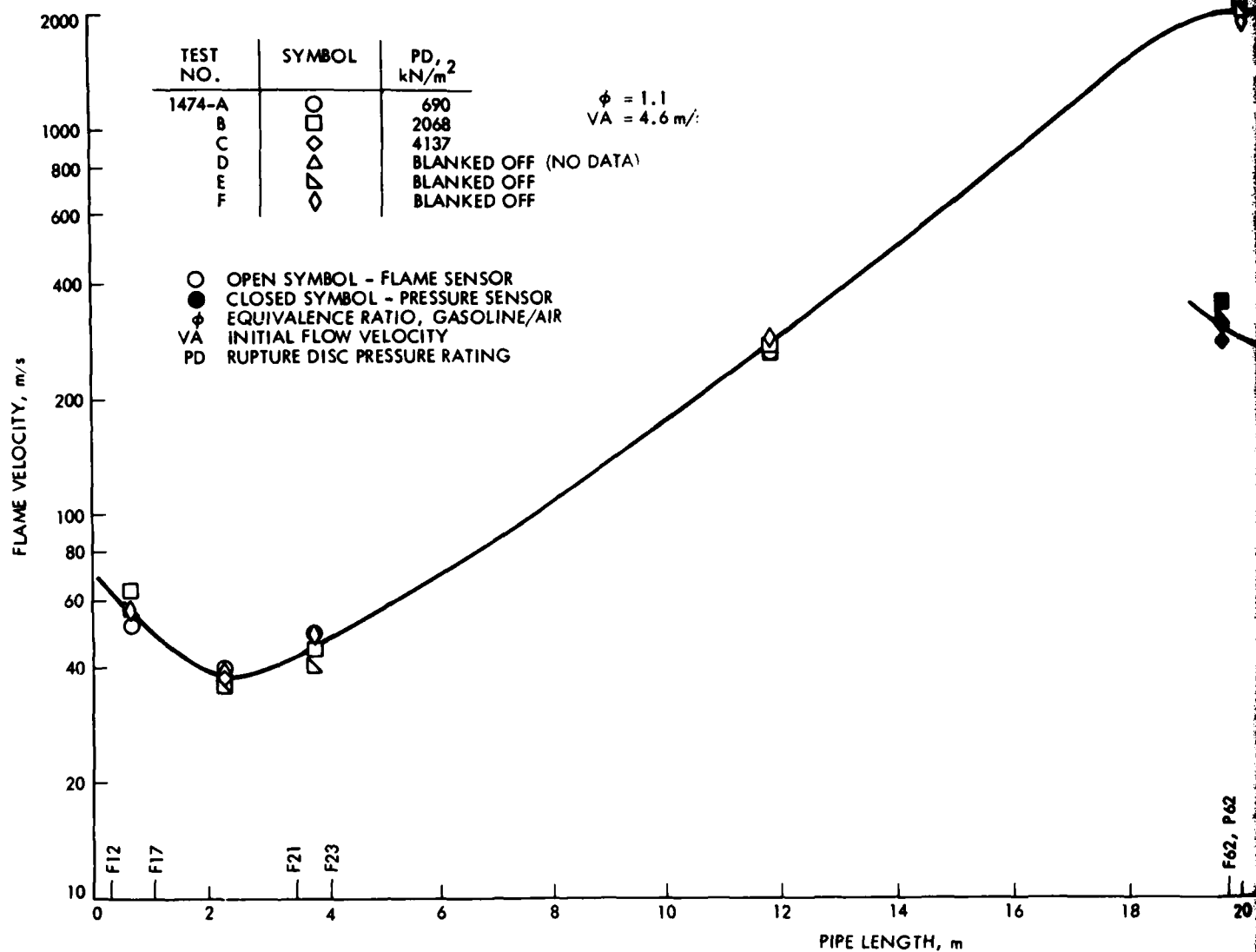
Figure 13-9. Shand and Jurs Sp...
Arrester Assembly
Length, Direct Co...
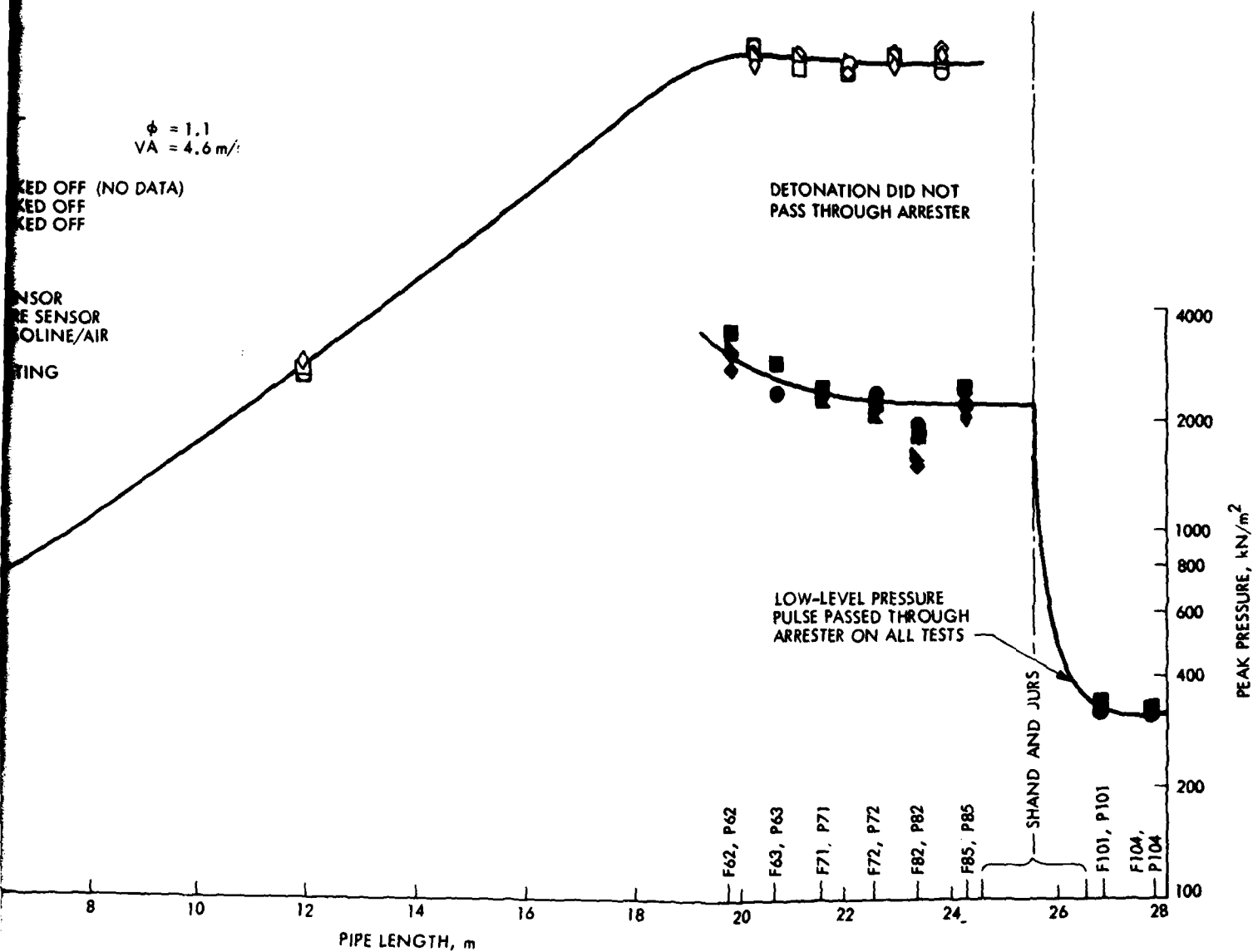
Figure 13-9. Shand and Jurs Spiral-Wound, Crimped Stainless-Steel Ribbon Arrester Assembly Test Results, 30.5-cm Diameter by 20.3-cm Length, Direct Connect Inlet

13-15
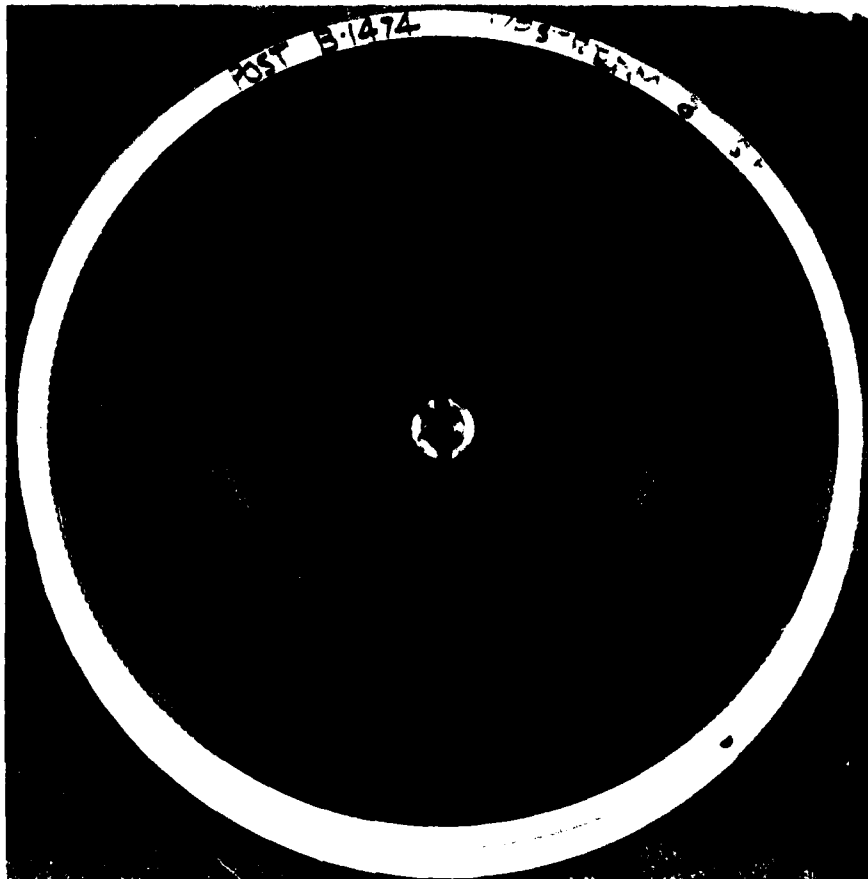
Figure 13-10. Spiral-Wound, Crimped Stainless-Steel Ribbon
Core Element, 30.5-cm Diameter by 20.3-cm
Length, Posttest Upstream Side

The inlet and outlet piping connections to the vertical bed of
Ballast rings arrester were the same combination of pipe tees, rupture-
disc not in line, and pipe-elbow assemblies as previously used. It
would have required a major modification to the facility piping and
support structures to accomplish a direct in-line inlet and outlet
connections to the arrester vessel housing. Rupture-disc assemblies
with a 690 kN/m^2 (100 psid) pressure rating were installed on the inlet
pipe tee, the vessel cover, and the outlet pipe tee. All test firings
were made using gasoline and air mixtures at the standard test conditions
with the upstream ignition location.

Figure 13-11. Spiral-Wound, Crimped Stainless-Steel Ribbon
Core Element, 30.5-cm Diameter by 20.3-cm
Length, Posttest Downstream Side

The first three bed depth parametric test configurations (No.
184, No. 185, and No. 186) were all packed with the 2.54-cm- (1.0-in.-)
diameter by 2.54-cm- (1.0-in.-) long aluminum Ballast rings. A new
bed of rings was installed at the start of each test series because
of the deformation that occurred in the rings. Starting with the full-
size bed that was 43.2 cm (17 in.) in diameter, the bed depth was reduced
in steps through 63.5 cm (25 in.), 45.7 cm (18 in.), and 22.9 cm (9
in.). Each configuration was subjected to six stable detonations.
Only the inlet rupture disc was blown out and the detonation was
arrested on all but two test firings. On the fourth and sixth test
firings, with the 22.9-cm (9-in.) bed depth, the detonation passed
through the arrester, blowing out all three rupture discs. Flame
velocity in the witness section on these tests was measured at around
660 m/s (2166 ft/s). When the detonation was arrested, the down-
stream peak pressure pulse ranged from 181 to 236 kN/m^2 (26.3 to 34.2
psia), and showed an increase in pressure level with the reduction
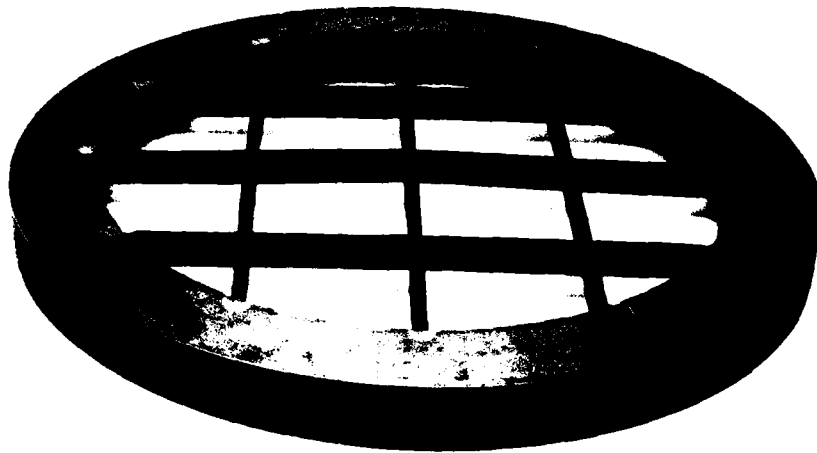
Figure 13-12. Spiral-Wound, Crimped Ribbon Arrester
Mounting Ring, Posttest Downstream
Side Showing Deformation of Retainer
Grid

5.08 cm   3.01 cm   2.54 cm
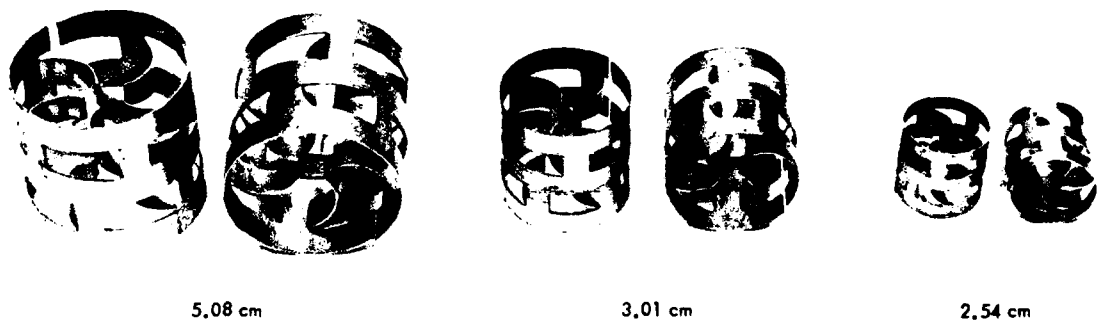
Figure 13-13. Aluminum Ballast Rings, Three Sizes

13-19
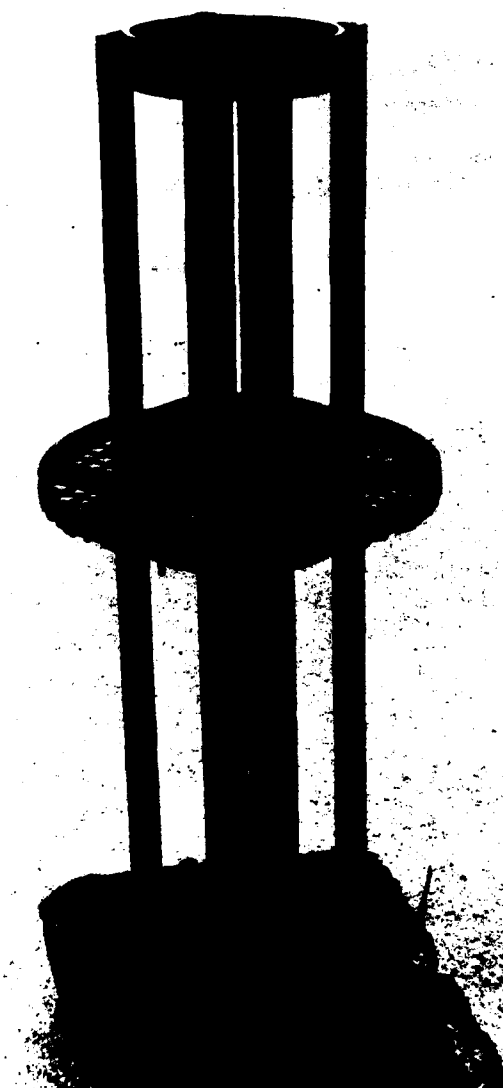
Figure 13-14.   Stacked Assembly of   Figure 13-15.   Stacked Assembly of
                Support Grid Rings   Support Grid Rings
                Covered with Heavy   Covered with Heavy
                Wire Mesh and Bed   Wire Mesh, Bed
                Depth Spacers   Diameter Insert,
                                                        and Spacer

in bed depth. On the test firings where the detonation passed through
the arrester, the peak pressure pulse exceeded the 450 kN/m^2 (65 psia)
upper range of the pressure sensors installed. Plots of the test data
results for these tests are shown in Figures 13-16, 13-17, and 13-18.
Table 1-3 is a summary of the test results.

Figure 13-16. Vertical Bed of Ba̲
Test Results, Bed
Depth, Ring Size:

FLAME VELOCITY AND PEAK PRESSURE VERSUS PIPE LENGTH
TEST CONFIGURATION NO. 184

DETONATION DID NOT
PASS THROUGH ARRESTER

LOW-LEVEL PRESSURE
PULSE PASSED THROUGH
ARRESTER ON ALL TESTS
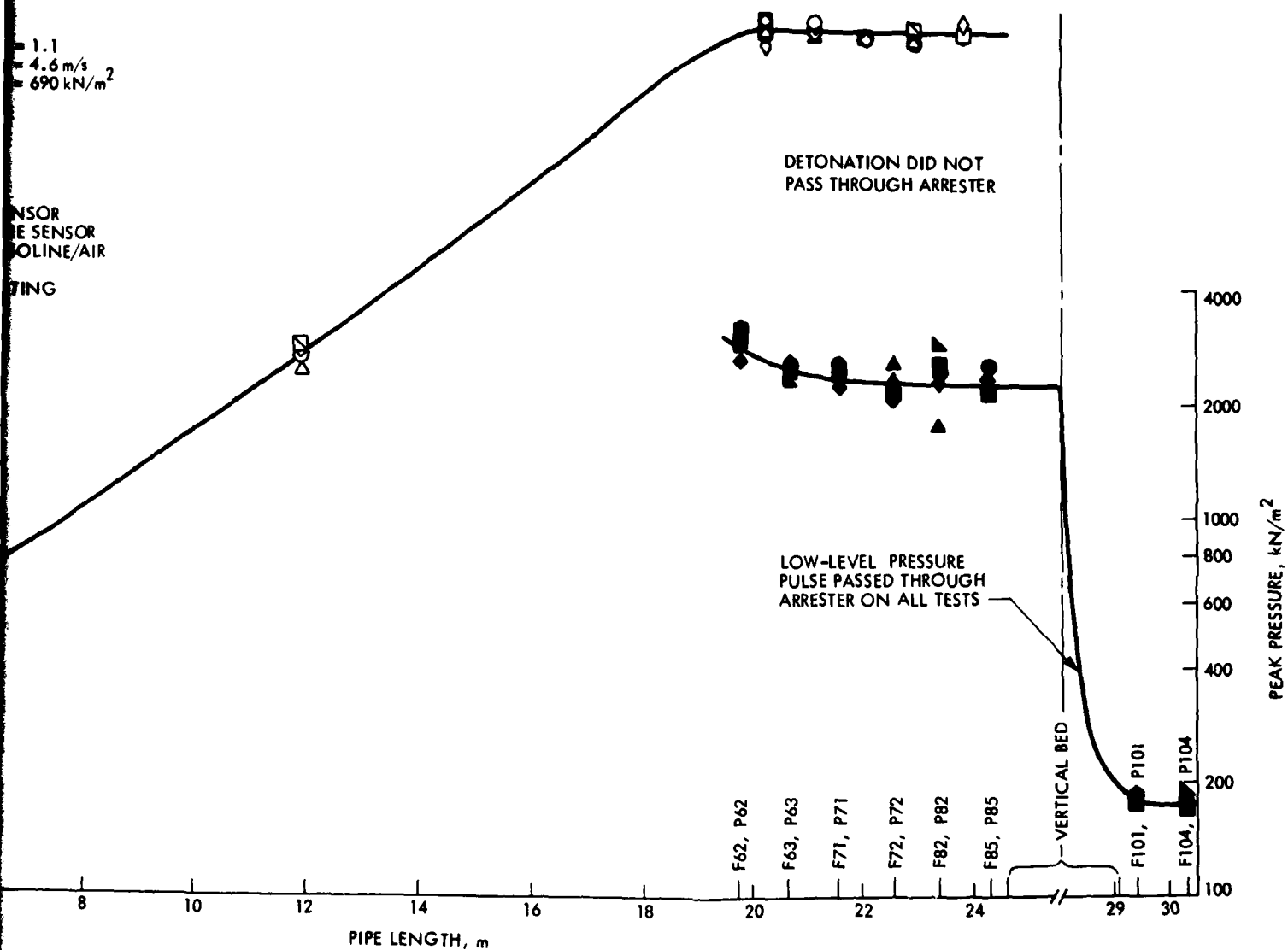
Figure 13-16. Vertical Bed of Ballast Rings Arrester Assembly Parameter
Test Results, Bed Size: 43.2-cm Diameter by 63.5-cm
Depth, Ring Size: 2.54-cm Diameter by 2.54-cm Length

13-21

FLAME VELOCITY AND PEAK PRESSURE VERSUS PIPE LENGTH
TEST CONFIGURATION NO. 185

TEST NO.	SYMBOL
1476-A	O
B	□
C	◇
D	△
E	◁
F	◇

ϕ = 1.1
VA = 4.6 m/s
PD = 690 kN/m^2

O OPEN SYMBOL – FLAME SENSOR
● CLOSED SYMBOL – PRESSURE SENSOR
ϕ EQUIVALENCE RATIO, GASOLINE/AIR
VA INITIAL FLOW VELOCITY
PD RUPTURE DISC PRESSURE RATING

FLAME VELOCITY, m/s

PIPE LENGTH, m

F12 F17   F21 F23   F62, P62

DETO
PASS

LOW-LEVE
PULSE PAS
ARRESTER

Figure 13-17. Vertical Bed of B
Test Results, Bed
Depth, Ring Size:

Figure 13-17. Vertical Bed of Ballast Rings Arrester Assembly Parametric
Test Results, Bed Size: 43.2-cm Diameter by 45.7-cm
Depth, Ring Size: 2.54-cm Diameter by 2.54-cm Length

FLAME VELOCITY AND PEAK PRESSURE VERSUS PIPE LENGTH
TEST CONFIGURATION NO. 186

TEST NO.	SYMBOL
1477-A	○
B	□
C	◇
D	△
E	◁
F	◇

$\phi = 1.1$
$VA = 4.6 \, m/s$
$PD = 690 \, kN/m^2$

○ OPEN SYMBOL – FLAME SENSOR
● CLOSED SYMBOL – PRESSURE SENSOR
ϕ EQUIVALENCE RATIO, GASOLINE/AIR
VA INITIAL FLOW VELOCITY
PD RUPTURE DISC PRESSURE RATING

DETONATION PAS
THROUGH ARRESTE
ON TESTS 1477D A

Figure 13-18.   Vertical Bed of B
Test Results, Bed
Depth, Ring Size:

Figure 13-18. Vertical Bed of Ballast Rings Arrester Assembly Parametric Test Results, Bed Size: 43.2-cm Diameter by 22.9-cm Depth, Ring Size: 2.54-cm Diameter by 2.54-cm Length

13-25

The pre- and posttest pressure loss across the arresters ranged from 0.052 to 0.075 kN/m^2 (0.007 to 0.011 psid) at an average air velocity of 4.58 m/s (15.03 ft/s). Pressure loss decreased with the reduction in bed depth, and generally increased slightly after the first test firing in a series. Posttest inspection of the packed bed of rings showed about a 35% compaction due to distortion of the Ballast rings. A posttest photograph of a compacted bed of rings is shown in Figure 13-19. Since the support grid rings were restrained from motion, the compaction had to be caused by the force of the detonation wave acting on the frontal area of the Ballast rings alone.

A full-size arrester bed was used in the parametric tests with different-size Ballast rings. The 2.54-cm (1.0-in.) rings were replaced by new 3.81-cm- (1.5-in.-) diameter by 3.81-cm- (1.5-in.-) long aluminum Ballast rings in a bed depth of 63.5 cm (25 in.). All other parameters remained the same. This new arrester configuration (No. 187) was subjected to four stable detonations. On the first two firings, only the inlet rupture disc was blown out and the detonation was arrested. On the last two firings, all three rupture discs were blown out and flame was recorded in the witness section with a velocity of around 770 m/s (2530 ft/s). When the detonation was arrested, the downstream peak pressure pulse averaged 290 kN/m^2 (42.1 psia) and then exceeded 450 kN/m^2 (65 psia) when flame penetrated the arrester. Pre and posttest pressure loss across the arrester averaged 0.067 kN/m^2 (0.010 psid) at an average air-flow velocity 4.73 m/s (15.52 ft/s). The arrester bed was repacked
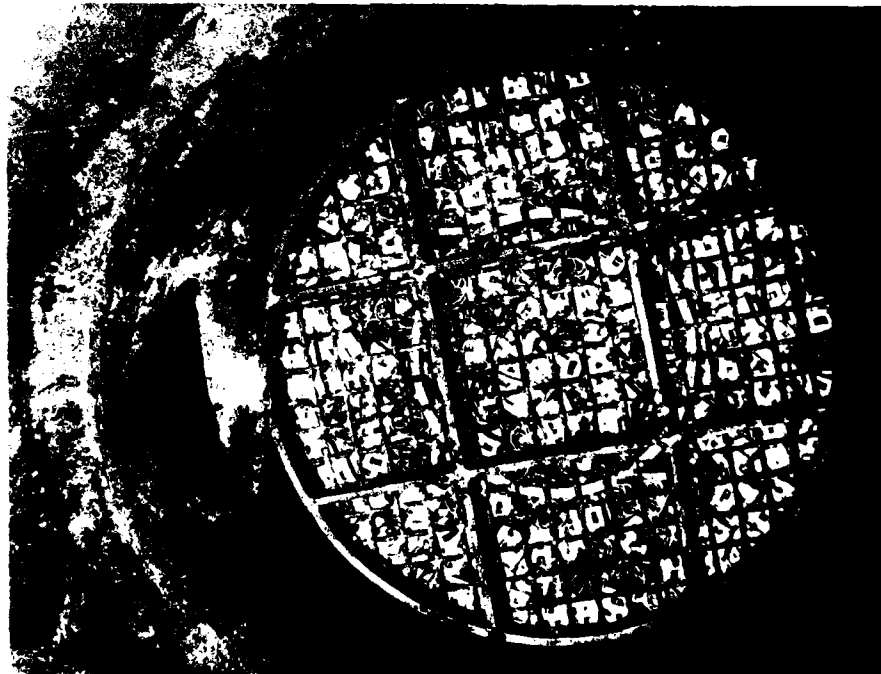
Figure 13-19. Posttest Compacted Bed of Aluminum Ballast Rings

with new 5.08-cm- (2.0-in.-) diameter by 5.08-cm- (2.0-in.-) long
aluminum Ballast rings at the same bed depth of 63.5 cm (25 in.). All
other parameters remained the same. This arrester configuration (No.
188) was subjected to three stable detonations. The detonation was
arrested on only the first test firing. On the last two test firings,
all rupture discs were blown out and flame was recorded in the witness
section with a velocity of around 733 m/s (2406 ft/s). When the detonation
was arrested, the downstream peak pressure pulse was 304 kN/m^2 (44.1
psia) and exceeded 450 kN/m^2 (65 psia) when flame penetrated the arrester.
Pre- and posttest pressure loss across the arrester averaged 0.056 kN/m^2
(0.008 psid) at an average air-flow velocity of 4.68 m/s (15.35 ft/s).
Posttest inspection showed a 28% compaction of the bed from distortion
of the Ballast rings. The results of this test are plotted in Figure
13-21 and summarized in Table 1-3.

The next three parametric test configurations (No. 189, No. 190 and
No. 191) for variations in bed diameter were all made with new 2.54-cm
(1.0-in.) aluminum Ballast rings. A full 43.2-cm- (17-in.-) diameter
bed was demonstrated in the first test series, so this test series
started with the largest cylindrical insert and in three steps reduced
the bed diameter through 33.7 cm (13.25 in.), 30.5 cm (12 in.), and
25.4 cm (10 in.), all at a constant bed depth of 63.5 cm (25 in.).
Ballast rings were packed into both the central flow passage of the
insert and the nonflowing annular space between the inner wall of the
housing vessel and the outer wall of the insert. Figure 13-22 is a
pretest photograph showing the ring packing of the 33.7-cm (13.25-in.)
diameter bed. Each configuration was subjected to six or more stable
detonations. The detonation was arrested on all test firings and only
the inlet rupture disc was blown out. The downstream peak pressure
pulse ranged from 181 to 132 kN/m^2 (26.3 to 19.1 psia) and showed a
slight reduction in pressure level as the bed diameter was reduced in
size. Pre- and posttest averaged pressure loss across the arresters
increased from 0.075 to 0.278 kN/m^2 (0.011 to 0.040 psid) as the bed
diameter was reduced. The averaged air-flow velocity was 4.55 m/s
(14.93 ft/s). Posttest inspections showed that each bed had compacted
about 30% from distortion of the Ballast rings. The results of these
tests are plotted in Figures 13-23, 13-24, and 13-25, and summarized
in Table 1-3.

The vertical bed of Ballast rings arrester test assembly used
to evaluate the inlet rupture-disc pressure rating parameter combined
the results of the previous parametric tests. The selected bed size
was 25.4-cm (10-in.) diameter by 45.7-cm (18-in.) deep, packed with
2.54-cm- (1.0-in.-) diameter by 2.54-cm- (1.0-in.-) long aluminum Ballast
Rings. The bed depth was obtained by cutting 17.8 cm (7 in.) off the
upper end of the 25.4-cm- (10-in.-) diameter cylindrical insert and em-
ploying the appropriate length spacer to complete the stack height.
This test configuration (No. 192 to No. 195) was subjected to six stable
detonations. In the first three tests, the inlet rupture-disc pressure
rating was increased in steps through 690, 2068, and 4137 kN/m^2 (100,
300, and 600 psid). On the last three tests, the rupture-disc assembly
was blanked-off with a blind flange. The detonation was arrested on
all test firings. Where the inlet rupture disc was blown out, the
downstream peak pressure pulse measured about 141 kN/m^2 (20.4 psia).

FLAME VELOCITY AND PEAK PRESSURE VERSUS PIPE LENGTH
TEST CONFIGURATION NO. 187

TEST NO.	SYMBOL
1478-A	O
B	□
C	◇
D	△

ϕ = 1.1
VA = 4.6 m/s
PD = 690 kN/m^2

O   OPEN SYMBOL – FLAME SENSOR
●   CLOSED SYMBOL – PRESSURE SENSOR
ϕ EQUIVALENCE RATIO, GASOLINE/AIR
VA   INITIAL FLOW VELOCITY
PD   RUPTURE DISC PRESSURE RATING

FLAME VELOCITY, m/s
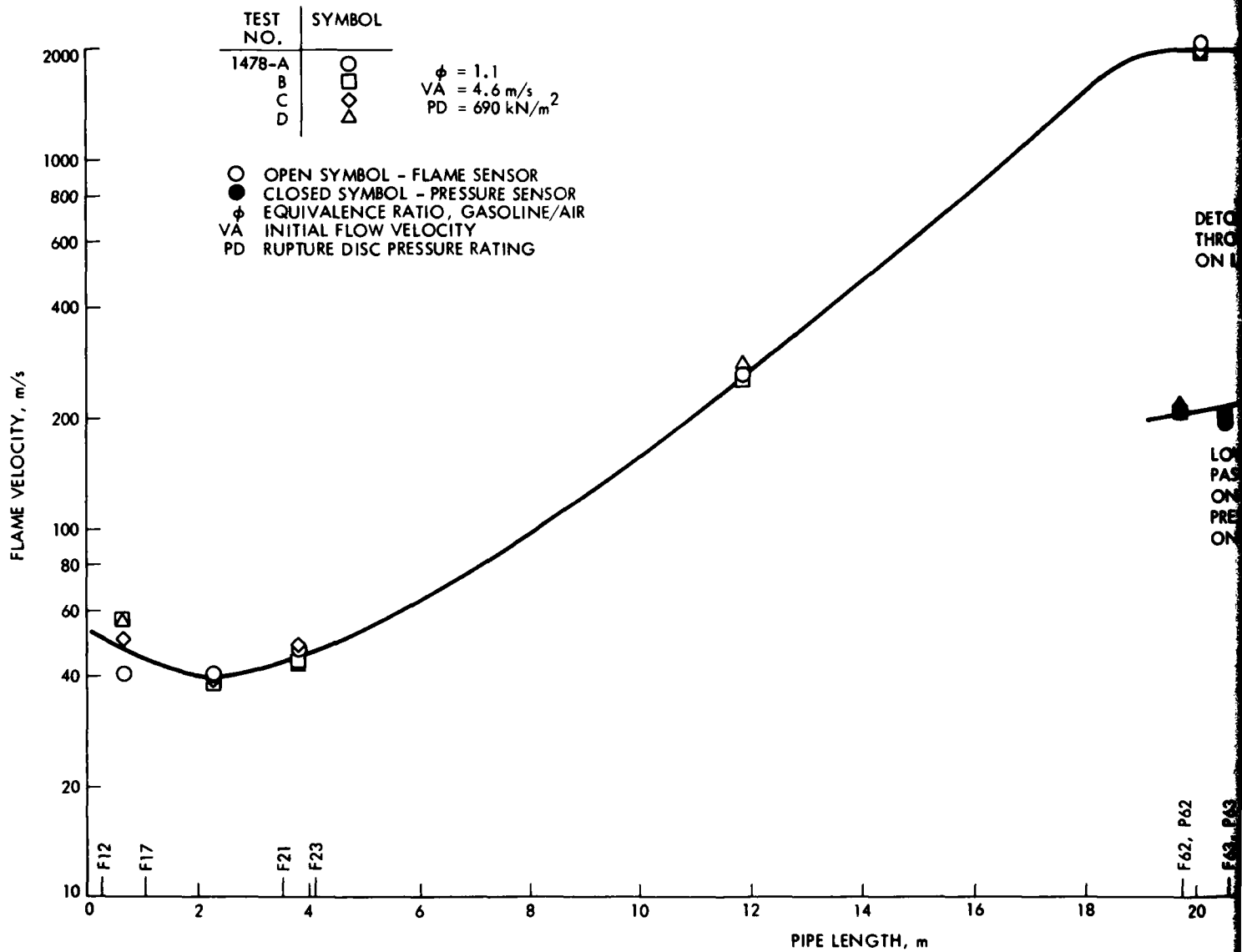
PIPE LENGTH, m

Figure 13-20.   Vertical Bed of Ball
Test Results, Bed S
Ring Size: 2.54-cm

FLAME VELOCITY AND PEAK PRESSURE VERSUS PIPE LENGTH
TEST CONFIGURATION NO. 187
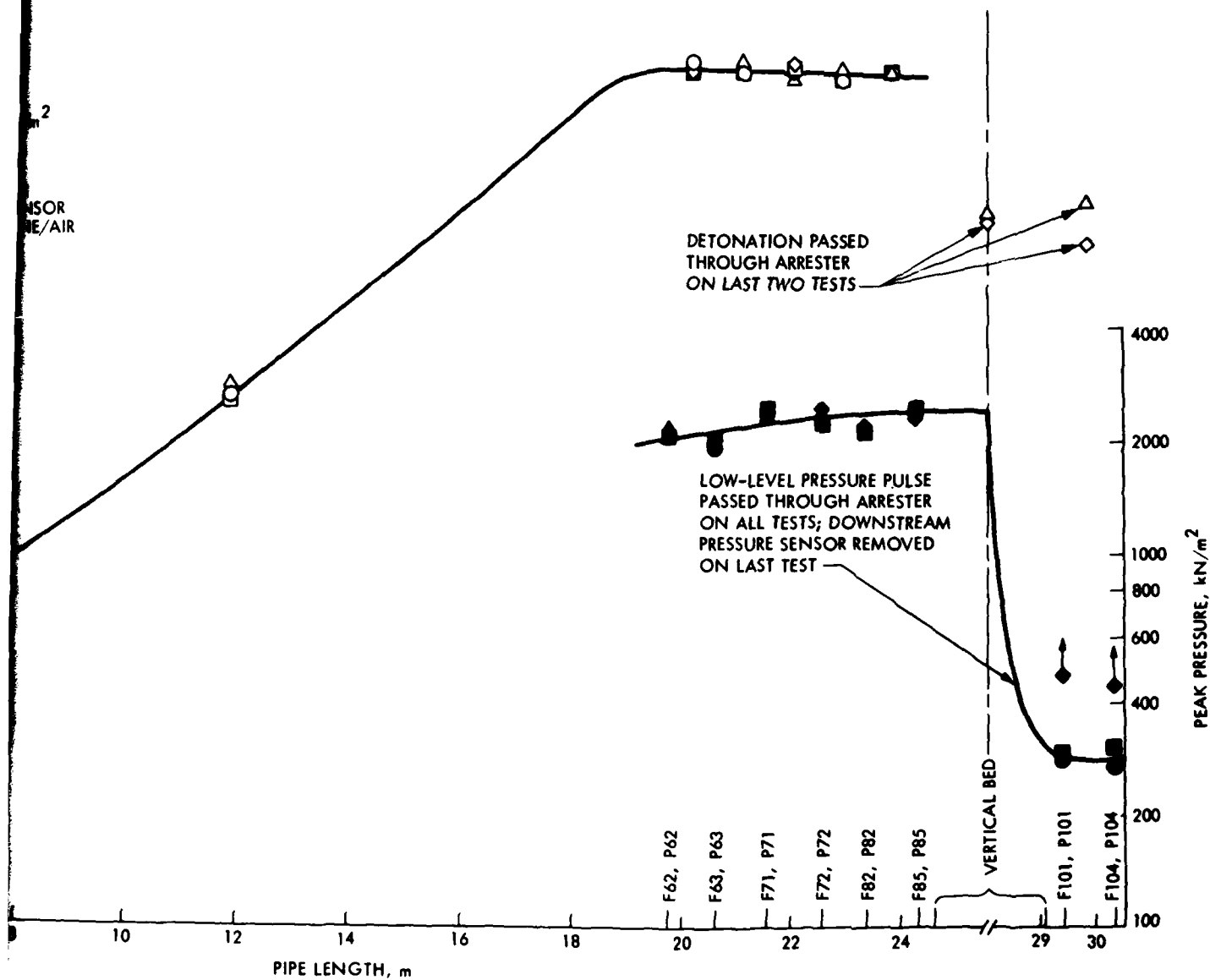
DETONATION PASSED
THROUGH ARRESTER
ON LAST TWO TESTS

LOW-LEVEL PRESSURE PULSE
PASSED THROUGH ARRESTER
ON ALL TESTS; DOWNSTREAM
PRESSURE SENSOR REMOVED
ON LAST TEST

4000

2000

1000
800

PEAK PRESSURE, kN/m²

600

400

200

100

F62, P62
F63, P63
F71, P71
F72, P72
F82, P82
F85, P85
VERTICAL BED
F101, P101
F104, P104

10   12   14   16   18   20   22   24   29   30

PIPE LENGTH, m

Figure 13-20.   Vertical Bed of Ballast Rings Arrester Assembly Parametric
Test Results, Bed Size: 43.2-cm Diameter by 22.9-cm Depth,
Ring Size: 2.54-cm Diameter by 2.54-cm Length

13-29

2

FLAME VELOCITY AND PEAK PRESSURE VERSUS PIPE LENGTH
TEST CONFIGURATION NO. 188
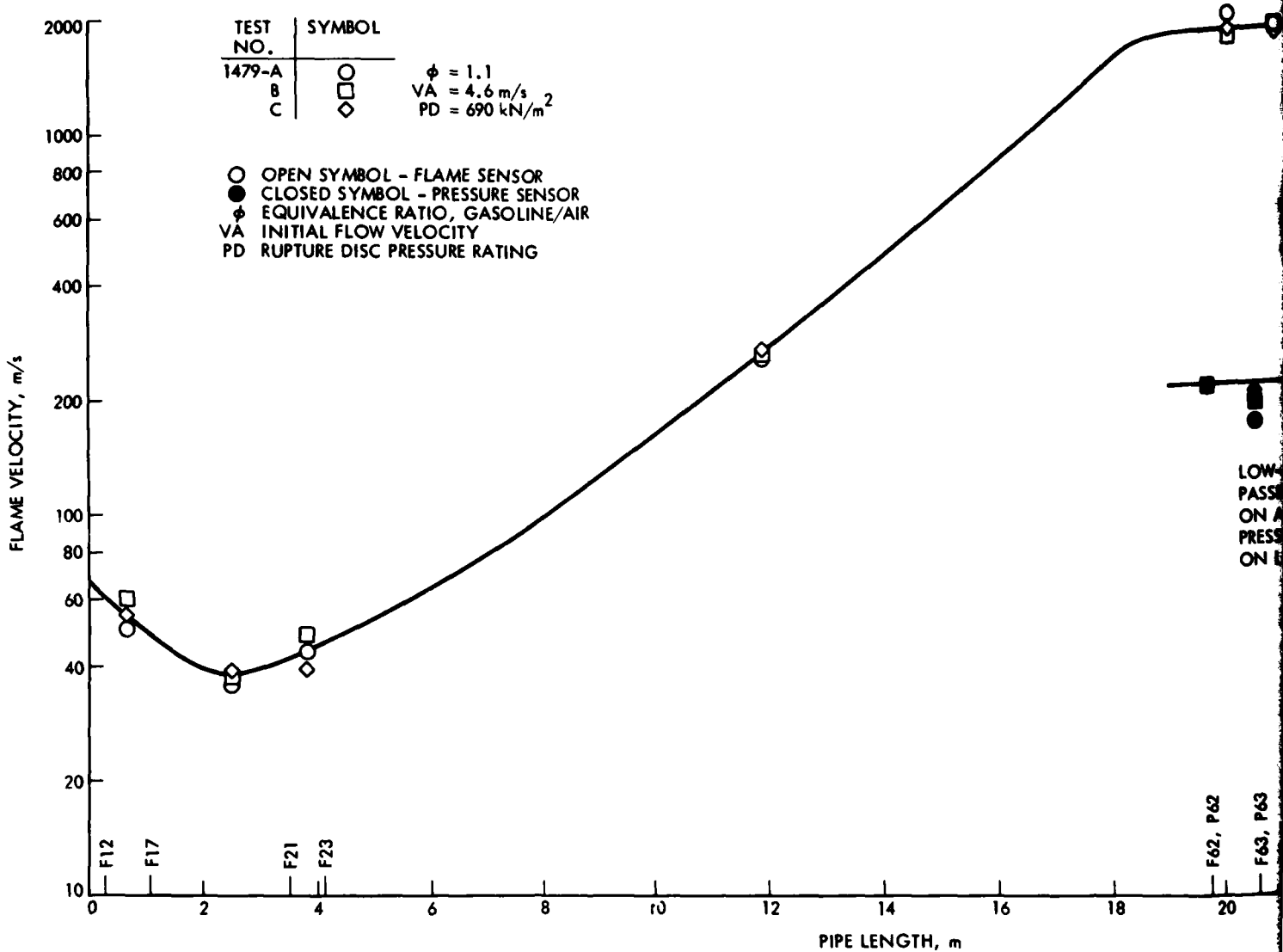
Figure 13-21. Vertical Bed of Ball
Test Results, Bed Si
Ring Size: 5.08-cm

FLAME VELOCITY AND PEAK PRESSURE VERSUS PIPE LENGTH
TEST CONFIGURATION NO. 188
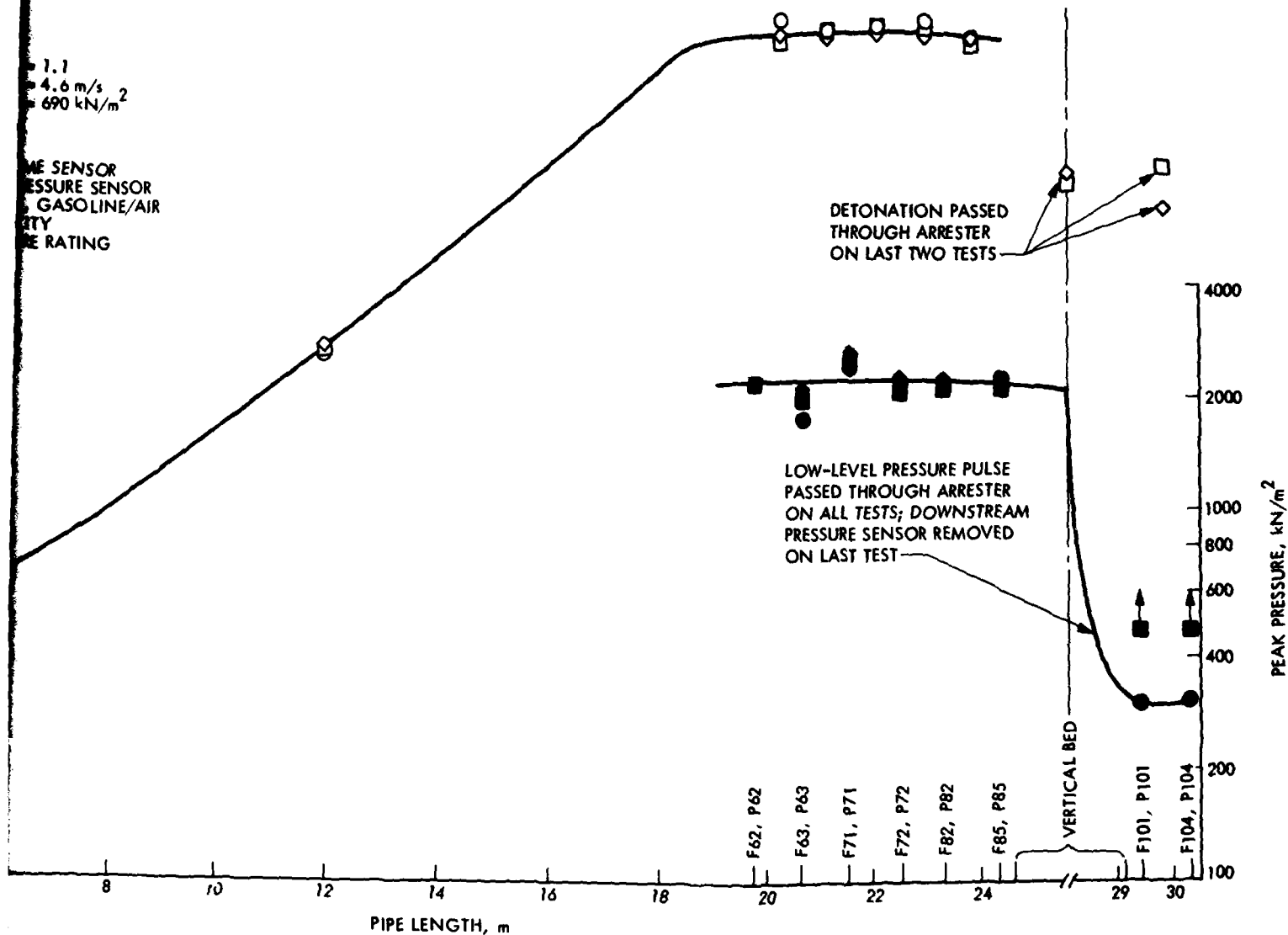
Figure 13-21. Vertical Bed of Ballast Rings Arrester Assembly Parametric
Test Results, Bed Size: 43.2-cm Diameter by 63.5-cm Depth,
Ring Size: 5.08-cm Diameter by 5.08-cm Length

13-31
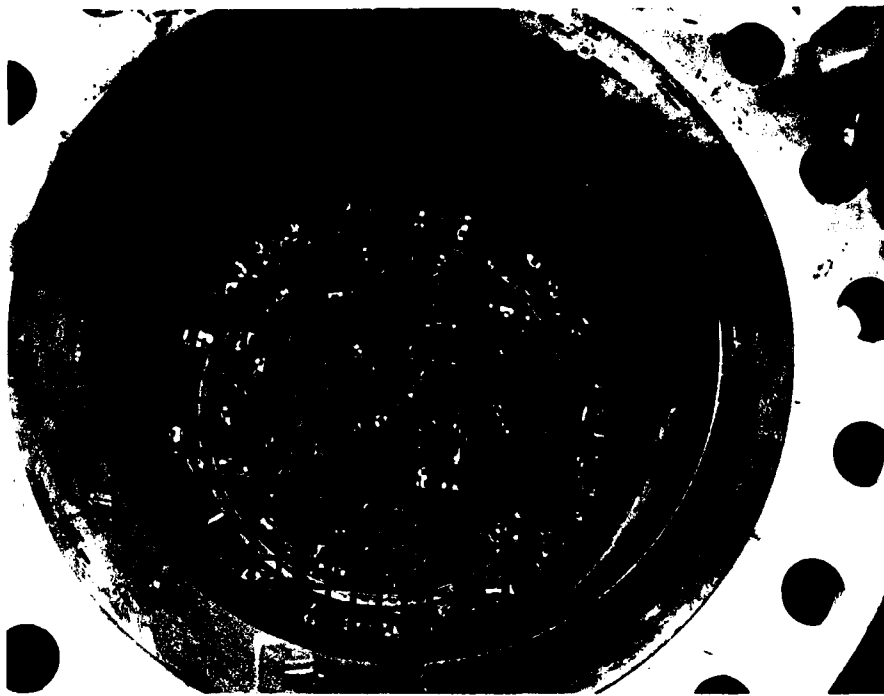
Figure 13-22.   Pretest Packed Bed of Aluminum Ballast Rings Around
the 33.7-cm Diameter Cylindical Insert

When the rupture disc was blanked-off, this same pressure increased
slightly to average 164 kN/m^2 (23.8 psia). Pre- and posttest pressure
loss across the arrester ranged from 0.162 to 0.220 kN/m^2 (0.023 to
0.032 psid) at an averaged air-flow velocity of 4.56 m/s (14.97 ft/s).
Posttest inspection showed that the bed had compacted 28% from distortion
of the Ballast rings. The results of this test are plotted in Figure
13-26, and summarized in Table 1-3.

This last test completed the parametric testing of detonation-
flame arresters. From these tests, two arrester configurations were
defined that were used in the continuous-flow testing described in the
next section.

FLAME VELOCITY AND PEAK PRESSURE VERSUS PIPE LENGTH
TEST CONFIGURATION NO. 189
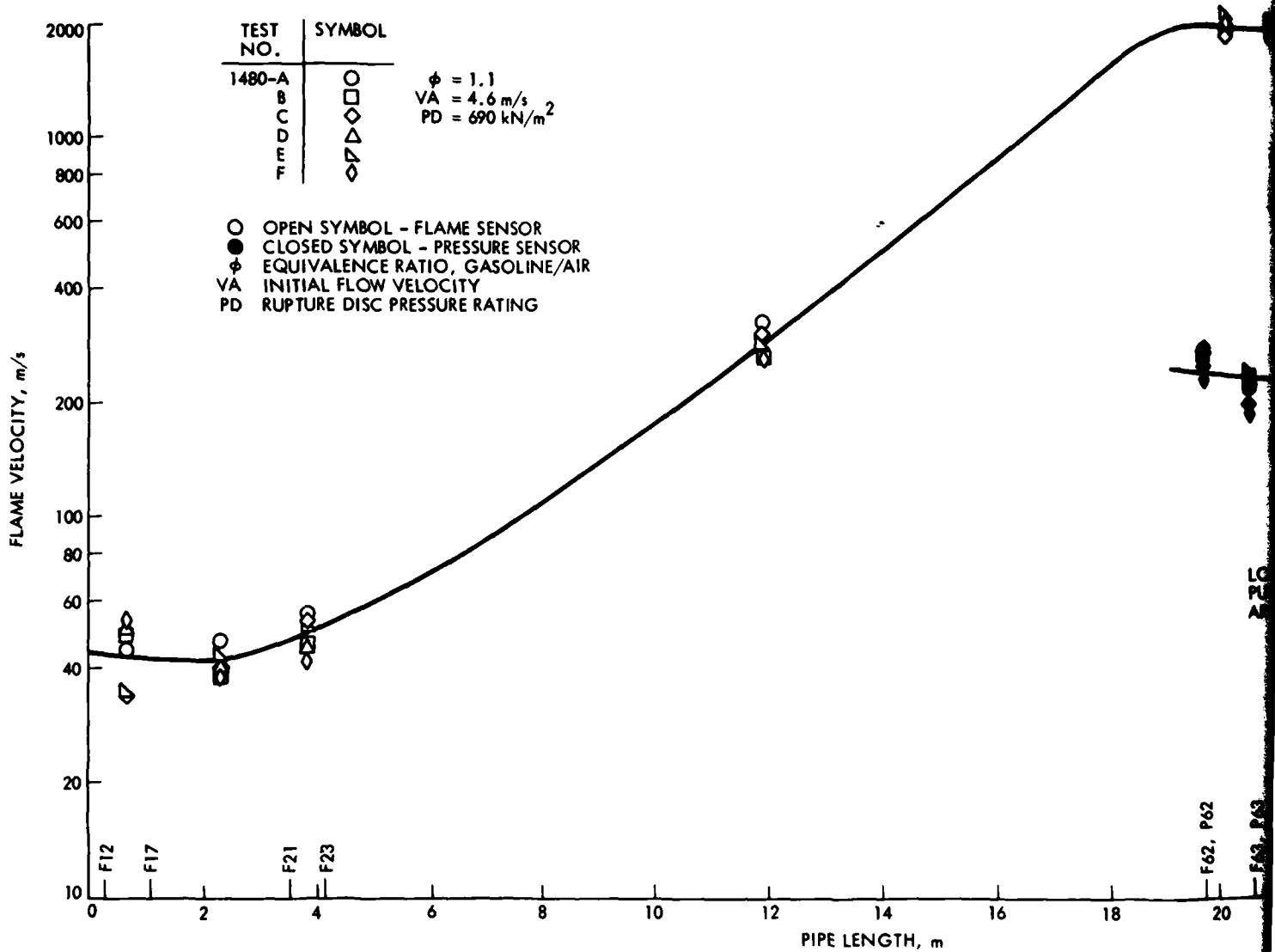
Figure 13-23. Vertical Bed of Bal
Test Results, Bed
Depth, Ring Size:
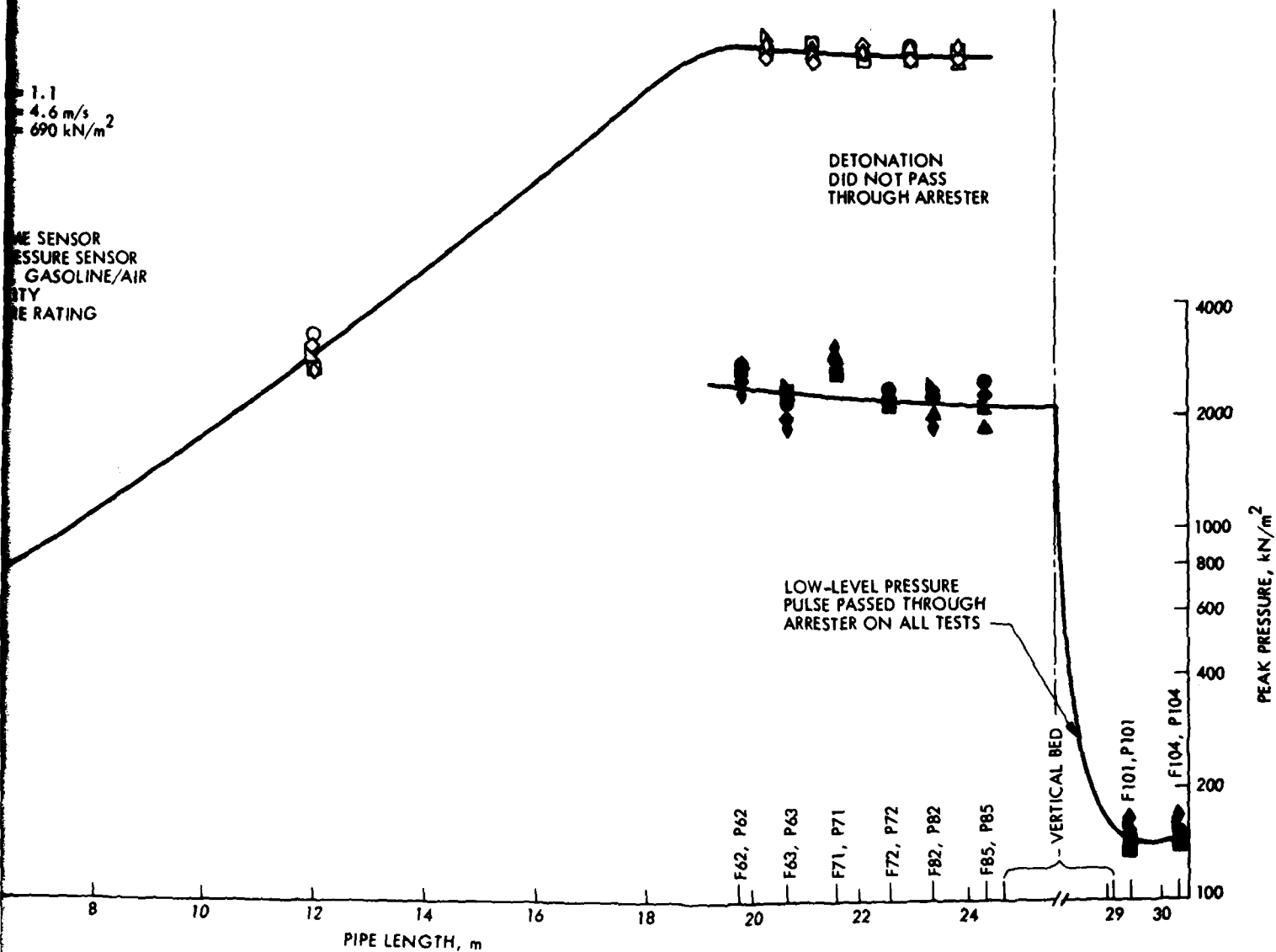
Figure 13-23. Vertical Bed of Ballast Rings Arrester Assembly Parametric Test Results, Bed Size: 33.7-cm Diameter by 63.5-cm Depth, Ring Size: 2.54-cm Diameter by 2.54-cm Length

13-35

FLAME VELOCITY AND PEAK PRESSURE VERSUS PIPE LENGTH
TEST CONFIGURATION NO. 190
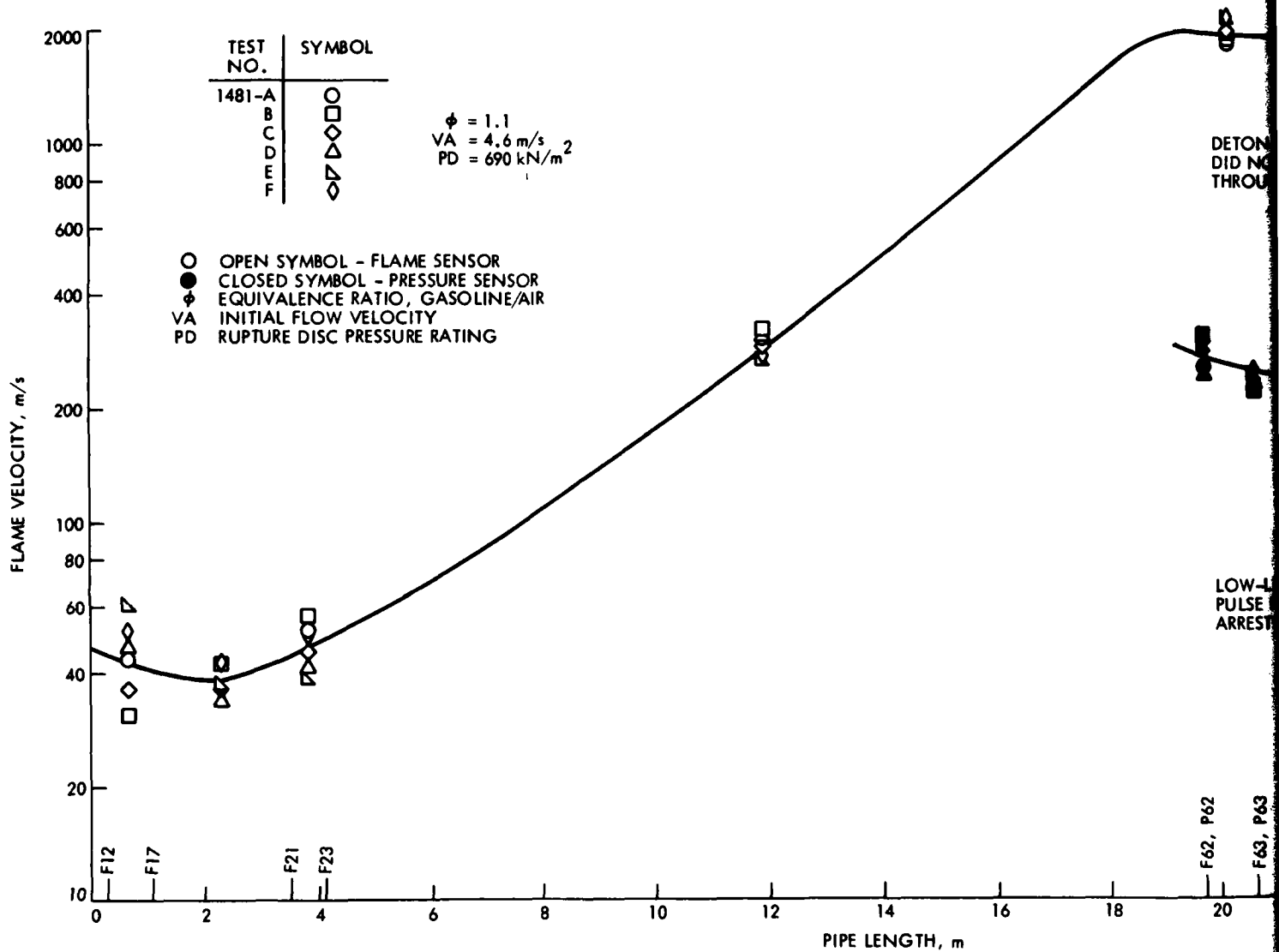
Figure 13-24. Vertical Bed
Parametric Te
by 63.5-cm De
2.54-cm Lengt

FLAME VELOCITY AND PEAK PRESSURE VERSUS PIPE LENGTH
TEST CONFIGURATION NO. 190
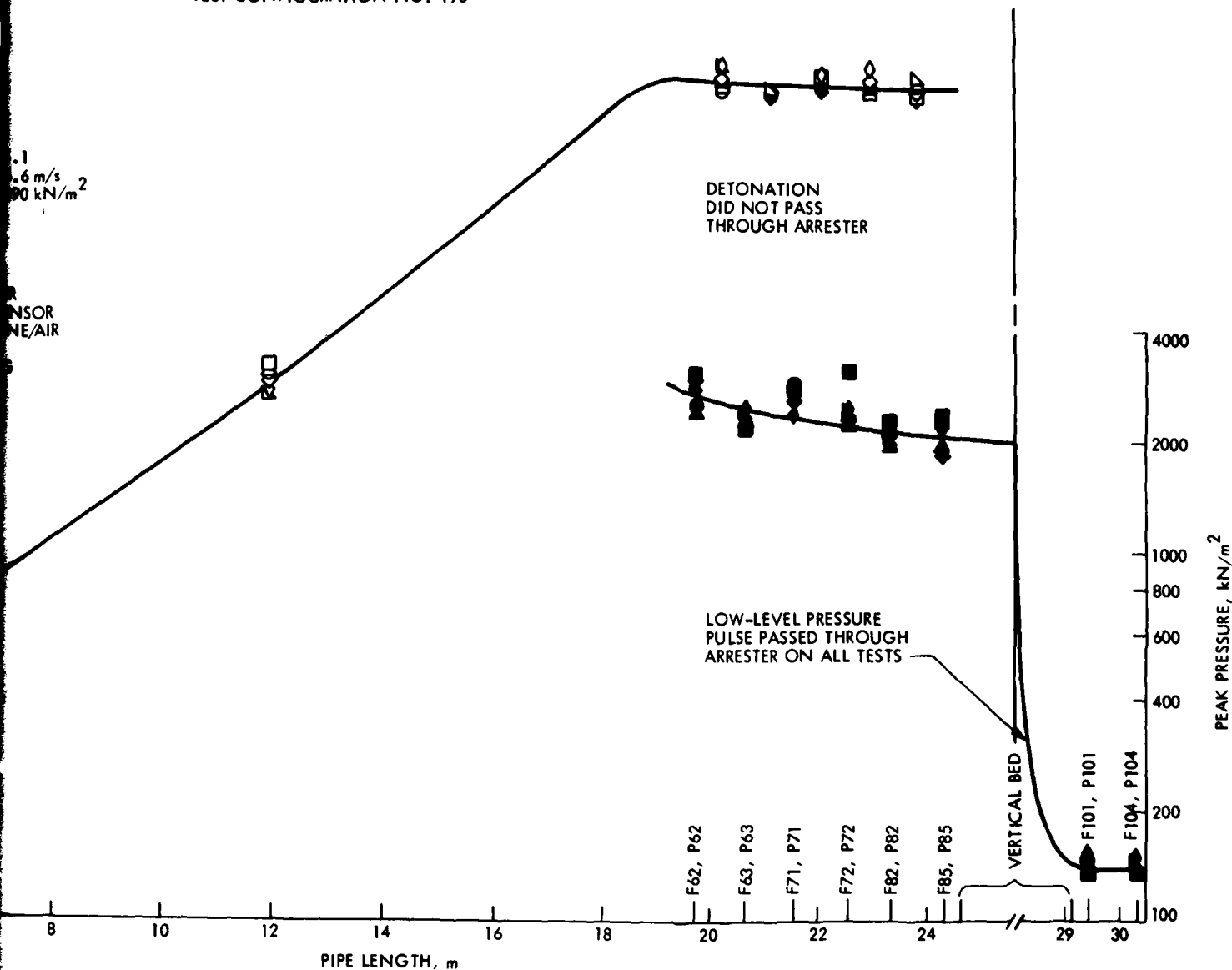
Figure 13-24. Vertical Bed of Ballast Rings Arrester Test Assembly
Parametric Test Results, Bed Size: 30.5-cm Diameter
by 63.5-cm Depth, Ring Size: 2.54-cm Diameter by
2.54-cm Length

13-37

FLAME VELOCITY AND PEAK PRESSURE VERSUS PIPE LENGTH
TEST CONFIGURATION NO. 191
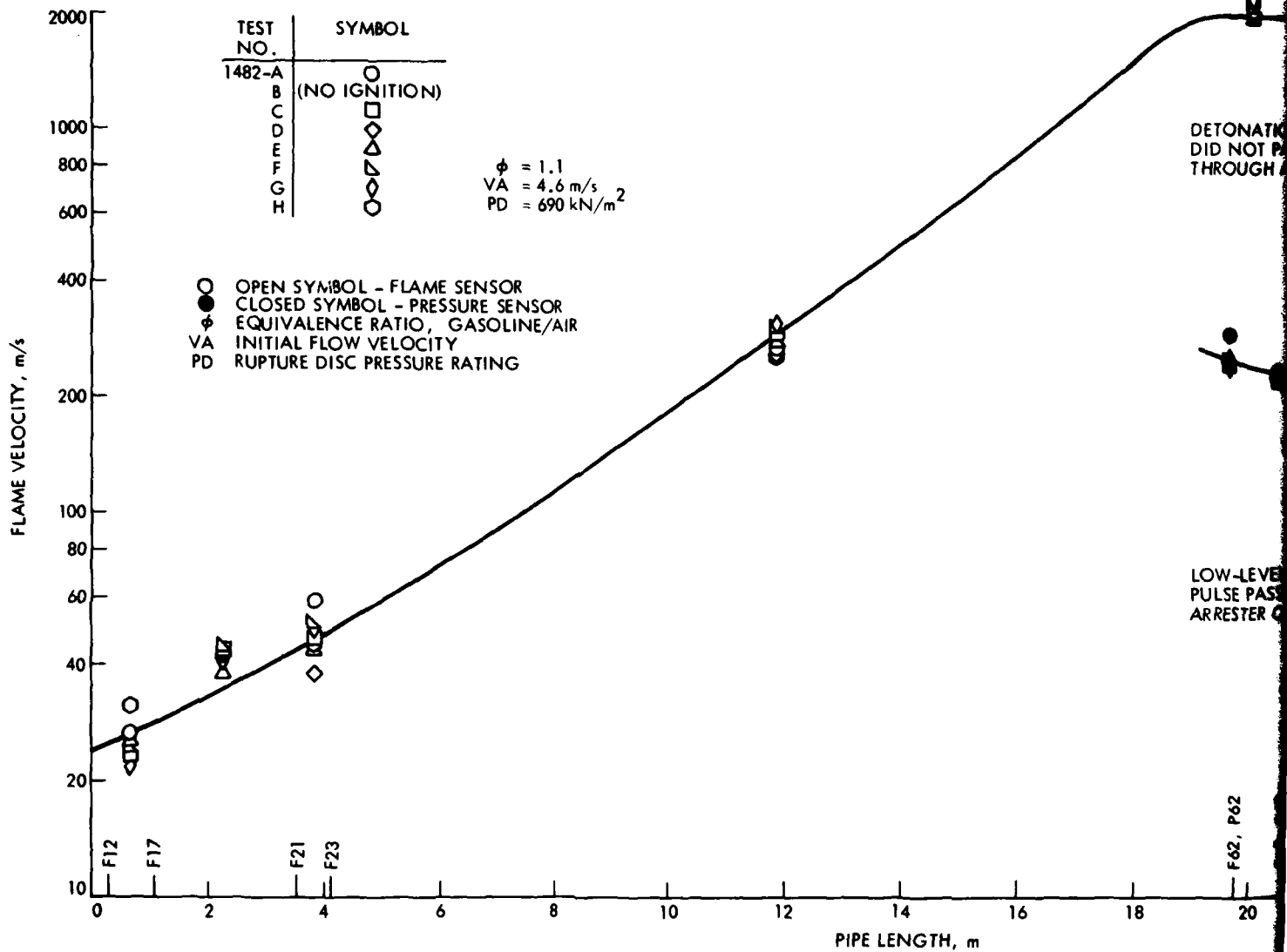
Figure 13-25. Vertical B
Parametric
by 63.5-cm
2.54-cm Le

Figure 13-25. Vertical Bed of Ballast Rings Arrester Test Assembly Parametric Test Results, Bed Size: 25.4-cm Diameter by 63.5-cm Depth, Ring Size: 2.54-cm Diameter by 2.54-cm Length

13-39

FLAME VELOCITY AND PEAK PRESSURE VERSUS PIPE LENGTH
TEST CONFIGURATION NO. 192 TO NO. 195

TEST NO.	SYMBOL	PD, kN/m^2
1483-A	○	690
B	□	2068
C	◇	4137
D	△	BLANKED OFF
E	▷	BLANKED OFF
F	◇	BLANKED OFF

ϕ = 1.1
VA = 4.6 m/s

○ OPEN SYMBOL – FLAME SENSOR
● CLOSED SYMBOL – PRESSURE SENSOR
ϕ EQUIVALENCE RATIO, GASOLINE/AIR
VA INITIAL FLOW VELOCITY
PD RUPTURE DISC PRESSURE RATING

FLAME VELOCITY, m/s

PIPE LENGTH, m

DETONA
DID NO
THROU

LOW-
PULSE
ARRES

F12 F17 F21 F23 F62, P62

Figure 13-26.   Vertical Bed
Parametric Te
by 45.7-cm De
cm Length

FLAME VELOCITY AND PEAK PRESSURE VERSUS PIPE LENGTH
TEST CONFIGURATION NO. 192 TO NO. 195

$\phi = 1.1$
VA = 4.6 m/s

DETONATION
DID NOT PASS
THROUGH ARRESTER

LOW-LEVEL PRESSURE
PULSE PASSED THROUGH
ARRESTER ON ALL TESTS

PEAK PRESSURE, kN/m^2

4000
2000
1000
800
600
400
200
100

F62, P62
F63, P63
F71, P71
F72, P72
F82, P82
F85, P85
VERTICAL BED
F101, P101
F104, P104

PIPE LENGTH, m

8   10   12   14   16   18   20   22   24   29   30

Figure 13-26.   Vertical Bed of Ballast Rings Arrester Test Assembly
Parametric Test Results, Bed Size: 25.4-cm Diameter
by 45.7-cm Depth, Ring Size: 2.54-cm Diameter by 2.54-
cm Length

13-41

SECTION XIV

CONTINUOUS-FLOW TESTING OF DETONATION-FLAME ARRESTERS

A.   TEST FACILITY MODIFICATION

Continous-flow testing, as referred to in this report, is defined as a type of test where the gasoline and air mixture, used to generate a stable detonation in the facility piping, continues to flow into the piping for a finite time period following ignition and detonation. At the end of the specified time period, the gasoline vapor is manually diverted into the fuel condenser. This differs from the normal detonation test where the vaporized gasoline flowing into the induction piping is automatically diverted into the fuel condenser 1.0 second before ignition. In both procedures, air continues to flow through the piping until a posttest inspection verifies that the facility is clear of residual gasoline and combustion by-products.

There was a high probability that continuous flow testing would cause a flame to flash back from the detonation test piping into the induction system piping. The rarefaction wave or the reflected detonation wave could be expected to drive any lingering flame in the ignition section upstream through the flow straightener and into the induction piping. This flame would undoubtedly persist in the mechanical mixer, a region of high turbulence, and burn out the hardware. The flow straightener, which was made from a spiral-wound, crimped stainless-steel ribbon core, 15.2 cm (6 in.) in diameter by 3.8 cm (1.5 in.) long with a flow passage hydraulic diameter of 0.269 cm (0.106 in.), was not considered to be an adequate arrester for high-velocity flames. Installed in its place was a larger Shand and Jurs spiral-wound, crimped aluminum ribbon arrester assembly, 25.4 cm (10 in.) in diameter by 15.2 cm (6 in.) long with a smaller flow passage hydraulic diameter of 0.114 cm (0.045 in.). The arrester assembly was mounted between two 25.4- to 15.2-cm- (10- to 6-in.-) diameter flanged-pipe reducer assemblies, as shown in Figure 14-1.

To explore the possibility of reignition occuring at some distance downstream of the experimental detonation-flame arrester, two lengths of standard steel pipe 15.2 cm (6.0 in.) in diameter, and each 6.7 m (22 ft) long, were installed at the exit of the witness section (No. 10). The upstream instrumented verification section (No. 6) was removed and replaced by the uninstrumented extension section (No. 11). The instrumented verification section (No. 6) was reversed 180 deg and installed at the exit of the new 13.4-m- (44-ft-) long extension sections (No. 12 and No. 13). By reversing the verification section, the instrumentation ports were placed at the upstream end of this pipe section, thus allowing some protection for the flame sensors from ambient sunlight. A schematic diagram of the continuous-flow testing arrangement of facility piping is shown in Figure 14-2. This new assembly provided sufficient run-up piping and instrumented sections to verify whether or not the low-level peak-pressure pulse passing through the experimental detonation arrester had sufficient energy to cause an ignition of the combustible gasoline and air mixture downstream. A photograph of the facility piping, showing the new extension sections, is presented in Figure 14-3.

Figure 14-1. Shand and Jurs Spiral-Wound, Crimped Aluminum Ribbon
Arrester Assembly Installed in the Inlet Flow Straight-
ener Location, Size: 25.4-cm Diameter by 15.2-cm
Length

The preprogrammed ignition and fuel diversion procedure, provided
by the automatic sequence timer, was modified to reduce the igniter
"on-time" from 500 milliseconds to 180 milliseconds and the fuel diversion
command changed from an automatic to a manual input. The reduction
in igniter "on-time" removed the source of ignition from the upstream
test piping by the time the detonation rarefaction and reflection waves
retrogressed back to the ignition section. The only source then available
for ignition of the continuing flow of combustible gasoline and air
mixture in the test piping would have to be a lingering flame or residual
wave energy from the initial detonation. Fast responding bare-wire
thermocouples were installed into the induction piping, run-up piping,
test section, and witness section to monitor the presence of any continuous
flame.

Figure 14-2. Facility Piping Schematic Diagram for Detonation-Flame Arrester Evaluation with Continuous Flow Testing
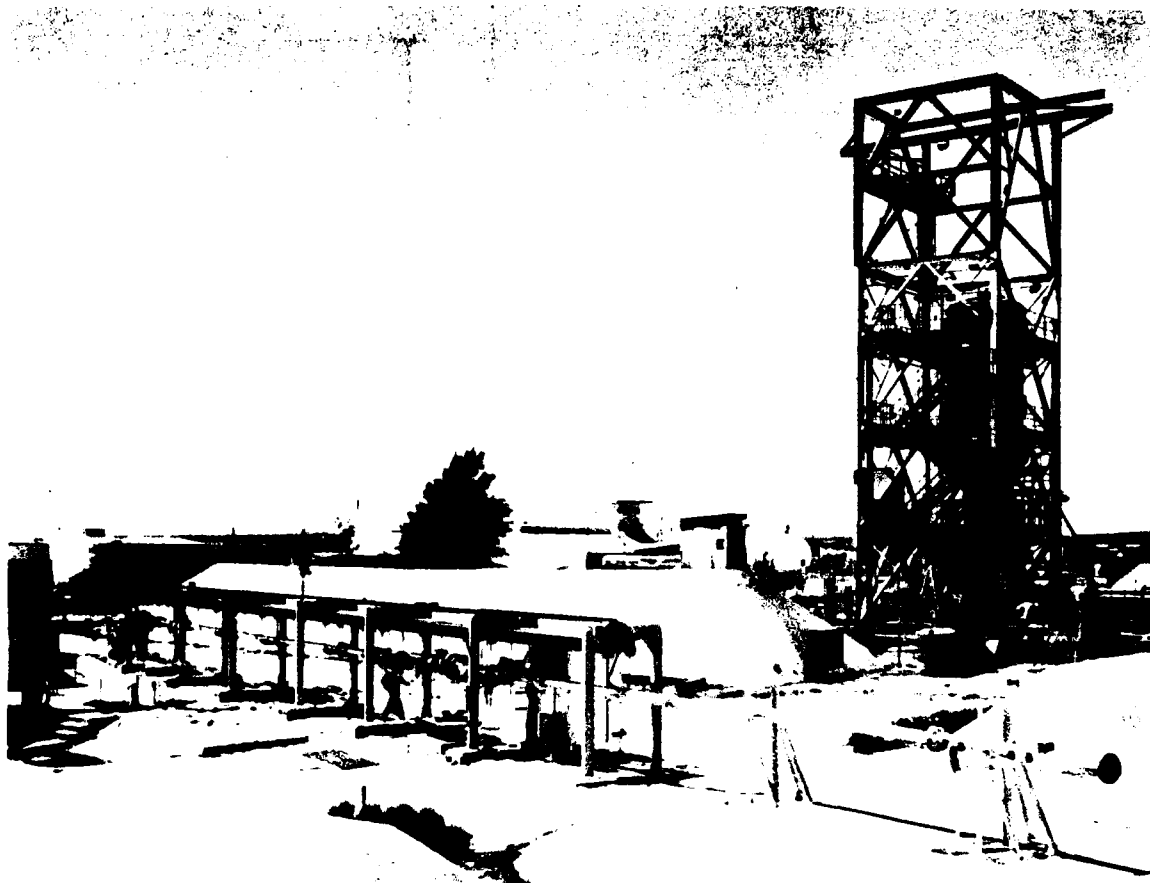
Figure 14-3. Facility Piping Assembly with the 13.4-m-Long Extension
Sections Installed

B. VERTICAL BED OF ALUMINUM BALLAST RINGS ARRESTER TEST ASSEMBLY

The test configuration for the vertical bed of aluminum Ballast
rings arrester used in the continuous-flow tests was identical to the last
one used in the parametric test series. Bed size was 25.4-cm (10-in.)
diameter by 45.7-cm (18-in.) depth, packed with new 2.54-cm- (1.0-in.-)
diameter by 2.54-cm- (1.0 in.-) long aluminum Ballast rings. The inlet
rupture-disc assembly was blanked-off, but the rupture-disc assemblies on
the vessel cover and the outlet pipe tee both contained discs with the 690
kN/m^2 (100 psid) pressure rating. Using a gasoline and air mixture at the
standard test conditions and the upstream ignition location, four stable
detonation firings were made on this test configuration (No. 196). The
first two firings were followed by a continuous flow of the gasoline
and air mixture for a period of 30 seconds. On the last two firings,
the flow period was extended to 60 seconds. The detonation was ar-
rested on all tests and was completely contained between the inlet
and test section arresters. None of the induction piping rupture discs

14-4

or the downstream piping rupture discs were blown out. There was no evidence of reignition in the witness or extension sections, and no lingering flames in the test run-up sections. The thermocouple in the ignition section (T12) registered the short-lived flame and the thermocouple in the witness section (T102) recorded only a few degrees rise in temperature due to the passage of the combustion gas products as they exhausted through the downstream piping. Most of the heat of combustion was apparently absorbed by the pipe wall or the heat sink capability within the arrester bed. The pre- and posttest pressure loss across the arrester bed averaged 0.30 kN/m^2 (0.044 psid) at an averaged air-flow velocity of 4.68 m/s (15.35 ft/s). Posttest inspection of the bed showed a 25% compaction due to distortion of the Ballast rings.

The arrester bed was repacked with new 2.54-cm- (1.0-in.-) size aluminum Ballast rings. Four more detonation test firings were made on this test configuration (No. 197). In this series, the first two firings were followed by 90 seconds of continous gasoline-and-air-mixture flow, and the last two firings by 120 seconds of continuous mixture flow. Again, the detonation was arrested on all test firings and was completely contained between the inlet and test section arresters. No rupture discs were blown out. There was no evidence of reignition in the witness or extension sections and no lingering flame in the test run-up section. Pre- and posttest pressure loss measurements averaged about the same as the previous test series. Posttest inspection showed a 27% bed compaction. Test data from these two test series are plotted in Figure 14-4 and summarized in Table 1-4. The peak pressure pulse measured in both the witness section and the downstream verification section averaged around 146 kN/m^2 (21.1 psia) and was traveling at an average velocity of 398 m/s (1306 ft/s). There was no evidence of increasing wave velocity or pressure in the extension section, as would have been the case had ignition and combustion been present.

C.   SHAND AND JURS SPIRAL-WOUND, CRIMPED STAINLESS-STEEL RIBBON
     ARRESTER TEST ASSEMBLY

The Shand and Jurs spiral-wound, crimped stainless-steel ribbon arrester test assembly was installed into the test section using the last test configuration developed during the parametric testing. It contained the 30.5-cm- (12-in.-) diameter by 20.3-cm- (8-in.-) long arrester assembly with the directly connected inline pipe tee and the blanked-off rupture-disc assembly shown in Figure 13-7. This test configuration (No. 198) was subjected to four stable detonations using the gasoline and air at the standard test condition and the upstream ignition location. The first two test firings were followed by the continuous mixture flow for a period of 30 seconds and the second two test firings by 60 seconds of continuous mixture flow. The detonation was arrested on all test firings and was completely contained between the inlet and test section arresters. There was no evidence of reignition in the witness or extension sections and no lingering flame in the test run-up section. Pre- and posttest pressure loss measurements showed no change from the parametric tests. A posttest inspection of the arrester assembly revealed a slight bowing of the downstream retainer grid as previously described and a few cracked welds in the

grid. The damage was repaired and the arrester was reinstalled into the test assembly.

Four more stable detonation test firings were made on the repaired arrester configuration (No. 200). The first two test firings were followed by 90 seconds of continuous mixture flow, and on the last two test firings the flow period was extended to 120 seconds. The results were the same as those of the previous test series. There was no evidence of reignition or lingering flames. Test data from these two test series are plotted in Figure 14-5 and summarized in Table 1-4. The low-level peak-pressure pulse measured in the witness section averaged 335 kN/m^2 (48.6 psia), and decayed to an average 240 kN/m^2 (34.8 psia) at the exit of the extension section. The velocity of this pressure pulse likewise decayed from an average of 640 m/s (2100 ft/s) in the witness section to 480 m/s (1575 ft/s) at the exit of the extension section. With both the intensity and velocity decreasing in this downstream pressure wave, there was no evidence of reignition or combustion taking place. Posttest inspection revealed no unusual damage or distortion to the crimped ribbon arrester test assembly.

The arrester core was removed from the test assembly and the two 30.5-cm- (12-in.-) diameter flanges were bolted together. Also, the low-pressure transducers were removed from the witness and extension sections. One last test firing was made where a stable detonation was recorded passing through the entire 13.4-m- (44-ft-) long extension piping.

Figure 14-4. Vertical Bed of Ball
Flow Test Results

WAVE VELOCITY AND PEAK PRESSURE VERSUS PIPE LENGTH
TEST CONFIGURATION NO. 196 AND NO. 197

ϕ = 1.1
VA = 4.6 m/s
PD = BLANKED OFF

DETONATION
DID NOT PASS
THROUGH ARRESTER

OR
ENSOR
NE/AIR

G

LOW-LEVEL PRESSURE
PULSE WAVE VELOCITY

LOW-LEVEL PRESSURE
PULSE PASSED THROUGH
ARRESTER ON ALL TESTS

VERTICAL BED

PEAK PRESSURE, kN/m²

F71, P71

F72, P72

F82, P82

F85, P85

F101, P101

F104, P104

F63, P63

F62, P62

4000

2000

1000
800
600

400

200

100

8   16   18   20   22   24   26   28   30   42   44

PIPE LENGTH, m

Figure 14-4.   Vertical Bed of Ballast Rings Arrester Assembly Continuous
Flow Test Results

14-7

WAVE VELOCITY AND PEAK PRESSURE VERSUS PIPE LENGTH
TEST CONFIGURATION NO. 198 TO NO. 200

TEST NO.	SYMBOL	FLOW TIME, s
1486-A	○	30
B	□	30
C	◇	60
D	△	60
1487-A	◭	90
B	◈	90
C	⬡	120
D	◭	120
E	⬠	5 (CORE REMOVED)

$\phi \approx 1.1$
VA ≈ 4.6 m/s
PD $\approx$ BLANKED OFF

○ OPEN SYMBOL – FLAME SENSOR
● CLOSED SYMBOL – PRESSURE SENSOR
ϕ EQUIVALENCE RATIO, GASOLINE/AIR
VA INITIAL FLOW VELOCITY
PD RUPTURE DISC PRESSURE RATING

DETONATION PASSED THROUGH ARRESTER ONLY AFTER CORE ELEMENT WAS REMOVED ON LAST TEST

LOW-LEVEL PRESSURE PULSE PASSED THROUGH ARRESTER ON ALL TESTS; DOWNSTREAM PRESSURE SENSOR REMOVED ON LAST TEST

SHAND AND JURS

WAVE VELOCITY, m/s

PIPE LENGTH, m

Figure 14-5. Shand and Jurs
Ribbon Arrester

WAVE VELOCITY AND PEAK PRESSURE VERSUS PIPE LENGTH
TEST CONFIGURATION NO. 198 TO NO. 200

$\phi = 1.1$
VA = 4.6 m/s
PD = BLANKED OFF

(E REMOVED)

OR
SENSOR
LINE/AIR

NG

DETONATION
PASSED THROUGH
ARRESTER ONLY AFTER
CORE ELEMENT WAS
REMOVED ON LAST TEST—

LOW-LEVEL PRESSURE
PULSE WAVE VELOCITY →

LOW-LEVEL PRESSURE PULSE
PASSED THROUGH ARRESTER
ON ALL TESTS; DOWNSTREAM
PRESSURE SENSOR REMOVED
ON LAST TEST —

SHAND AND JURS

F71, P71
F72, P72
F82, P82
F85, P85
F101, P101
F104, P104
F63, P63
F62, P62

PEAK PRESSURE, kN/m²

4000

2000

1000
800
600

400

200

100

6   8   10   16   18   20   22   24   26   28   40   42

PIPE LENGTH, m

Figure 14-5.   Shand and Jurs Spiral-Wound, Crimped Stainless-Steel
Ribbon Arrester Assembly Continuous Flow Test Results

14-9

2

SECTION XV

CONCLUSIONS

The following conclusions have been reached from the results of this experimental evaluation of flame-control devices in a simulated vapor recovery system using 15.2-cm- (6.0-in.-) diameter piping where combustible mixtures of gasoline and air flowed at pressures slightly above one atmosphere and temperatures ranged from 23 to 65°C (74 to 149°F).

(1) The deflagration-to-detonation run-up distance is 11.2 m (36.7 ft), or an L/D of 74 for 15.2-cm- (6.0-in.-) diameter piping artificially roughened to a Darcy friction factor ranging from 0.040 to 0.047, or a relative roughness ranging from 0.010 to 0.015.

(2) The deflagration-to-detonation run-up distance does not change significantly for gasoline-and-air equivalence ratios ranging from 0.9 to 1.4, or for initial flow velocities ranging from 0 to 6.1 m/s (0 to 20 ft/s).

(3) The stable detonation after transition has a measured flame velocity of 1800 m/s (5906 ft/s) and a peak pressure of 1900 kN/m^2 (276 psia).

(4) During the transition from deflagration to detonation, flame velocity reaches 2700 m/s (8860 ft/s) and peak pressure exceeds 4000 kN/m^2 (580 psia).

(5) A reflected detonation wave had a measured peak pressure of 3300 kN/m^2 (479 psia), or double the level of the stable propagating detonation wave.

(6) Four generic types of flame control devices found effective in arresting detonations are:

    (a)   Spiral-wound, crimped metal ribbon.

    (b)   Foamed nickel-chrome metal.

    (c)   Vertical bed of aluminum Ballast rings.

    (d)   Water-trap or hydraulic back-pressure valve.

(7) Combinations of standard pipe fittings, such as tees and elbows, with rupture-disc assemblies and restricter orifice plates, are ineffective in arresting detonations.

(8) Rupture-disc assemblies installed on the inlet side of detonation arresters do not reduce the intensity of the detonation wave pressure, but do provide a controlled release of the hot combustion gases behind the detonation wave.

(9)   The smallest-size vertical bed of metal rings arrester
        found to be effective in arresting detonations is
        25.4 cm (10 in.) in diameter by 45.7 cm (18 in.) in depth
        and packed with 2.54-cm- (1.0-in.-) diameter by 2.54-cm-
        (1.0-in.-) long aluminum Ballast rings.

(10)   Aluminum Ballast rings in larger sizes, 3.81 (1.5 in.) and 5.08
        cm (2.0 in.), are not effective in repeatedly arresting
        detonations.

(11)   Increasing the rupture-disc pressure rating from 690 kN/m^2
        (100 psid) up to a blanked-off condition on the inlet piping
        of a vertical bed of aluminum Ballast rings arrester does
        not affect the arrester's ability to stop a detonation.
        Also, it has very little influence on the level of peak-
        pressure pulse passed through the arrester.

(12)   Repeated exposure to the impact of detonation shock waves
        caused distortion of the aluminum Ballast rings, resulting
        in compaction of the bed of rings in the arrester. The
        amount of compaction ranged from 25 to 35% of the starting
        depth; larger diameter beds experience a higher percentage
        of compaction. The resulting pressure drop across the bed
        increases with each succeeding detonation, but reaches an
        upper limit after three to four detonations.

(13)   The smallest core length of a 30.5-cm- (12-in.-) diameter
        spiral-wound, crimped metal ribbon arrester found to be
        effective in arresting detonations is 15.2 cm (6 in.) with
        a crimp passage hydraulic diameter of 0.114 cm (0.045 in.).
        Stainless-steel ribbon material is better able to withstand
        the impact of detonation shock waves without distortion
        than aluminum ribbon, providing the core wingings are made
        from continuous length ribbons.

(14)   The downstream peak-pressure pulse passing through a spiral-
        wound, crimped stainless-steel ribbon arrester was reduced
        from 344 to 260 kN/m^2 (49.9 to 37.7 psia) when the core length
        was increased from 15.2 to 30.5 cm (6 to 12 in.). Assuming a
        linear relationship between core length and downstream peak-
        pressure pulse, the core for a 30.5-cm- (12-in.-) diameter
        arrester would have to be 58.5 cm (23 in.) long to reduce the
        downstream pressure pulse to one atmosphere or 101.4 kN/m^2
        (14.7 psia).

(15)   Increasing the rupture-disc pressure rating from 690 kN/m^2
        (100 psid) up to a blanked-off condition on the inlet piping
        of a spiral-wound, crimped stainless-steel ribbon arrester does
        not affect its ability to stop a detonation. Also, it has
        very little influence on the level of the peak pressure pulse
        passed through the arrester.

(16) Both the vertical bed of aluminum Ballast rings arrester
and the spiral-wound, crimped stainless-steel ribbon arrester
are effective in stopping detonations followed by continuous
combustible mixture flow for periods up to 120 seconds.
There is no indication that lingering flames remain in
the 25 m (80 ft) of run-up piping upstream of the arrester,
and no evidence of reignition in the 18 m (60 ft) of exit
piping downstream of the arrester. In this limited configuration,
a rupture disc upstream of the arrester was not required
to relieve the hot combustion gases following the detonation.

SECTION XVI

RECOMMENDATIONS

In the design of a closed-loop vapor recovery system for gasoline cargo transfer at a marine terminal, the following recommendations are made regarding the selection and installation of detonation-flame arresters:

(1) Ranked in order of preference, the selection of an arrester based on the least drop in system pressure is (1) packed bed of Ballast rings, (2) spiral-wound, crimped metal ribbon, (3) 80-grade foamed metal, (4) water trap, and (5) hydraulic back-pressure valve.

(2) Ranked in order of preference, the selection of an arrester based on the ability to withstand repeated detonation is (1) spiral-wound, crimped metal ribbon, (2) packed bed of Ballast rings, (3) water-trap or hydraulic back-pressure valve, and (4) 80-grade foamed metal.

(3) Ranked in order of preference, the selection of an arrester based on minimum maintenance, least susceptibility to fouling, and reduced contamination is (1) packed bed of Ballast rings, (2) spiral-wound, crimped metal ribbon, (3) 80-grade foamed metal, and (4) water-trap or hydraulic back-pressure valve.

(4) The selection of materials used in the construction of arresters should be based on their compatibility with the environment and the fuel vapors to be encountered. However, stainless steel is recommended over aluminum or similar lower-strength metals.

(5) Because of the short deflagration-to-detonation run-up distance, it would be impractical to install a series of detonation-flame arresters in a vapor transfer line at spacing intervals that would prevent the occurence of a detonation. The combined arrester pressure losses in such an installation would soon exceed the available operating pressure differential between storage and receiver tanks. It would be better to place the arresters as close to the individual tanks as possible, making sure that they are located between the tanks and any source of ignition.

(6) To minimize the possibility of a detonation, a flame arrester device should be placed as close as possible to any potential ignition source, at a position well within the detonation run-up distance.

(7) For operational safety, the arrester, vapor transfer lines, valves, and other components in the vapor recovery system should be designed to withstand the instantaneous pressure spikes ranging from 1900 kN/m^2 (276 psia) to 4000 kN/m^2

(580 psia) as associated with stable, transitional, and
reflected detonation waves, should they occur.

(8)   Rupture-discs or rupture-disc/relief-valve combination
       assemblies should be included in vapor transfer lines to
       vent the hot combustion gases produced by a detonation.
       This would minimize the danger of over pressurizing the
       tanks attached to these lines.

The data and experience obtained from these detonation arresting
tests is limited to gasoline and air mixtures in 15.2-cm (6.0-in.-)
diameter pipe sizes. It is recommended that extrapolation of this
data should be limited to the following:

(1)   Application to other fuels should be limited to those hydro-
       carbons that have flame propagating characteristics similar
       to gasoline. This does not include such fuels as hydrogen
       and acetylene or any type of fuel in an oxygen enriched
       environment.

(2)   Scaled-down applications to pipe sizes smaller than a
       15.2-cm (6.0-in.) diameter are considered to be conservative.

(3)   Scaled-up applications should be limited to pipe sizes
       no larger than a 20.3-cm (8.0-in.) diameter, providing
       adequate consideration is given to structural strength.

It is recommended that the following experimental work be considered
as possible follow-on programs to extend the data base and experience
already achieved:

(1)   Using the existing test facility and with a moderate increase
       in air flow and fuel flow capability, detonation-flame
       arrester testing could be conducted with enlarged conical
       transition pipe sections up to and larger than 30.5-cm
       (12.0-in.) diameter.

(2)   Detonation-flame arrester testing should be made with other
       fuel/air combinations that would normally require a closed-loop
       type of vapor recovery system for transfers operations.

(3)   Detonation qualification-type testing should be made on vapor
       recovery system components other than arresters including:
       (1) valves, (2) pumps, (3) blowers, (4) filters, (5) condensors,
       and (6) separators.

(4)   Flame arrester qualification type testing should be conducted
       at conditions other than detonations including atmospheric
       flashback from fuel/air vapor plumes and under the heat-up
       characteristics achieved by sustained burning where fuel/air
       mixture flow rates are representative of a vapor recovery
       system or normal tank venting systems.

REFERENCES

2-1. Lewis, B., and von Elbe, G., _Combustion, Flames and Explosions of Gases_, pp. 546-554. Academic Press, Inc., New York, 1961.

2-2. Courant, R., and Friedrichs, K. O., _Supersonic Flow and Shock Waves_, pp. 224-226. Intersciences, New York, 1948.

2-3. Martin, F. J., "Transition from Slow Burning to Detonation in Gaseous Explosives," _Phys. Fluids_, 1, pp. 399-407, 1958.

2-4. Urtiew, P. A., and Oppenheim, A. K., "Experimental Observations of the Transition to Detonations in an Explosive Gas," _Proc. Roy. Soc. Lond._, A 295, pp. 13-28, 1966.

2-5. Lewis, B., and von Elbe, G., _op. cit._, p. 547.

2-6. Urtiew, P. A., and Oppenheim, A. K., "Onset of Detonation," _Comb. and Flame_, 9, pp. 405-407, 1965.

2-7. Urtiew, P. A., and Oppenheim, A. J., "Transverse Flame-Shock Interactions in an Explosive Gas," _Proc. Roy. Soc. Lond._, A 304, pp. 379-385, 1968.

2-8. Bollinger, L. E., Fong, M. C., and Edse, R., "Experimental Measurements and Theoretical Analysis of Detonation Induction Distances," _ARS Journal_, 31, pp. 588-595, 1961.

2-9. Lewis, B., and von Elbe, G., _op. cit._ pp. 540-546.

2-10. Strehlow, R. A., "Gas Phase Detonations: Recent Developments," _Comb. and Flame_ 12, pp. 81-101, 1968.

2-11. Mooradian, A. J., and Gordon, W. E., "Gaseous Detonation, I. Initiation of Detonation," _J. Chem. Phys._, 19, pp. 1116-1172, 1951.

2-12. See, e.g., Ref. 10 and references contained therein.

2-13. Bollinger, L. E., Fong, M. C., and Edse, R., _Detonation Induction Distances in Combustible Gaseous Mixtures at Atmospheric and Elevated Initial Pressures. IV Hydrogen-Nitric Oxide; V. Hydrogen-Oxygen-Diluent; VI. Theoretical Analysis_, Wright Air Development Center Technical Report 58-591, Part II, 1959.

2-14. Holmes, L. B., and Weymann, H. D., "Precursors Ahead of Shock Waves: II. Photoionization," _Phys. Fluids_, 12, pp. 1200-1210, 1963.

2-15. Kistiakowsky, G. D., and Richards, L. W., "Emission of Vacuum Ultraviolet Radiation from Acetylene-Oxygen and Methane-Oxygen Reactions in Shock Waves," _J. Chem. Phys._, 36, pp. 1707-1712, 1962.

2-16. Strauss, W. A., and Edse, R., "Burning Velocity Measurements by the Constant-Pressure Bomb Method," _Seventh Symposium (International) on Combustion_, Butterworths, London, pp. 377-385 (1959).

2-17. Garforth, A. M., and Rallis, C. J., "Laminar Burning Velocity of Stoichiometric Methane-Air: Pressure and Temperature Dependence," _Comb. and Flame_, 31, pp. 53-68, 1978.

2-18. Shchelkin, K. I., and Troshin, Ya. K., _Gasdynamics of Combustion_, pp. 174-179, (B. W. Kuvshinoff and L. Holtschlag, transl.), Mono Book Corp., Baltimore, 1965.

2-19. Holzapfel, G., and Schoen, G., "Zur Ausbilding von Gasdetonationen in Rohren," (The Formation of Gas Detonation in Pipes), _Chemie-Ing.-Techn._, Vol. 37, No. 5, pp. 493-497, 1965. Translated by SCITRAN; translation available from the authors of this report, JPL Publication 80-18.

2-20. Gorden, S. and McBride, B. J., _Computer Program for Calculation of Complex Chemical Equilibrium Compositions, Rocket Performance, Incident and Reflected Shocks and Chapman - Jouguet Detonations_, _NASA Specification Publication SP 273_, National Aeronautics and Space Administration, Washington, D.C., 1971.

2-21. Courant, R. and Friedricks, K. O., _op. cit_, pp. 150.

2-22. Schalla, R. L. and Hibbard, R. R., _Smoke and Coke Formation in the Combustion of Hydrocarbon-Air-Mixtures_, Chapter 9. National Advisory Council on Aeronautics _Report 1300_ (1957), Rayle, W.D.

7-1. "Gasoline Fuels Specification," _Federal Register_, 43, No. 140, Thr. pp. 310, 134-310, 138, Jul. 20, 1978.

12-1. Moody, L. F., "Friction Factors for Pipe Flow," _American Society of Mechanical Engineers Transactions_, 66, No. 8, pp. 671-684, Nov. 1944.

APPENDIX A

ANALYSIS OF INSTRUMENTATION MEASUREMENT AND CALCULATION UNCERTAINTIES

The following is an analysis of the uncertainties associated with pressure, temperature, and IDAC program calculations. Although these values can be assured with only a 95% (2σ) probability, this is most likely a conservative estimate. Many of the uncertainty values used are absolute in that the procedures specify a maximum limit. Others are difficult to ascertain precisely, so "safe" estimates must be large. The calibration of pressure transducers, for example, are always subject to the uncertainties of accidental, fixed, or operational errors. However, considerable effort has been expended on procedures, techniques, and training to minimize effects of this type. Certainly encouraging is the fact that data taken on B-Stand as well as other stands supports the conclusions reached by this type of analysis.

In this analysis it will be assumed that:

(1) All elemental errors are normally distributed and hence are in "statistical control."

(2) All elemental errors are based on at least 20:1 odds, i.e., 95% probability; hence the overall accuracy determination has that probability.

A.   PRESSURE MEASUREMENTS

1.   Component Errors

Figure A-1 shows the various components of error $e_1, \cdots, e_7$ in a strain-gage instrumentation channel from the sensed parameter to the digitized tape record, and is typical for pressure measurements. These error components are first evaluated by estimating the elemental errors making up each component and then combining them (where appropriate) by the standard "square-root-of-the-sum-of-the-squares" technique.
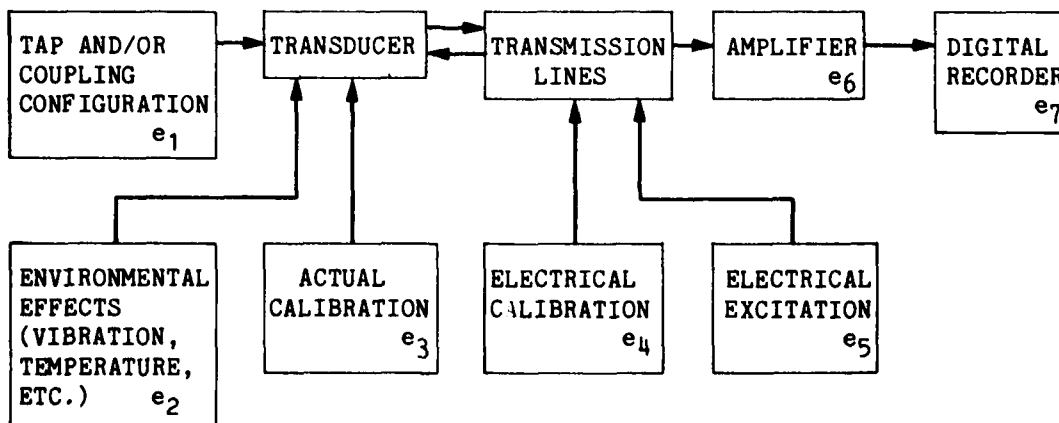
Figure A1. Typical Strain-Gage-Type Instrumentation Channel

2.   Tap and/or Coupling Errors e_1

These consist of amplitude error when the nature (frequency, amplitude, wave shape) of the fluctuating components of the measurements exceeds the response capabilities of the coupling/transducer system. However, the system will produce a nearly-average electrical analog for small amplitude fluctuations at frequencies beyond the response of the system. It is assumed that this analog is a true average of the noise-like fluctuations during steady-state conditions. Therefore, e_1 = nil.

3.   Environmental Errors e_2

Bonded strain gage construction provides low vibration sensitivity for pressure transducers. Noise introduced by mechanical vibration for pressure will be assumed to be of small amplitude and to be effectively averaged at the digital recorder input filter (0 to 10 cps low pass).

Transducers are not exposed to heat radiation from exhaust gases and are normally shielded from the direct rays of the sun. Temperature errors are assumed to result from ambient temperature changes between the time of electrical calibration and run time, and not from nonuniform case temperature. Ambient temperature change is estimated to be within $\pm 2.8^{\circ}C$ ($\pm 5^{\circ}F$). Temperature effects on pressure and force transducers are minimized by compensation circuitry and quoted by the manufacturers to be in the range of 0.009% full scale/$^{\circ}C$ (.005% full scale/$^{\circ}F$) for the pressure transducers.

$$e_2 = \pm 0.04\% \text{ of run level pressure}$$

4.   Actual Calibration Error e_3

The component error e_3 will be considered as the error in the parameter equivalent.

(1)   Calibrator combined accuracy (linearity, hysteresis, resolution, repeatability) -------------------- $\pm 0.05\%$

(2)   Transducer
Linearity (determined for near run level) ---- nil
Temperature effects (temperature assumed constant during calibration) ----------------- $\pm 0.10\%$
Interconnecting wiring (negligible current flow with high-impedance system) ------------- nil
Combined hysteresis and repeatability -------- 0.25%
Excitation (short-term stability) ------------ $\pm 0.10\%$
Readout (digital voltmeter overall accuracy at 30-mV full-scale and 24-mV reading) ------- $\pm 0.033\%$

Thus, $e_3 = \pm 0.29\%$

5. Electrical Calibration Error e_4

   (1) Repeatability ----------------------------------- $\pm 0.10\%$

   (2) Thus, $e_4 = \pm 0.10\%$

6. Electrical Excitation Error e_5

   (1) Excitation stability (from prerun electrical
       calibration through run) --------------------- $\pm 0.10\%$

   (2) Thus, $e_5 = \pm 0.10\%$

7. Amplifier Error e_6

   (1) Amplifier stability (from prerun electrical
       calibration through run):

       Gain stability ------------------------------- $\pm 0.01\%$

       Nonlinearity --------------------------------- $\pm 0.01\%$

       Balance -------------------------------------- $\pm 0.01\%$

   (2) Thus, $e_6 = \pm 0.02\%$

8. Digital Recorder Error e_7

   (1) Resolution ($\pm 16,384$ counts full scale) ------- $\pm 0.006\%$

   (2) Short term stability (from prerun calibration
       through run) --------------------------------- $\pm 0.05\%$

   (3) Linearity -------------------------------------- $\pm 0.02\%$

   (4) Electrical noise (combined effects of entire
       system) -------------------------------------- $\pm 0.10\%$

   (5) Conversion error ------------------------------ $\pm 0.05\%$

   (6) Thus, $e_7 = \pm 0.13\%$

9. Uncertainty

   The uncertainty (U_p) in a pressure measurement involves e_1 through
e_7 plus the uncertainty (U_{CAL}) in the calibration step. The uncertainty
in the calibrate step involves e_4, e_6, and e_7:

A-4

$$U_{?4} = [(e_4)^2 + (e_6)^2 + (e_7)^2]^{1/2}$$

$$= [(0.10)^2 + (0.02)^2 + (0.13)^2]^{1/2} = \pm 0.17\%$$

$$U_P = [(e_1)^2 + (e_2)^2 + (e_3)^2 + (e_4)^2 + (e_5)^2 + (e_6)^2 + (e_7)^2]^{1/2}$$

$$= [(0)^2 + (0.04)^2 + (0.29)^2 + (0.10)^2 + (0.10)^2 + (0.02)^2 + (0.13)^2 + (0.17)^2]^{1/2}$$

$$= \pm 0.39\%$$

B. THERMOCOUPLE MEASUREMENTS

Figure A-2 shows the various components of error $e_1, \cdots, e_5$ in a thermocouple instrumentation channel from the sensed parameter to the digitized tape record. These error components are first evaluated by estimating the elemental errors making up each component and then combining them (where appropriate) by the "square-root-of-the-sum-of-the-squares" technique.

1. Thermocouple Errors e_1

All thermocouple probes at ETS meet the standard limits of error of premium grade thermocouples recommended by the Instrument Society of America (ISA). All of the thermocouples used were type-K, chromel-alumel, and therefore only this type will be evaluated. The ISA limits of error are given as percentages applied to the temperature being measured. The ISA limits of error for type K thermocouples are:

$\pm 1.1^\circ C$ ($\pm 2^\circ F$) from -17.8 to $276.7^\circ C$ (0 to $530^\circ F$)

$\pm 0.375\%$ from 276.7 to $1260^\circ C$ (530 to $2300^\circ F$)

```
THERMOCOUPLE  →  REFERENCE   →  TRANSMISSION  →  AMPLIFIER  →  DIGITAL
    e_1           JUNCTION        LINES            e_4          RECORDER
                    e2                                            e5
                                     ↑
                               ELECTRICAL
                               CALIBRATION
                                   e_3
```
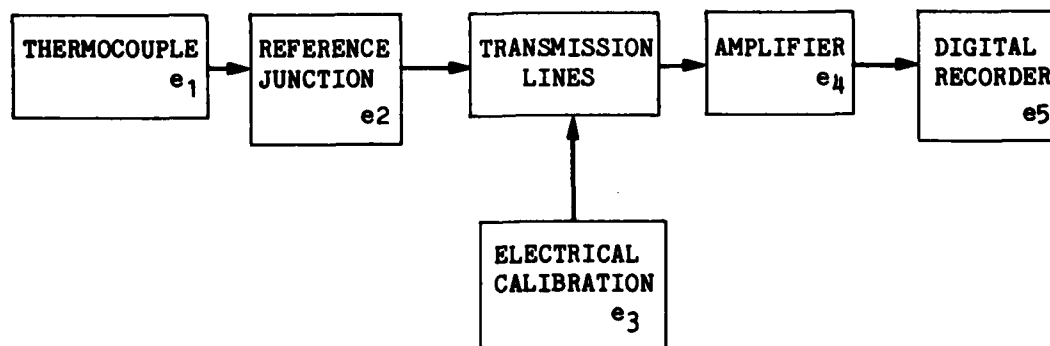
Figure A-2. Typical Thermocouple-Type Instrumentation Channel

2.   Reference Junction Error e_2

The reference junction used at ETS is the Pace Engineering Company 65.6°C (150°F) reference junction. The manufacturer lumps its total inaccuracy as ±0.28°C (±0.5°F).

Temperature °C (°F):

	10.0 to 37.8 (50 to 100)	37.8 to 93.3 (100 to 200)	93.3 to 148.9 (200 to 300)
e_2 :	0.67%	0.33%	0.20%

	148.9 to 204.4 (300 to 400)	204.4 to 276.7 (400 to 530)	276.7 to 1260 (530 to 2300)
e_2 :	0.14%	0.11%	0.03%

3.   Calibration Voltage Error e_3

The thermocouple systems at ETS calibrate the records by voltage substitution using a Video Power Supply Model 200. The power supply stability is ±0.05%. The voltage divider resistors are ±0.05%.

$$e_3 = \pm0.07\%$$

4.   Amplifier Error e_4

    (1)   Amplifier stability (from prerun electrical calibration through run):

        Gain stability ---------------------------------- ±0.01%

        Non linearity ---------------------------------- ±0.02%

        Balance -- ±0.01%

    (2)   Thus, $e_4 = \pm0.02\%$

5.   Digital Recorder Error e_5

    (1)   Resolution (±16,384 counts full scale) ------- ±0.006%

    (2)   Short-term stability (from prerun calibration through run) ---------------------------------- ±0.05%

    (3)   Linearity ------------------------------------- 0.02%

(4)   Electrical noise (combined effects of entire
        system) -------------------------------------- ±0.10%

(5)   Conversion error ----------------------------- ±0.05%

(6)   Thus, e_5 = ±0.13%

6.   Uncertainty

The uncertainty (U_{TC}) in a thermocouple measurement involves
e_1 through e_5 plus the uncertainty (U_{CAL}) in the calibrate step.
The uncertainty in the calibrate step involves e_3, e_4 and e_5:

$$U_{CAL} = [(e_3)^2 + (e_4)^2 + (e_5)^2]^{1/2}$$

$$= [(0.07)^2 + (0.02)^2 + (0.13)^2]^{1/2}$$

$$= 0.15\%$$

U_{TC} for type K (CR-AL) thermocouples for the range 10.0 to 37.8°C (50°F
to 100°F):

$$U_{TC} = [(e_1)^2 + (e_2)^2 + (e_3)^2 + (e_4)^2 + (e_5)^2 + (U_{CAL})^2]^{1/2}$$

$$= [(2.6)^2 + (0.67)^2 + (0.07)^2 + (0.02)^2 + (0.13)^2 + (0.15)^2]^{1/2}$$

$$= ±2.7\%$$

For range 37.8 to 93.3°C (100 to 200°F):

$$U_{TC} = [(1.3)^2 + (0.33)^2 + (0.07)^2 + (0.02)^2 + (0.13)^2 + (0.15)^2]^{1/2}$$

$$= ±1.4\%$$

Uncertainties for other ranges of type K are calculated the same way and
are listed below.

Temperature °C (°F):

	10.0 to 37.8 (50 to 100)	37.8 to 93.3 (100 to 200)	93.3 to 148.9 (200 to 300)
U_{TC}:	±2.7%	±1.4%	±0.85%

	148.9 to 204.4 (300 to 400)	204.4 to 276.7 (400 to 530)	276.7 to 1260 (530 to 2300)
U_{TC}:	±0.62%	±0.49%	±0.43%

C.   CALCULATION PROGRAM UNCERTAINTIES

There are three error sources in an IDAC calculation program:
input data exceeding the input range of the program, resolution of the
engineering units conversion, and calculation round-off errors. The
first error nearly always shows as a major discrepancy in the calculated
data. The latter two have a relatively small magnitude and are inherent
in the IDAC, so will remain throughout use of the program.

In general, there have been no problems with the calculations
in other IDAC programs when the range of the source data is within
the general range used for the program verification. Problems may
be found if the range of the source data is greatly exceeded. However,
such errors typically produce a calculated result that is obviously
incorrect, so there is relatively little chance of obtaining invalid
data.

Engineering units data displayed for the source channels are
obtained by multiplying a digital value proportional to the physical
quantity by a parameter equivalent (PE) value. The digital value is
referred to as "raw data," and has a range of $\pm16,384$ counts. The PE
typically has a value in the range of 4000 to 10,000 counts. If the PE
has a relatively small magnitude, the engineering units value displayed
by the IDAC will stay at the same value while the raw data bits are
changed through a range of at least several bits. Typically, the raw
data must change on the order of 4 counts before change will be shown
in the engineering units data. A small PE may require a change of
over 10 raw data counts to cause a change in the engineering units
data. The typical engineering units data have a resolution of 4 digits;
this does not represent a significant error for real-time data. However,
this characteristic will affect the calculated data since several source
channels may all have their maximum resolution errors at the same time.
The combined resolution error is thus present in the calculated data.

The round-off errors are caused by the limited word length of the
IDAC. All calculations are performed in a two-word format; one defines
the magnitude and the other the exponent. The magnitude word has 16 bits,
so the least significant bit represents 0.006% of the full scale value.
Each operation of the calculation sequence can thus lose 0.006%.
The air-flow calculation involves about 30 operations, so the round-
off error can be on the order of 0.2%.

To verify the calculation program results, source channel data was
entered into IDAC, read on the video display, and logged. A Texas
Instruments SR51 calculator was used to calculate the air- and fuel-flow
rates from the logged data. The calculator result was compared to the
IDAC result and the difference noted. The maximum percentage difference
of reading is, air flow 0.54% and fuel flow 0.13%. Multiplying the
percent difference by 1.5 gives a safe uncertainty number for the IDAC
program calculation. The results:

Air flow = $\pm0.81\%$ of reading; fuel flow = $\pm0.20\%$ of reading

D.   FUEL FLOW MEASUREMENTS

1.   Component Errors

Figure A-3 shows the various components of error e_1, $\cdots$, e_5 in
a turbine flowmeter instrumentation channel from the transducer to the
digitized tape record. These error components are first evaluated by
estimating the elemental errors making up each component and then combining
them (where appropriate) by the "square-root-of-the-sum-of-the-squares"
technique.

2.   Environmental Errors e_1

Magnetic coil pickups are receptive to external ac signals. Good
instrumentation shielding and grounding techniques virtually eliminate
externally induced signals. Thus, e_1 is nil.

3.   Actual Calibration Errors e_2

The turbine flowmeter used was calibrated at the Jet Propulsion
Laboratory where the overall calibration uncertainty is 1.3%. Thus,
$e_2 = \pm 1.3\%$.

4.   Electrical Calibration Errors e_3

The electrical calibration is a known frequency substitution
and is not used in the flow-rate calculation, and therefore introduces
no error in the measurement. Thus, $e_3 = 0$

5.   Electrical Shaping Errors e_4

The shaping electronics convert the transducer output to a fast-
rise-time pulse. This is straightforward electrical process and the
error will be assumed to be nil. Thus, e_4 = nil.
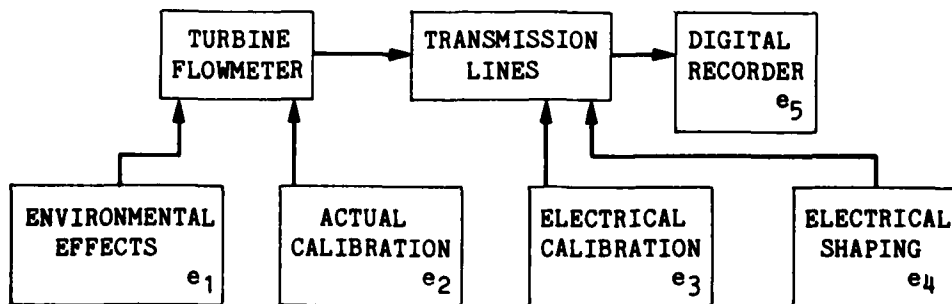
Figure A-3. Typical Turbine Flowmeter Instrumentation Channel

6. Digital Recorder e_5

The turbine flowmeter output is recorded on the IDAC period counters. The inherent uncertainty of the period measurement is $\pm0.20\%$. Thus, $e_5 = \pm0.20\%$.

7. Uncertainty

The uncertainty (U_F) in a turbine flowmeter measurement involves e_1 through e_5:

$$U_F = [(e_1)^2 + (e_2)^2 + (e_3)^2 (e_4)^2 + (e_5)^2]^{1/2}$$

$$= [(0)^2 + (1.3)^2 + (0)^2 (0)^2 + (0.20)^2]^{1/2}$$

$$= \pm1.32\%$$

The uncertainty (U_{MF}) in the mass fuel-flow measurement involves the fuel-flow measurement uncertainty (U_F) plus the fuel-temperature measurement uncertainty (U_{TC}) plus the calculation program uncertainty (U_{CPF}):

$$U_{MF} = [(U_F)^2 + (U_TC)^2 + (U_{CPF})^2]^{1/2}$$

$$= [(1.32)^2 + (1.4)^2 + (0.20)^2]^{1/2}$$

$$= \pm1.93\%$$

E. MASS AIR-FLOW MEASUREMENT

1. Component Errors

Figure A-4 shows the various components required to make the mass air-flow measurement. The error of each component is combined by the "square-root-of-the sum-of-the-squares" technique to determine the uncertainty for this measurement.

2. Laminar Flow Element Errors e_1

The laminar flow element (LFE) has no direct output but requires that three measurements be taken on it. The manufacturer lists the LFE measurement uncertainty at $\pm0.50\%$. Thus, $e_1 = \pm0.50\%$
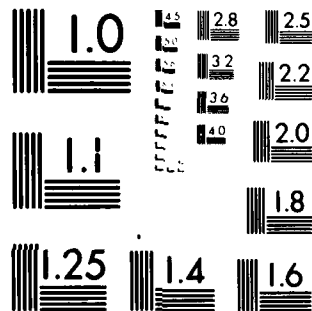
MICROCOPY RESOLUTION TEST CHART

NATIONAL BUREAU OF STANDARDS 1963 A
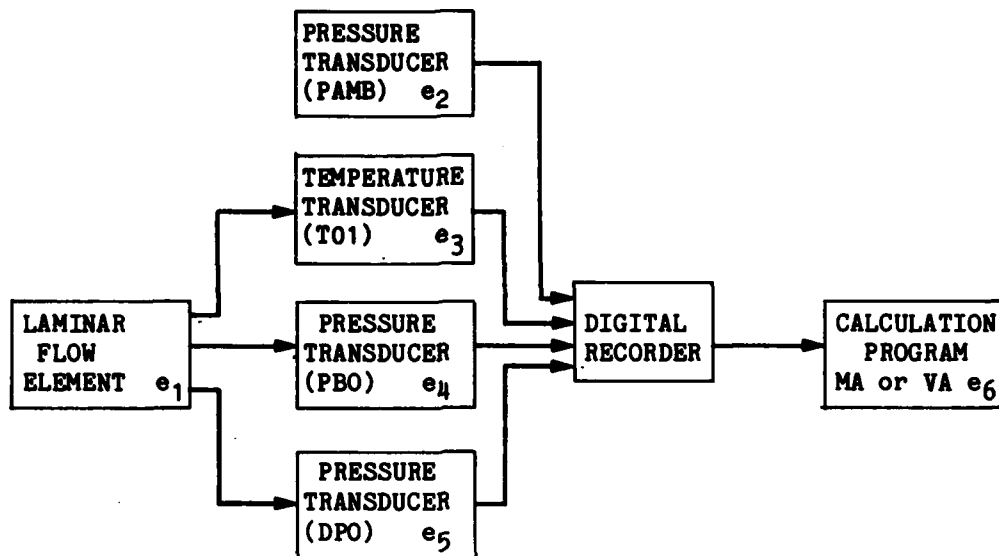
Figure A-4. Mass Air-Flow Measurement

3.   Transducer Measurement Uncertainties

   (1)   PAMB, e_2 = ±0.39%

   (2)   T01, e_3 = ±1.4%

   (3)   PBO, e_4 = ±0.39%

   (4)   DP2, e_5 = ±0.39%

   (5)   Mass air flow calculation program uncertainties e_6 = ±0.81%

4.   Uncertainty

   The uncertainity (U_{MA}) in the mass air-flow measurement involves e_1 through e_6.

$$U_{MA} = [(e_1)^2 + (e_2)^2 + (e_3)^2 (e_4)^2 + (e_5)^2 + (e_6)^2]^{1/2}$$

$$= [(0.50)^2 + (0.39)^2 + (1.4)^2 (0.39)^2 + (0.39)^2 + (0.18)^2]^{1/2}$$

$$= ± 1.82\%$$

F.   MIXTURE RATIO (MR) AND EQUIVALENCE RATIO (ER) CALCULATIONS

   The MR and ER calculation uncertainty involves the mass fuel-flow uncertainity (U_{MF}), mass air-flow uncertainty (U_{MA}), and calculation program uncertainty (U_{CP}). In this case, the calculation program involves only 2 operations, so the round-off error is 0.012%.

$$U_{MR} = U_{ER} = [(U_{MF})^2 + (U_{MA})^2 + (U_{CP})^2]^{1/2}$$

$$= [(1.93)^2 + (1.82)^2 + (0.012)^2]^{1/2}$$

$$= \pm 2.65\%$$

G. QUARTZ-CRYSTAL PRESSURE TRANSDUCER MEASUREMENTS

1. Component Errors

Figure A-5 shows the various components of error $e_1, \cdots, e_8$ in a quartz-piezoelectric instrumentation channel from the sensed parameter to the recorder. These error components are first evaluated by estimating the elemental errors making up each component and then combined (where appropriate) by the standard "square-root-of-the-sum-of-the-squares" technique.
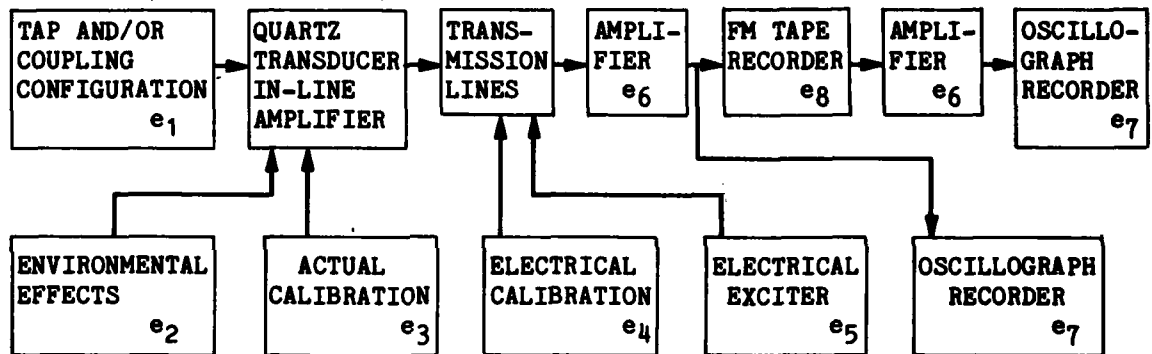
Figure A-5. Typical Quartz-Piezoelectric Type of Instrumentation Channel

2. Tap and/or Coupling Errors e_1

These consist of amplitude error when the nature (frequency, amplitude, waveshape) of the fluctuating components of the measurements exceed the response capabilities of the coupling/transducer system. Quartz-crystal pressure transducers are high-frequency (500-kHz) sensors that are normally flush-mounted to eliminate tap and/or coupling errors. Therefore, e_1 = nil.

3. Environmental Errors e_2

The rigid structure of quartz-crystal pressure transducers with an integral compensating accelerometer reduce vibration sensitivity and suppress resonance effects.

Transducers in the flame arrester detonation piping are exposed to flame and heat for milliseconds as the flame moves down the piping.

Heat radiation absorbed by the transducer is minimal due to the short duration and is estimated to be within $5.6^\circ C$ ($10^\circ F$). The manufacturers quoted temperature coefficient is $0.054\%/^\circ C$ ($0.03\%/^\circ F$). Thus, $e_2 = \pm 0.30\%$.

4.   Actual Calibration Error e_3

    The component error e_3 will be considered as the error in the parameter equivalent.

      (1)   Calibrator combined inaccuracy (linearity, hysteresis, resolution, repeatability) -------------------- $\pm 0.20\%$

      (2)   Quartz-crystal pressure Transducers:

            Linearity (determined for near run level) ---- $\pm 0.10\%$

            Temperature effects (temperature assumed constant during calibration) ------------------ $\pm 0.10\%$

            Interconnecting wiring (negligible current flow with high-impedance system) ------------- nil

            Combined hysteresis and repeatability -------- 0.25%

            Excitation (short-term stability) ------------ $\pm 0.10\%$

            Readout (X-Y plotter combined linearity, hystersis, resolution, repeatability) -------- $\pm 0.50\%$

      (3)   Thus, $e_3 = \pm 0.62\%$

5.   Electrical Calibration Error e_4

      (1)   Repeatability --------------------------------- $\pm 0.10\%$

      (2)   Thus, $e_4 = \pm 0.10\%$

6.   Electrical Excitation Error e_5

      (1)   Excitation stability (from prerun electrical calibration through run) --------------------- $\pm 0.10\%$

      (2)   Thus, $e_5 = \pm 0.10\%$

7.   Amplifier Error e_6

      (1)   Amplifier stability (from prerun electrical calibration through run):

<pre>
                    Gain stability ------------------------------ ±0.01%

                    Nonlinearity -------------------------------- ±0.01%

                    Balance ------------------------------------- ±0.01%
</pre>

    (2)   Thus, $e_6 = \pm 0.02\%$

8.   Oscillograph Recorder Error e_7

    (1)   Resolution [±10.16-cm (± 4-in.) full-scale
deflection] ------------------------------- ±0.50%

    (2)   Linearity [±10.16-cm (± 4-in.) full-scale
deflection] ------------------------------- ±2.00%

    (3)   Electrical noise (combined effects of entire
system) ----------------------------------- ±0.10%

    (4)   Thus, $e_7 = \pm 2.1\%$

9.   FM Tape Recorder Error e_8

    (1)   DC Linearity -------------------------------- ±0.50%

    (2)   Short-term stability (from pressure
calibration through run) -------------------- ±0.05%

    (3)   Electrical noise (combined effects of entire
system) ------------------------------------- ±0.10%

    (4)   Flutter (instantaneous tape speed errors) ---- ±0.10%

    (5)   Resolution ---------------------------------- ±0.01%

    Thus, $e_8 = \pm 0.53\%$

10.   Uncertainty

The uncertainty (U_{QT}) in a quartz-crystal pressure transducer
measurement recorded on FM tape and played back onto an oscillograph
involves e_1 through e_8 plus the uncertainty (U_{CAL}) in the calibration
step. The uncertainty in the calibrate step involves e_4, e_6, e_7, and e_8:

$$U_{CAL} = [(e_4)^2 + (e_6)^2 + (e_7)^2 + (e_6)^2 + (e_8)^2]^{1/2}$$

$$= [(0.10)^2 + (0.02)^2 + (2.06)^2 + (0.02)^2 + (0.53)^2]^{1/2}$$

$$= \pm 2.17\%$$

$$U_{QT} = [(e_1)^2 + (e_2)^2 + (e_3)^2 + (e_4)^2 + (e_5)^2 + (e_6)^2 + (e_8)^2$$
$$+ (e_6)^2 + (e_7)^2 + U_{CAL})^2]^{1/2}$$

$$= [(0)^2 + (6.30)^2 + (0.62)^2 + (0.10)^2 + (0.10)^2 + (0.02)^2$$
$$+ (0.53)^2 + (0.02)^2 + (2.06)^2 + (2.17)^2]^{1/2}$$

$$= \pm 3.1\%$$

The uncertainty (U_{OG}) in a quartz-crystal pressure transducer measurement recorded directly onto an oscillograph involves e_1 through e_7 plus the uncertainty (U_{CAL}) in the calibration step. The uncertainty in the calibrate step involves e_4, e_6, and e_7:

$$U_{CAL} = [(e_4)^2 + (e_6)^2 + (e_7)^2]^{1/2}$$

$$= [(0.10)^2 + (0.02)^2 + (2.06)^2]^{1/2}$$

$$= \pm 2.06\%$$

$$U_{QG} = [(e_1)^2 + (e_2)^2 + (e_3)^2 + (e_4)^2 + (e_5)^2 + (e_6)^2 + (e_7)^2$$
$$+ (U_{CAL})^2]^{1/2}$$

$$= [(0)^2 + (0.30)^2 + (0.62)^2 + (0.10)^2 + (0.10)^2 + (0.02)^2$$
$$+ (2.06)^2 + (2.06)^2]^{1/2}$$

$$= \pm 3.0\%$$

H.   QUARTZ-CRYSTAL PRESSURE TRANSDUCER RISE-TIME RESPONSE

1.   Component Limitations

Figure A-6 shows the various components for a quartz-piezoelectric instrumentation channel that limit the rise-time response. These components are first evaluation individually for rise-time limiting characteristics; the lowest response component(s) in the system determines the maximum rise-time response capability of the system.
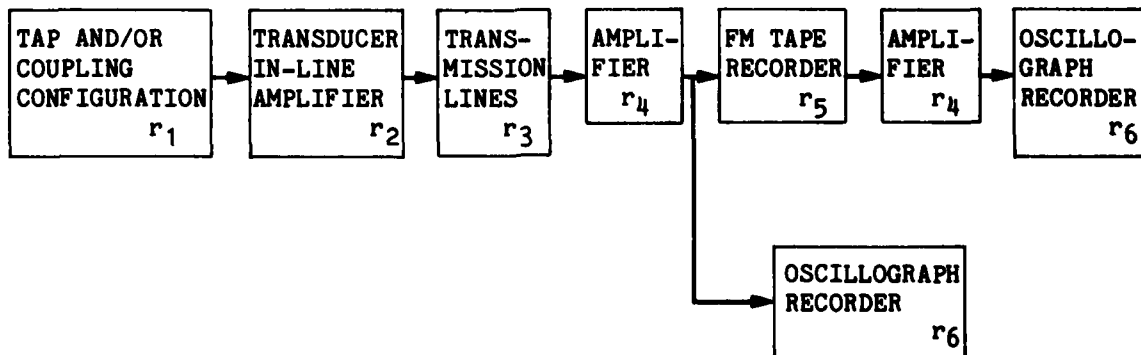
Figure A-6.   Typical Quartz-Piezoelectric Type of Instrumentation Channel

2. Tap and/or Rise-Time Response Limitations r_1

These consist of amplitude damping, waveshape distortion or frequency filtering when the nature of the fluctuation components of the measurement exceed the response capabilities of the coupling/transducer system. Quartz-crystal pressure transducers are fast rise-time, high-frequency (500-kHz) sensors that are normally flush-mounted to eliminate tap and/or coupling errors. Therefore, $r_1 < 1$-μs rise time.

3. Transducer In-Line Amplifier Rise-Time Limitations r_2

The manufacturer's quoted rise-time response for a quartz-crystal pressure transducer, in-line amplifier system is 1 μs. Thus, r_2 is 1-μs rise time.

4. Transmission Line Rise-Time Limitations r_3

All coaxial lines are used. Thus, r_3 is negligible.

5. Amplifier Rise-Time Limitations r_4

The manufacturer's quoted rise-time response is 2.5 μs. Thus, r_4 is 2.5 μs rise time.

6. FM Tape Recorder Rise-Time Limitations r_5

When frequency data and/or rise-time response data is required for a test, the data is recorded at maximum FM tape recorder speed. If more than 13 channels of data are required, two tape recorders are used and they have different capabilities:

Parameter	Recorder No. 1 (Ampex FR 3020)	Recorder No. 2 (Ampex PR 2200)
Tape speed, cm/s (ips)	304.8 (120)	152.4 (60)
Bandwidth, kHz ($\pm$ 1/2 dB)	DC to 80	DC to 40
Rise Time, μs	3.5	7.0
Flutter, %	0.13	0.20
Dynamic Skew, μs	0.2	0.4

Dynamic skew is the relative time displacement of an event recorded simultaneously on any two adjacent tracks within the same head stack as observed on playback. The dynamic skew of the recorders can be accounted for by simultaneously recording a square wave on all tape channels and making note of the time displacement between all channels.

A-16

A technique used to improve the time resolution between step functions on different tape tracks is to time expand the playback by decreasing the tape speed. A one-step speed reduction [from 304.8 to 152.4 cm/s (120 to 60 ips)] reduces the recorded frequency output by 1/2 and increases the time resolution by a factor of 2. This is very useful when playing back onto an oscillograph recorder whose galvanometers have a limited frequency and rise-time response.

7.   Oscillograph Recorder Frequency Limitations r_6

The response limitations are dependent on the type of galvanometer used. Included here are galvanometers used for this test program:

Galvanometer Type	Undampened Natural Frequency, Hz	Rise-Time Response, μs
M600	DC to 600	757
7-362	DC to 4150	110

8.   Results

The quartz-crystal pressure transducer system response limit when recorded directly on the oscillograph is:

757-μs rise time response

When recorded on FM tape and playback with a time expansion of 32 onto the oscillograph, the response limits are:

3.5-μs rise time on tape recorder No. 1
7.0-μs rise time on tape recorder No. 2

I.   PHOTODETECTOR RISE-TIME LIMITATIONS

1.   Component Limitations

Figure A-7 shows the various components of a photodetection system that limit the rise-time response. These components are first evaluated individually for rise-time response limiting characteristics; the lowest response components in the system determine the maximum rise-time response capability of the system.

TAP AND/OR COUPLING CONFIGURATION r_1	PHOTO-DETECTOR r_2	TRANS-MISSION LINE r_3	AMPLI-FIER r_4	FM TAPE RECORDER r_5	AMPLI-FIER r_4	OSCILLO-GRAPH RECORDER r_6
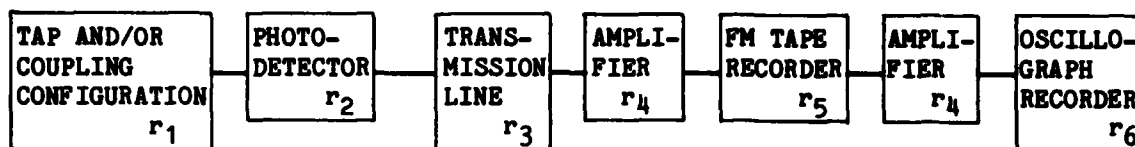
Figure A-7. Typical Photodetector Type of Instrumentation Channel

2. Tap and/or Coupling Rise-Time Limitations r_1

With photodetectors, the tap or coupling may decrease the photo intensity and affect the spectral response. These characteristics may result in lower output amplitudes, but have minimum effect on rise-time response. However, the field of vision, reflections, flame-front characteristics, and flame speed will affect rise-time response. These characteristics are unknown and indeterminate at this time. Therefore, r_1 is indeterminate, and the rise-time limitation analysis will begin with r_2.

3. Photovoltaic Rise-Time Limitations r_2

The manufacturer's quoted rise-time response is 1.5 μs.

4. Multiplier Phototubes Rise-Time Limitations r_2

The manufacturer's quoted rise-time response is 0.05 μs.

5. Rise-Time Limitations r_3 Through r_6

These rise-time limitations are the same as for quartz-crystal transducer systems.

6. Results

The photodetector system response is limited by the rise-time response limitations of the recorders. Therefore, for real-time recordings, the limit is the 757-μs rise-time response of the oscillograph.

For time-expanded data recorded on FM tape and played out onto an oscillograph, the limits are:

Time Expansion	Rise-Time Response, μs	
	Tape No. 1	Tape No. 2
1:1	110	110
2:1	55	55
4:1	28	28
8:1	14	14
16:1	7	7
32:1	3.5	7
64:1	3.5	7

APPENDIX B

TEST CONFIGURATION LOG

Configu-ration No.	Test No.	Description
100 to 117	1415 to 1428	The first eighteen test configurations were evolved during the facility check-out tests designed to produce a stable detonation with propane and air mixtures. They covered the development of the hydrogen-air-spark igniter, the fuel-and-air-mixture sampling procedure, the increase in pipe run-up length from 8.4 to 31.5-m (25.5 to 103.5-ft), the changes in propane fuel from chemically pure to commercial grade, and the eventual addition of the expanded metal liners to produce turbulence in the fuel-and-air mixture burning in the run-up piping.
118	1429 (A-F)	This configuration was similar to that shown in Figure 3-1. The only difference was that two 4.6-m (15.0-ft) sections of turbulent liners were installed at this time. The orifice plate was not installed.
119	1430 (A,B)	The orifice plate was installed at the outlet of the extension Section No. 11.
120	1431 (A)	The third turbulent liner was added to the remaining 4.6-m (15.0-ft) Section No. 5, making the total run-up length of lined piping 13.7-m (45.0-ft).
121	1431 (B-D)	Installed orifice plate at the exit of the verification sections; that is, between Sections No. 8 and No. 9.
122	1432 (A-D) 1433 (A,B)	Changed fuel in the test supply tank from commercial grade propane to Indolene HO III clear gasoline. Removed the orifice plate.
123	1433 (C-E)	Installed the orifice plate between Sections No. 8 and No. 9.
124	1434 (A)	Removed the 3.1-m (10.0-ft) test Section No. 9 and installed the two pipe tees and in-line rupture-disc test assembly as shown in Figure 8-1. Two 4137-kN/m^2 (600-psid) pressure-rated rupture discs were installed. Orifice plate was installed at entrance to witness Section No. 10.

Configuration No.	Test No.	Description
125	1434 (B)	Rupture discs with 2068-kN/m^2 (300-psid) pressure rating were installed.
126	1434 (C)	Rupture discs with 690-kN/m^2 (100-psid) pressure rating were installed.
127	1434 (D)	Rupture discs with 345-kN/m^2 (50-psid) pressure rating were installed.
128	1435 (A)	Rearranged the upstream pipe tee and replaced the downstream pipe tee with a pipe elbow as shown in Figure 8-3. Installed a rupture disc with 4137-kN/m^2 (600-psid) pressure rating. Orifice plate remained at the entrance to witness Section No. 10.
129	1435 (B)	Rupture disc with 2068-kN/m^2 (300-psid) pressure rating was installed.
130	1435 (C)	Rupture disc with 690-kN/m^2 (100-psid) pressure rating was installed.
131	1435 (D)	Rupture disc with 345-kN/m^2 (50-psid) pressure rating was installed.
132	1436 (A-E) 1437 (A)	Removed the orifice plate from the entrance to Section No. 10 and installed the 30.5- to 15.2-cm (12-to 6-in.-) diameter pipe reducer assembly containing the Shand and Jurs arrester as shown in Figure 8-6. Installed a rupture disc with 690-kN/m^2 (100-psid) pressure rating.
133	1437 (B)	Rupture disc with 1379-kN/m^2 (200-psid) pressure rating was installed.
134	1437 (C)	Rupture disc with 2068-kN/m^2 (300-psid) pressure rating was installed.
135	1437 (D)	Rupture disc with 4137-kN/m^2 (600-psid) pressure rating was installed.
136	1437 (E)	Removed the Shand and Jurs arrester and bolted the 30.5-cm- (12-in.-) diameter flanges back together with only a gasket seal. Rupture disc with 4137-kN/m^2 (600-psid) pressure rating installed.

Configuration No.	Test No.	Description
137	1438 (A-D)	Replaced the 30.5- to 15.2-cm- (12- to 6-in.-) diameter pipe reducer assembly with a 25.4- to 15.2-cm- (10- to 6-in.-) diameter pipe reducer assembly containing the Amal arrester as shown in Figure 8-10. Installed a rupture disc with a 690-kN/m^2 (100-psid) rating.
	NOTE:	The rupture-disc pressure rating was 690 kN/m^2 (100-psid) on all subsequent test assemblies unless otherwise noted.
138	1439 (A-C,	Replaced the Amal arrester with the Whessoe 80-grade foamed metal arrester.
139	1439 (D)	Replaced the Whessoe 80-grade with a 45-grade foamed metal arrester.
140	1440 (A-E)	Replaced the 25.4- to 15.2-cm- (10- to 16-in.-) diameter pipe reducer assembly with the water-trap arrester assembly as shown in Figure 8-15.
141	1440 (F)	Removed all the water from the water-trap arrester.
142	1441 (A-E)	Reversed the water-trap inlet and exit ports and installed the vertical-packed bed of aluminum Ballast rings arrester as shown in Figure 8-18.
143	1442 (A-E) 1433 (C)	Replaced the vertical-packed bed arrester with the Linde hydraulic back-pressure valve arrester as shown in Figure 8-21.
144	1442 (F)	Removed all the water from the Linde arrester.
145	1444 (A-B)	Reversed all the detonation test piping from the inlet pipe tee Section No. 0 to the exit extension Section No. 11 to arrange the downstream ignition test assembly. The Linde arrester was installed in the normal flow-through direction. Orifice plate was installed at exit of Section No. 11.
146	1444 (C)	Reversed hydrogen-air-spark igniter orientation by 180 degrees.
147	1444 (D)	Removed all water from the Linde arrester.

Configu-ration No.	Test No.	Description
148	1445 (A-F)	Interchanged ignition Section No. 1 with stabilizer Section No. 2 and installed the orifice plate between Sections No. 1 and No. 2. as shown in Figure 9-1. Refilled the Linde arrester with water up to the gaging port.
149	1446 (A-E)	Replaced the Linde arrester with the water-trap arrester and filled with water to the gaging port.
150 to 156	1447 to 1449	Removed the water-trap arrester and reassembled all the detonation test piping back to the upstream ignition arrangement so that it was identical to Configuration No. 121. Replaced the gasoline in the test fuel supply tank with chemically pure (CP) propylene.
157 to 164	1450 to 1449	Various lengths of both lined and unlined piping were used during the unsuccessful measurement of air-flow pressure loss to determine pipe-wall friction factor.
165	1458 (A-C)	Removed the turbulent liner from Section No. 5 and cut it into required lengths for installation into Sections No. 7, No. 8, and No. 10. Provided instrumentation ports in the liners so that the ports were coincident with the flame sensor and pressure sensor locations in these sections. Reassembled all sections in the following order: No. 1, No. 2, No. 3, No. 4, No. 7, No. 8, No. 10, No. 6, No. 5, orifice plate, No. 9, and No. 11. Removed the CP propylene from the fuel supply tank and replaced it with gasoline.
166	1459 (A-G)	Removed the turbulent liner from Section No. 4, cut it into required length, and installed it into Section No. 6. Reinstalled Section No. 6 between Sections No. 3 and Section No. 7. Reinstalled Section No. 4 between Sections No. 10 and No. 5 as shown in Figure 11-1.
167	1460 (A-F) 1461 (A-I)	Section No. 10 liner broke loose and jammed up into Section No. 8. The damaged liner was removed from Section No. 8 and a new liner installed into Section No. 10.

Configu-ration No.	Test No.	Description
168 to 175	1462 to 1469	Various lengths of both lined and unlined piping were used during the successful measurement of air-flow pressure loss to determine pipe-wall friction factor.
176	1470 (A-C)	Reassembled the detonation test shock-tube piping to the upstream ignition configuration shown in Figure 3-1. Two new expanded metal tube liners were installed into the run-up Sections No. 4 and No. 5. The liners were removed from the verification Sections No. 6, No. 7, and No. 8 and the witness Section No. 10. Installed the 30.5-to 15.2-cm- (12- to 6-in.-) diameter pipe reducer assembly into the test Station No. 9 as shown in the arrester test assembly, Figure 8-6. A 30.5-cm- (12-in.-) diameter by 15.2-cm- (6-in.-) long Shand and Jurs spiral-wound, crimped stainless-steel ribbon core element was installed into the arrester assembly. Replaced the two high-pressure quartz-crystal-type pressure transducers in the witness Section No. 10 (P101 and P104) with two lower-range bonded strain-gage-type pressure transducers.
177	1471 (A,B)	Installed the two high-pressure quartz-crystal-type pressure transducers into verification Section No. 7 (P71 and P72).
178	1472 (A-F)	Replaced the arrester core element with a 30.5-cm- (12-in.-) diameter by 20.3-cm- (8-in.-) long spiral-wound, crimped stainless-steel ribbon core element and high-pressure housing.
179	1473 (A-F)	Replaced the arrester core element with a 30.5-cm- (12-in.-) diameter by 30.5-cm- (12-in.-) long spiral-wound, crimped stainless-steel ribbon core element and high-pressure housing.
180	1474 (A)	Rearranged the test assembly inlet pipe tee to an in-line position with the branch line containing the rupture-disc assembly directed vertically up and eliminated the inlet pipe elbow as shown in Figure 13-7. Reinstalled the Shand and Jurs arrester test assembly containing the 30.5-cm- (12-in.-) diameter by 20.3-cm- (8-in.-) long core element.

Configuration No.	Test No.	Description
181	1474 (B)	Rupture disc with 2068-kN/m^2 (300-psid) pressure rating installed.
182	1474 (C)	Rupture disc with 4137-kN/m^2 (600-psid) pressure rating installed.
183	1474 (D-F)	Replaced the rupture-disc assembly on the inlet pipe tee of the test assembly with a blind flange.
184	1475 (A-F)	Removed the Shand and Jurs arrester test assembly and installed the vertical bed of Ballast rings arrester test assembly as shown in Figure 8-18. Bed size is 43.2-cm (17-in.) in diameter by 67.5-cm (25-in.) in depth containing 2.54-cm- (1.0-in.-) diameter by 2.54-cm- (1.0-in.-) long aluminum Ballast rings. Bed depth controlled by special spacers between lower and upper grids and between upper grid and dome cover.

NOTE: Aluminum Ballast ring size was 2.54-cm (1.0 in.) in diameter by 2.54-cm (1.0 in.) in length on all subsequent test assemblies unless otherwise noted.

185	1476 (A-E)	Changed bed size to 43.2-cm (17 in.) in diameter by 45.7-cm (18 in.) in depth, containing new Ballast rings.
186	1477 (A-E)	Changed bed size to 43.2 cm (17 in.) in diameter by 22.9 cm (9 in.) in depth containing new Ballast rings.
187	1478 (A-D)	Changed bed size to 43.2 cm (17 in.) in diameter by 63.5 cm (25 in.) in depth containing new 3.81-cm- (1.5-in.-) diameter by 3.81-cm- (1.5-in.-) long aluminum Ballast rings.
188	1479 (A-C)	Replaced the bed with new 5.08-cm-(2.0 in.-) diameter by 5.08-cm- (2.0-in.-) long aluminum Ballast rings.
189	1480 (A-F)	Installed cylindrical insert to change bed size to 33.7 cm (13.25 in.) in diameter by 63.4 cm (25 in.) in depth containing new Ballast rings.

Configuration No.	Test No.	Description
190	1481 (A-F)	Changed bed size to 30.5 cm (12 in.) in diameter by 63.5 cm (25 in.) in depth containing new Ballast rings.
191	1482 (A-H)	Changed bed size to 25.4 cm (10 in.) in diameter by 63.5 cm (25 in.) in depth containing new Ballast rings.
192	1483 (A)	Changed bed size to 25.4 cm (10 in.) in diameter by 45.7 cm (18 in.) in depth containing new Ballast rings.
193	1483 (B)	Rupture disc with 2068-kN/m^2 (300-psid) pressure rating installed on inlet pipe tee.
194	1483 (C)	Rupture disc with 4137-kN/m^2 (600-psid) pressure rating installed on inlet pipe tee.
195	1483 (D-F)	Replaced the rupture-disc assembly on the inlet pipe tee with a blind flange.
196	1484 (A-D)	Modified the detonation test piping installation for continuous flow as shown in Figure 14-2. Replaced the 15.2-cm- (6-in.-) diameter flow straightener at the exit of the inlet pipe tee Section No. 0 with the 25.4- to 15.2-cm- (10- to 6-in.-) diameter flanged pipe reducer arrester assembly containing a 25.4-cm- (10-in.-) diameter by 15.2-cm- (6-in.-) long Shand and Jurs spiral-wound, crimped aluminum ribbon core element mounted in a high-pressure housing. The instrumented verification Section No. 6 was replaced by the extension Section No. 11. The vertical bed arrester assembly remained installed in test Section No. 9 with a blind flange on the inlet pipe tee. The bed size remained at 25.4 cm (10 in.) in diameter by 45.7 cm (18 in.) in depth containing new Ballast rings. Two flanged 15.2-cm- (6-in.-) diameter standard pipe extension Sections No. 12 and No. 13, each 6.8 -m (22.4-ft) long, were installed at the exit of the witness Section No. 10, downstream of the gas sample rake. The instrumented verification Section No. 6 was reversed 180 degrees and installed at the exit of extension Section No. 13. In reversing Section No. 6, instrument ports

Configuration No.	Test No.	Description
		F63 and P63 are now upstream of instrument ports F62 and P62. This change provided better protection of the flame sensors from ambient light at the pipe exit.
197	1485 (A-D)	Replaced the bed with new Ballast rings.
198	1486 (A-D)	Replaced the vertical bed arrester test assembly with the Shand and Jurs 30.5-cm- (12-in.-) diameter by 20.3-cm-(8-in.-) long spiral-wound, crimpled stainless-steel ribbon arrester test assembly using the inline pipe tee connection with the rupture-disc assembly replaced by a blind flange in a configuration identical to No. 183.
199	1487 (A-D)	Removed the Shand and Jurs arrester assembly to straighten and repair cracked welds in the downstream retainer grid ring. Reversed the upstream and downstream retainer grid rings and reinstalled the Shand and Jurs arrester test assembly.
200	1487 (E)	Removed the Shand and Jurs arrester assembly and bolted the 30.5-cm- (12-in.-) diameter flanges together without an arrester.

APPENDIX C

TABULAR SUMMARY OF STEADY-STATE MEASURED AIR

AND FUEL SYSTEM TEST CONDITIONS

Test No.	Configuration No.	PBO, kN/m²	DPO, kN/m²	TO1, °C	PFL, kN/m²	TFL, °C	FMF, Hz	PVL, kN/m²	TV1, °C	TV2, °C	TMF, °C	PM1, kN/m²	TM1, °C	T12, °C	T102, °C	PA1, kN/m²	DPA1, kN/m²	DPA2, kN/m²	PAMB, kN/m²	VA[a], m/s	HA, kg/h	MF, kg/h	A/F RATIO	φ E.R.	HCA E.R.
1429A	118	125.09	0.2951	85.6	2212	33.4	238.0	117.1	75.3	91.9	66.6	93.96	58.9	48.2	38.6	—[b]	—	—	93.680	1.878	125.10	9.58	13.00	1.21	1.05
B	118	125.08	0.5640	83.9	1931	33.3	454.3	163.3	93.2	138.5	79.9	94.40	63.6	49.1	39.9	—	—	—	93.624	3.606	236.28	17.85	13.23	1.19	1.03
C	118	125.04	0.8453	83.9	1941	36.5	682.5	223.2	86.8	146.2	76.4	94.84	66.3	51.9	39.4	—	—	—	93.618	5.337	350.85	26.40	13.28	1.18	0.99
D	118	125.55	1.1452	82.1	1931	36.7	941.7	303.2	86.4	165.4	79.4	95.59	68.6	55.2	39.7	—	—	—	93.624	7.321	472.64	36.26	13.02	1.21	1.03
E	118	124.83	0.2848	83.1	1959	39.0	230.0	114.9	95.7	108.4	84.2	93.24	59.7	48.1	40.8	—	—	—	93.562	(1.811)	120.93	9.10	13.28	1.18	1.03
F	118	124.75	0.2820	80.2	1961	39.6	237.5	113.5	66.8	85.1	57.9	93.78	53.8	45.2	41.6	—	—	—	93.487	(1.850)	121.29	9.42	12.88	1.22	1.04
1430A	119	126.11	0.8122	78.3	1906	28.7	673.5	233.2	108.7	175.0	99.0	95.27	64.7	49.4	35.8	—	—	—	93.921	5.243	349.04	26.58	13.13	1.20	1.04
B	119	125.84	0.8315	78.9	1953	32.3	690.0	230.5	86.0	147.0	76.9	95.47	61.8	47.7	36.5	—	—	—	93.949	5.337	355.21	27.07	13.12	1.20	1.01
C	118	125.82	0.8315	78.3	1967	33.6	688.3	229.1	87.9	148.7	79.4	95.19	62.6	49.2	37.1	—	—	—	93.990	5.358	356.11	26.84	13.27	1.18	1.01
D	118	125.74	0.8467	78.9	1970	34.3	691.3	230.4	91.8	154.0	81.5	95.16	63.2	49.8	37.3	—	—	—	92.928	5.358	355.21	26.93	13.19	1.19	1.02
1431A	120	126.65	0.8150	73.4	1838	26.7	678.2	233.2	98.3	164.9	92.1	94.99	59.3	43.8	31.8	—	—	—	94.017	5.328	360.11	27.02	13.32	1.10	1.04
B	121	126.46	0.8142	74.5	1856	28.4	684.3	229.2	90.9	156.0	79.8	95.25	58.2	44.0	33.9	94.29	0.276	—	94.024	5.307	357.29	27.04	13.21	1.11	1.04
C	121	126.16	0.8122	76.9	1878	31.2	687.3	236.7	114.7	184.7	105.1	95.36	64.6	48.9	33.2	94.29	0.248	—	94.017	5.240	351.44	26.98	13.02	1.12	1.03
D	121	125.99	0.8253	80.0	1878	32.2	689.1	231.8	97.3	157.0	91.2	94.62	66.3	51.4	34.1	94.21	0.248	—	93.949	5.267	351.26	26.98	13.01	1.12	1.03
E	121	125.83	0.8205	77.7	1884	33.1	706.2	223.6	78.1	137.6	70.3	95.18	59.5	46.8	35.4	94.13	0.248	—	93.873	5.267	352.71	27.42	12.86	1.14	1.02
1432A	122	125.53	0.9591	78.7	574	32.3	531.2	199.3	186.1	286.4	174.2	95.38	73.8	54.7	36.7	—	—	—	93.818	6.197	407.64	31.20	13.03	1.12	0.91
B	122	125.42	0.7246	81.2	591	35.3	392.1	160.6	201.7	277.2	189.9	94.68	74.2	53.3	36.2	—	—	—	93.735	4.512	306.54	23.28	13.16	1.11	0.91
C	122	125.24	0.4888	83.9	625	37.1	274.5	127.5	195.1	256.8	166.2	94.24	70.2	51.2	37.7	—	—	—	93.693	3.115	205.52	16.48	12.46	1.17	0.93
D	122	125.18	0.2441	80.7	708	37.7	132.6	101.3	212.8	277.1	206.3	93.95	64.0	45.4	37.7	—	—	—	93.666	1.585	105.51	8.29	12.72	1.15	0.93
1433A	122	125.23	0.2434	83.0	667	46.6	133.9	101.3	182.3	296.4	209.3	94.27	64.5	44.3	36.1	—	—	—	93.700	(1.554)	103.96	8.33	12.84	1.17	0.89
B	122	125.00	0.7557	85.1	532	46.7	429.6	177.3	182.3	345.3	233.7	94.37	83.2	56.4	38.1	—	—	—	93.693	4.779	312.39	25.25	12.36	1.18	0.88
C	123	124.85	0.7467	87.7	522	48.2	417.8	170.9	180.3	326.5	224.0	94.62	84.6	59.4	40.6	93.89	0.166	—	93.700	4.697	305.13	24.53	12.43	1.18	0.87
D	123	124.89	0.7474	86.4	518	48.7	418.2	177.1	179.1	363.1	242.6	94.59	85.7	59.8	40.8	93.90	0.172	—	93.700	4.730	306.90	24.57	12.49	1.17	0.86
E	123	124.89	0.7419	83.7	517	48.9	420.7	171.8	180.3	373.9	251.3	94.49	84.1	58.2	40.6	93.84	0.166	—	93.666	4.746	308.62	24.68	12.50	1.17	0.87
1434A	124	125.93	0.7233	76.0	359	40.9	419.5	172.3	170.6	341.7	221.7	94.70	74.8	49.8	32.1	93.93	0.193	—	93.735	4.709	314.79	24.69	12.74	1.15	0.87
B	125	125.69	0.7205	75.6	565	43.9	408.4	169.6	179.2	408.3	268.8	94.73	79.3	52.2	31.8	93.94	0.214	—	93.707	4.663	310.71	23.93	12.98	1.13	0.88
C	126	125.56	0.7267	78.7	599	43.9	418.0	176.4	191.6	395.0	268.1	94.74	80.9	52.1	32.2	93.95	0.207	—	93.700	4.673	311.34	24.39	12.76	1.15	0.87
D	127	125.48	0.7219	77.7	609	45.6	418.9	173.6	166.4	394.8	257.5	94.64	78.5	52.0	32.7	93.87	0.193	—	93.625	4.666	310.39	24.51	12.66	1.15	0.89
1435A	128	125.32	0.7405	82.3	515	44.4	411.8	169.4	172.9	344.7	234.7	94.51	82.3	56.1	33.6	93.74	0.214	—	93.521	4.271	311.16	24.15	12.88	1.13	0.94
B	129	125.25	0.7384	82.9	625	45.7	403.9	163.8	162.1	356.4	217.1	94.47	78.2	53.7	34.0	93.74	0.221	—	93.514	4.679	309.30	23.66	13.06	1.12	0.94
C	130	125.06	0.7281	80.2	725	46.3	405.1	163.7	159.2	311.4	210.6	94.36	75.2	52.1	34.1	93.62	0.214	—	93.404	4.663	308.71	23.74	13.00	1.12	0.96
D	131	125.06	0.7508	82.2	831	47.0	416.3	167.9	166.5	317.1	214.7	94.38	77.7	54.0	35.4	93.60	0.214	—	93.390	4.779	314.56	24.35	12.91	1.13	0.96

[a] VA values given in parentheses are the air flow velocities at the time DPA measurements were taken. Flow velocity at the time of ignition was zero.

[b] The dash signifies the lack of an event.

Test No.	Configuration No.	PBO, kN/m²	DPO, kN/m²	TO1, °C	PFL, kN/m²	TFL, °C	FMF, Hz	PV1, kN/m²	TV1, °C	TV2, °C	TMF, °C	PM1, kN/m²	TM1, °C	T12, °C	T102, °C	PA1, kN/m²	DPA1, kN/m²	DPA2, kN/m²	PAMB, kN/m²	VA, m/s	MA, kg/h	MF, kg/h	A/F RATIO	φ E.R.	HCA E.R.
1436A	132	125.48	0.7439	79.8	686	42.2	427.1	174.8	184.0	335.2	219.1	94.36	76.1	50.9	30.7	93.65	0.152	0.159	93.473	4.746	316.42	25.15	12.58	1.16	0.83
B	132	125.24	0.7474	81.7	946	43.2	413.3	168.6	198.2	357.6	234.2	94.47	78.7	53.1	32.7	93.64	0.145	0.145	93.480	4.755	314.48	24.44	12.86	1.14	0.82
C	132	125.98	0.7391	82.0	1073	44.8	405.0	165.8	187.5	348.9	227.6	94.47	78.2	52.9	34.6	93.59	0.138	0.152	93.438	4.700	310.21	23.79	13.03	1.12	0.86
D	132	125.92	0.7343	82.8	1072	45.4	418.9	163.0	179.2	329.1	212.1	94.40	79.4	55.8	35.6	93.61	0.159	0.159	93.411	4.676	306.81	24.52	12.51	1.17	0.87
E	132	125.83	0.7329	82.4	1171	46.4	409.3	164.4	183.6	333.1	211.7	94.36	76.9	53.7	35.8	93.56	0.138	0.152	93.390	4.654	306.26	24.00	12.75	1.15	0.86
1437A	132	125.66	0.7219	81.0	1010	40.8	409.3	167.4	184.4	313.6	203.2	94.56	75.4	51.2	32.1	93.80	0.152	0.159	93.631	4.599	306.45	24.27	12.62	1.16	0.86
B	133	125.54	0.7212	80.4	1016	42.2	399.7	161.9	181.9	313.6	198.3	94.58	73.3	51.1	32.2	93.85	0.166	0.159	93.680	4.599	306.58	23.46	13.06	1.12	0.86
C	134	125.28	0.7350	80.9	1026	44.2	414.0	163.9	188.9	312.6	201.9	94.68	75.1	51.6	34.4	93.85	0.152	0.152	93.670	4.682	310.71	24.28	12.79	1.14	0.87
D	135	125.14	0.7391	83.2	1021	45.0	401.2	161.2	190.3	307.7	200.4	94.70	77.4	54.8	35.7	93.84	0.145	0.145	93.660	4.691	308.99	23.59	13.10	1.12	0.87
E	136	125.01	0.7391	84.3	1026	46.3	417.2	164.5	199.9	317.3	208.2	94.59	78.7	54.5	36.8	93.70	0.035	—ᵃ	93.631	4.666	306.67	24.36	12.58	1.16	0.87
1438A	137	125.73	0.8053	84.8	794	42.4	399.6	162.8	163.2	261.6	163.6	95.27	78.9	54.8	31.9	94.31	0.428	0.421	93.886	4.694	312.80	23.60	13.26	1.10	0.85
B	137	125.28	0.8274	89.1	794	43.9	411.6	166.3	191.3	307.0	202.4	95.31	84.4	61.4	35.2	94.29	0.428	0.434	93.852	4.785	313.79	24.16	12.98	1.13	0.86
C	137	124.76	0.8322	91.2	794	47.6	414.8	168.9	217.1	339.4	229.3	95.33	88.8	63.8	38.9	94.16	0.421	0.428	93.714	4.825	312.93	24.27	12.83	1.14	0.85
D	137	124.69	0.8308	91.3	797	48.2	428.2	165.4	184.5	301.9	195.9	95.49	87.0	64.8	40.6	94.14	0.428	0.441	93.700	4.813	310.89	25.14	12.36	1.18	0.85
1439A	138	125.79	0.7439	85.6	953	42.5	405.8	166.2	163.7	262.0	163.2	94.85	79.5	55.9	33.6	94.05	0.234	0.234	93.811	4.676	309.21	23.93	12.91	1.13	0.86
B	138	125.56	0.7619	87.6	957	43.2	423.5	169.0	171.1	283.3	180.0	95.01	81.7	54.9	32.6	94.12	0.248	0.255	93.859	4.712	312.89	24.92	12.55	1.16	0.87
C	138	125.11	0.7646	89.8	967	47.2	404.3	164.8	191.8	313.2	209.8	94.91	74.3	62.4	38.8	94.02	0.214	0.110	93.769	4.776	310.12	23.70	13.08	1.12	0.86
D	139	124.98	0.7633	88.5	975	48.7	410.5	170.1	205.8	328.4	215.0	94.67	82.6	58.8	38.7	93.71	0.131	0.124	93.562	4.779	310.98	24.04	12.93	1.13	0.88
1440A	140	125.03	0.7633	88.1	792	42.3	402.6	167.7	163.4	263.5	163.2	95.65	85.8	60.2	29.7	95.25	1.517	1.558	93.562	4.648	311.16	23.73	13.11	1.11	0.86
B	140	124.44	0.7695	91.5	784	45.8	421.5	168.0	218.8	304.4	199.9	96.38	85.6	62.1	36.4	95.21	1.648	1.655	93.556	4.654	307.35	24.63	12.47	1.17	0.88
C	140	124.27	0.7688	89.7	775	46.1	411.0	161.0	204.3	279.7	180.4	95.72	82.6	61.5	35.8	95.28	1.709	1.758	93.383	4.679	309.67	24.11	12.84	1.13	0.86
D	140	124.29	0.7639	89.1	788	47.7	404.6	159.6	205.5	275.2	171.8	96.12	80.1	61.7	36.8	95.15	1.655	1.620	93.425	4.676	308.53	23.66	13.03	1.12	0.85
E	140	125.16	0.7529	87.1	791	50.3	408.8	156.7	172.3	246.1	136.7	95.82	74.9	58.2	38.7	95.05	1.724	1.710	93.231	4.648	307.17	23.82	12.89	1.14	0.87
F	141	124.07	0.7701	87.3	939	50.3	417.8	160.1	194.6	263.8	121.6	93.61	78.3	59.6	38.8	93.27	0.028	—	93.225	4.837	312.89	24.33	12.85	1.14	0.86
1441A	142	125.16	0.7660	90.7	811	43.9	404.6	151.7	169.5	231.7	125.8	94.78	79.6	61.6	34.1	93.82	0.042	0.042	93.776	4.734	309.30	23.76	13.01	1.12	0.86
B	142	124.89	0.7812	91.8	875	45.2	414.4	155.1	183.3	245.2	140.4	94.82	82.3	63.1	35.3	93.82	0.055	0.048	93.762	4.810	313.02	24.29	12.88	1.13	0.88
C	142	124.66	0.7750	92.2	909	47.9	414.6	158.4	180.2	243.8	139.3	94.76	80.3	62.1	40.6	93.67	0.055	0.042	93.618	4.798	309.62	24.23	12.77	1.14	0.88
D	142	124.52	0.7743	92.2	816	47.9	420.1	156.4	167.9	234.1	126.7	94.78	80.4	63.6	41.0	93.68	0.055	0.048	93.618	4.801	308.94	24.54	12.58	1.16	0.89
E	142	124.53	0.7722	91.3	918	48.6	418.4	159.1	194.7	252.4	152.6	94.71	82.3	64.3	42.4	93.67	0.055	0.055	93.604	4.825	309.35	24.35	12.65	1.16	0.88
1442A	143	125.04	0.7570	87.2	802	39.3	404.4	160.4	210.4	260.8	157.5	96.33	77.1	56.2	33.1	95.80	2.158	2.137	93.528	4.599	310.03	23.80	13.02	1.12	0.85
B	143	125.83	0.7653	87.2	897	40.7	415.7	157.6	165.6	233.4	123.6	96.13	73.4	56.7	33.3	95.72	2.062	1.931	93.493	4.633	313.16	24.41	12.82	1.14	0.86
C	143	125.51	0.7653	87.2	904	42.9	422.5	150.6	150.9	221.2	113.9	95.68	72.1	56.8	36.4	95.40	2.027	1.999	93.369	4.682	312.52	24.83	12.58	1.16	0.86

ᵃThe dash signifies the lack of an event.

Test No.	Configuration No.	PB5, kN/m²	PPJ, kN/m²	IO2, °C	PIL, kN/m²	TFL, °C	FMF, Hz	PV1, kN/m²	TV1, °C	TV2, °C	IMF, °C	PM1, kN/m²	TM1, °C	T12, °C	TIO2, °C	PA1, kN/m²	DPA1, kN/m²	DPA2, kN/m²	PAMB, kN/m²	VA[a], m/s	MA, kg/h	MF, kg/h	A/F RATIO	¢ E.R.	HCA E.R.
1442D	143	124.42	0.7667	86.3	907	43.2	431.0	162.3	171.9	241.2	136.2	96.51	76.2	58.6	35.7	95.60	2.241	2.206	93.356	4.706	314.07	25.35	12.39	1.18	0.87
E	143	124.35	0.7722	85.8	909	44.9	415.4	159.5	172.5	262.2	155.4	96.05	78.2	60.4	36.2	95.11	1.793	1.724	93.266	4.791	316.79	24.38	12.99	1.13	0.86
F	144	124.35	0.7502	82.7	899	44.5	415.6	165.6	201.3	295.5	182.9	94.46	76.2	56.5	36.5	93.59	0.407	—b	93.187	4.773	312.43	24.39	12.80	1.14	0.88
1443A	144	126.15	0.7164	74.7	863	37.2	418.9	166.9	193.9	292.1	178.8	94.96	67.7	45.6	28.7	94.22	0.393	0.393	93.818	4.633	314.56	24.82	12.66	1.15	0.87
B	144	125.93	0.7095	77.1	859	39.0	405.8	163.4	200.5	295.4	183.4	94.18	69.4	48.3	30.7	94.18	0.372	0.393	93.797	4.569	307.62	24.02	12.80	1.14	0.88
C	143	125.63	0.7281	79.1	867	40.7	405.8	164.1	193.1	287.3	177.3	96.33	70.8	49.8	30.6	95.63	1.862	1.868	93.728	4.566	311.43	24.13	12.90	1.13	0.87
D	144	125.53	0.7205	77.9	866	40.9	409.6	162.0	199.4	293.7	183.8	94.92	71.2	49.9	31.4	94.10	0.393	—	93.700	4.621	309.67	24.02	12.89	1.13	0.87
1444A	145	126.78	0.2372	74.4	850	41.1	136.8	104.4	207.6	259.9	158.0	95.96	53.9	29.7	29.4	95.98	1.731	1.779	94.017	1.570	106.91	8.46	12.63	1.16	0.86
B	145	126.22	0.2379	77.7	864	43.5	136.9	104.3	216.6	271.9	166.9	96.11	58.6	35.2	34.8	95.93	1.779	1.772	93.990	(1.570)	105.14	8.58	12.25	1.19	0.88
C	146	126.04	0.2337	77.5	861	44.8	128.1	100.1	213.3	273.2	147.3	95.16	57.6	35.4	36.0	—	—	—	93.880	(1.634)	103.42	7.96	12.99	1.12	0.88
D	147	125.93	0.2392	77.3	861	44.9	138.1	100.7	205.3	263.1	146.3	94.05	58.1	36.5	35.2	—	—	—	93.811	(1.609)	105.51	8.50	12.41	1.18	0.89
1445A	148	125.80	0.2420	82.9	785	39.8	131.0	101.9	227.6	281.1	182.6	95.64	59.9	29.8	27.6	95.79	1.655	0.979	93.666	(1.545)	104.10	8.29	12.55	1.16	0.87
B	148	124.78	0.2606	88.8	788	34.3	135.8	98.4	205.0	259.6	163.7	95.08	66.4	40.6	42.4	95.62	1.979	0.779	93.583	(1.652)	108.14	8.60	12.57	1.16	0.83
C	148	124.73	0.2517	89.7	789	35.8	132.4	99.2	184.7	240.6	146.6	95.44	67.6	44.2	44.7	95.78	2.062	1.965	93.659	(1.594)	103.78	8.30	12.50	1.17	0.89
D	148	124.50	0.2565	91.9	788	36.7	136.5	101.8	197.0	252.3	139.2	95.89	69.1	45.2	46.1	95.56	1.965	1.717	93.562	1.618	104.73	8.51	12.30	1.19	0.89
E	148	124.44	0.2530	87.6	787	40.6	135.7	96.9	192.6	251.6	134.5	96.72	65.8	45.9	46.3	95.59	1.924	1.793	93.425	1.612	104.82	8.44	12.41	1.18	0.88
F	148	124.34	0.2537	90.6	784	40.6	130.8	99.0	187.3	234.6	146.6	95.61	70.2	45.2	45.9	95.54	2.109	2.006	93.438	1.609	103.92	8.16	12.72	1.15	0.87
1446A	149	126.00	0.2365	74.1	821	26.1	123.1	101.7	199.6	276.0	133.1	95.24	51.2	27.9	26.3	95.24	1.062	0.979	93.445	1.558	106.09	7.85	13.51	1.08	0.89
B	149	126.02	0.2310	71.3	828	24.8	133.7	102.3	198.6	260.1	143.5	94.79	48.4	24.6	23.9	95.06	1.607	1.469	93.349	1.530	105.01	8.50	12.35	1.18	0.87
C	149	126.00	0.2303	71.6	827	25.6	133.3	100.3	213.2	266.2	156.7	95.05	50.9	24.7	23.8	95.00	1.448	1.413	93.390	1.530	104.46	8.46	12.36	1.18	0.87
D	149	126.15	0.2248	67.8	837	24.0	130.5	101.0	199.6	259.4	139.9	96.16	45.9	24.6	22.8	94.83	1.448	1.607	93.383	1.512	104.10	8.33	12.48	1.17	0.86
E	149	126.77	0.2130	60.2	841	20.3	123.1	100.2	231.9	287.9	160.8	95.51	39.4	18.9	19.3	95.07	1.496	1.379	93.266	1.469	103.37	7.92	13.05	1.12	0.84
1447A	150	127.55	0.6929	73.1	1532	33.9	581.2	226.6	135.2	244.9	139.8	95.67	61.4	42.1	25.1	94.42	0.199	—	94.197	4.505	309.94	22.28	13.91	1.13	0.90
B	151	127.40	0.6736	73.8	1568	41.4	563.7	211.4	136.2	215.8	111.8	95.18	58.6	41.5	26.0	—	—	—	94.197	4.371	299.82	21.51	13.93	1.13	0.89
C	151	127.19	0.6853	72.6	1565	41.4	575.3	218.9	128.8	224.3	123.8	95.08	59.7	41.7	25.9	—	—	—	94.059	4.478	306.67	21.92	13.99	1.12	0.74
1448A	152	126.81	0.7184	79.7	1741	36.6	581.1	216.8	101.6	213.6	108.9	95.46	64.3	47.1	32.3	94.31	0.193	—	94.114	4.596	309.17	22.50	13.74	1.14	0.89
B	152	126.58	0.7136	81.3	1772	37.5	559.7	214.1	122.4	224.2	128.5	95.50	68.7	50.8	33.0	94.32	0.179	—	94.080	4.551	304.54	21.59	14.07	1.12	0.91
C	152	126.38	0.7295	83.6	1781	39.4	570.1	213.4	108.7	211.6	113.5	95.52	71.0	54.2	34.8	94.31	0.186	—	94.095	4.630	307.40	22.36	14.02	1.12	0.90
D	153	125.24	0.7267	83.2	1818	40.2	574.3	196.7	85.4	186.1	65.8	95.32	66.4	51.2	35.4	94.19	0.186	—	93.990	4.602	306.31	22.00	13.91	1.13	0.88
1449A	154	126.33	0.7281	82.6	1938	36.7	568.0	207.1	84.3	193.8	89.8	95.36	66.2	49.7	31.6	94.32	0.193	—	94.004	4.581	309.99	21.98	14.01	1.12	0.86
B	155	126.62	0.7591	85.1	2004	40.9	589.0	207.6	80.3	180.8	82.3	95.42	67.9	53.5	38.2	94.18	0.221	—	93.838	4.776	315.25	22.54	13.98	1.12	0.88
C	156	125.39	0.7467	86.7	2020	42.0	590.7	217.2	119.4	219.4	124.5	95.21	74.6	58.3	40.3	93.93	0.002	—	93.811	4.724	307.62	22.47	13.69	1.15	0.88

aVA values given in parentheses are the air flow velocities at the time DPA measurements were taken. Flow velocity at the time of ignition was zero.

bThe dash signifies the lack of an event.

Test No.	Config-uration No.	PBO, kN/m²	DPO, kN/m²	TO1, °C	PFL, kN/m²	TFL, °C	FMF, Hz	PV1, kN/m²	TV1, °C	TV2, °C	TMF, °C	PM1, kN/m²	TM1, °C	T12, °C	T1O2, °C	PA1, kN/m²	DPA1, kN/m²	DPA2, kN/m²	PAMB, kN/m²	VA[a], m/s	MA, kg/h	MF, kg/h	A/F RATIO	φ E.R.	HCA E.R.
1458A	165	126.08	0.7839	82.6	830	31.4	406.8	161.2	173.2	253.1	149.8	94.85	75.2	55.6	35.8	93.76	—[b]	—	93.604	4.697	308.71	24.29	12.71	1.15	0.88
B	165	125.69	0.7991	83.6	821	36.7	418.9	161.0	167.1	252.3	145.7	94.71	73.8	55.6	38.5	93.58	—	—	93.404	4.846	316.65	24.83	12.56	1.16	0.89
C	165	125.53	0.7970	83.7	824	39.7	406.2	159.6	182.2	265.5	167.6	94.67	77.1	57.9	39.4	93.55	—	—	93.376	4.855	315.52	23.99	12.95	1.13	0.96
1459A	166	127.03	0.6978	75.8	756	30.5	390.5	158.5	171.8	261.9	158.3	94.73	68.1	45.1	25.1	93.86	—	—	93.673	4.508	306.76	23.36	13.12	1.11	0.86
B	166	126.57	0.7219	79.2	778	32.2	330.5	142.7	191.4	270.1	175.9	94.93	71.9	50.0	30.6	93.96	—	—	93.742	4.642	310.98	19.69	15.79	0.93	0.81
C	166	125.91	0.7371	84.1	755	35.9	469.3	174.9	159.7	256.8	149.1	94.93	75.6	54.8	37.8	93.78	—	—	93.569	4.703	308.58	27.65	11.15	1.31	0.92
D	166	125.66	1.0060	84.1	746	36.4	526.0	192	149.2	256.3	132.1	95.72	76.0	58.7	39.1	93.94	—	—	93.535	6.392	416.85	31.17	13.37	1.09	0.86
E	166	126.65	0.7584	86.7	766	38.2	424.9	163.8	186.6	278.4	176.6	94.98	82.1	61.4	41.5	93.78	—	—	93.521	4.846	313.02	25.26	12.38	1.18	0.89
F	166	124.93	0.4902	85.4	786	40.4	262.6	126.5	203.2	274.7	176.4	94.30	67.4	54.0	40.7	93.55	—	—	93.425	3.149	205.57	15.84	12.98	1.13	0.88
G	166	125.53	0.2537	84.4	800	41.8	134.0	99.7	192.1	241.5	162.2	94.00	69.5	52.7	41.6	93.44	—	—	93.445	1.655	108.05	8.39	19.04	0.77	0.89
1460A	167	124.29	0.2365	72.1	818	20.7	134.0	105.8	285.9	340.6	233.9	93.67	59.0	35.2	25.6	93.42	—	—	93.376	(1.655)	107.86	8.50	12.68	1.15	0.88
B	167	126.37	0.2324	75.2	844	23.0	127.3	103.6	231.5	265.9	199.9	93.70	59.3	38.7	31.0	93.35	—	—	93.307	(1.536)	104.14	8.15	12.78	1.14	0.91
C	167	126.15	0.2448	77.8	842	23.6	137.5	102.9	228.1	288.8	180.7	93.97	55.3	40.1	31.7	93.32	—	—	93.266	(1.597)	107.91	8.61	12.52	1.17	0.91
D	167	125.87	0.2434	78.8	848	25.2	133.6	102.2	210.3	248.6	180.1	93.71	62.1	42.8	34.2	93.32	—	—	93.259	1.591	106.50	8.49	12.53	1.17	0.91
E	167	126.12	0.4833	78.6	827	25.1	260.5	126.3	216.2	288.6	190.7	94.05	67.5	46.5	33.8	93.37	—	—	93.238	3.152	209.97	15.85	13.24	1.10	0.88
F	167	125.91	0.9653	77.1	741	25.0	532.8	197.3	154.9	264.8	145.5	95.31	71.8	53.1	33.4	93.64	—	—	93.231	6.264	414.40	31.85	13.00	1.12	0.87
1461A	167	127.88	0.7336	69.3	654	15.7	391.4	163.4	179.6	273.2	169.1	94.93	62.5	40.2	21.1	93.95	—	—	93.728	4.526	312.93	23.81	13.13	1.11	0.83
B	167	127.63	0.7219	71.9	680	16.9	453.7	175.6	166.3	267.3	156.7	94.88	67.3	46.2	24.8	93.92	—	—	93.707	4.462	303.45	22.85	11.08	1.32	0.84
C	167	126.69	0.7529	75.6	730	21.4	325.7	143.1	191.8	271.7	173.1	94.82	67.2	47.7	29.7	93.74	—	—	93.507	4.587	308.21	19.81	15.55	0.94	0.78
D	167	126.50	0.7750	76.7	759	21.5	253.4	125.9	186.1	244.6	177.1	94.87	69.6	51.2	32.8	93.73	—	—	93.514	4.740	315.11	15.48	20.35	0.72	0.74
E	167	126.47	0.7467	78.3	753	21.8	279.5	133.4	193.4	265.8	174.7	94.82	66.2	53.7	34.2	93.67	—	—	93.459	4.566	301.68	16.96	17.79	0.82	0.77
F	167	126.45	0.7764	78.4	744	22.8	350.1	152.8	192.3	273.6	178.3	95.05	74.9	55.6	35.9	93.78	—	—	93.549	4.755	312.48	21.86	14.29	1.02	0.83
G	167	126.29	0.7598	78.2	723	22.6	421.6	162.4	152.4	243.8	148.8	94.90	73.2	55.3	36.4	93.67	—	—	93.459	4.660	305.99	25.36	12.06	1.21	0.84
H	167	126.28	0.7777	78.1	684	24.1	508.3	190.7	171.0	281.7	161.1	94.99	73.2	54.1	35.1	93.72	—	—	93.438	4.749	313.02	30.39	10.03	1.42	0.89
I	167	126.13	0.7770	78.5	689	24.6	542.6	200.9	185.0	301.1	174.1	94.98	76.8	56.2	35.4	93.68	—	—	93.369	4.749	311.84	32.30	9.65	1.52	0.90
1462 to 1469	Air flow pressure loss calibration tests.																							

[a] VA values given in parentheses are the air flow velocities at the time DPA measurements were taken. Flow velocity at the time of ignition was zero.

[b] The dash signifies the lack of an event.

Test No.	Configuration No.	PBO, kN/m²	DPO, kN/m²	TO1, °C	PFL, kN/m²	TFL, °C	FMF, Hz	PV1, kN/m²	TV1, °C	TV2, °C	TMF, °C	PM1, kN/m²	TM1, °C	T12, °C	TIO2, °C	PA1, kN/m²	DPA1, kN/m²	DPA2, kN/m²	PAMB, kN/m²	VA, m/s	MA, kg/h	MF, kg/h	A/F RATIO	φ E.R.	HCA E.R.
1470A	176	126.65	0.7336	78.4	726	18.8	416.7	168.6	180.7	276.1	169.3	94.90	75.9	55.8	31.6	93.85	0.145	0.145	93.680	4.758	315.0	25.20	12.58	1.17	0.86
B	176	126.24	0.7508	80.1	717	22.2	413.9	166.8	171.3	264.7	162.7	94.72	75.5	59.2	31.8	93.63	0.145	0.145	93.459	4.849	318.6	24.99	12.76	1.14	0.86
C	176	126.16	0.7433	80.9	716	25.5	416.1	166.2	176.1	270.9	162.8	94.77	76.6	59.5	32.3	93.63	0.145	0.138	93.452	4.788	314.1	24.98	12.57	1.16	0.85
1471A	177	126.52	0.7488	74.3	789	15.1	397.3	163.6	185.1	276.4	172.3	94.38	71.9	53.9	24.3	93.42	0.166	0.152	93.231	4.737	316.8	24.19	13.10	1.12	0.85
B	177	125.77	0.7943	78.1	725	21.1	417.5	167.0	176.3	271.0	165.9	94.39	73.2	52.5	29.6	93.22	0.166	0.159	93.045	4.770	316.4	25.31	12.54	1.16	0.85
1472A	178	127.71	0.7157	65.2	744	14.3	413.8	166.8	167.2	265.8	153.3	94.63	58.7	37.9	15.3	93.70	0.145	0.152	93.556	4.612	322.3	25.21	12.78	1.14	0.82
B	178	127.65	0.7046	66.5	757	15.7	399.5	166.1	185.0	280.4	168.7	94.55	60.1	37.2	16.1	93.65	0.152	0.159	93.487	4.514	315.3	24.29	12.97	1.13	0.82
C	178	127.40	0.7012	64.7	766	15.7	408.5	168.1	190.1	287.4	169.0	94.47	58.4	37.0	16.9	93.58	0.159	0.152	93.418	4.535	316.2	24.85	12.72	1.15	0.83
D	178	127.39	0.7164	67.5	771	16.4	390.9	163.3	184.6	275.4	164.6	94.56	59.1	37.4	18.4	93.60	0.159	0.159	93.433	4.578	318.1	23.79	13.36	1.09	0.83
E	178	127.26	0.7012	70.1	768	18.4	390.0	161.4	167.7	254.2	158.1	94.45	61.6	38.8	19.9	93.57	0.145	0.145	93.425	4.444	307.2	23.67	12.97	1.13	0.83
F	178	127.12	0.7198	72.2	772	18.9	412.1	168.6	174.0	266.2	165.9	94.51	66.5	43.7	20.3	93.57	0.152	0.145	93.418	4.542	311.2	24.97	12.48	1.17	0.85
1473A	179	127.82	0.7136	68.4	784	11.7	390.5	166.3	196.5	290.7	177.6	94.87	65.1	43.7	14.8	93.78	0.248	0.228	93.528	4.569	316.7	23.92	13.23	1.10	0.91
B	179	127.37	0.6950	67.3	814	12.7	396.1	165.4	182.0	274.5	163.7	94.52	61.3	41.1	17.5	93.61	0.228	0.234	93.342	4.471	309.3	24.18	12.77	1.14	0.90
C	179	127.33	0.6978	66.2	804	13.7	399.1	158.1	152.5	245.3	141.4	94.47	56.7	36.7	18.7	93.60	0.235	0.228	93.342	4.487	311.9	24.35	12.80	1.14	0.89
D	179	127.19	0.6750	61.8	808	16.1	387.8	160.4	195.2	291.8	171.9	94.27	54.9	33.8	19.7	93.44	0.228	0.228	93.183	4.456	308.9	23.63	13.06	1.12	0.81
E	179	127.17	0.6729	60.1	814	17.5	393.4	161.0	168.3	262.6	148.3	94.31	50.6	33.8	20.1	93.41	0.228	0.228	93.169	4.462	310.5	23.89	13.00	1.12	0.81
F	179	127.26	0.6598	58.8	808	17.5	392.1	161.3	192.7	311.7	167.3	94.22	50.5	32.2	19.5	93.38	0.228	0.220	93.128	4.441	310.0	23.84	13.00	1.12	0.81
1474A	180	127.44	0.6522	55.8	793	10.4	401.9	163.9	163.3	261.4	139.7	93.91	45.3	27.7	12.4	92.99	0.131	0.138	92.828	4.353	308.6	24.60	12.54	1.17	0.82
B	181	127.28	0.6619	58.3	821	11.6	402.6	161.1	160.3	254.9	142.6	93.88	48.8	29.9	14.0	92.97	0.138	0.138	92.818	4.380	308.5	24.62	12.52	1.17	0.79
C	182	126.99	0.6888	60.0	840	13.1	407.3	166.8	189.6	289.2	168.8	93.95	54.6	33.6	15.7	92.94	0.138	0.138	92.790	4.554	317.6	24.83	12.78	1.14	0.83
D	183	127.08	0.6764	60.1	842	14.7	400.2	165.8	193.1	303.7	145.1	94.00	55.4	34.3	15.8	92.98	0.138	0.144	92.825	4.471	311.8	24.36	12.78	1.14	0.83
E	183	127.00	0.6778	60.3	844	14.7	399.3	169.0	203.8	301.6	181.3	93.86	53.4	33.2	15.6	92.96	0.145	0.131	92.804	4.468	312.0	24.34	12.82	1.14	0.79
F	183	127.13	0.6571	60.4	848	15.4	401.4	166.8	181.7	278.6	154.4	93.91	52.5	34.3	15.6	93.00	0.131	0.138	92.838	4.432	309.0	24.44	12.64	1.16	0.82
1475A	184	127.16	0.7053	60.2	743	15.4	405.7	168.4	197.3	297.4	174.0	94.05	52.4	31.9	16.7	93.07	0.055	0.055	93.004	4.490	314.0	24.69	12.71	1.15	0.78
B	184	126.86	0.7019	61.6	756	16.9	398.8	166.4	197.7	293.6	171.7	94.03	53.7	33.9	19.2	93.07	0.076	0.076	92.976	4.468	309.4	24.23	12.77	1.15	0.77
C	184	126.40	0.7267	64.9	756	18.1	403.9	165.9	193.8	290.1	168.3	93.96	58.1	37.9	20.4	93.00	0.076	0.083	92.907	4.560	313.5	24.52	12.78	1.14	0.80
D	184	126.33	0.7184	65.3	760	19.7	401.7	163.8	193.3	289.2	166.6	93.89	57.6	38.1	21.7	92.91	0.083	0.076	92.818	4.508	309.1	24.32	12.70	1.15	0.79
E	184	126.17	0.7274	67.3	762	20.1	388.9	167.1	215.3	310.7	196.6	93.80	60.8	38.6	21.0	93.51	0.076	0.069	92.770	4.517	309.5	23.56	13.13	1.11	0.29
F	184	126.15	0.7295	65.8	778	20.2	395.6	162.6	201.3	297.0	178.8	93.78	58.8	38.3	20.1	92.80	0.069	0.076	92.714	4.557	312.6	23.98	13.03	1.12	0.29
1476A	185	127.97	0.7288	69.9	814	14.5	393.1	165.1	187.0	279.8	167.3	94.91	64.5	44.1	18.1	93.95	0.055	0.055	93.893	4.508	311.2	23.98	12.97	1.13	0.78
B	185	127.28	0.7536	73.8	833	18.5	397.2	166.4	196.1	370.6	178.3	94.94	70.1	50.2	22.8	93.85	0.055	0.048	93.790	4.633	313.8	24.12	13.00	1.12	0.80
C	185	127.23	0.7474	74.4	822	20.1	398.3	163.5	193.9	370.7	172.9	94.89	69.7	49.6	23.4	93.80	0.048	0.055	93.735	4.581	310.3	24.12	12.86	1.14	0.80

Test No.	Config-uration No.	PBO, kN/m²	DPO, kN/m²	TO1, °C	PFL, kN/m²	TFL, °C	FMF, Hz	PV1, kN/m²	TV1, °C	TV2, °C	TMF, °C	PM1, kN/m²	TM1, °C	T12, °C	TIO2, °C	PA1, kN/m²	DPA1, kN/m²	DPA2, kN/m²	PAMB, kN/m²	VA, m/s	MA, kg/h	MF, kg/h	A/F RATIO	o E.R.	HCA E.R.
1476D	185	127.19	0.7667	75.3	817	21.3	396.5	166.1	195.1	373.6	176.9	94.93	72.2	52.3	24.6	93.76	0.055	0.048	93.693	4.709	316.7	23.97	13.20	1.11	0.77
E	185	127.17	0.7536	74.3	834	21.5	397.4	165.0	199.2	377.3	178.7	94.84	69.6	49.8	25.4	93.74	0.048	0.048	93.680	4.642	312.9	24.00	13.01	1.12	0.78
1477A	186	126.72	0.7426	64.4	733	19.1	407.4	164.7	165.8	352.7	144.8	94.19	56.6	38.1	21.6	93.22	0.041	0.041	93.169	4.538	312.1	24.68	12.64	1.16	0.81
B	186	126.63	0.7398	64.9	731	19.7	309.2	163.7	184.9	366.2	159.6	94.19	55.8	37.4	21.4	93.20	0.055	0.048	93.149	4.502	310.0	24.12	12.85	1.14	0.81
C	186	126.47	0.7481	64.5	732	20.1	407.3	164.2	181.3	364.3	152.7	94.22	56.3	38.2	22.8	93.14	0.048	0.055	93.073	4.572	313.6	24.65	12.73	1.15	0.82
D	186	126.25	0.7591	66.6	739	22.3	408.3	164.3	192.0	374.8	164.0	94.16	59.3	40.6	24.0	93.08	0.055	0.055	93.011	4.612	314.2	24.65	12.74	1.15	0.83
E	186	126.29	0.7619	66.6	743	22.1	411.5	166.3	183.3	368.2	155.5	94.17	57.4	38.9	23.6	93.10	0.055	0.062	93.032	4.615	315.5	24.82	12.70	1.15	0.83
F	186	126.21	0.7715	66.1	741	22.2	410.5	167.8	200.4	377.1	171.2	94.10	57.6	37.9	23.4	93.07	0.062	0.062	92.990	4.673	320.0	24.77	12.92	1.13	0.83
1478A	187	127.42	0.7005	59.1	769	12.8	402.9	168.9	185.4	375.1	155.6	93.96	50.4	32.1	13.6	93.03	0.069	0.069	92.956	4.767	315.4	24.60	12.81	1.14	0.77
B	187	127.31	0.6957	59.8	779	13.1	407.3	167.7	194.4	377.9	166.6	93.91	51.2	31.1	13.0	93.00	0.069	0.062	92.928	4.712	311.8	24.86	12.54	1.17	0.78
C	187	127.17	0.7060	60.7	773	13.7	393.6	162.4	177.1	363.6	151.7	93.97	50.2	30.8	13.6	93.01	0.062	0.069	92.928	4.746	314.5	24.02	13.09	1.12	0.76
D	187	126.84	0.7067	63.8	786	15.7	398.5	164.2	191.5	377.9	162.9	93.88	55.2	29.8	16.5	92.93	0.069	0.069	92.838	4.700	309.3	24.24	12.75	1.15	0.79
1479A	188	127.20	0.6929	58.1	736	14.1	397.6	163.4	191.6	375.6	162.8	93.83	50.1	31.4	14.4	92.94	0.048	0.062	92.866	4.730	313.2	24.24	12.91	1.13	0.80
B	188	127.20	0.6840	57.2	738	14.3	404.8	166.7	185.7	372.0	153.1	93.87	46.7	29.9	14.2	92.97	0.062	0.055	92.901	4.654	310.6	24.68	12.58	1.16	0.80
C	188	127.24	0.6784	56.3	738	15.4	403.0	168.4	201.6	387.8	167.6	93.87	47.8	30.1	14.7	92.91	0.055	0.055	92.852	4.651	309.7	24.53	12.62	1.16	0.81
1480A	189	126.34	0.7274	68.4	733	21.1	414.8	167.3	182.6	367.8	159.6	93.90	58.8	39.3	24.4	93.05	0.110	0.110	92.924	4.353	309.3	25.06	12.33	1.18	0.83
B	189	125.20	0.7288	70.6	736	21.8	406.8	167.7	196.6	378.2	177.7	93.95	62.2	41.1	24.6	93.08	0.145	0.131	92.931	4.548	309.2	24.56	15.58	1.16	0.84
C	189	125.93	0.7447	70.6	738	23.3	413.7	165.4	186.6	371.4	163.5	93.93	61.8	42.0	26.7	93.03	0.138	0.138	92.889	4.602	311.3	24.94	12.47	1.17	0.85
D	189	125.70	0.7371	68.0	748	25.1	403.5	163.4	190.9	372.6	162.1	93.83	60.1	42.2	27.6	92.90	0.138	0.131	92.752	4.636	312.6	24.30	12.84	1.14	0.85
E	189	125.95	0.7267	67.1	749	26.3	411.9	166.0	191.1	376.3	166.1	93.76	58.9	40.1	28.6	92.86	0.131	0.131	92.717	4.590	310.0	24.72	12.54	1.17	0.82
F	189	125.81	0.7309	67.7	749	26.2	409.2	166.4	188.0	371.4	162.0	93.77	58.9	40.4	27.9	92.88	0.131	0.138	92.717	4.596	310.4	24.57	12.63	1.16	0.80
1481A	190	127.43	0.7289	69.4	730	12.7	403.3	167.5	184.6	370.1	162.6	94.17	63.9	42.7	15.0	93.33	0.110	0.138	93.186	4.484	309.7	24.63	12.58	1.16	0.81
B	190	127.28	0.7536	70.8	741	14.7	407.7	164.6	186.3	371.2	169.0	94.27	64.7	43.9	16.9	93.36	0.152	0.145	93.200	4.633	318.5	24.82	12.82	1.14	0.82
C	190	127.16	0.7198	66.2	744	15.6	404.7	164.4	186.8	369.9	163.2	94.13	59.3	39.8	18.7	93.32	0.145	0.145	93.165	4.517	311.5	24.63	12.65	1.16	0.86
D	190	127.30	0.7047	62.1	738	17.4	399.3	165.8	211.5	394.6	188.7	94.08	57.6	36.8	20.4	93.28	0.145	0.152	93.110	4.514	312.0	24.23	12.87	1.14	0.83
E	190	127.34	0.6791	61.4	744	17.4	406.0	164.4	183.4	369.6	155.9	94.00	53.6	34.6	20.3	93.26	0.152	0.159	93.103	4.356	302.1	24.64	12.26	1.19	0.83
F	190	127.46	0.7040	60.5	741	17.0	407.9	166.0	180.2	367.8	151.9	94.18	52.6	34.0	19.7	93.34	0.159	0.159	93.172	4.526	314.7	24.79	12.69	1.15	0.82
1482A	191	127.47	0.7591	73.1	758	13.6	408.1	166.7	184.6	368.2	168.9	94.75	68.8	47.3	16.6	93.75	0.186	0.262	93.579	4.465	306.9	24.88	12.33	1.19	0.82
B	191	127.17	0.7833	75.4	766	16.6	401.2	164.5	181.7	364.4	169.3	94.71	69.7	49.3	20.7	93.83	0.262	0.269	93.558	4.590	312.4	24.39	12.80	1.14	0.82
C	191	126.99	0.7853	75.9	766	16.9	399.7	164.0	190.7	367.0	178.3	94.92	71.9	51.2	22.9	93.81	0.269	0.283	93.524	4.615	311.9	24.30	12.83	1.14	0.76
D	191	126.44	0.7847	78.1	771	21.6	395.4	154.9	144.3	340.3	130.3	94.82	71.9	54.4	28.9	93.70	0.283	0.283	93.413	4.615	307.1	23.88	12.85	1.14	0.76
E	191	126.03	0.7936	79.6	766	26.0	392.9	162.9	189.2	365.4	168.8	94.70	74.6	55.8	29.9	93.57	0.283	0.290	93.276	4.642	307.4	23.61	13.01	1.12	0.78

Test No.	Configuration No.	PBO, kN/m²	DPO, kN/m²	TO1, °C	PH1, kN/m²	TH1, °C	FMF, Hz	PV1, kN/m²	TV1, °C	TV2, °C	TMF, °C	PM1, kN/m²	TM1, °C	T12, °C	TTO2, °C	PA1, kN/m²	WFA1, kN/m²	WFA2, kN/m²	PAMB, kN/m²	VA, m/s	WA, kg/h	WF, kg/h	A/F RATIO	L.R.	HCA E.R.
1482F	191	126.29	0.7929	79.9	770	23.2	402.3	162.0	181.7	359.9	165.8	94.79	74.6	55.2	29.4	93.66	0.290	0.297	93.358	4.670	309.9	24.26	12.77	1.14	0.7?
G	191	126.01	0.7929	75.9	763	25.8	401.5	160.9	191.1	365.6	175.3	94.59	70.3	50.3	30.1	93.55	0.297	0.297	93.241	4.685	312.6	24.13	12.95	1.13	0.?2
H	191	126.14	0.7819	74.1	766	25.6	411.0	167.8	186.9	367.3	164.4	94.56	67.4	52.8	28.6	93.52	0.297	0.292	93.220	4.640	311.2	24.70	12.59	1.16	0.79
1483A	192	126.09	0.7502	74.0	737	23.2	404.8	163.0	170.1	355.4	150.2	94.30	64.8	45.4	23.7	93.57	0.138	0.186	93.420	4.553	309.5	24.41	12.67	1.15	0.82
B	193	125.91	0.7467	73.2	748	23.7	410.7	165.6	173.8	358.1	153.0	94.40	63.6	44.2	24.6	93.61	0.200	0.193	93.386	4.532	308.5	24.73	12.46	1.17	0.84
C	194	125.08	0.7529	73.6	751	24.9	406.6	163.7	174.4	358.7	151.7	94.48	65.6	46.4	27.2	93.58	0.186	0.207	93.358	4.596	310.2	24.46	12.68	1.15	0.85
D	195	123.45	0.7529	70.6	766	27.0	400.7	165.5	202.1	382.3	179.9	94.29	62.0	41.9	28.1	93.48	0.221	0.214	93.248	4.563	309.5	24.65	12.86	1.14	0.82
E	195	123.68	0.6970	70.7	763	27.3	403.8	164.0	194.9	375.0	169.7	94.21	61.9	42.1	28.2	93.48	0.214	0.207	93.234	4.532	307.1	24.68	12.67	1.15	0.83
F	195	123.74	0.7578	70.4	766	26.8	404.2	166.3	192.0	374.3	166.1	94.30	63.1	43.2	27.2	93.48	0.234	0.228	93.234	4.612	312.5	24.26	12.86	1.13	0.?2
1484A	196	125.94	0.7702	78.7	742	21.7	408.6	163.2	175.9	361.6	160.5	95.53	71.6	43.7	26.8	93.63	0.166	0.310	93.448	4.569	310.0	24.67	12.56	1.16	.84
B	196	125.64	0.7853	79.8	750	23.4	401.6	164.6	189.6	369.0	177.0	94.70	73.1	45.9	29.9	93.67	0.310	0.331	93.351	4.663	313.8	24.21	12.96	1.13	0.83
C	196	125.56	0.7964	81.7	743	25.4	412.7	166.8	174.4	359.0	161.8	94.80	75.0	48.7	32.7	93.69	0.331	0.324	93.338	4.721	315.1	24.80	12.70	1.13	0.84
D	196	125.40	0.7998	84.2	748	28.1	403.4	164.6	194.5	376.3	183.6	94.77	71.3	56.1	35.3	93.61	0.310	0.317	93.282	4.761	312.4	24.18	12.91	1.13	0.84
1485A	197	127.40	0.7019	61.4	741	16.2	414.2	169.0	184.2	376.8	156.6	93.94	51.3	28.1	16.8	93.10	0.179	0.303	92.924	4.496	316.6	25.17	12.29	1.18	0.80
B	197	127.27	0.7040	61.7	747	16.4	407.6	165.1	185.5	375.4	157.3	93.99	52.2	29.6	18.3	93.17	0.303	0.310	92.869	4.456	312.4	24.76	12.60	1.16	0.80
C	197	127.10	0.7081	62.4	748	18.3	410.8	166.2	183.2	374.8	155.7	93.90	54.8	32.2	20.9	93.16	0.310	0.338	92.848	4.496	312.5	24.90	12.54	1.16	0.82
D	197	127.01	0.7219	62.9	744	18.4	408.9	167.4	182.0	374.6	155.9	93.99	54.6	31.3	21.5	93.17	0.338	0.318	92.834	4.566	317.5	24.77	12.81	1.14	0.81
1486A	198	128.10	0.7626	76.4	765	17.1	412.1	166.9	183.6	372.2	164.1	94.97	68.8	39.1	23.6	93.99	0.145	0.138	93.841	4.569	315.3	25.03	12.59	1.16	0.81
B	198	127.65	0.7688	76.8	776	18.8	410.8	167.9	184.9	369.4	165.8	94.77	63.8	38.3	25.0	93.94	0.138	0.138	93.786	4.590	316.3	24.90	12.70	1.15	0.82
C	198	127.45	0.7564	77.5	777	21.1	395.8	166.9	196.1	377.4	179.8	94.77	69.1	42.5	26.7	93.96	0.138	0.138	93.806	4.538	309.8	23.94	12.93	1.11	0.82
D	198	127.07	0.7660	80.3	778	24.4	403.0	164.7	194.7	373.9	180.6	94.88	73.1	44.6	29.1	93.89	0.138	0.138	93.731	4.560	308.7	24.26	12.72	1.15	0.83
1487A	199	127.38	0.7516	80.2	734	21.3	402.4	164.1	190.3	374.8	174.9	94.43	75.6	47.5	29.8	93.28	0.131	0.138	93.117	4.545	304.0	24.32	12.49	1.17	0.83
B	199	127.16	0.7688	80.9	747	24.2	401.9	166.0	190.6	376.8	176.9	94.50	73.8	50.1	36.0	93.25	0.138	0.131	93.096	4.691	309.1	24.20	12.77	1.14	0.84
C	199	126.80	0.7757	81.1	750	28.2	406.8	166.8	194.3	380.1	176.1	94.40	72.3	47.8	33.2	93.20	0.131	0.131	93.027	4.676	310.6	24.38	12.74	1.15	0.83
D	199	126.78	0.7791	81.4	741	29.3	408.0	166.6	184.6	363.9	167.0	94.46	72.3	47.7	34.1	93.17	0.124	0.124	92.993	4.697	311.5	24.42	12.75	1.15	0.83
E	200	126.85	0.7688	79.9	748	31.0	407.4	168.4	192.3	373.9	171.8	94.25	69.0	43.3	33.0	NI	NI	NI	92.972	4.633	309.8	24.30	12.74	1.15	0.82

APPENDIX D

TABULAR SUMMARY OF TRANSIENT STATE MEASURED

FLAME VELOCITY AND PEAK-PRESSURE TEST DATA

Test No.	Configuration No.	φ E.R.	VA, m/s	F12-F17, m/s	F17-F31, m/s	F31-F32, m/s	F32-F41, m/s	F41-F43, m/s	F43-F72, m/s	F72-F73, m/s	F73-F81, m/s	F81-F85, m/s	F85-F101, m/s	F101-F104, m/s	P72, kN/m²	P73, kN/m²	P81, kN/m²	P85, kN/m²	P101, kN/m²	P104, kN/m²	P72-P73, m/s	P73-P81, m/s	P81-P85, m/s	P85-P101, m/s	P101-P104, m/s
1429A	118	1.1	1.5	31.52	34.32	68.15	62.97	67.21	175.4	1037	1164	1435	1666	2177	875	1564	1626	1378	3524	3014	864	1169	1337	1555	2181
B	118	1.1	3.0	56.45	41.24	57.03	81.96	84.28	284.1	1170	1638	1176	2211	1976	1775	1844	1425	1445	2632	2335	1510	1218	1339	2012	1974
C	118	1.1	4.6	81.69	46.73	59.22	80.35	106.07	287.6	1436	1914	2320	2092	1852	1843	2124	3558	3203	2070	2064	1507	1470	2184	2033	2048
D	118	1.1	6.1	47.61	52.30	75.93	77.51	78.85	279.7	1908	1908	1908	1994	1908	2179	2404	2226	1986	2015	1792	2202	1780	1948	1985	1964
E	118	1.1	0	35.94	37.43	73.58	75.80	68.31	231.9	1019	2038	2002	2060	1840	1574	1844	3624	3406	2084	2132	1504	1191	2177	2063	1971
F	118	1.1	0	37.37	35.63	68.52	64.65	61.75	195.1	1170	1638	2011	2052	1791	1036	1844	4890	5839	2358	2132	923	1394	2309	2027	1971
1430A	119	1.1	4.6	68.00	46.79	61.36	65.56	71.23	139.9	1023	896	956	581	299	767	1119	1227	1493	1013	893	923	969	1104	1076	953
B	119	1.1	4.6	74.40	52.03	66.75	64.16	76.14	142.7	793	985	955	570	303	565	1050	1160	1128	1210	1160	688	830	1060	1120	1041
C	118	1.1	4.6	68.64	48.10	68.21	78.21	118.26	313.5	2393	1688	1963	2001	1794	4131	2961	2559	2300	1933	2093	2206	2116	1954	1957	1732
D	118	1.1	4.6	70.01	53.00	68.98	72.97	102.93	337.9	1686	1791	1911	1998	1791	2784	2892	2226	2507	1866	n.a.ᵃ	2040	2009	1963	1917	n.a.ᵃ
					F17-F21, m/s	F21-F23, m/s	F23-F62, m/s	F62-F63, m/s	F63-F71, m/s	F71-F72, m/s	F72-F81, m/s				P62, kN/m²	P63, kN/m²					P62-P63, m/s	P63-P31, m/s			
1431A	120	1.1	4.6	79.37	54.96	90.62	513.7	2039	1836	1874	1590	1774	1926	1846	1776	1886	2129	1895	1662	1574	1784	1836	1859	1876	1971
B	121	1.1	4.6	72.57	44.90	78.09	220.9	1588	2060	1891	1763	1905	1148	828	2448	2369	2392	3489	1009	968	2041	2061	1892	1292	1079
C	121	1.1	4.6	67.73	51.60	92.75	464.3	1791	1814	1874	1766	1861	1008	724	1977	2024	1866	2865	813	901	1910	1814	1954	1190	1003
D	121	1.1	4.6	69.28	59.10	50.32	458.4	1904	1731	1867	1671	1858	1020	804	2044	2162	2326	3004	911	935	1905	1752	1859	1184	1039
E	121	1.1	4.6	75.44	41.82	50.29	200.8	2036	1964	1978	1665	1898	1627	1837	2448	2507	2785	3489	1891	1809	2036	1885	1908	1722	1908

ᵃNot available.

Test No.	Config-uration No.	φ E.R.	VA, m/s	F12-F17, m/s	F17-F21, m/s	F21-F23, m/s	F23-F62, m/s	F62-F63, m/s	F63-F71, m/s	F71-F72, m/s	F72-F81, m/s	F81-F85, m/s	F85-P101, m/s	F101-F104, m/s	P62, kN/m²	P63, kN/m²	P81, kN/m²	P85, kN/m²	P101, kN/m²	P104, kN/m²	P62-P63, m/s	P63-P81, m/s	P81-P85, m/s	P85-P101, m/s	P101-P104, m/s
1432A	122	1.1	6.1	87.08	46.33	54.91	254.8	2048	1633	1984	1984	1905	1957	1905	1834	2026	2083	1792	1626	1652	1912	1862	1862	1911	1847
B	122	1.1	4.6	59.22	39.44	46.57	214.6	2203	1630	2113	1668	1902	1920	1783	1834	1959	1751	1860	1626	1818	1909	1817	1957	1895	1908
C	122	1.1	3.0	46.92	31.46	35.02	187.3	1912	1729	1981	1864	1855	1904	1783	1834	1959	1917	1724	1826	1818	1912	1864	1911	1914	1911
D	122	1.1	1.5	30.45	25.21	34.05	190.0	1910	1843	1924	1763	1858	1957	1843	2033	2159	1585	1792	1726	1884	1791	1982	1957	1879	1847
1433A	122	1.1	0	32.13	28.47	31.97	184.7	2045	1734	1870	1870	1861	1926	1683	2083	2118	1726	1844	1581	1793	2046	1888	1960	1852	1849
B	122	1.1	4.6	62.54	40.14	51.66	211.9	1907	1734	1870	1987	1861	1977	1734	n.a.ᵃ	2118	1759	1774	1750	1793	1907	1929	1963	1908	1905
C	123	1.1	4.6	57.79	38.34	41.33	177.9	1909	1735	1870	1987	1818	1106	817	2281	2324	1993	3278	906	960	1909	1938	1914	1276	1083
D	123	1.1	4.6	58.22	37.31	50.78	189.9	1909	1849	1873	1873	1820	1092	785	2878	2461	2059	3244	939	896	1909	1888	1911	1274	1082
E	123	1.1	4.6	58.34	36.91	49.90	196.8	2046	1734	1817	1870	1817	1231	1010	2514	2392	2059	3453	1041	1088	2046	1842	1865	1357	1170

ᵃNot available.

For tests 1438A–1440C the columns F72–F81, F81–F85, P81, P63–P81, and P81–P85 are labeled F72–F62, F82–F85, P82, P63–P82, and P82–P85 respectively.

Test No.	Config. No.	φ E.R.	VA, m/s	F12–F17, m/s	F17–F21, m/s	F21–F23, m/s	F23–F62, m/s	F62–F63, m/s	F63–F71, m/s	F71–F72, m/s	F72–F81, m/s	F81–F85, m/s	F85–F101, m/s	F101–P104, m/s	P62, kN/m²	P63, kN/m²	P81, kN/m²	P85, kN/m² [a]	P101, kN/m²	P104, kN/m²	P62–P63, m/s	P63–P81, m/s	P81–P85, kN/m²	P85–P101, m/s	P101–P104, m/s
1434A	124	1.1	4.6	63.7	34.3	46.8	200.3	2204	1593	1722	2123	1737	1593	1686	2268	2381	1868	n.a.	1260	1480	2204	1796	1748	1748	1788
B	125	1.1	4.6	62.2	34.3	35.1	171.7	2383	1635	1767	2272	1735	1928	1506	2335	2347	2035	1988	1759	1615	2384	1839	1862	1994	1735
C	126	1.1	4.6	62.4	34.6	38.3	170.9	2041	1973	1817	2120	1817	1568	1636	2166	2448	2370	2223	1626	1615	2042	1888	1865	1932	1792
D	127	1.1	4.6	55.7	36.5	38.6	196.9	2044	1627	1711	1978	1853	1802	1676	2743	2617	1901	2088	1593	1581	2044	1799	1865	1660	1911
1435A	128	1.1	4.6	59.1	37.5	48.5	200.6	1845	2116	1814	1868	1858	1798	1732	2359	2257	1801	n.a.	1595	1608	1845	1929	2059	1630	1681
B	129	1.1	4.6	59.5	37.0	46.8	204.6	1909	1692	1880	1880	1917	1733	974	2231	2257	1968	1968	1070	1157	1909	1881	1859	1674	1143
C	130	1.1	4.6	58.9	39.0	37.1	185.4	2044	1789	1767	1988	1862	1855	1684	2231	2189	1868	1935	1850	1575	2044	1796	1862	1724	1789
D	131	1.1	4.6	66.5	37.3	42.9	189.9	2046	1633	1868	1764	1814	1698	969	2231	2223	2289	2336	1070	1028	2046	1836	1859	1722	1121
1436A	132	1.1	4.6	58.1	41.9	51.1	203.0	2200	2117	1764	1984	1859	—[b]	—	2031	2097	1716	2000	329	322	2200	1926	1856	1091	607
B	132	1.1	4.6	65.8	37.6	41.5	195.9	2043	1789	1817	1871	1862	—	—	1866	1965	1885	1827	296	284	2043	1879	1902	1122	601
C	132	1.1	4.6	63.5	40.1	49.6	207.6	2041	1908	1871	1988	1862	—	—	2031	1933	1818	1688	—	—	2042	1932	1908	—	—
D	132	1.1	4.6	61.1	36.1	43.0	196.7	2042	1846	1871	1871	1862	—	—	1866	1834	1750	1930	—	—	2042	1820	1865	—	—
E	132	1.1	4.6	62.9	40.3	50.4	201.7	2043	1905	1814	1984	1859	—	—	2195	1933	1784	1861	—	—	2043	1905	1859	—	—
1437A	132	1.1	4.6	63.8	39.8	46.5	278.1	1908	1731	1761	1865	1856	—	—	1941	1974	1878	1801	314	217	1908	1856	1902	1091	607
B	133	1.1	4.6	64.3	32.9	39.7	269.9	2040	1971	1716	1868	1814	—	—	2040	1909	1775	1801	314	290	2040	1929	1814	1093	608
C	134	1.1	4.6	66.8	36.2	35.5	260.6	1908	1841	1761	1981	1811	—	—	1971	1909	1740	1734	334	290	1908	1882	1859	1105	602
D	135	1.1	4.6	66.1	35.2	40.4	273.1	1903	1905	1764	1984	1814	—	—	1941	1909	1638	1667	314	290	1903	2002	1769	1109	601
E	136	1.1	4.6	63.6	37.2	41.8	280.6	1904	1908	1871	1871	1862	1855	1431	1776	1842	1638	1700	1933	1760	1904	1929	1905	1653	1905
1438A	137	1.1	4.6	70.0	44.2	45.5	272.5	2039	1737	1820	1699	1911	—	—	1977	2002	1750	1756	377	351	2039	1789	1847	1200	636
B	137	1.1	4.6	61.1	41.1	52.9	290.8	1907	1786	1814	1882	1905	1042	595	2011	1935	1847	1685	659	530	1907	1824	1905	1230	706
C	137	1.1	4.6	68.2	34.2	41.1	288.2	1905	1908	1927	1755	1847	1075	622	1977	1834	1784	1614	719	549	1906	1808	1847	1249	734
D	137	1.1	4.6	67.0	36.5	46.7	273.9	1908	1970	1924	1752	1905	1060	628	1809	1767	1818	1685	578	589	1908	1933	1791	1243	708
1439A	138	1.1	4.6	68.3	42.9	50.9	273.3	2044	1686	1930	1820	1849	—	—	2126	2226	1851	1926	290	312	2044	1773	1849	1042	541
B	138	1.1	4.6	66.0	38.3	44.9	280.7	1788	1729	1865	1811	1902	—	—	2059	2059	1919	1759	290	253	1788	1808	1908	1046	535
C	138	1.1	4.6	61.4	33.1	40.2	237.3	1906	1732	1924	1752	1905	—	—	2126	2159	1919	1826	329	312	1906	1905	1844	1076	549
D	139	1.1	4.6	62.8	30.4	39.1	227.1	2199	1732	1814	1882	1786	1106	457	2093	2026	1919	1826	388	370	2198	1827	1847	1145	578
1440A	140	1.1	4.6	65.0	40.5	42.9	254.8	1907	1786	1924	1752	1844	—	—	1924	2315	1625	1446	—	—	1907	1905	1905	—	—
B	140	1.1	4.6	63.2	36.7	39.3	240.2	1906	2041	1984	1954	1905	—	—	2250	2248	1693	1412	—	—	1906	1951	1847	—	—
C	140	1.1	4.6	65.3	36.9	41.6	247.9	1907	1971	1924	1954	1905	—	—	1859	1919	1693	1345	—	—	1907	1905	1844	—	—

[a] Not available.

[b] The dash signifies the lack of an event.

Test No.	Configuration No.	φ E.R.	VA, m/s	F12-F17, m/s	F17-F21, m/s	F21-F23, m/s	F23-F62, m/s	F62-F63, m/s	F63-F71, m/s	F71-F72, m/s	F72-F82, m/s	F82-F85, m/s	F85-F101, m/s	F101-F104, m/s	P62, kN/m²	P63, kN/m²	P82, kN/m²	P85, kN/m²	P101, kN/m²	P104, kN/m²	P62-P63, m/s	P63-P82, m/s	P82-P85, m/s	P85-P101, m/s	P101-P104, m/s
1440D	140	1.1	4.6	57.2	35.6	38.4	224.0	1906	1786	1868	1814	1844	—[a]	—	2185	2282	1726	1412	—	—	1907	1902	1841	—	—
E	140	1.1	4.6	55.8	41.9	43.3	230.8	1906	1844	1924	1882	1844	1000	—	2218	2149	1826	1412	—	—	1906	1844	1844	—	—
F	141	1.1	4.6	68.2	37.4	45.3	276.5	1908	1902	1921	1811	1786	1000	939	1565	1884	1393	1108	865	949	1908	1881	1902	926	935
1441A	142	1.1	4.6	59.1	40.4	51.2	280.6	1895	1905	1868	1954	1844	—	—	1874	1950	1682	1633	—	—	1895	1905	1844	—	—
B	142	1.1	4.6	64.2	36.0	41.8	287.2	1890	1905	1924	1814	1844	—	—	1874	1784	1716	1667	—	—	1890	1884	1844	—	—
C	142	1.1	4.6	66.2	42.0	46.4	260.5	2031	1905	1924	1814	1844	—	—	2068	2050	1750	1667	—	—	2031	1884	1844	—	—
D	142	1.1	4.6	53.3	38.6	41.2	264.4	1899	1905	1924	1814	1844	—	—	1906	2083	1615	1700	—	—	1898	1887	1908	—	—
E	142	1.1	4.6	63.8	41.8	54.2	253.3	2008	1835	1915	1806	1961	—	—	2036	2116	1750	1633	—	—	2008	1899	1899	—	—
1442A	143	1.1	4.6	65.7	36.6	47.5	227.8	1904	1971	1868	1814	1844	—	—	2448	2469	1834	2176	—	—	1904	1926	1844	—	—
B	143	1.1	4.6					No ignition: no data recorded.																	
C	143	1.1	4.6	62.5	35.4	43.3	221.0	1903	1844	1984	1814	1844	—	—	2515	2568	1834	2126	—	—	1903	1867	1908	—	—
D	143	1.1	4.6	65.8	32.8	47.9	211.3	1901	1971	1924	1882	1844	—	—	2481	2370	1801	2126	—	—	1901	1884	1844	—	—
E	143	1.1	4.6	64.6	35.3	41.6	230.1	1902	1841	1921	1811	1902	—	—	2515	2271	1600	2073	—	—	1902	1905	1905	—	—
F	144	1.1	4.6	63.7	36.5	43.1	247.3	1902	1899	1978	1809	1838	—	—	2044	2106	1567	1869	—	—	1902	1905	1844	—	—
1443A	144	1.1	4.6	63.1	37.0	41.8	263.2	1903	1726	1809	1746	1899	857	475	2236	2228	1560	1903	530	534	1903	1818	1838	870	750
B	144	1.1	4.6	64.1	40.1	47.7	286.4	1784	1844	1814	1814	1786	1017	608	1941	1866	1726	1835	510	554	1784	1818	1838	1023	730
C	143	1.1	4.6	61.2	35.3	39.9	220.3	2040	1905	1868	1814	1905	—	—	2572	2359	1693	2005	—	—	2040	1884	1844	—	—
D	144	1.1	4.6	65.7	35.4	49.1	281.3	2040	1876	1901	1846	1875	942	559	2172	2129	1593	2005	430	574	2040	1902	1841	960	722

[a] The dash signifies the lack of an event.

Test No.	Config-uration No.	φ E.R.	VA, m/s	F21-F23, m/s	F12-F17, m/s	F17-F62, m/s	F62-F63, m/s	F63-F71, m/s	F71-F72, m/s	F72-F82, m/s	F82-F85, m/s	F85-F101, m/s	F101-F104, m/s	P62, kN/m²	P63, kN/m²	P82, kN/m²	P85, kN/m²	P101, kN/m²	P104, kN/m²	P62-P63, m/s	P63-P82, m/s	P82-P85, m/s	P85-P101, m/s	P101-P104, m/s
1444	Obtained ignition, but flame did not propagate upstream.																							
1445A	148	1.1	(1.5)	137.5	78.3	522.9	2034	2054	1936	1763	1917	a	-	1988	1979	1787	1861	-	-	2190	1840	1732	-	-
B	148	1.1	(1.5)	136.6	61.6	467.3	1678	1683	1871	1696	1789	-	-	1784	1844	1820	1896	-	-	1678	1769	1735	-	-
C	148	1.1	(1.5)	131.1	68.6	455.1	2035	1951	1913	1847	1829	-	-	1886	1844	1787	1763	-	-	2035	1811	1908	-	-
D	148	1.1	1.5	135.6	163.7	378.6	1898	1654	2010	1774	1867	-	-	1954	2216	1987	1861	-	-	2034	1783	1857	-	-
E	148	1.1	1.5	147.5	172.2	413.0	2038	1803	1832	1768	1861	-	-	2022	2216	1854	1661	-	-	2038	1784	1785	-	-
F	148	1.1	1.5	147.2	178.6	424.3	2035	1873	1897	1843	1760	-	-	1988	2047	1987	1727	-	-	2035	1806	1753	-	-
1446A	149	1.1	1.5	135.6	154.2	475.4	1900	1876	1838	1774	1867	-	-	1781	1937	1787	1869	-	-	1900	1786	1786	-	-
B	149	1.1	1.5	141.7	184.1	530.4	1900	1765	1849	1849	1879	-	-	1847	1834	1787	1766	-	-	1900	1819	1780	-	-
C	149	1.1	1.5	139.0	155.8	512.7	2057	1713	1961	1917	1879	-	-	1847	1971	1854	1800	-	-	2214	1780	1726	-	-
D	149	1.1	1.5	143.2	137.5	526.7	1915	1852	1881	1881	1911	-	-	1716	2006	1787	1800	-	-	2052	1777	1835	-	-
E	149	1.1	1.5	133.5	160.0	495.6	1788	1899	1808	1808	1780	-	-	1849	1834	1554	1732	-	-	1788	1744	1726	-	-
1447 to 1449	Chemically pure propane and propylene mixture tests; no repeatable detonations.																							
1450 to 1457	Air flow pressure loss calibration tests.																							

a The dash signifies the lack of an event.

Table (rotated; values read left-to-right across columns). Primary header applies to tests 1458A–C; the alternate header (shown as an interior row) applies to tests 1459A–1461H.

Test No.	Configuration No.	φ E.R.	VA, m/s	F12-F17, m/s	F17-F21, m/s	F21-F23, m/s	F23-F71, m/s	F71-F2, m/s	F72-F82, m/s	F82-F85, m/s	F85-F101, m/s	F101-F104, m/s	F104-F62, m/s	F62-F63, m/s	P82, kN/m^2	P85, kN/m^2	P101, kN/m^2	P104, kN/m^2	P62, kN/m^2	P63, kN/m^2	P82,P85, m/s	P85,P101, m/s	P101,P104, m/s	P104,P62, m/s	P62,P63, m/s
1458A	165	1.1	4.6	62.8	37.2	43.0	183.8	2182	1962	1838	1999	1838	1997	1904	2852	2490	2572	2253	1951	1980	1902	1811	1967	1995	1904
B	165	1.1	4.6	65.5	39.0	45.4	196.0	2264	1861	1902	2002	1902	1836	1679	2507	2359	2408	2213	1918	2086	1902	1902	1902	1836	1679
C	165	1.1	4.6	72.5	42.4	47.6	168.9	2183	1801	1838	1808	1780	1777	1788	2266	2294	2326	1948	1825	1878	1838	1808	1808	1863	1788
(alt. header)							F23-F62, m/s	F62-F63, m/s	F63-F71, m/s	F71-F72, m/s	F72-F82, m/s	F82-F85, m/s	F85-F101, m/s	F101-F104, m/s	P71, kN/m^2	P72, kN/m^2	P82, kN/m^2	P85, kN/m^2	P101, kN/m^2	P104, kN/m^2	P71-P72, m/s	P72-P82, m/s	P82-P85, m/s	P85-P101, m/s	P101-P104, m/s
1459A	166	1.1	4.6	64.0	36.9	42.7	126.8	618.7	868.1	990.6	1170	1268	2238	1902	1081	1354	1374	4189	4129	3162	909.5	1031	1208	2034	1932
B	166	0.9	4.6	61.6	38.1	43.0	111.9	444.7	628.2	797.4	1133	1359	2135	1967	800	1188	1633	3982	4068	3166	723.0	827.0	1160	2169	2070
C	166	1.3	4.6	61.3	32.6	42.4	120.4	537.1	615.1	777.9	1002	1085	1423	1630	1103	1208	1473	1942	2662	3078	659.0	854.0	1017	1220	1449
D	166	1.1	6.1	78.6	47.9	59.1	149.1	678.8	1000	1329	2004	1902	1922	1841	1709	2939	2752	2721	2601	2426	1181	2324	1951	1877	1888
E	166	1.1	4.6	64.0	36.0	41.5	112.8	458.7	628.2	817.8	1042	1783	2135	1841	1426	1447	1633	4065	2682	2232	635.8	786.1	1672	1971	1951
F	166	1.1	3.0	51.5	30.2	44.5	94.8	490.7	694.6	898.6	1063	1585	2135	1841	1527	1387	2493	3920	2254	3201	837.3	894.9	1400	2200	1960
1460A	167	1.1	0	43.3	41.2	44.8	110.0	475.2	685.5	849.2	1107	1838	2741	1838	1094	1674	2263	4350	3928	2640	602.0	929.0	1356	2257	2035
B	167	1.1	0	45.1	41.1	45.4	109.1	394.7	607.8	827.2	1062	1499	2558	1838	994	1460	1861	4013	4251	3117	657.8	666.9	1212	2020	2035
C	167	1.1	1.5	36.0	26.8	36.9	82.3	325.8	403.9	597.1	776.6	982.1	1421	1899	493	1097	1937	1895	3081	3416	625.1	619.4	919.0	1096	1899
D	167	1.1	1.5	35.1	23.8	34.4	91.1	452.3	607.8	819.3	1062	1676	2132	1899	694	1323	2203	3400	3666	2958	665.7	713.8	1214	2261	2038
E	167	1.1	3.0	54.3	32.0	42.4	103.0	418.2	572.4	770.0	1062	1356	2257	1964	1273	1205	1742	3993	4049	3078	724.8	752.9	980.5	2016	2031
F	167	1.1	6.1	78.0	50.0	55.5	157.6	592.8	1052	1420	1794	1838	1918	1838	1953	3391	3910	3598	2576	2143	1228	1637	1911	2033	1850
1461A	167	1.1	4.6	70.1	39.0	43.6	128.3	566.3	765.7	953.7	1182	1628	2257	1838	1413	1991	1785	4171	2446	2390	717.5	912.9	1325	2132	1899
B	167	1.3	4.6	67.4	43.3	54.6	145.4	572.7	671.8	863.5	881.8	933.9	1163	863.2	1473	1143	1174	1367	1693	2271	885.4	947.6	877.8	985.4	1542
C	167	0.9	4.6	57.9	40.2	42.1	109.4	364.9	487.1	620.3	812.9	1095	1421	1726	446	558	1011	1506	1673	3400	551.5	582.5	844.6	1289	1826
D	167	0.7	4.6	No ignition.																					
E	167	0.8	4.6	45.4	37.5	35.4	80.5	138.4	239.9	260.3	330.7	414.5	562.4	613.9	n.a.[a]	105	156	273	434	985	n.a.	330.7	480.1	562.4	654.4
F	167	1.0	4.6	64.9	42.1	47.6	128.6	592.8	710.2	1014	1369	2109	2132	1838	1074	2092	3334	3893	2972	2509	759.9	1091	1911	2033	1977
G	167	1.2	4.6	65.5	42.1	47.6	133.5	650.8	810.4	1183	1734	1964	2019	1964	1373	2899	3273	2958	2512	2014	1065	1533	2282	1921	1841
H	167	1.4	4.6	64.2	44.2	60.7	139.0	616.3	756.8	924.8	983.3	1164	1201	1902	1473	1709	2030	2143	3631	3360	819.6	981.8	1075	1199	1899
1462 to 1469	Air flow pressure loss calibration tests.																								

[a] Not available.

Test No.	F12-F17, m/s	F17-F21, m/s	F21-F23, m/s	F23-F62, m/s	F62-F63, m/s	F63-F71, m/s	F71-F72, m/s	F72-F82, m/s	F82-F85, m/s	P85-P101, m/s	P101-P104, m/s	P62, kN/m²	P63, kN/m²	P71, kN/m²	P72, kN/m²	P82, kN/m²	P85, kN/m²	P101, kN/m²	P104, kN/m²	P62-P63, m/s	P63-P71, m/s	P71-P72, m/s	P72-P82, m/s	P82-P85, m/s	P101-P104, m/s
1470A	48.6	37.9	48.3	235.8	1902	2040	1987	2035	1847	—	—	2064	1935	n.i.b	n.i.	2281	2313	424.6	357.5	1902	—	1852	—	1847	755.0
B	54.8	37.9	39.7	261.0	2038	1903	1984	1812	1783	—	—	2158	1905	n.i.	n.i.	2072	1858	356.0	374.0	2037	—	1831	—	1783	687.6
C	47.5	36.2	41.7	289.3	2035	2044	1988	1957	1908	—	—	3345	2560	n.i.	n.d.	2718	2524	336.0	206.0	2035	—	1951	—	2044	597.7
1471A	25.2	31.4	41.5	269.8	1908	1914	1876	1982	1914	—	—	2919	2230	2480	2246	2632	2530	324.1	279.0	2051	2051	1987	1982	1914	582.3
B	33.9	34.9	47.9	290.0	1908	2038	1981	1951	1783	870.0	570.6	2540	2100	1850	1573	2029	2040	464.1	453.4	1908	1902	1864	1951	1783	695.9
1472A	32.8	38.2	43.2	253.5	2078	2078	1981	1951	1902	—	—	3326	3472	2958	2525	2743	2945	331.4	316.6	2078	2078	1981	1951	1783	594.4
B	55.6	36.3	43.1	271.3	2036	1902	1981	1951	2039	—	—	3076	2713	2492	2492	2471	2548	334.8	306.7	2036	1903	1982	1812	1691	583.0
C	58.6	37.0	38.8	276.8	1902	2040	2116	1814	1904	—	—	2723	2713	2392	2192	2029	2476	331.0	307.0	2038	1902	1981	1953	1904	571.0
D	43.2	37.1	42.4	263.0	2038	1902	1865	1951	1902	—	—	3076	2713	2525	2325	2505	2332	328.0	306.7	1902	1903	1981	1811	1783	570.6
E	48.7	37.5	45.0	277.5	1903	1962	1865	1811	1962	—	—	2402	2576	2492	2225	2607	2512	331.4	303.5	1963	1901	1865	2038	1902	594.0
F	47.6	40.3	54.0	291.4	2037	1903	1866	1952	1784	—	—	2857	2541	2292	2192	2131	2296	328.0	297.2	1901	1903	1981	1813	1784	583.0
1473A	47.0	36.7	38.4	260.9	1903	1733	1981	1951	1678	—	—	2523	2637	2347	2195	2334	2359	268.0	255.7	1903	1783	1982	1811	1678	529.0
B	61.0	38.4	43.8	271.3	1903	1783	1866	1952	1903	—	—	2720	2436	2515	2129	1899	2228	263.3	252.3	2039	1783	1865	1813	1903	509.5
C	57.8	38.1	43.2	269.7	1902	1903	1866	1952	1784	—	—	2950	2436	2448	2195	2401	2260	270.0	252.3	1902	1903	1855	1952	1784	529.0
D	58.5	39.1	41.1	265.5	2039	1901	1865	1951	1901	—	—	3354	2570	2650	2485	2434	2423	266.7	259.0	1903	1902	1866	1951	1901	519.0
E	59.2	37.0	41.0	230.0	2040	1908	1870	1957	1908	—	—	3311	2704	2515	2260	2501	2490	266.7	259.0	1904	1903	1865	1957	1908	529.0
F	60.4	36.9	42.1	258.7	2038	1902	1981	1811	1902	—	—	2819	2369	2616	2359	2568	2523	263.3	259.0	2038	1783	1866	1951	1783	528.0
1474A	51.8	40.1	50.4	261.9	2036	1902	1855	1952	1784	—	—	2984	2359	2380	2358	1916	2199	321.8	314.9	1902	1785	1865	1813	1784	607.4
B	63.5	37.6	45.0	271.6	2048	1785	1763	1952	1903	—	—	3048	2831	2413	2225	1790	2437	343.9	325.2	2048	1901	1763	1952	1903	607.4
C	n.a.c	n.a.	n.a.	n.a.	n.a.	n.a.	n.a.	n.a.	n.a.	n.a.	n.a.	2698	n.a.	2313	2192	1419	2369	328.1	321.8	1901	1901	1761	1949	2035	619.8
D	n.a.	n.a.	n.a.	n.a.	n.a.	n.a.	n.a.	n.a.	n.a.	n.a.	n.a.	n.a.	n.a.	n.a.	n.a.	n.a.	n.a.	n.a.	n.a.	n.a.	n.a.	n.a.	n.a.	n.a.	n.a.
E	57.3	36.4	40.0	269.2	1902	1902	1865	1950	1902	—	—	3015	n.a.	2246	2058	1585	2369	325.0	322.0	1902	1902	1865	1950	1902	634.0
F	57.0	39.8	48.7	285.2	1782	1901	1863	1811	1902	—	—	2921	n.a.	2347	2092	1850	2029	328.1	318.3	1782	1901	1863	1811	1902	636.0
1475A	50.8	39.8	46.9	268.7	1898	2034	1861	1811	1902	—	—	2915	2539	2588	2172	2403	2556	185.4	183.4	1898	2034	1861	1811	1902	663.5
B	40.1	39.9	50.9	282.6	2033	1897	1860	1951	1902	—	—	3140	2403	2490	2139	2535	2162	176.4	170.1	2033	1897	1860	1951	1902	731.5
C	46.0	37.2	50.1	280.9	2034	1898	1861	1951	1902	—	—	2562	2369	2233	2007	2337	2293	179.4	173.4	2034	1898	1861	1951	1902	663.5
D	55.5	36.7	44.9	242.7	1902	1902	1865	1811	1902	—	—	2915	2505	2490	2568	1874	2458	179.3	183.5	1902	1902	1865	1811	1902	365.8
E	50.8	37.2	42.5	289.4	1902	1902	1865	1949	1901	—	—	2883	2335	2293	2007	2403	2260	181.3	186.8	1902	1902	1865	1949	1901	407.3
F	47.6	39.3	50.1	277.1	1783	1902	1865	1950	2036	—	—	3172	2539	2359	2337	2271	2359	185.3	183.5	1783	1902	1865	1950	2036	419.3
1476A	39.4	43.7	55.2	301.2	1781	2035	1862	1938	1890	—	—	1876	2110	2208	2053	2053	2244	178.6	180.6	1781	1890	1853	1938	1890	405.0
B	40.5	38.3	49.3	260.7	1898	1898	1861	2110	1900	—	—	1843	1687	2045	2053	1952	2176	185.5	187.5	1898	1900	1759	2110	1900	425.3
C	26.0	37.6	47.9	294.1	1900	2035	1759	1811	1902	—	—	1775	1655	1980	2054	2020	2210	195.7	204.2	1900	1902	1864	1811	1902	380.4

a The dash signifies the lack of an event.

b Not installed: pressure transducer removed.

c Not available.

Test No.	F12-F17, m/s	F17-F21, m/s	F21-F23, m/s	F23-F62, m/s	F62-F63, m/s	F63-F71, m/s	F71-F72, m/s	F72-F82, m/s	F82-F85, m/s	F85-F101, m/s	F101-F104, m/s	P62, kN/m²	P63, kN/m²	P71, kN/m²	P72, kN/m²	P82, kN/m²	P85, kN/m²	P101, kN/m²	P104, kN/m²	P62-P63, m/s	P63-P71, m/s	P71-P72, m/s	P72-P82, m/s	P82-P85, m/s	P101-P104, m/s
1476D	26.0	44.4	52.9	309.4	1900	1900	1862	1808	1779	—[a]	—	1843	1753	1948	1884	1918	2210	199.3	204.2	1781	1898	1977	946	1779	418.7
E	23.7	41.5	50.2	307.8	1896	1896	1858	1944	2031	—	—	1708	1655	1948	2020	2020	2244	215.9	214.3	1777	2031	1859	944	1896	418.2
1477A	29.1	45.9	54.2	317.9	2032	1780	1860	2106	1724	—	—	2141	1809	2337	1851	2279	2294	230.0	235.6	1897	1839	1915	1872	1896	415.2
B	27.4	44.5	55.6	304.6	2038	1783	1865	1951	1783	—	—	2312	1776	2240	1919	2010	2456	244.0	248.9	1902	1902	1854	1951	1902	445.7
C	42.4	37.6	48.3	290.4	2034	1780	1861	1944	1777	—	—	2039	1809	2142	2222	2111	2327	250.8	245.4	1898	1896	1859	1944	1777	437.5
D	38.9	40.4	47.9	275.9	2035	1781	1979	1948	1900	576.4	633.2	1971	1841	1947	1884	2044	1938	>473.8[b]	>451.1	1781	1900	1979	1809	1900	518.0
E	41.3	37.7	45.4	269.2	1900	1781	1862	1951	1902	—	—	2210	1971	2272	2155	2178	2327	n.i.	n.i.	1900	2038	1865	1811	1902	n.i.
F	31.4	43.5	48.7	277.2	2035	2035	1979	1948	1900	832.9	678.4	2243	1841	2207	2222	2178	2133	n.i.	n.i.	2035	1900	1862	1948	1900	n.i.
1478A	40.3	40.1	47.9	262.7	2035	1900	1979	1809	1900	—	—	2068	1923	2403	2239	2125	2482	284.4	270.5	1900	1900	1862	1948	1900	390.3
B	57.5	38.9	44.2	253.4	1901	1901	1980	1810	1901	—	—	2068	2021	2467	2274	2158	2482	298.2	307.3	1901	1901	1980	1949	1901	407.3
C	50.4	39.6	49.6	255.1	1900	1900	1979	1809	1900	764.7	678.4	2032	1988	2305	2450	2192	2346	>473.1	>447.8	1900	1900	1862	1948	1781	919.1
D	56.6	39.7	43.6	280.2	1900	2035	1862	1948	1900	803.5	863.4	2104	2021	2305	2239	2192	2482	n.i.	n.i.	1900	1900	1862	1948	1900	n.i.
1479A	50.5	36.2	44.2	258.6	2030	1897	1979	2028	1837	—	—	2187	1744	2419	2199	2101	2250	299.4	307.6	1900	1902	1761	1951	1841	380.4
B	60.6	38.1	49.4	262.3	1781	1900	1979	1948	1780	748.4	825.6	2187	1971	2517	2029	2118	2114	>479.8	>475.1	1900	1781	1862	1948	1900	1017
C	55.4	39.8	39.8	272.5	1840	1840	1920	1878	1840	808.2	640.8	2133	2132	2662	2301	2218	2165	n.i.	n.i.	1920	1878	1840	1878	1840	n.i.
1480A	44.8	47.5	56.5	326.6	1893	1965	1863	1948	1899	—	—	2739	2187	2739	2363	2290	2475	146.9	151.3	1890	1960	1860	1948	1900	419.0
B	49.5	38.2	46.2	270.8	1893	1900	1809	1876	1899	—	—	2667	2300	2590	2160	2256	2112	137.4	139.7	1900	1900	1809	1876	1900	425.1
C	34.5	40.8	54.3	302.7	1837	1780	1918	1811	1840	—	—	2433	1930	2672	2228	2205	2180	140.6	141.3	1900	1780	1809	1811	1840	419.5
D	50.1	40.9	45.3	260.1	1900	1781	1919	1875	1779	—	—	2703	2365	2970	2278	1986	1873	142.2	144.7	1900	1781	1918	1875	1779	452.0
E	34.2	43.0	51.8	279.0	2033	1836	1860	1877	1900	—	—	2685	2332	2606	2160	2408	2163	159.6	158.0	2033	1836	1810	1877	1900	509.0
F	53.8	38.1	41.8	265.0	1965	1839	1918	1809	1899	—	—	2253	1849	3003	2312	1834	2180	166.0	163.0	1965	1839	1918	1809	1900	369.9
1481A	43.5	37.2	51.3	297.9	1779	1779	1976	1876	1838	—	—	2482	2332	2889	n.a.[c]	2223	2386	144.7	143.1	1920	1779	n.a.	1878	1840	395.5
B	30.5	42.3	56.6	317.0	1838	1780	1918	1809	1727	—	—	3079	2138	2738	3142	2273	2334	135.0	134.8	1900	1780	1918	1809	1727	390.2
C	35.4	36.3	45.6	296.3	1927	1752	1890	1875	1780	—	—	2971	2186	2572	2346	2121	1817	138.3	139.8	1927	1898	1977	1947	1898	418.7
D	47.4	33.6	41.2	291.1	1897	1725	1916	1875	1898	—	—	2410	2300	2835	2296	1986	1920	144.7	143.1	1897	1725	1916	1875	1898	379.7
E	62.2	37.2	38.3	262.3	2035	1781	1862	1808	1899	—	—	2844	2332	2671	2414	2037	2334	140.0	143.1	1900	1899	1861	1947	1837	406.8
F	55.2	41.6	49.2	274.4	2033	1725	1916	2028	1872	—	—	2734	2397	2441	2414	2240	2196	151.1	146.4	1897	1902	1811	1878	1968	335.6
1482A	26.3	43.4	58.5	263.3	1969	1731	1866	1876	1838	—	—	2827	2280	2376	2020	1902	2209	131.2	130.4	1904	1731	1866	1876	1838	474.9
B									1780	Delayed Ignition: no data recorded															418.7
C	23.0	43.6	46.4	296.5	2038	1729	1864	1875	1780	—	—	2362	2167	2146	2003	1953	1813	132.9	130.4	1902	1898	1861	1947	1898	418.7
D	n.a.	n.a.	37.1	262.8	1899	1899	1862	1924	1876	—	—	2416	2231	2113	2037	1767	2106	129.6	128.7	1899	1875	1953	1923	1875	365.3
E	24.8	38.3	44.8	278.8	1822	1875	1846	1915	2001	—	—	2434	2103	2080	2156	1919	2020	129.6	123.7	1822	1875	1838	1923	1875	493.5

[a]The dash signifies the lack of an event.

[b]Not installed: pressure transducer removed.

[c]Not available.

Test No.	F12-F17, m/s	F17-F21, m/s	F21-F23, m/s	F23-F62, m/s	F62-F63, m/s	F63-F71, m/s	F71-F72, m/s	F72-F82, m/s	F82-F85, m/s	F85-F101, m/s	F101-F104, m/s	P62, kN/m²	P63, kN/m²	P71, kN/m²	P72, kN/m²	P82, kN/m²	P85, kN/m²	P101, kN/m²	P104, kN/m²	P62-P63, m/s	P63-P71, m/s	P71-P72, m/s	P72-P82, m/s	P82-P85, m/s	P101-P104, m/s
1482F	24.5	-44.9	50.2	289.1	1964	1780	1918	1872	1895	—[a]	—	2416	2199	2129	2003	2003	2037	136.1	135.4	1837	1896	1858	1944	1896	418.1
G	20.2	42.6	49.2	290.8	2033	1837	1861	1797	1826	—	—	2326	2231	2179	2206	2037	2071	137.8	132.1	1897	1769	1850	1936	1887	312.5
H	33.6	43.9	45.9	257.6	1831	1831	1855	1948	1780	—	—	2416	2199	2179	2139	2020	1899	137.8	137.1	2027	1896	1859	1944	1834	437.5
1483A	45.6	37.9	45.6	265.4	1766	1766	1962	1863	1952	—	—	2404	2188	2157	2044	1742	2283	142.0	142.4	2016	2018	1903	1793	1884	415.5
B	41.3	41.5	45.1	245.4	1825	1825	1905	1855	1818	—	—	2422	2220	2157	2212	2027	2110	140.3	140.7	1875	1761	1789	1855	1878	385.9
C	38.1	45.2	53.9	268.8	1896	1719	1890	1782	1754	—	—	2657	2204	2272	2229	2128	2076	140.3	140.7	1833	1878	1897	1926	1942	375.5
D	26.4	45.1	54.3	293.6	1832	1832	1856	1806	1835	—	—	2476	2285	1830	2190	2061	2001	158.1	159.3	1831	1961	1915	1944	1896	418.2
E	48.0	41.7	54.1	323.5	1897	1836	1916	1948	1781	—	—	2458	2172	2174	2162	1960	2007	177.5	162.6	1898	1965	1809	1948	1837	390.2
F	30.0	46.2	51.8	284.2	1839	1839	1863	1812	1841	—	—	2603	2204	2305	2196	2061	1990	166.2	157.6	1901	1841	1865	1951	1968	370.6

[a] The dash signifies the lack of an event.

Test No.	F12-F17, m/s	F17-F21, m/s	F21-F23, m/s	F23-F71, m/s	F71-F72, m/s	F72-F82, m/s	F82-F85, m/s	F85-F101, m/s	F101-F104, m/s	F104-F63, m/s	F63-F62, m/s	P71, kN/m²	P72, kN/m²	P82, kN/m²	P85, kN/m²	P101, kN/m²	P104, kN/m²	P63, kN/m²	P62, kN/m²	P71-P72, m/s	P72-P82, m/s	P82-P85, m/s	P101-P104, m/s	P104-P63, m/s	P63-P62, m/s
1488A	44.3	66.9	85.5	492.7	1936	1917	1838	—a	—	—	—	1916	1902	1939	2123	152.9	146.4	144.2	144.2	1978	1808	1899	409.8	339.4	430.7
B	44.6	65.9	82.3	477.5	2000	1847	1899	—	—	—	—	2113	2003	2039	2037	148.1	144.7	141.0	138.4	1978	1947	1899	413.3	389.0	618.3
C	44.9	66.5	78.9	494.3	1990	1915	1724	—	—	—	—	2064	1851	2056	2174	151.3	146.4	145.8	138.4	1859	1945	1897	360.1	398.0	616.1
D	45.9	66.9	83.1	491.1	2053	1828	1763	—	—	—	—	2146	2037	2023	2088	149.7	151.1	142.2	136.6	1959	1791	1880	394.5	395.8	416.0
1485A	43.1	66.4	72.9	463.3	1864	1809	1780	—	—	—	—	2369	2199	2235	2092	150.3	151.1	151.4	147.2	1864	1809	1780	385.1	409.5	407.5
B	44.4	68.3	73.4	455.8	1862	1807	1898	—	—	—	—	2370	n.a.	2235	1644	147.1	146.1	148.1	n.a.b	n.a.	n.a.	1898	390.1	395.2	n.a.
C	45.1	67.8	75.1	486.6	2105	1944	1777	—	—	—	—	2304	2267	2201	2161	147.1	149.4	131.9	n.a.	2105	1944	1777	374.2	392.5	n.a.
D	44.6	67.9	75.5	475.6	1976	1944	1895	—	—	—	—	2403	2233	2135	2058	147.1	142.8	n.a.	n.a.	1859	1944	1896	418.2	n.a.	n.a.
1486A	46.1	67.9	79.2	490.8	2110	1946	1898	—	—	—	—	2283	2082	2116	2132	354.0	331.2	222.5	n.a.	1977	1809	1898	619.0	523.9	491.0
B	45.9	65.7	79.8	490.3	1979	1949	1780	—	—	—	—	2217	2049	2184	2098	354.0	341.2	219.9	n.a.	1862	1948	1900	633.2	525.7	508.8
C	46.1	67.5	82.2	492.7	1852	1946	1673	—	—	—	—	2217	2150	2082	2098	360.6	334.5	225.8	n.a.	1258	1946	1779	646.7	531.6	450.0
D	46.7	67.6	76.9	502.1	1976	1944	1895	—	—	—	—	2207	2116	2217	2098	354.0	331.2	231.6	233.7	1859	1944	1895	622.0	532.6	508.1
1487A	45.4	69.7	86.5	498.1	1974	1944	1895	—	—	—	—	2068	2135	1995	2103	350.8	333.9	247.1	248.4	1975	1944	2031	605.1	526.0	507.5
B	45.3	63.7	91.7	478.4	1976	1946	1897	—	—	—	—	2262	2034	2267	2137	350.8	339.0	251.7	248.2	1975	1946	2032	618.6	529.6	527.0
C	46.2	68.4	79.0	495.5	1858	1945	1897	—	—	—	—	2133	2101	2199	2033	344.1	327.3	259.0	258.2	1976	1945	1897	661.8	534.3	517.1
D	46.4	67.0	85.0	494.9	1856	1805	1777	—	—	—	—	2262	1967	2233	2103	343.6	324.0	259.0	254.9	1859	1805	1896	632.0	564.9	489.7
E	46.1	66.0	78.7	480.7	1975	1945	1896	1711	1777	1840	1895	2262	2000	2232	3137	n.i.c	n.i.	>585	>556	1859	1806	1896	n.i.	n.i.	1895

a The dash signifies the lack of an event.

b Not available.

c Not installed: pressure transducer removed.

DATE
ILMED

-8